Strontium isotope tracing of prehistoric human mobility in France

Malte Willmes, MSc.

A thesis submitted for the degree of Doctor of Philosophy of The Australian National University

March 2015

Declaration

Hereby I declare and confirm that this thesis represents my own work, except where otherwise acknowledged.

Malte Willmes

Malte Willmes

Abstract

Human mobility in recent history is well documented and often related to drastic external changes, including war, famine, and the discovery and exploration of new geographic regions and resources. Reconstruction of mobility patterns in prehistory is thus a crucial part of understanding the forces that drove our ancestors, but it is complicated by the fact that the archaeological evidence becomes scarce as we go back in time. The application of stable isotopes in archaeological research has revolutionised palaeomobility studies by providing independent data, which can be used to evaluate models of migration, trade, and cultural change. This research project explores the use of strontium isotope ratios ($^{87}Sr/^{86}Sr$) to trace prehistoric human mobility patterns. Strontium isotope ratios vary across the landscape based on the age and composition of the underlying geology. Through diet humans incorporate strontium into their skeletal tissues such as bones and teeth. Teeth form during childhood and are resistant to weathering and geochemical alteration, often preserving the original isotope values. By comparing the strontium isotope ratios in teeth to the variations of strontium isotopes in the landscape it becomes possible to investigate mobility across geologically different areas between childhood and death.

This study establishes the Isotopic Reconstruction of Human Migration (IRHUM) reference database and provides the first dataset of $^{87}Sr/^{86}Sr$ isotope ratios of plant and soil samples, covering all major geologic units of France. This provides a new powerful tool for the archaeological science community as it allows the mapping of the variations of bioavailable $^{87}Sr/^{86}Sr$ isotope across the landscape. Utilizing this dataset, a bioavailable $^{87}Sr/^{86}Sr$ isotope map for archaeological provenance studies in France is created.

For the application of this method to human fossil teeth new analytical methods to detect diagenetic overprint were tested. These now allow for rapid scanning to investigate the suitability of samples, minimising the damage to fossil remains. Least destructive analytical techniques for strontium isotope analysis, such as micro drilling thermal ionisation mass spectrometry and *in situ* laser-ablation MC-ICP-MS, were further developed and applied to a range of materials of known composition, including shark and dugong teeth, modern and archaeological fauna samples, and fossil and modern human teeth.

Finally, strontium isotope tracing was applied to three key archaeological sites in France, including the Neanderthal sites of Moula-Guercy, and the Neolithic sites of Le Tumulus des Sables and La Grotte des Perrats. Strontium isotope tracing proved to be a valuable technique and in combination with additional strings of evidence from archaeological material and other isotopic tracers, such as oxygen, improved our understanding of prehistoric human mobility at these sites. By covering different geographic locations and different time periods this study tests geochemical fingerprinting and offers new insights into these renowned archaeological sites.

Acknowledgements

This research project has been more challenging, and maybe surprisingly, also more enjoyable than I could have imagined. I am immensely grateful to my principle supervisor Rainer Grün for providing me with an interesting research project, for allowing me to make this project my own, and for his guidance and frank discussions to keep me on track. Thank you to Richard Armstrong, who took on the role as my secondary supervisor, and without his expertise, dedication, and ongoing support this project would have surely failed. Thanks also to my co-supervisors Stephen Eggins and Matthew Spriggs for their helpful suggestions and comments over the last 4 years.

The technical and analytical aspects of this research project were supported by a large number of people within the Research School of Earth Sciences and I am immensely thankful for their unwavering support. Linda McMorrow was instrumental in setting up the geochemistry laboratory and spend countless hours in front of the column chemistry, and the MC-ICP-MS. Her dedication and hard work made this all possible. Les Kinsley was always eager to explore new analytical techniques and allowed me to run the instruments day and night once everything was working. Thanks to Graham Mortimer for showing me the ropes of isotope geochemistry, when I first got here, and for his help in setting up the strontium isotope lab. I would also like to thank Sonja Zink, Vickie Bennett, and Yuri Amelin for their help in analysing the samples on the TIMS and helpful suggestions on the treatment and interpretation of the data. Rachel Wood and Stewart Fallon introduced me to radiocarbon dating and were happy to share their expertise. David Heslop was a great source of sound statistical advice and Ian Williams' comments on the treatment of data and the art of scientific writing were most valued.

Eric Ward and Nigel Craddy were trusted sources of support during the various moves of the lab and sample collection. They were of great help during the first water leak flooding the lab – and maintained their enthusiasm during the second flooding as well. Robyn Petch and Josephine Magro were directly involved in all of the logistical parts of this project and their dedication and encouragement was very much appreciated. Robyn and Eric chased a sample box all the way from France to Canberra, via Frankfurt, Sydney, Singapore, Hamburg, Sydney, Canberra. Without their help we would have to go back to northern France.

I would also like extend my thanks to the people of the Engineering and Electronic workshop at RSES for their support in designing, building, and fixing parts of our laboratory equipment. Specifically, to Ben Tranter for his help with finding a way to drill tooth enamel samples and to Andrew Wilson for his excellent advice. Thank you to Hashantha Mendis and Duncan Bolt for their support with anything remotely IT related.

The fieldwork in France, which involved ~35000 km of driving along narrow French country roads, 820 stops to collect samples, boxes and boxes of soils, plants and rocks, and a rogue camembert, would not have been possible without the enthusiastic support of Rainer Grün, Ceridwen Boel and Magdalena Huyskens.

Thanks to our colleagues at the archaeological sites in France. Bruno Maureille was a great host at our various stays in Bordeaux and provided valuable feedback. Patrice Courtaud showed us around Le Tumulus des Sables, introduced us to the best wines of the region, and hosted us in the Pyrenees. We also thank Fanny Derym, from the Museum Archéologique de Soyons, for her immense help with the project at Moula-Guercy. A thank you also to our hosts in Corsica from DRAC for their hospitality, and for showing us the exciting archaeology of this island. Philippe Rossi hosted us at the BRGM and shared his knowledge of French geology.

Jurian Hoogewerff was a great source of advice at the beginning of this project and together with Clemens Reimann arranged for us to analyse the GEMAS soil standards.

Teeth samples from Rainer, Alex, and Jiamin were greatly appreciated. The Grey Nurse Shark tooth was provided from the Australian Museum Sydney, in collaboration with Mark McGrouther, and the Dugong tooth from School of Archaeology and Anthropology, ANU, with the kind help of Colin Groves.

My colleges at the Research School of Earth Sciences formed the backbone of this endeavour, providing insightful discussion and advice, as well as coffee and food at sometimes unreasonable hours. In particular, I am thankful to my fellow Archaeogeochemistry group members Kelsie Long, Hannah James, Fang Fang, and Mathieu Duval for their friendship and advice.

To my family, you are a constant source of happiness and I only wish I could see you more often. Your patience, support, and understanding kept me going. To my friends, present, past, and beyond, I am grateful to have shared this time with you. I am thankful for your company and friendship, from late night dinners at RSES when running the instruments, to adventurous bush walks in the Australian wilderness and weeks of swimming and camping along the South Coast. For teaching me that falling of a rock cliff can be as much fun as being dragged upside down in kayak through the waves. Long days often ended with amazing house dinners, and weeks were finished off with the sudden appearance of food and drinks on Friday nights. Regular trips to the coffee shops on campus sparked interesting discussions, sometimes even related to science, and lifted the spirit when it was most needed. Fierce competitions for the prestigious mytournament8, conquering the world in the early hours of the morning, casual rides to the hospital, disgusting Sundays and renowned Halloween parties kept me distracted enough so that I could finish this project. Finally, thank you for offering places to sleep and rest in Hobart, Paris, Freiburg, Vienna and Münster, and for the wonderful home we had in Canberra.

To Bella No-biting, for her excellent advice on previous versions of this manuscript and for kindly introducing me to all the possums in the neighbourhood. Finally, to my wife Magda, for her insights, support, and for embarking on this incredible adventure together with me.

Funding was provided by ARC DP110101415 (Grün, Spriggs, Armstrong, Maureille and Falguères) *Understanding the migrations of prehistoric populations through direct dating and isotopic tracking of their mobility patterns*. Part of this research was supported by the Australian French Association for Science & Technology through the ACT Science Fellowship program (2013). The National Science

Foundation Travel Grant (2012) allowed me to participate in the SPATIAL summer school program at the University of Utah. The Vice-Chancellor's HDR travel grant for allowing to attend the EGU conference 2012 in Vienna. Parts of the study at Moula-Guercy were funded by the CEPAM, UMR7264-CNRS and by Géoazur, UMR7329-CNRS. The GeoNode community was a great resource for setting up the IRHUM database and supported this project with discussions and detailed assistance.

Dedication

To my sister Inga, who roams on the other side of this planet but is never far from my mind

Table of contents

List of Figures

List of Tables

List of acronyms

AMS	Accelerator Mass Spectrometry
BBP	Bell Beaker Phenomenon
BEB	Buccal Enamel Boundary
CL imaging	Cathodoluminescence imaging
DL	Detection Limit
DEJ	Dentine Enamel Junction
EBK	Empirical Bayesian Kriging
EDS	Energy Dispersive X-ray Spectroscopy
ESR dating	Electron Spin Resonance dating
GNIP	Global Network of Isotopes in Precipitation
IAEA	International Atomic Energy Agency
ICP-AES	Inductively Coupled Plasma Atomic Emission Spectroscopy
ICP-MS	Inductively Coupled Plasma Mass Spectrometer
IQR	Interquartile range
IR spectroscopy	Infra-red spectroscopy
IRHUM database	Isotopic reconstruction of human migrations database
IRMS	Isotope-ratio mass spectrometry
IU	*In Utero*
LA-MC-ICP-MS	LASER ablation Multi-Collector Inductively Coupled Plasma Mass Spectrometer
MC-ICP-MS	Multi-Collector Inductively Coupled Plasma Mass Spectrometer
MIS	Marine Isotope Stage
NIST	National Institute of Standards and Technology
REEs	Rare Earth Elements
RSES, ANU	Research School of Earth Sciences, The Australian National University
SHRIMP II	Sensitive High Resolution Ion MicroProbe II
TIMS	Thermal Ionisation Mass Spectrometer
TL dating	Thermoluminescence dating
TLD	Thermoluminescent Dosimeter
$\Delta_{LA\text{-}TIMS}$	Strontium isotopic ratio difference between LA-MC-ICP-MS analysis and TIMS analysis
Δ_{PS}	Strontium isotopic ratio difference between plant sample and soil leachate

List of publications

Benson, L. Kinsley, **M. Willmes**, A. Defleur, H. Kokkonen, M. Mussi, R. Grün (2013), Laser ablation depth profiling of U-series and Sr isotopes in human fossils. Journal of Archaeological Science, 2991–3000. doi: 10.1016/j.jas.2013.02.028.

M. Willmes, L. McMorrow, L. Kinsley, R. Armstrong, M. Aubert, S. Eggins, C. Falguères, B. Maureille, I. Moffat, R. Grün (2014), The IRHUM (Isotopic Reconstruction of Human Migration) database – bioavailable strontium isotope ratios for geochemical fingerprinting in France. Earth System Science Data 6, 117–122. doi: doi:10.5194/essd-6-117-2014.

M. Willmes, I. Moffat, L. McMorrow, L. Kinsley, R. Armstrong, S. Eggins, R. Grün (in review), Spatial variability of bioavailable $^{87}Sr/^{86}Sr$ isotope ratios in France as a framework for archaeological provenance studies. Applied Geochemistry.

M. Willmes, L. Kinsley, M.-H. Moncel, R. A. Armstrong, M. Aubert, S. Eggins, R. Grün (in review), Improvement of laser ablation *in situ* micro-analysis to identify diagenetic alteration and measure strontium isotope ratios in fossil human teeth. Journal of Archaeological Science.

M. Willmes, H. F. James, C. A. Boel, P. Courtaud, A. Chancerel, R. Wood, S. Fallon, L. McMorrow, R. A. Armstrong, I. S. Williams, L. Kinsley, M. Aubert, S. Eggins, I. Moffat, R. Grün (in preparation), Radiocarbon dating and isotopic tracing of human diet and mobility at the collective burial site, Le Tumulus des Sables, France. Journal of Archaeological Science: Reports.

M. Willmes, R. Grün, K. Douka, V. Michel, R. A. Armstrong, A. Benson, E. Crégut-Bonnoure, E. Desclaux, F. Fang, L. Kinsley, T. Saos, A. R. Defleur (in preparation), Chronology and human mobility at the Neanderthal site of Moula-Guercy (Ardèche, France). PLOS ONE.

Scope of the project

The chapters in this thesis are written as manuscripts for journal publication and are in various stages of the review process. The contributions of the author to the different publications are outlined at the beginning of each chapter. This thesis pursued three main aims: (i) defining the bioavailable strontium isotope range of France, (ii) development of least-destructive analytical techniques to screen for diagenetic overprint and to perform strontium isotope analysis of fossil human teeth, and (iii) application of isotopic tracing to key archaeological sites in France. The introduction to strontium isotope tracing, given in chapter 1, discusses the complexities involved in strontium isotope tracing of mobility patterns, including the effects such as preferential weathering, mixing of strontium reservoirs, input of strontium from the atmosphere or through anthropogenic influences, and the effects of post burial diagenesis on the skeletal remains. Conclusions and future directions are given at the end of the thesis in chapter 6. The appendix found in chapter 8 contains detailed laboratory methods as well as the supplementary material from the journal publications.

(i) Defining the bioavailable strontium isotope range of France

Archaeological provenance studies in France are currently limited due to the lack of baseline strontium isotope maps. In order to define the bioavailable strontium isotope range of France we developed the IRHUM (isotopic reconstruction of human migration) database (www.irhumdatabase.com, Willmes et al., 2014), see chapter 2. This online database allows the user to explore and map isotopic datasets and exchange data in a variety of formats. It is based on the open source software GeoNode (Boundless) and all modifications are tracked in GitHub, to allow future developments. To ensure the longevity of the dataset it is deposited in the Pangaea data repository (doi:10.1594/PANGAEA.819142). Since strontium isotope ratios are used as a geochemical tracer in a wide range of fields outside of archaeology, including ecology, soil, food and forensic sciences, the IRHUM database will hopefully prove to be a useful tool for the wider science community and encourage collaboration between the different fields of science for geochemical fingerprinting. The data found in the IRHUM database was then used to create a bioavailable $^{87}Sr/^{86}Sr$ isotope map of France for archaeological provenance studies, see chapter 3 (Willmes et al., submitted). This baseline map now allows the investigation of prehistoric mobility patterns in France in great detail and provides the framework for future archaeological provenance studies.

(ii) Development of least-destructive analytical techniques for strontium isotope analysis of fossil human skeletal remains

The analysis of human remains is a particularly sensitive topic and has been hindered in the past because destructive sampling (drilling) was required for traditional strontium isotope analysis. In order to select suitable samples for strontium isotope analysis *in situ* methods to detect diagenetic overprint using laser-

ablation ICP-MS were explored by Boel (2011) and Grün et al. (2008). We improved on these methods, see chapter 4, and now have a protocol in place that allows for the rapid scanning of human dental remains to select the best suited samples for isotopic tracing. An exploratory study by Benson et al. (2013) showed the potential of *in situ* strontium isotopic analysis from the outer sample surface, which avoids cutting of the sample. However, there are considerable analytical problems associated with *in situ* laser-ablation MC-ICP-MS analysis of strontium isotope ratios in teeth. A thorough investigation of these analytical problems and a new sample acquisition protocol are discussed in chapter 4. These methods were then evaluated using samples of known isotopic composition, including shark and dugong teeth, modern and archaeological fauna samples, and fossil and modern human teeth using micro drilling thermal ionisation mass spectrometry and *in situ* laser-ablation MC-ICP-MS.

(iii) Application of isotopic tracing to key archaeological sites in France

Combining least-destructive analysis with the baseline strontium isotope map proved to be a powerful technique and opened the doors to previously unavailable human fossil samples, such as Neanderthal teeth. The strontium isotope tracing conducted at the archaeological sites is often part of larger scale projects. The study at Moula-Guercy of two Neanderthal individuals and one Neolithic individual was part of a larger effort to investigate the chronology and mobility of this important Neanderthal site (chapter 5.2). Le Tumulus des Sables, an important Neolithic site near Bordeaux, was the focus of a new radiocarbon dating campaign combined with multi-isotope study to reconstruct mobility and diet using strontium, oxygen (James et al., 2013), nitrogen and carbon isotopes (chapter 5.3). The study at La Grotte des Perrats, chapter 5.4, is an ongoing investigation and only the strontium isotope data on human remains is presented here. The application of the strontium isotope tracing method to different geographic locations and different time periods tests the potentials and pitfalls of this method, and offers new insights into these renowned archaeological sites.

1 Fundamentals of strontium isotope tracing

1.1 Strontium isotope geochemistry

Strontium is a lithophile alkaline earth metal with a typical valence state of 2^+ and an ionic radius of 1.13 Å, which is similar to that of Ca^{2+} (0.99 Å). Sr^{2+} thus substitutes easily for Ca^{2+} in the mineral structures of plagioclase feldspar, gypsum, calcite, dolomite, aragonite and, most important in the archaeological context, biogenic apatite. Strontium is a major cation in strontianite ($SrCO_3$) and celestite ($SrSO_4$), which occur in hydrothermal deposits. As a trace element it is found in many igneous, metamorphic and sedimentary rock types, in the ocean, river and ground water, in soils, plants, and animal and human tissues. It has four naturally occurring isotopes, all of which are stable, namely ^{84}Sr (~0.56%), ^{86}Sr (~9.87%), ^{87}Sr (~7.04%) and ^{88}Sr (~82.53%), de Laeter et al. (2003). The isotopic abundances of Sr vary because of the production of radiogenic ^{87}Sr by the decay of ^{87}Rb by emission of a negative β-particle with a half-life of ~4.88 x 10^{10} years (Faure and Mensing, 2005). Fission reactions have also produced a small amount of ^{90}Sr, a short lived (half-life ~30 years) radioactive isotope, present in modern environments (Capo et al., 1998).

$$\frac{87}{37}Rb \rightarrow \frac{87}{38}Sr + \beta^- + \overline{\nu} + Q$$

β^-	beta particle
$\overline{\nu}$	antineutrino
Q	decay energy

Rubidium is an alkali metal and a large ion lithophile element that has two naturally occurring isotopes, ^{85}Rb and ^{87}Rb. It has an ionic radius of 1.48 Å, which is similar to that of potassium (1.33 Å). Therefore, Rb^+ can substitute for K^+ in all K-bearing minerals like potassium feldspar, micas, certain clay minerals, and evaporate minerals such as sylvite. Many common rock types contain significant concentrations of Rb and Sr on the order of tens to hundreds ppm. Geochemically Rb and Sr behave very differently leading to high Rb/Sr variations in magmatic, metamorphic and sedimentary environments. All of these features make the Rb-Sr decay system widely applicable for geochronology and geochemical tracing (Faure and Mensing, 2005). In the context of tracing animal and human mobility with Sr isotopes several other factors are also important. Recent studies have shown that the stable isotopes of strontium can be fractioned by physical and chemical processes (Fietzke and Eisenhauer, 2006; Halicz et al., 2008; Krabbenhöft et al., 2009; Knudson et al., 2010). When measuring $^{87}Sr/^{86}Sr$ for provenance studies these changes are corrected during the mass spectrometry measurements, by normalizing the $^{87}Sr/^{86}Sr$ ratio to a constant $^{86}Sr/^{88}Sr$ value of 0.1194. The decay of ^{87}Rb to ^{87}Sr does not influence the $^{87}Sr/^{86}Sr$ of each component in these cycles, since these processes operate on a much shorter timescales (Bentley, 2006

and references therein). Typical Sr, Ca and Rb/Sr concentrations are given in Table 1-1. For geochemical tracing the $^{87}Sr/^{86}Sr$ notation is commonly used.

An alternative notation is $\boldsymbol{\delta^{87}Sr} = \left[\frac{^{87}Sr/^{86}Sr_{\text{ Sample}}}{^{87}Sr/^{86}Sr_{\text{ Seawater}}} - \mathbf{1}\right] * \mathbf{1000}$ (Capo et al. 1998).

Table 1-1: Typical concentrations for Sr and Ca in different materials and corresponding Rb/Sr ratios. These values are a guide and specific values can vary significantly. Table adapted from Bentley, (2006) with data compiled from various sources (Burton et al., 1999; Kohn et al., 1999; Aubert et al., 2002; Bashkin and Howarth, 2002).

	Material	*Sr [ppm]*	*Ca [ppm]*	*Rb/Sr*
Geologic	Sandstone	20	40 000	3
	Low-Ca granite	100	5000	2
	Deep-sea clay	180	30 000	0.6
	Syenite	200	20 000	0.6
	Shale	300	20 000	0.5
	High-Ca granite	440	25 000	0.3
	Ultramafic rock	1	25 000	0.2
	Basalt	500	75 000	0.07
	Deep-sea carbonate	2000	300 000	0.005
	Carbonate	600	300 000	0.005
Soils	Soil minerals	10-1000	240 00	
	Labile soil minerals	0.2-20	1000	
	Soil moisture	0.001-0.07	1-4	
Water	Seawater	8	400	
	Rivers	0.006-0.8	15	
	Rain	0.001-0.4	1-100	
	Snow	0.00001-0.001	0.01-0.1	
Biological	Edible plants	1-100	3000-6000	
	Mammal bone	100-1000+	~370 000	
	Mammal enamel	50-500+	~370 000	

1.2 Strontium isotope reservoirs

This chapter describes the different $^{87}Sr/^{86}Sr$ isotope reservoirs and discusses the pathways and interactions between them. Figure 1-1 shows a sketch of the different processes that potentially influence the strontium composition before it enters the skeletal material of animals and humans.

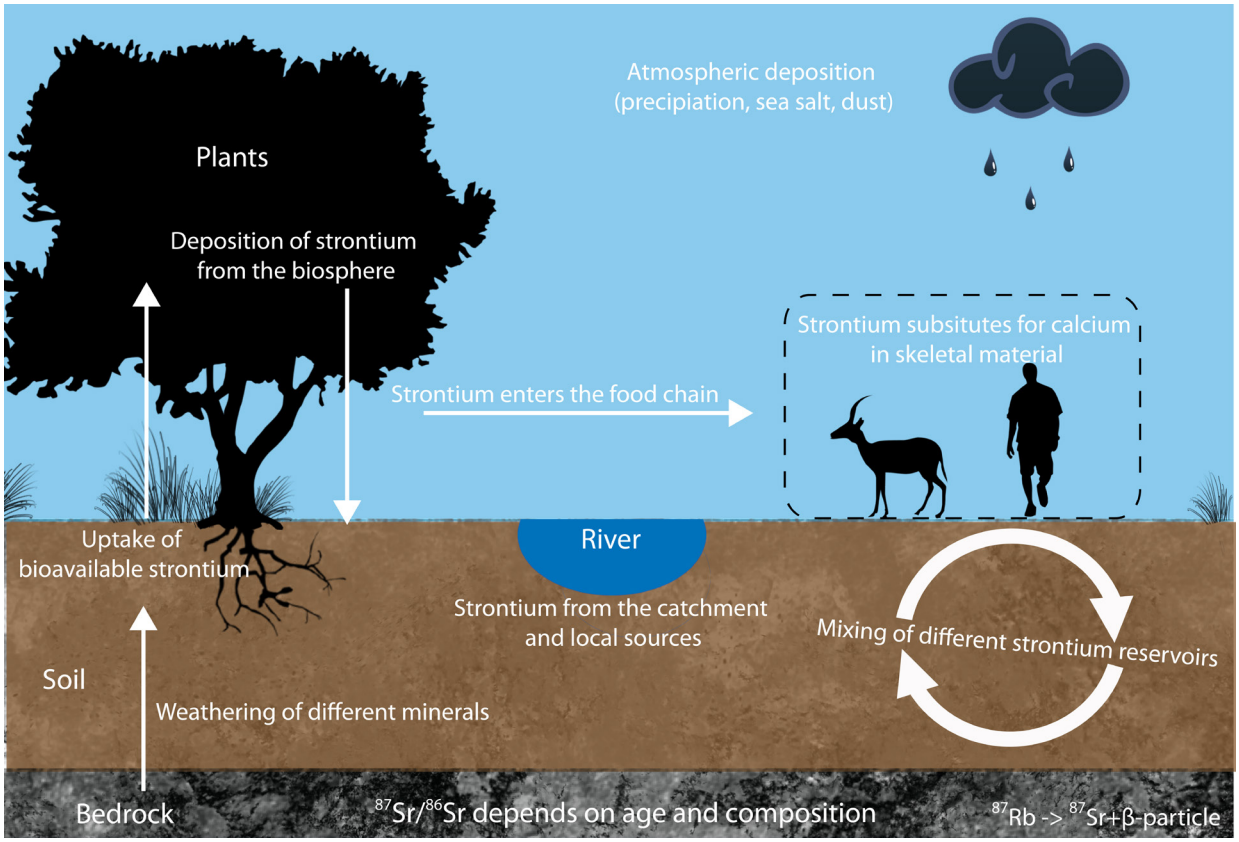

Figure 1-1: Simplified sketch of the strontium cycle showing important processes that affect the strontium composition before it reaches the skeletal material of animals and humans.

1.2.1 Bedrock

The $^{87}Sr/^{86}Sr$ isotope ratio in a rock depends on its initial $^{87}Sr/^{86}Sr$ ratio, its Rb concentration, and its age. Due to geochemical differences, the Rb/Sr ratio in rocks varies by several orders of magnitude (Table 1-1) and geologic regions can have very different ages, resulting in $^{87}Sr/^{86}Sr$ ratios that vary substantially between different geological terrains (Table 1-2). High $^{87}Sr/^{86}Sr$ ratios are usually found in very old rocks with high Rb/Sr ratios, while younger rocks with small Rb/Sr ratios have generally low $^{87}Sr/^{86}Sr$ ratios. Igneous rocks show a large range of $^{87}Sr/^{86}Sr$ isotope ratios, from low values close to the isotopic composition of the mantle in mafic volcanic rocks, to high values in old granitic rocks. Carbonaceous sedimentary rocks exhibit $^{87}Sr/^{86}Sr$ isotope ratios that reflect the isotopic composition of the liquid they formed in, while clastic sediments reflect the sources of their components and thus can be highly variable. Subsequent changes and exchange during deposition can alter their $^{87}Sr/^{86}Sr$ ratios

from their source and metamorphic rocks often show $^{87}Sr/^{86}Sr$ isotope ratios very different from their unmetamorphosed source rock.

Table 1-2: Common $^{87}Sr/^{86}Sr$ ratios for different geologic settings taken from Bentley (2006) and references therein. These numbers present a rough guide and specific settings can be highly variable.

Geologic setting	**$^{87}Sr/^{86}Sr$**
Basalts along mid oceanic ridges and volcanic islands	0.702-0.704
Oceanic island arcs formed by subduction-related magmatism	0.703-0.707
Overall continental crust	0.702-0.750
Phanerozoic marine limestone and dolomite	0.707-0.709
Old Granites	0.710-0.740>

As a first order approximation the bedrock age can be used to estimate the bioavailable $^{87}Sr/^{86}Sr$ isotope range (Beard and Johnson, 2000) of a certain region. However, this has limited application because different minerals within a single rock can have vastly different Sr concentrations and $^{87}Sr/^{86}Sr$ isotope ratios and have varying resistance to weathering. This means that the bulk $^{87}Sr/^{86}Sr$ isotope ratios can vary significantly from the $^{87}Sr/^{86}Sr$ isotope ratios of the weathered material which is transported into the soils, plants, water reservoirs, and finally into the food chain. Models using bedrock lithology, age and weathering rates have been successful in providing large scale bioavailable $^{87}Sr/^{86}Sr$ isotope ranges (Beard and Johnson, 2000; Bataille and Bowen, 2012; Bataille et al., 2012), but need to be tested to investigate their usability across different geologic and geographic terrains.

1.2.2 Surface water

Strontium concentrations in river water vary between ~0.006 to ~0.8 ppm (Capo et al., 1998). The $^{87}Sr/^{86}Sr$ isotope ratio in rivers is primarily determined by the eroding rocks in the catchment area, augmented by atmospheric deposition for example from precipitation. Tectonic activity and climate affect both the intensity of weathering processes as well as the type of rock subject to weathering and thus can have a strong effect on the amount and isotopic composition of the Sr in rivers and the ocean (Capo et al., 1998). Generally speaking, elevated areas are eroded more strongly than low plains and therefore contribute more to the sediments in the river. At high elevations the $^{87}Sr/^{86}Sr$ signal in river water can be closely correlated to the underlying bedrock (e.g., Hoogewerff et al., 2001; Aubert et al., 2002). At lower elevations, this close correlation may be lost, due to the mixture of strontium from different bedrocks and other reservoirs. River water and floodplain sediments deposited by rivers can thus introduce a significantly different $^{87}Sr/^{86}Sr$ isotope range, possibly related to a distant upper catchment to an area. This is of particular importance for archaeological provenance studies as floodplains can represent an important food and thus strontium source for animals and humans. Discharge variation of a river can also have an effect on the Sr concentration and $^{87}Sr/^{86}Sr$ isotope ratio. This means, that depending on the hydrological and moisture conditions of the catchment different Sr

isotopes will be measured for the same river on a homogenous bedrock (Aubert et al., 2002). $^{87}Sr/^{86}Sr$ isotope ratios from lake water will reflect the mixture of incoming rivers, precipitation, and potential equilibration with the lake bed sediments (Hodell et al., 2004). Frei and Frei (2011) studied surface waters in Denmark and found a $^{87}Sr/^{86}Sr$ isotope distribution related to two major sources, one being Sr from carbonaceous sediments and one from water that shows a radiogenic component due to the interaction of precipitation with Pleistocene glaciogenic soils and Precambrian granitoids. However, they also observe an offset between the $^{87}Sr/^{86}Sr$ isotope ratios measured in surface water compared to soil and snail shells, indicating that the topsoil might have a relatively lower $^{87}Sr/^{86}Sr$ isotope ratio, possibly due to the downward movement of Sr into the water tables.

1.2.3 Groundwater

The $^{87}Sr/^{86}Sr$ isotope ratios in groundwater are controlled by the process of dissolution and reprecipitation of Sr from the minerals it comes into contact with (Åberg, 1995) and in many cases reflect the underlying geology more closely than surface waters. In evaporates and marine limestones, the $^{87}Sr/^{86}Sr$ isotope ratio will reflect the isotopic composition of the rocks closely, due to their simple geochemical composition and high solubility of their main minerals. On the other hand, groundwater aquifers in regions with clastic sediments, magmatic, and metamorphic rocks, will show the $^{87}Sr/^{86}Sr$ isotope ratio of the easily soluble minerals and differ significantly from the bulk host rock (Blum et al., 1993; Åberg, 1995; Négrel et al., 2001; Jacobson et al., 2002; Montgomery et al., 2006). Large scale studies on natural mineral waters have shown a good correlation between the aquifer geology and variations in strontium isotope ratios in the water (Montgomery et al., 2006; Voerkelius et al., 2010). However, the mixing of different ground water sources, differences in flow rates, and the possibility of contamination by anthropogenic activities, such as agriculture, can have significant influences on the strontium isotope ratio in water samples and complicate the correlation with aquifer geology.

1.2.4 Seawater

The Sr concentration in the oceans is relatively high with 8100 µg/l compared to for example Rb (120 µg/l) and Pb (0.03µg/l) and about 100 times that of average river water (~0.07 ppm). At depths of >1500 m the Sr concentration is mainly a function of salinity. Both salinity and Sr concentration in surface water decrease regionally in response to the dilution of the seawater by meteoric water, river water and glacial melt water (Faure and Mensing, 2005). In times of evaporation or formation of sea ice, salinity and Sr concentration will increase. The $^{87}Sr/^{86}Sr$ isotope ratio at present is 0.70918 (McArthur et al., 2001) and is homogenous throughout the ocean. The homogenous distribution of $^{87}Sr/^{86}Sr$ isotope ratios in the ocean is caused by the much shorter turnover time of the ocean ~10^3a, compared to the long residence time of Sr in seawater ~10^6a (Stosch, 2004). The $^{87}Sr/^{86}Sr$ isotope ratio of the ocean is driven by the average of the weathered continental crust, the amount of volcanic activity, and the influence from dissolution of marine carbonates on the continents and continental shelfs (Stosch, 2004; Faure and Mensing, 2005). The Sr isotopic composition of the oceans has changed significantly

over the history of the Earth depending on which of these three factors was dominating (Burke et al., 1982; Stosch, 2004). Figure 1-2 shows the evolution of Sr isotope ratios in the ocean for the geologic history of the Earth.

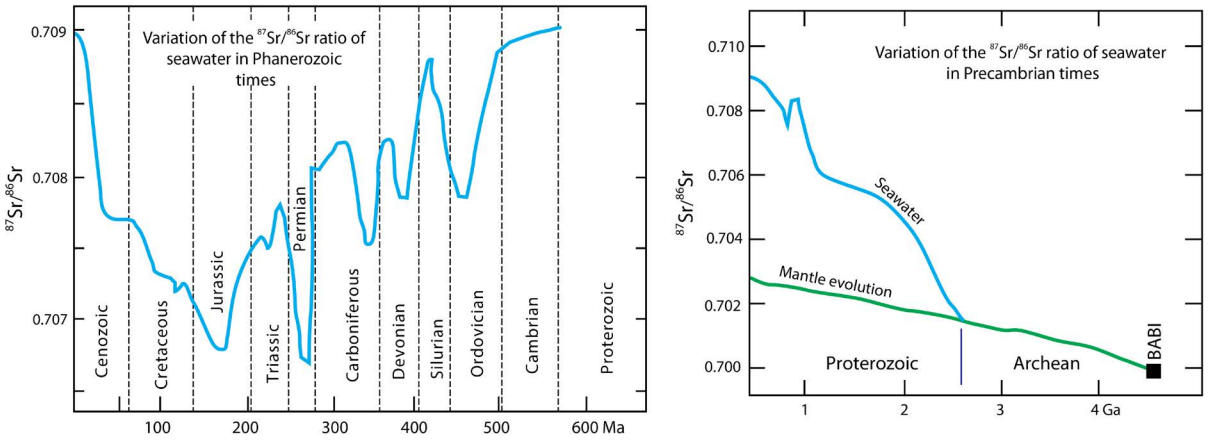

Figure 1-2: Variation of the $^{87}Sr/^{86}Sr$ ratio of seawater in Phanerozoic and Precambrian times. BABI is the Basaltic Achondrite Best Initial. Modified from Stosch (1999). Data for the strontium isotope composition of seawater through time from Burke et al., (1982).

During the Phanerozoic, $^{87}Sr/^{86}Sr$ varied between 0.707-0.709. The increase since the Middle Jurassic can be attributed to an increase in continental weathering, caused by the young orogenies. The same is proposed for the increase at the Ordovician-Silurian boundary (Caledonian orogeny) and Cambrian period (Pan-African orogeny). These time-dependent variations provide the possibility for global correlation of marine sediments. The rise of $^{87}Sr/^{86}Sr$ over the last 2 Ma is primarily due to the change of Sr entering the ocean through the rivers connected to an increase of overall chemical weathering of the continents. Data for the Precambrian is sparse since carbonate outcrops for that time are rare and have been altered geochemically. It seems that starting in the Proterozoic the Sr isotope signal of the ocean diverged from the mantel signal (Stosch, 2004). This would indicate that weathering of old continental crust did not play a major role in the Archean, compared to volcanism and weathering of young crust. Overall, the Sr isotopic curve of the ocean seems to be a time-delayed indicator for large scale tectonics. It may thus be used to date sedimentary rocks of marine origin. In turn this correlation also can be used to predict the $^{87}Sr/^{86}Sr$ isotope ratio of marine origin and known age (Hodell et al., 2004). In archaeological studies this can be used to identify the source of shell artefacts (e.g., Shackleton and Elderfield, 1990; Vanhaeren et al., 2004). However, differences between the predicted $^{87}Sr/^{86}Sr$ from the seawater curve compared to the sediments have been observed, possibly due to the presence of Rb-rich clays as well as additional atmospheric inputs and secondary modification (Hodell et al., 2004; Bentley, 2006).

1.2.5 Soils and regolith

Strontium occurs in all parts of the soil, including the bioavailable fraction, carbonate fraction and silicate fraction. The bioavailable Sr fraction is the part of the Sr in the soil, that is available for uptake to plants and only represents a part of the total strontium (Capo et al., 1998; Sillen et al., 1998; Price et al., 2002). Typical concentrations of bioavailable Sr in soil range from ~0.2 to ~20 ppm (Elias et al., 1982; Miller et al., 1993; Capo et al., 1998). Usually, mineral weathering from bedrock dominates the Sr in the soils, but additional input comes from river and ground water, atmospheric deposition such as dust, seaspray, and precipitation (Bentley, 2006; Evans et al., 2009, 2010; Slovak and Paytan, 2012). Areas that are not extremely weathered or under high annual levels of precipitation show $^{87}Sr/^{86}Sr$ isotope ratios dominated by bedrock weathering (Capo et al., 1998; Sillen et al., 1998; Bern et al., 2005; Bentley, 2006), while deeply weathered regions or areas under high annual rainfall or atmospheric deposition can be significantly altered towards the external $^{87}Sr/^{86}Sr$ ratio. The use of soil leachates to determine the local bioavailable Sr isotope ratio has shown varying degrees of success in different regions (Sillen et al., 1998; Price et al., 2002; Hodell et al., 2004; Bentley, 2006; Maurer et al., 2012; Slovak and Paytan, 2012). Some areas can be relatively homogenous while geologically complex regions can have high local variability in their $^{87}Sr/^{86}Sr$ values (Sillen et al., 1998; Hodell et al., 2004). A good example of low local variability is the study by Hodell et al. (2004) on the Yucatan Peninsula. They were able to distinguish five $^{87}Sr/^{86}Sr$ isotope regions, representing large geographic distances. A study by Sillen et al. (1998) in South Africa, on the other hand, found high variability of $^{87}Sr/^{86}Sr$ values ranging from 0.718 in soils on a shale to 0.900 in soils on an Archean granite within a 15 km radius.

The strontium isotope ratio in soils is also a function of soil depth, with increasing soil depth bedrock weathering becomes more important relative to atmospheric influences (Probst et al., 2000; Prohaska et al., 2005). A study by Prohaska et al. (2005) in the Günser Mountains, Eastern Austria found that the Sr isotope signature in the first 10 cm of soil was dominated by atmospherically deposited dust. They found a gradual increase in the Sr isotope ratio down to 120 cm, reflecting a mixture of the underlying geology and recently deposited Sr from dust. The depth to which the soil is influenced by Sr from atmospheric deposition will vary greatly depending on the soil and the local climatological and hydrological conditions. Thus, the Sr isotopic composition in soil is the result of dynamic processes, that may vary spatially and through time as the surrounding conditions change.

1.2.6 Plants

Strontium is taken up by plants from the soil solution and the soil exchange complex (Capo et al., 1998). In general, plant samples have shown a good comparability with other direct indicators of bioavailable Sr like snail shells, caterpillars, and rodent teeth (Blum et al., 2000; Laffoon et al., 2012). The $^{87}Sr/^{86}Sr$ ratio in plants is influenced by the depth of the roots, the source water, and the addition of strontium from biomass and atmospheric deposition (Graustein and Armstrong, 1983; Gosz and Moore, 1989; Bentley, 2006). Atmospheric deposition and the addition of Sr from biomass is especially important for

the upper soil layers and as such affects plants with shallow roots the most. Thus, while no fractionation of $^{87}Sr/^{86}Sr$ isotope ratios occurs within plants, differences in plant anatomy and varying contributions of strontium from different reservoirs can lead to significantly different $^{87}Sr/^{86}Sr$ isotope ratios within a single plant and between different plant species in the same area (Graustein and Armstrong, 1983; Reynolds et al., 2012). Shallow rooted plants should more closely reflect the $^{87}Sr/^{86}Sr$ isotope ratio of the topsoil then plant species with deeper roots that might sample deeper soil horizons with different $^{87}Sr/^{86}Sr$ isotope ratios (Poszwa et al., 2002, 2004; Drouet et al., 2007; Maurer et al., 2012).

1.2.7 Atmospheric deposition

Atmospheric deposition of strontium through processes such as precipitation, seaspray, and dust can have a significant influence on the strontium isotopic composition of a region. The effect atmospheric deposition of Sr will have on the strontium isotopic composition of a region primarily depends on the concentrations and differences in $^{87}Sr/^{86}Sr$ isotope ratios of the different end members. In general, the lower total the Sr concentration in the underlying lithological material, the higher the possible influence of atmospheric influences on the strontium isotope composition of a region. Evaporated seawater starts with a low strontium concentration and $^{87}Sr/^{86}Sr$ isotope ratio close to modern seawater 0.70918. The strontium concentration and isotopic ratio is then changed by the addition of terrestrial dust and aerosols (Miller et al., 1993; Åberg, 1995; Capo et al., 1998; Faure and Mensing, 2005). Rainwater $^{87}Sr/^{86}Sr$ isotope ratios measured in France range from 0.709-0.713 (Négrel and Roy, 1998; Probst et al., 2000; Négrel et al., 2001, 2007) show that rainwater $^{87}Sr/^{86}Sr$ can be highly variable. Due to the generally low Sr concentration in precipitation in comparison to most soils and plants, only areas with high annual precipitation are expected to show a significant effect. The western part of Britain exhibits high annual precipitation in excess of 2000 mm/a, which results in a pronounced influence on the $^{87}Sr/^{86}Sr$ isotope ratio in the biosphere (Evans et al., 2009, 2010). The island of Bornholm, Denmark, on the other hand, shows low annual precipitation of around ~550 mm, which has only minute effects on the $^{87}Sr/^{86}Sr$ isotope ratio (Frei and Frei, 2013). Predicting the Sr isotope signal of rainfall for a certain area is not simple due to changes in the different sources and mixing of strontium with time. Sr from rainwater, for example in the Massif Central, shows $^{87}Sr/^{86}Sr$ values that vary from 0.7090 to 0.7106 (Négrel et al., 2001). Seaspray can also have a significant effect on the bioavailable $^{87}Sr/^{86}Sr$ isotope ratio in coastal areas (Whipkey et al., 2000; Montgomery et al., 2006; Evans et al., 2009; Frei and Frei, 2013), causing a shift towards marine isotope values. Seaspray affects coastal areas more strongly and the effect decreases further inland. Studies in the Hawaiian rainforest have shown that atmospheric deposition of marine strontium can dominate the $^{87}Sr/^{86}Sr$ ratios of plants on highly weathered surfaces (Chadwick et al., 1999) and even on fresher surfaces may form a significant contribution (Vitousek et al., 1999). Terrestrial dust can also be a major source of strontium in the environment, especially in arid regions (Graustein and Armstrong, 1983; Capo and Chadwick, 1999; Benson et al., 2008). A study on basalt flows in New Mexico observed a pattern where the $^{87}Sr/^{86}Sr$ ratios on young basalt flows was dominated by atmospheric deposition, while older flows were more influenced by bedrock weathering (Reynolds

et al., 2012). Saharan dust from Africa is transported across the Atlantic and also north into the Mediterranean and Europe (Goudie and Middleton, 2001; Engelstaedter et al., 2006; Israelevich et al., 2012). Dust from the Sahara region of Africa is considered a significant component of the biogeochemical budget in Europe, and it might have been of even greater importance during the last glacial period. The strontium concentration and isotopic composition of dust may be highly variable since it can come from distant and from local sources and these sources change over time. Atmospheric deposition of strontium from precipitation, seaspray, and dust can have a significant contribution to the $^{87}Sr/^{86}Sr$ isotope ratios of plants and soils in a given area and thus need to be considered.

1.2.8 Exogenic surface deposits

Regions with exogenic surface deposits (loess, peat, glacial deposits), may show bioavailable $^{87}Sr/^{86}Sr$ isotope ratios that are partially disconnected from the underlying geology. Loess can be locally derived or come from far distances, which makes it difficult to predict, whether a patch of loess has a local or non-local strontium isotope signature (Chadwick et al., 1999). Large areas of central Europe are covered by loess influencing the $^{87}Sr/^{86}Sr$ isotope ratio. Peat deposits are thought to mute the $^{87}Sr/^{86}Sr$ isotope ratio from the bedrock geology, due to their high rainwater content (Evans et al., 2009). Glacial deposits can contain material moved over vast distances and this material can in certain areas dominate the bioavailable $^{87}Sr/^{86}Sr$ isotope ratio. However, in some areas the till may contain exotic boulders while the surrounding matrix is of local origin (Evans et al., 2010). In addition, the timing and occurrence of exogenous surface deposits may be disconnected from the archaeological material in question.

1.2.9 Anthropogenic influences

Strontium in the environment can be heavily influenced by anthropogenic activity. Artificial fertilizers are commonly used in Europe and may contribute a significant component to the Sr content in local surface water, groundwater, soil, and plant material. Only very restricted information is available on the Sr concentration and isotopic composition of artificial fertilizers. A comprehensive study of fertilizers in Spain (Vitòria et al., 2004) found that there is a large variation in $^{87}Sr/^{86}Sr$ isotope ratios for different fertilizers covering the full range found in rocks on the Earth. Most fertilizers showed $^{87}Sr/^{86}Sr$ isotope ratios around 0.708-0.709 thus overlapping with modern seawater compositions. Other anthropogenic sources are urban and industrial wastes ~0.708 and detergents ~0.709-0.710 (Vitòria et al., 2004). A study on Danish surface waters found that unrealistically high amounts of fertilizer input would be needed to change their strontium isotopic composition (Frei and Frei, 2011). Varying degrees of fertilizer influence have been observed suggesting that while bedrock weathering is the dominant process that fertilizers can have a significant effect $^{87}Sr/^{86}Sr$ isotope ratios in surface water (Négrel and Deschamps, 1996; Hosono et al., 2007). One important aspect is that while for example the Ca, Na, Mg, and K concentration in a watershed in the Massif Central was heavily influenced by fertilizer input (~40-80%), Sr was still largely derived from the bedrock with only a ~7% influence from the fertilizer (Négrel and Deschamps, 1996). This shows that even in areas with potentially high fertilizer application, strontium

concentration and $^{87}Sr/^{86}Sr$ isotope ratio in the environment and in the applied fertilizer need to be considered before the influence on soil and plant values can be evaluated.

1.3 Strontium isotopes in skeletal remains

1.3.1 Biopurification

Calcium plays a vital role in many biological processes and strontium can substitute for calcium due to its similar atomic properties. Along biochemical pathways non-essential elements, such as strontium, are preferentially removed, in comparison to Ca, leading to a decrease of the Sr/Ca ratio with each progressive step. This process is called biopurification and it has been observed that the Sr/Ca ratio decreases per trophic level in terrestrial food chains (Elias et al., 1982; Blum et al., 2000). Many plants do not discriminate strongly between strontium and calcium and thus exhibit relatively high Sr/Ca ratios. Sr/Ca ratio in herbivores is lower than that of their average plant die, and carnivores would in turn exhibit even lower Sr/Ca ratios. This effect can be used to constrain the composition of prehistoric diets, however, this approach is limited by the large geographic and individual variability of these ratios (Schoeninger, 1985; Sillen, 1992). The variability of Sr/Ca ratios is also affected by biopurification and decreases with each step in the food chain. This reduction in variability also applies to $^{87}Sr/^{86}Sr$ isotope ratios. Animal groups higher in the food chain thus exhibit a reduced variability in the standard deviation of their $^{87}Sr/^{86}Sr$ ratios compared to their feeding source (Blum et al., 2000; Price et al., 2002). The biopurification effect is not identical for different species and dietary patterns. Animals with a large migratory range across geologically vastly different terrains are expected to show a relatively large variation of their $^{87}Sr/^{86}Sr$ isotope ratios, while local animals with small migratory ranges show low variations and very low standard deviations in their $^{87}Sr/^{86}Sr$ isotope ratios (Price et al., 2002; Bentley et al., 2004; Bentley, 2006).

1.3.2 Tooth formation

Human teeth consist of the hard inert enamel, supported by the less mineralised dentine and pulp (Figure 1-3) and attached to the jaw by the alveolar bone, periodontal ligament, and cementum (Nanci, 2012). Tooth formation is a complex process beginning *in utero* and depending on the tooth takes years to complete (Ash and Nelson, 2003; Simmons et al., 2013). The primary dentition, which forms to accommodate for the small initial size of the jaw is later replaced by the permanent dentition, normally before the age of 12 (Ash and Nelson, 2003). Teeth consist of bioapatite, which is similar to hydroxyapatite, but is affected by numerous substitutions of the Ca, PO_4, and OH groups in the mineral structure with secondary groups, such as Sr, Mg, and Ba. These secondary groups are under biological selection and thus vary in concentration based on changes in trophic levels, between different species, and with the element abundance in the underlying substrate (Burton and Wright, 1995; Elliott, 2002). Enamel formation is called Amelogenesis and is a multi-step process. After the induction stage the first enamel forms in the secretion stage as a partially crystallised (~30%) mineral by the release of enamel proteins from ameloblasts. Enamel first appears early during pregnancy at the cusps of the teeth and

then grows outwards from the center of the tooth. During the maturation stage the organic matrix breaks down and the enamel layer becomes fully mineralised (Nanci, 2012). Mature tooth enamel consists of ~96 wt% Ca phosphate with a composition of $Ca_{4.5}$ $[(PO_4)_{2.7}(HPO_4)_{0.2}(CO_3)_{0.3}]$ $(OH_{0.5})$. The ameloblasts are lost during the maturation stage, meaning that enamel cannot replace or regenerate itself (Nanci, 2012). Dentine formation called dentinogenesis, is controlled by odontoblasts and occurs before the formation of enamel. Dentine forms the bulk of the tooth and is used to support the more rigid and brittle enamel. Like enamel it consists of bioapatite but it includes larger amounts of organic compounds, including collagen. Related to their timing of formation different types of dentine can be distinguished. Mantle and primary dentine form during the tooth formation process. Secondary dentine only starts to form after the root formation has been completed and forms at a much slower rate and may continue throughout the lifetime of the individual do the presence of the odontoblasts (Nanci, 2012). Finally, tertiary dentine is deposited at specific sites in the tooth as response to injury. The central chamber within the tooth is filled with pulp, a soft tissue related to dentine but often lost in tooth remains leaving a characteristic cavity.

Strontium is taken into the body through food and water and serves no metabolic function and substitutes for calcium. The Sr isotopic ratio ($^{87}Sr/^{86}Sr$) measured in skeletal material thus reflects the concentration-weighted average of dietary Sr, that was consumed while the skeletal tissue was formed (Beard and Johnson, 2000; Bentley, 2006). After formation, tooth enamel is closed to chemical exchange and thus forms an archive of the $^{87}Sr/^{86}Sr$ isotope ratios acquired during formation. Intra tooth isotopic variations are related to the sequential mineralisation and maturation of the tooth. Measurements along the growth axis of the tooth enamel in large mammals have connected the intra tooth isotopic variations to mobility (Balasse et al., 2002; Britton et al., 2009). However, while the timing of tooth development in humans is well constrained, the mineralisation and maturation times and rates of tooth enamel are not well understood. Intra tooth isotopic studies in human teeth are possible (Eerkens et al., 2011; Beaumont et al., 2013), but complicated by the fact that incremental features (e.g. Retzius lines) may not reflect the pattern of later mineralisation and maturation during which the minerals are incorporated into the enamel apatite (Suga, 1989). This hinders the development of a time sensitive record from human teeth for a direct comparison to mobility patterns (Balasse et al., 2002; Viner et al., 2010). Recent studies have shown that different tooth types show variability in their maturation patters but that it may be possible to gain time sensitive information when choosing the sampling path across the tooth carefully (Montgomery et al., 2012). Inter isotopic analysis of human teeth, measuring multiple teeth with different formation and maturation times from the same individual, can also be used to extend the temporal information (Poulson et al., 2013; Eerkens et al., 2014).

In contrast to teeth, bones remodel throughout life and therefore their strontium isotope composition reflect more recent dietary intake (Sealy et al., 1995). Different individual bones have different rates of turnover, depending on their ratio of active osteoclasts, which precipitate hydroxyapatite, and

osteoblasts, which dissolve hydroxyapatite (Price et al., 2002 and references therein). Bone turnover rates also vary between different individuals including their age and diet (Cox and Sealy, 1997; Hedges and Reynard, 2007) complicating a direct inference of timing. Generally, it can be assumed that the bones will approach the local Sr isotope signature, depending on their turnover rate and the time the individual spends in the specific geologic region.

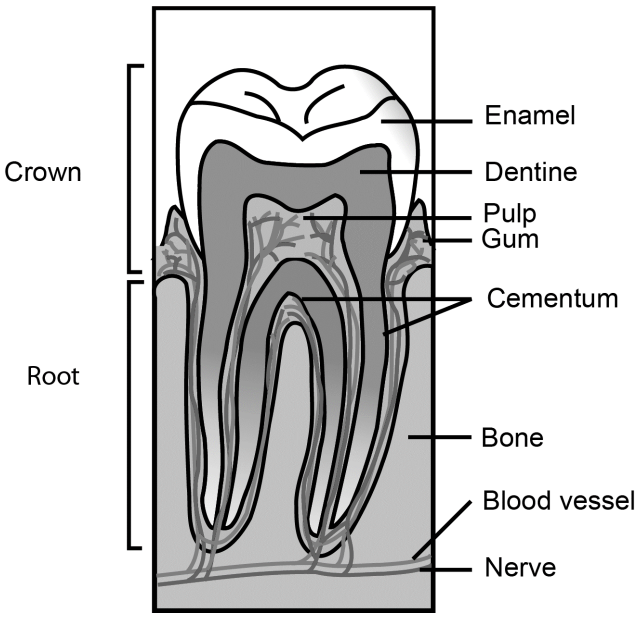

Figure 1-3: The anatomy of the tooth (Sam Fentress, Wikimedia Commons).

1.3.3 Diagenesis

Diagenesis is one of the major obstacles for isotopic studies in archaeology. Skeletal material is affected by both physical and chemical changes, potentially leading to the loss of the original $^{87}Sr/^{86}Sr$ isotope ratio. The degree of diagenetic overprint depends on a large number of factors, including the length of burial, the surrounding environment and the kind of skeletal material (Lee-Thorp, 2002, 2008; Hoppe et al., 2003) and may vary from sample to sample and within different domains of the same sample. Bone material is prone to local contamination due to its high content of organic matter (~30%), high porosity and poorly crystalline structure (Slovak and Paytan, 2011 and references therein). Similar to bone, dentine is easily altered because it has pores ~1 µm, which are larger than its phosphate crystals (Kohn et al., 1999), allowing contaminants from soil and water to enter into the pore space. In addition, dissolution and recrystallization of bone and dentine can occur (Koch et al., 1997). Both of these processes may alter element concentrations and the overall Sr isotope composition of the sample, rendering it unsuitable to determine the original isotopic signature. Tooth enamel has phosphate crystals above 1 µm, a compact structure and little pore space (Hillson, 2005; Nanci, 2012). It is thus much denser, harder and more inert than bone and dentine and consequently much more resistant towards post-burial diagenesis and often retains the original strontium isotopic signature (Budd et al., 2000; Hoppe et al., 2003; Trickett et al., 2003; Bentley, 2006; Slovak and Paytan, 2012).

For the investigation of diagenetic changes in tooth enamel, a variety of methods have been used, including infra-red (IR) spectroscopy (Sponheimer and Lee-Thorp, 1999) and cathodoluminescence (CL) imaging (Schoeninger et al., 2003). Nearly all of these studies have employed bulk analysis with the aim of testing cleaning techniques (Price et al., 1992; Hoppe et al., 2003; Trickett et al., 2003) or coarse sub-sampling using mineralogical information (e.g. by CL) as a guide. While these approaches provide some information as to the mineralogical state of the hydroxyapatite or functional groups within this mineral (such as hydroxyl or phosphate sites), any conclusions about sample integrity for isotopic analysis are derived from conjecture. Mapping of element distributions has been used for the identification of the degree of diagenesis in bones (Trueman et al., 2008; Koenig et al., 2009; Fernandes et al., 2013). In addition, a few studies have investigated the mechanisms of diagenetic alteration using high resolution elemental or isotopic analysis (Kohn et al., 1999; Jacques et al., 2008; Martin et al., 2008; McCormack et al., 2015). Systematic mapping of U and Th concentrations can help identify domains within a tooth that are diagenetically overprinted. The basic principle is that modern teeth and bones contain only trace amounts of uranium (low ppb range) and thorium and thus their presence in archaeological skeletal remains can be used to identify zones of diagenetic overprinting (Budd et al., 2000; Eggins et al., 2003; Rainer Grün et al., 2008; Koenig et al., 2009; Hinz and Kohn, 2010; Boel, 2011).

1.4 Tracing mobility

In order to identify and trace human mobility across the landscape, the $^{87}Sr/^{86}Sr$ isotope ratio of the skeletal material is compared to the $^{87}Sr/^{86}Sr$ isotope range of the target areas. The method was first introduced to archaeological research by Ericson (1985), and since then has been rapidly developed and applied in numerous studies that showcased the huge potential, but also the limitations and pitfalls of the method (reviewed by Bentley, 2006; Slovak and Paytan, 2011). The ability to trace mobility is directly related to how tightly the isotope ranges of the different target regions can be constrained. This in turn is related to the internal isotopic variability of the local geology and the mixing with external Sr inputs. A multitude of different sample types can be used to constrain the strontium isotope range of different regions, each having its advantages and drawbacks, as summarised in Table 1-3. The different parts of a single individual thus archive a detailed record of the strontium isotopic composition of dietary intake over different timescales and potentially allow for the detailed reconstruction of past mobility. Teeth reflect the childhood signal, while bones average the dietary strontium isotope composition over the last years of an individual's life, depending on their turnover rate. Soft tissues, hair, and nails also contain strontium and are used for isotope tracing in forensic cases to investigate mobility over the last few weeks to years. However, at most archaeological sites they are not preserved.

Several assumptions have to be met for the archaeological interpretation of the data in terms of mobility. One assumption is that the people ate local food. Even small amounts of Sr rich non local food, like dairy products, fish and sea salt can significantly alter the $^{87}Sr/^{86}Sr$ isotope ratio of the skeletal remains. The definition of isotopically local simply means that an individual has an isotope range that is similar or overlaps with the isotope range of the target area. The Sr isotope values obtained from skeletal material are not necessarily directly related to a single defined residence area e.g., if the individual was highly mobile it will represent an average of multiple regions. A non-local $^{87}Sr/^{86}Sr$ ratio in tooth enamel means that the individual ate non-local food averaged over the tooth growth period. In a simple case this may indicate mobility from one place to another, but it could also be caused by movement over a wide area. A fundamental limitation is that strontium isotope ratios are often not unique to a single area, but can overlap with other, sometimes distant, regions. In general, the most robust case for the use of isotopes to trace mobility is when a specific geographic question is asked, because this minimizes the chance of overlap between the target areas. However, often the data do not fall neatly into two different groups, but form a range of values with no clear identifiable break. This creates a challenge to determine cut-off values between local and non-local data. Several studies (Grupe et al., 1997; Bentley et al., 2004) suggested the use of statistical methods (e.g. 2 standard deviation) to distinguish between local and non-local individuals. However, this is not directly transferable because the cut-off will be specific for a certain the region with its different geologic units and the archaeological population and culture in question (Price et al., 2002; Evans and Tatham, 2004; Montgomery et al., 2007). The internal structure of the strontium isotope data of a population may offer additional information such as identifying simple

two end member mixing relationships (e.g. bedrock and precipitation) or a diffuse cloud of data, which would suggest multiple strontium end members (Montgomery et al., 2007).

This is further complicated by the fact that an individual will be subject to changing sources of strontium as it moves across the landscape. In order to start to untangle all these different factors, we need to take the different areas and isotope reservoirs into account and use detailed baseline maps to define the internal variability of the different target regions. Based on this knowledge the strontium isotopic variability in the human dataset can be explored and appropriate cut-off values can be chosen based on the archaeological setting such as food sourcing practices. In some cases, even small variations in strontium isotope ratios may indicate significant movement, such as when the region and the population exhibit very homogenous strontium isotope ratios and there are some outliers. In other cases, highly variable strontium isotope ratios within a population may simply reflect the complex geologic substrate of the site and its immediate surrounding area. Strontium isotope tracing can provide one line of evidence to investigate past mobility. Additional lines of evidence such as geochemical methods, like element concentrations and other isotope systems are essential to gain a better understanding of past mobility. Element concentrations can help to constrain possible atmospheric and anthropogenic influences. $\delta^{13}C$ and $\delta^{15}N$ can be used to identify dietary bias, e.g., marine vs. terrestrial foods. Other isotope systems like $\delta^{18}O$ and $^{207}Pb/^{206}Pb$, $^{208}Pb/^{206}Pb$ add another layer of spatially variable independent data to the interpretation, and when overlayed with each other greatly enhance our ability to characterise different residence regions and mobility across the landscape.

Table 1-3: Overview of sample types and their characteristics for strontium isotope tracing.

Bedrock Geology	The clear advantage of using the bedrock geology to predict the bioavailable $^{87}Sr/^{86}Sr$ isotope range is that depending on the quality of the available geologic maps and already available samples no additional sampling is needed and that this method it is applicable on a global scale. However, relating the bedrock signal to the bioavailable Sr in the surrounding environment requires complex mixing models which need to be tested with direct sampling to evaluate their predictive capabilities for different geologic units and different climatic and environmental conditions. Exogenic surface deposits (loess, glacial deposits), can disconnect the $^{87}Sr/^{86}Sr$ range of the region from the underlying geology.
Water	Overall, surface waters provide a good estimate of the average $^{87}Sr/^{86}Sr$ isotope ratios over their catchment area. A good correlation exists between the aquifer rocks and the strontium isotope ratios in ground water. Problems with surface and ground water samples can come from pollution, precipitation and flow rate effects. Due to the averaging effect these samples do not allow us to establish the $^{87}Sr/^{86}Sr$ isotope ratios of the individual geologic units. Since water is an important part of the dietary strontium intake, and is often sourced locally, water samples can provide a powerful tool to establish local strontium isotope ranges.

Soils and Plants	Soils and plants average Sr over a small area and are thus good candidates to establish $^{87}Sr/^{86}Sr$ isotope ratios for individual geologic units. The use of soil leachates to determine the local bioavailable Sr isotope ratio has shown varying degrees of success in different regions. Soil leachates are only an estimate of the bioavailable Sr pool, whereas plant samples on the other hand are a direct biosphere measurement. Plant samples are thus generally considered to be a better sample choice across different environments and can also offer insights into the variation of the Sr isotope ratio with depth, as different plant samples source Sr from different soil depths, depending on their root depth. Atmospheric inputs (precipitation, seaspray, dust) and anthropogenic inputs (fertilizers, land use) can influence both soil and plant samples. Both soil and plant samples are readily available in most areas and easy to collect, store, and transport.
Archaeological and modern	Archaeological and modern fauna samples are good indicators of the $^{87}Sr/^{86}Sr$ isotope range over their feeding area. In case of snails or small mammals this feeding area can be well constrained and thus these samples offer a high spatial resolution and direct measurement of the $^{87}Sr/^{86}Sr$ isotope range for a specific location. For animals with continuously growing teeth it can be possible to investigate seasonal patterns. Disadvantages for the use of archaeological fauna is it's restricted availably to excavation sites and their possible influence by diagenesis. Modern fauna is more easily found, but is possibly influenced by non-local food sources and fertilizers. Domestic animals are not necessarily of local origin and thus cannot be used to determine the local strontium isotope range.
Archaeological and modern humans	Tooth enamel contains the Sr isotope signature acquired during infancy and childhood and is most resistant to weathering and diagenetic overprint. It thus represents the best choice of sample to identify the original Sr isotope signature of an individual, while dentine is often diagenetically altered towards the local strontium isotope signature. Different bones have different rates of turnover and it can be possible to gain a very high temporal resolution of mobility for an individual. However, bones are also prone to contamination and thus often not that useful in archaeological cases. Dentine and bones can however be used to gain some insights into the Sr isotope signature of the archaeological site. In addition, if different isotopic values are found between dentine and enamel this can directly be used to identify non-local food sources. Soft tissues, hair and nails are potentially useful to investigate mobility of the last few weeks and years of an individual's life, but are often not preserved in archaeological sites. To identify complex mobility patterns across different regions multiple samples of teeth, bones, and soft tissues, all representing different formation times can be used. Using the skeletal remains of known local human fossils can be a very effective measure to determine the strontium isotope range, however these are often not available.

2 The IRHUM (Isotopic Reconstruction of Human Migration) database

This chapter has been published in the Journal of Earth System Science Data.

M. Willmes, L. McMorrow, L. Kinsley, R. Armstrong, M. Aubert, S. Eggins, C. Falguères, B. Maureille, I. Moffat, R. Grün (2014), The IRHUM (Isotopic Reconstruction of Human Migration) database – bioavailable strontium isotope ratios for geochemical fingerprinting in France. Earth System Science Data 6, 117–122. doi: 10.5194/essd-6-117-2014

The author's contribution to the publication is as follows: The author led the sampling campaigns (2012-2014), conducted the analysis in cooperation with L. McMorrow, and performed the evaluation of the data. The database and spatial infrastructure was implemented by the author. The article was written by the author with helpful comments from all co-authors. Additional unpublished information about the laboratory and analytical methods, including updated blank and standard values, can be found in the appendix 8.1.

Abstract

Strontium isotope ratios ($^{87}Sr/^{86}Sr$) are a key geochemical tracer used in a wide range of fields including archaeology, ecology, food and forensic sciences. These applications are based on the principle that the Sr isotopic ratios of natural materials reflect the sources of strontium available during their formation. A major constraint for current studies is the lack of robust reference maps to evaluate the source of strontium isotope ratios measured in the samples. Here we provide a new dataset of bioavailable Sr isotope ratios for the major geologic units of France, based on plant and soil samples (Pangaea data repository doi:10.1594/PANGAEA.819142). The IRHUM (Isotopic Reconstruction of Human Migration) database is a web platform to access, explore and map our dataset. The database provides the spatial context and metadata for each sample, allowing the user to evaluate the suitability of the sample for their specific study. In addition, it allows users to upload and share their own datasets and data products, which will enhance collaboration across the different research fields. This article describes the sampling and analytical methods used to generate the dataset and how to use and access of the dataset through the IRHUM database. Any interpretation of the isotope dataset is outside the scope of this publication.

2.1 Introduction

Strontium isotope ratios ($^{87}Sr/^{86}Sr$) can be used as a geochemical tracer in a wide range of fields, including archaeology (Bentley, 2006; Slovak and Paytan, 2012), ecology (West et al., 2010), food (Kelly et al., 2005; Voerkelius et al., 2010) and forensic sciences (Beard and Johnson, 2000). The Sr isotopic ratios of natural materials reflect the sources of strontium available during their formation. Sr isotope ratios in bedrock are a function of age and composition of the rock and thus vary between

geologic units (Faure and Mensing 2005). Through weathering Sr is released and transported into the soil, ground and surface water, where it becomes available for uptake by plants and eventually enters the food cycle (Capo et al., 1998; Bentley, 2006). Due to their large atomic mass, Sr isotope ratios ($^{87}Sr/^{86}Sr$) are not measurably affected by kinetic and equilibrium fractionations during processes at low temperatures and biologic processes (Faure and Mensing 2005). The isotopic composition of bioavailable Sr (the Sr taken up into the food cycle) can differ from the bulk Sr isotopic composition of the bedrock, mainly through to the preferential weathering of different minerals (Sillen et al., 1998). However, the bioavailable Sr isotope ratios can also be influenced by processes like precipitation, dryfall, seaspray, and in modern context by fertilizer application (Price et al., 2002; Bentley, 2006; Evans et al., 2010; Maurer et al., 2012; Slovak and Paytan, 2012; Frei and Frei, 2013). In addition, the range of Sr isotope compositions varies not only laterally between different regions, but also with depth and time as the local environmental conditions change. In summary, a direct connection exists between the measured Sr isotope ratio of a material and its source region, but determining the Sr isotope composition of different regions is complicated by the diverse range of possible influences on the bioavailable Sr isotope ratio composition.

2.2 Mapping strontium isotopes

The choice of sample material to constrain the bioavailable isotope ratio is a fundamental consideration and is discussed in detail in the literature (Price et al., 2002; Bentley, 2006; Maurer et al., 2012; Slovak and Paytan, 2012). In general, three different approaches can be distinguished:

Fauna or human samples that are local to a region are considered to represent a robust average bioavailable Sr isotope composition over their feeding area (Price et al., 2002; Bentley, 2006). However, these samples are restricted in their availability in the context of a country wide study. In addition, fossil samples are subject to diagenetic overprint, while modern samples might be influenced by non-local food sources and fertilizer (Bentley, 2006; Maurer et al., 2012).

The bioavailable Sr isotope ratio for different geologic units can be determined by analysing a number of soils, plants, ground and surface waters (Sillen et al., 1998; Price et al., 2002; Hodell et al., 2004; Evans et al., 2010; Maurer et al., 2012). Overall, surface and groundwater samples provide a good estimate of the bioavailable Sr isotope signal over their catchment area, but are influenced by seasonal changes and changes in precipitation (e.g. Shand et al., 2009). Soils and plants average Sr over a very small area and are readily available in many different environments and easily analysed. The use of soil leachates to determine the local bioavailable Sr isotope ratio has shown varying degrees of success in different regions (Sillen et al., 1998; Price et al., 2002; Hodell et al., 2004; Bentley, 2006; Frei and Frei, 2011, 2013; Maurer et al., 2012; Slovak and Paytan, 2012). Plant samples are generally considered to be a better sample choice across different environments and can also offer insights into the variation of the Sr isotope ratio with depth, as different plant samples source Sr from different soil depths.

The bioavailable Sr isotope ratio can also be modelled based on the bedrock lithology, age, and weathering rates (Beard and Johnson, 2000; Bataille and Bowen, 2012; Bataille et al., 2012). These

models have shown significant potential and the next step is to assess their predictive ability across different geologic and geographic regions using direct measurements.

In many regions mineral weathering is the dominant influence on the bioavailable Sr isotope ratio and thus different geologic units can be differentiated. However, there are other processes including atmospheric Sr input (seaspray, dryfall), and in modern context fertilizers and other anthropogenic influences that can significantly affect the Sr isotope ratio. In addition, in regions with exogenic surface deposits (loess, glacial deposits) the local bioavailable Sr isotope ratio can be completely disconnected from the underlying geology. In conclusion, the choice of sample location and material and its value as a reference for mapping the geologic unit need to take these effects into consideration. This interpretative step will also depend on the focus of the study e.g., modern studies in contrast to archaeological studies. Strontium isoscapes have been published on a country scale for Mesoamerica (Hodell et al., 2004), United Kingdom (Evans et al., 2010), and Denmark (Frei and Frei, 2011, 2013), using a combination of directly sampled materials. Modelling of the bioavailable Sr isotope ratio has been undertaken for the contiguous USA (Beard and Johnson, 2000; Bataille and Bowen, 2012) and the Circum-Caribbean region (Bataille et al., 2012). Sr data also exist as smaller scale maps from different archaeological studies summarised in Slovak and Paytan (2011). While data are still lacking for many regions a robust approach is to combine as many different sample materials as possible to investigate their differences. Moreover, where possible, strontium isotope analyses should be undertaken in conjunction with other lines of evidence, including other isotope systems such as oxygen and lead, to validate a samples provenance. As a final note, a fundamental limitation of provenance studies is that it is only possible to disprove a source hypothesis, not to prove origin from a specific source.

2.3 Dataset of bioavailable Sr isotope ratios of France

The bioavailable Sr isotope ratio dataset of France is based on plant and soil samples. By sampling both sample types over a wide range of geologic units and large geographic regions, we hope to reliably constrain the local bioavailable Sr isotope ratios and gain insight into the possibly different sources of Sr to plants and soils. Ground and surface water samples would be a valuable addition to this dataset and are being considered for future sample collection.

The dataset presently contains 840 sample locations, covering the major geologic units of France (Figure 2-1, Table 2-1). As only small amounts of the collected sample material have been used for our analysis we have established a large archive of plant, soil and rock samples that is available to the scientific community for further investigation. The analysis of these samples is ongoing and new results will be added to the database as they become available with the aim of analysing all major geologic units of France within the next year. Finally, because the geology of France is varied and incorporates some of Europe's dominant geologic units, the data gathered for France might be useable to infer Sr isotope values for similar geologic regions across Europe.

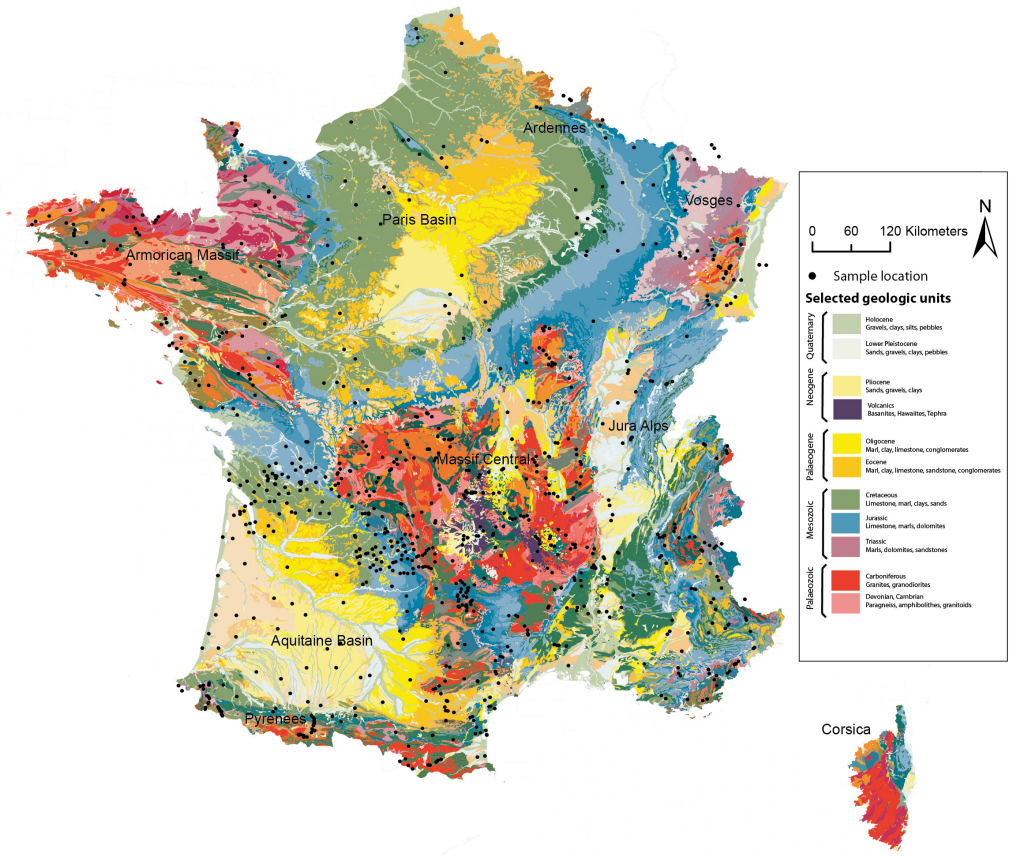

Figure 2-1: Map showing the sample locations (black dots) overlain on the 1:1M Geologic map of France (Chantraine et al., 2005).

Table 2-1: Metadata available for each sample site.

Sample ID	The sample ID can be used to identify the sample in our data tables and archives. Current standard is F-year-sample#, for example F11-02 means the second sample collected in 2011.
Researcher	Names of the researchers collecting the samples
Latitude, Longitude, Elevation	Coordinates of the sample site
Site image	If available, a picture of the outcrop or sampling site will be shown here
Outcrop type	We distinguish different types of outcrops: Outcrop: A natural outcrop of rock, as far as we could identify. Not uncovered through recent human activity. Roadcut: Along a major road, rocks unearthed by human activity. Quarry: Outcrop created by human activity, often no longer in use. Field: A sample collected from a field or meadow. Turned over tree: A sample collected from or beneath a turned over tree that has excavated some fresh soil layers. Shallow pit: A sample collected from ~10-20 cm deep hole dug by us.
Setting	This is a short description of our observations in the field, such as the proximity of human activities (agriculture, forest plantations) or clear indications of other recent influences.
Sample descriptions	Field observations during sample collection, such as rock, soil and plant type and characteristics.
$^{87}Sr/^{86}Sr$	Bioavailable strontium isotope ratios
Geologic setting	Summary of the geologic information from the 1:1M BRGM geologic map including the geologic region, rock type, geologic unit, major lithologies and age ranges.

2.4 Methods

2.4.1 Sample collection

The selection and density of the sample sites is based on the distribution of the geologic units on the 1:1M Geologic map of France (Chantraine et al., 2005). There is a wide spacing of sample sites in sedimentary basins, where the geology does not change over large areas, and closer spacing in geologically complex regions. Some geologic units contain several very different lithologies and our sampling was aimed at covering each of these lithologies. Areas where the bioavailable Sr isotope ratios are likely to be detached from the bedrock geology, like coastal areas influenced by seaspray, areas covered with glacial or loess deposits, swamps and peat deposits, were targeted to investigate these processes. In addition, close-spaced samples were taken around sites of special interest, such as archaeological sites and we collected a number of samples from agricultural fields to investigate the possible influence of fertilizers in France. Typical sample sites include roadcuts, outcrops, fields, areas of forest, and shallow pits. At each site plant, soil and rock samples were collected in close proximity to each other. Each sample site was photographed and described in detail, including information about the rock, soil and plant type collected, as well as an assessment of possible recent geomorphic and anthropogenic influences.

2.4.2 Analytical methods

Strontium is abundant in many materials in the environment. While this is an advantage for its use as a tracer it also increases the potential of contamination during sample preparation, especially for samples with low natural Sr concentrations. The samples were transported in sealed containers to Australia and irradiated at 50 Gy by the Australian Quarantine and Inspection Service to comply with quarantine procedures. All work is carried out under clean laboratory conditions. Only ultrapure reagents are used, and blanks are monitored at each step during the laboratory procedures to check for possible contamination. A summary of the sample preparation steps is illustrated in Figure 2-2 and described in detail in this section.

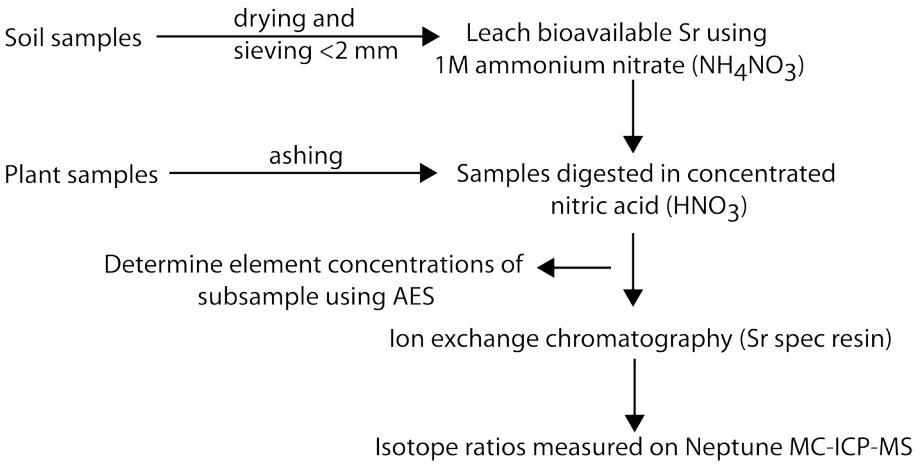

Figure 2-2: Overview of the preparation procedure for Sr analysis of plant and soil samples.

2.4.3 Sample treatment

A ~30 g subsample of each soil sample was dried overnight at 60°C and then sieved through a 2 mm sieve. A 1 g aliquot was subsampled and leached by adding 2.5 ml 1 M ammonium nitrate (NH_4NO_3) following the protocol DIN ISO 19730 and shaking for 8 hours. Samples are then centrifuged at 3000 rpm for 15 minutes, the supernatant extracted (~1-2 ml) and evaporated to dryness and then redissolved in 2 ml 2 M nitric acid (HNO_3). Plant samples were placed in heat resistant ceramic crucibles and ashed in an oven at 800°C for 8 hours. A 0.1 g aliquot of each sample was then digested in 1 ml ultrapure concentrated nitric acid (HNO_3) for at least 1 hour, before being evaporated to dryness overnight and redissolved in 2 ml 2 M nitric acid (HNO_3). A 0.1 ml subsample was extracted and placed in a vial with 4.9 ml 2% nitric acid (HNO_3). These solutions were then analysed using the ICP-AES to determine Sr and other major and trace element concentrations. The samples are further processed by ion exchange chromatography to isolate Sr from other interfering elements, in particular ^{87}Rb (isobaric interference), using two sets of columns filled with Eichrom Sr specific resin (pre-filter and Sr spec resin). In order to reach a target concentration of Sr in each sample volume eluted (600 ng in 2 ml) the amount of sample

added to the ion exchange columns is adjusted based on the Sr concentration determined by ICP-AES. The samples were finally diluted by a factor of 4 prior to MC-ICP-MS analysis to allow for reanalysis if necessary.

2.4.4 Neptune MC-ICP-MS measurements

Sr isotope ratios were measured in the Environmental Geochemistry and Geochronology Laboratory at the Research School of Earth Sciences, ANU, using a Neptune multi-collector inductively coupled plasma mass spectrometer (MC-ICP-MS). MC-ICP-MS was chosen over TIMS due to the requirement of high sample throughput for this project. A Quartz Dual Cyclonic Spray Chamber, PFA 100 µl nebulizer and standard Ni cones were used for sample introduction, and the instrument was tuned for maximum signal strength, stability and peak shape. The isotopes and Faraday cup configuration employed for analysis is shown in Table 2-2**.** Data reduction is performed offline in Microsoft Excel and includes Kr and ^{87}Rb isobar corrections, an exponential mass bias correction, and 3 sigma outlier rejection.

Table 2-2: Standard cup configuration and analysed masses (amu or isotope mass) employed for solution Sr isotope analysis on the Neptune MC-ICP-MS at RSES.

L4	L3	L2	L1	C	H1	H2	H3	H4
82.152	^{83}Kr	83.466	^{84}Sr	^{85}Rb	^{86}Sr	86.469	^{87}Sr	^{88}Sr

2.4.5 Quality control

To assure dataset precision, accuracy, reproducibility and comparability to other international data sources we record and report blank and standard analyses as a long-term reference for our laboratory in the database. Total procedural blanks vary between 50-250 pg Sr, and were analysed by isotope dilution with an ^{84}Sr enriched isotope spike using a TRITON Plus Thermal Ionisation Mass Spectrometer (TIMS) at RSES, ANU. These blank levels represent insignificant contributions to the amount of sample Sr measured (i.e. >100 ng). We tested the reproducibility of our analysis by running duplicate samples through the entire procedure and found differences between ^{87}Sr/^{86}Sr ratios measured for the same sample to be <0.004% (n=42).

Biases between measured ^{87}Sr/^{86}Sr ratios in different laboratories relate to differences in instrument design, problems of resolution of mass peaks and differences in measurement protocols (Faure and Mensing, 2005). Measurements of the Sr carbonate standard SRM987 (National Institute of Standards and Technology) on the Neptune MC-ICP-MS gave an average ^{87}Sr/^{86}Sr value of 0.71023±0.00001 (n=167, 2σ). This is in excellent agreement with measurements of the same standard by TIMS at RSES, ANU, which gave an average ^{87}Sr/^{86}Sr value of 0.71023±0.00002 (n=99, 2σ). It is also in agreement with the accepted ^{87}Sr/^{86}Sr value for SRM987 of 0.71025 (Faure and Mensing, 2005), and is within uncertainty of the original, albeit imprecise, certified value of 0.71034±0.00026 (Moore et al., 1982).

To assess the comparability of our dataset we carried out a blind test on a grazing soil standard from the GEMAS project (Geochemical Mapping of Agricultural and Grazing Land Soil). Measurements at

RSES gave an average value of 0.70631±0.00005 (n=10, 2σ) which is in agreement with the GEMAS value of 0.70638±0.00003 (n=39, 2σ). For future comparability studies we have commenced measuring an in-house soil standard which will be made available upon request.

2.5 Database architecture

The IRHUM (Isotopic Reconstruction of Human Migration) database is a web platform to explore and share strontium isotope datasets and data products. It is built upon a highly flexible open source software stack (Opengeosuite, GeoNode) maintained by Boundless (http://boundlessgeo.com) and follows common web standards. Its current functionality allows the user to explore our datasets, upload their own data, and create basic isotope maps. It is also possible to connect to an external WMS server to load background data such as geologic and soil maps. In addition to the spatial isotope data the IRHUM website stores metadata and allows the user to upload documents to describe their project and methods. This will enable others to assess the suitability of specific data for their study. Finally, the data can be exported in a variety of formats (.csv, .kml, .shp, .pdf) for GIS analysis. In summary IRHUM provides easy access to datasets, which facilitate the reuse of data and collaborative development of isotope maps at a variety of scales.

2.6 Data access

The dataset can be viewed and downloaded on the IRHUM webpage (http://rses.anu.edu.au/research-areas/archaeogeochemistry/tracing-human-migration or www.irhumdatabase.com). The full dataset is also available through the Pangaea data repository (doi:10.1594/PANGAEA.819142). Updates of the dataset are added to the IRHUM webpage as soon as they become available and will be passed on to the Pangaea data repository at the end of the project in 2014.

3 Spatial variability of bioavailable $^{87}Sr/^{86}Sr$ isotope ratios in France as a framework for archaeological provenance studies

This chapter has been submitted to the journal of Applied Geochemistry

M. Willmes, I. Moffat, L. McMorrow, L. Kinsley, R. Armstrong, S. Eggins, R. Grün (in review), Spatial variability of bioavailable $^{87}Sr/^{86}Sr$ isotope ratios in France as a framework for archaeological provenance studies. Applied Geochemistry

The author's contribution to the publication is as follows: The author was responsible for the analysis and interpretation of the data, as well as the spatial modelling. The article was written by the author with comments from all co-authors. Supplementary material for this chapter is found in appendix 8.2.

Abstract

Strontium isotope ratios ($^{87}Sr/^{86}Sr$) of archaeological samples (teeth and bone) can be used to trace the movement of animals, people, and their associated materials, across geologically different regions. Archaeological provenance studies in France are currently hindered by the lack of a baseline map to evaluate the variation of bioavailable $^{87}Sr/^{86}Sr$ isotope ratios across the landscape. Here we investigate the suitability of plant samples and soil leachates from the IRHUM database (www.irhumdatabase.com) to create a bioavailable $^{87}Sr/^{86}Sr$ isotope map for archaeological provenance studies in continental France. $^{87}Sr/^{86}Sr$ isotope ranges were classified for all major lithological units and isotope packages were created using cluster analysis to minimize in group variance and maximize the difference between the isotope packages. In this study it was not possible to untangle and quantify the processes that lead to variability between different sample types at some sample locations. However, these differences do not affect the overall variability of most lithological units, allowing us to create a robust $^{87}Sr/^{86}Sr$ isotope map for archaeological provenance studies.

3.1 Introduction

Strontium isotope ratios ($^{87}Sr/^{86}Sr$) are applied as provenance tracers in a wide range of fields such as archaeology, ecology, food and forensic sciences (Beard and Johnson, 2000; Hobbs et al., 2005; Kelly et al., 2005; Bentley, 2006; Voerkelius et al., 2010; West et al., 2010; Slovak and Paytan, 2012). $^{87}Sr/^{86}Sr$ isotope ratios vary between different geologic regions as a function of bedrock age and composition (Faure and Mensing 2005). Strontium is released by weathering of bedrock into the soils, ground and surface waters, from which it becomes available for uptake by plants and enters the food cycle (Capo et al., 1998; Bentley, 2006). Through their diet strontium is taken up by animals and humans and substitutes for calcium in biological apatite (bones, teeth), where it serves no metabolic function.

Recent studies have shown that the stable isotopes of strontium can be fractioned by physical and chemical processes (Fietzke and Eisenhauer, 2006; Halicz et al., 2008; Krabbenhöft et al., 2009; Knudson et al., 2010). This effect is removed when measuring $^{87}Sr/^{86}Sr$ for archaeological provenance studies during the mass spectrometry measurements, by normalizing the $^{87}Sr/^{86}Sr$ ratio to a constant $^{86}Sr/^{88}Sr$ value of 0.1194.

The isotopic composition of bioavailable strontium (i.e. the Sr that enters the food chain) can differ from the bulk $^{87}Sr/^{86}Sr$ isotopic composition of the bedrock, due to the preferential weathering of different minerals with different $^{87}Sr/^{86}Sr$ isotope ratios (Sillen et al., 1998). In addition, the isotopic composition of the bioavailable strontium can be influenced by atmospheric deposition (precipitation, seaspray, dust), the presence of exogenous surface deposits (loess, glacial till, cover sands, peat), mixing processes between different reservoirs, and anthropogenic influences such as fertilizer application and air pollution (Price et al., 2002; Bentley, 2006; Evans et al., 2010; Maurer et al., 2012; Slovak and Paytan, 2012; Frei and Frei, 2013). These processes vary between different areas and may introduce significant shifts in the bioavailable $^{87}Sr/^{86}Sr$ isotope ratio compared to the expected values based on bedrock geology.

A variety of samples types have been used to create baseline bioavailable $^{87}Sr/^{86}Sr$ isotope maps including rock leachates, soil leachates, plant samples, surface and ground water samples, archaeological and modern fauna or human remains (Price et al., 2002; Evans and Tatham, 2004; Bentley, 2006; Evans et al., 2009; Maurer et al., 2012; Slovak and Paytan, 2012). The best suited sample material for archaeological provenance studies would be archaeological samples with the same food source range as the archaeological samples in question, e.g. well preserved teeth of known local origin. However, these are invariably not available for large-scale (e.g. country wide) studies and thus substitute sample materials are needed. The choice of sample material is a fundamental consideration for any study and currently no consensus exists in the literature as to what type of sample material is best suited to determine the overall spatial variability of bioavailable $^{87}Sr/^{86}Sr$ isotope ratios for a country wide study.

Baseline $^{87}Sr/^{86}Sr$ isotope ratio maps using different sample types or modelling have been produced for a number of regions at different scales, including Europe (Voerkelius et al., 2010), Britain (Evans et al., 2009, 2010), Denmark (Frei and Frei, 2011, 2013), Israel (Hartman and Richards, 2014), the contiguous USA (Beard and Johnson, 2000; Bataille and Bowen, 2012), the Caribbean region (Bataille et al., 2012; Laffoon et al., 2012), Mesoamerica (Hodell et al., 2004), Puerto Rico (Pestle et al., 2013), South Africa (Sillen et al., 1998), and South Korea (Song et al., 2014). In addition, archaeological provenance studies on smaller spatial scales have been carried out in many areas around archaeological sites producing local baseline maps (Price et al., 2002, 2004; Bentley, 2006; Slovak and Paytan, 2012). Currently, no baseline $^{87}Sr/^{86}Sr$ isotope map exists for France, hindering the use of $^{87}Sr/^{86}Sr$ isotope ratios to investigate provenance of samples from the vast archaeological record of France. The aim of this study is to use our recently published dataset of $^{87}Sr/^{86}Sr$ isotope ratios of plants and soil leachates for continental France (Willmes et al., 2014) to produce a bioavailable $^{87}Sr/^{86}Sr$ isotope baseline map for archaeological provenance studies.

3.2 Data and methods

3.2.1 The IRHUM dataset

The IRHUM (isotopic reconstruction of human migration) database presently contains 843 sample locations from continental France, for which plant samples and top soil leachates have been analysed for $^{87}Sr/^{86}Sr$ isotope ratios (Pangaea data repository doi:10.1594/PANGAEA.819142, www.irhumdatabase.com). We selected 610 sample locations from the dataset, which cover all major geologic units and lithologies of France (Figure 3-1). This subset excludes sample locations that are situated on geologic units that are not characteristic for their geographic area, such as minor geologic outcrops, river terraces, as well as sample sites that are likely to represent modern anthropogenic activity, such as agricultural fields.

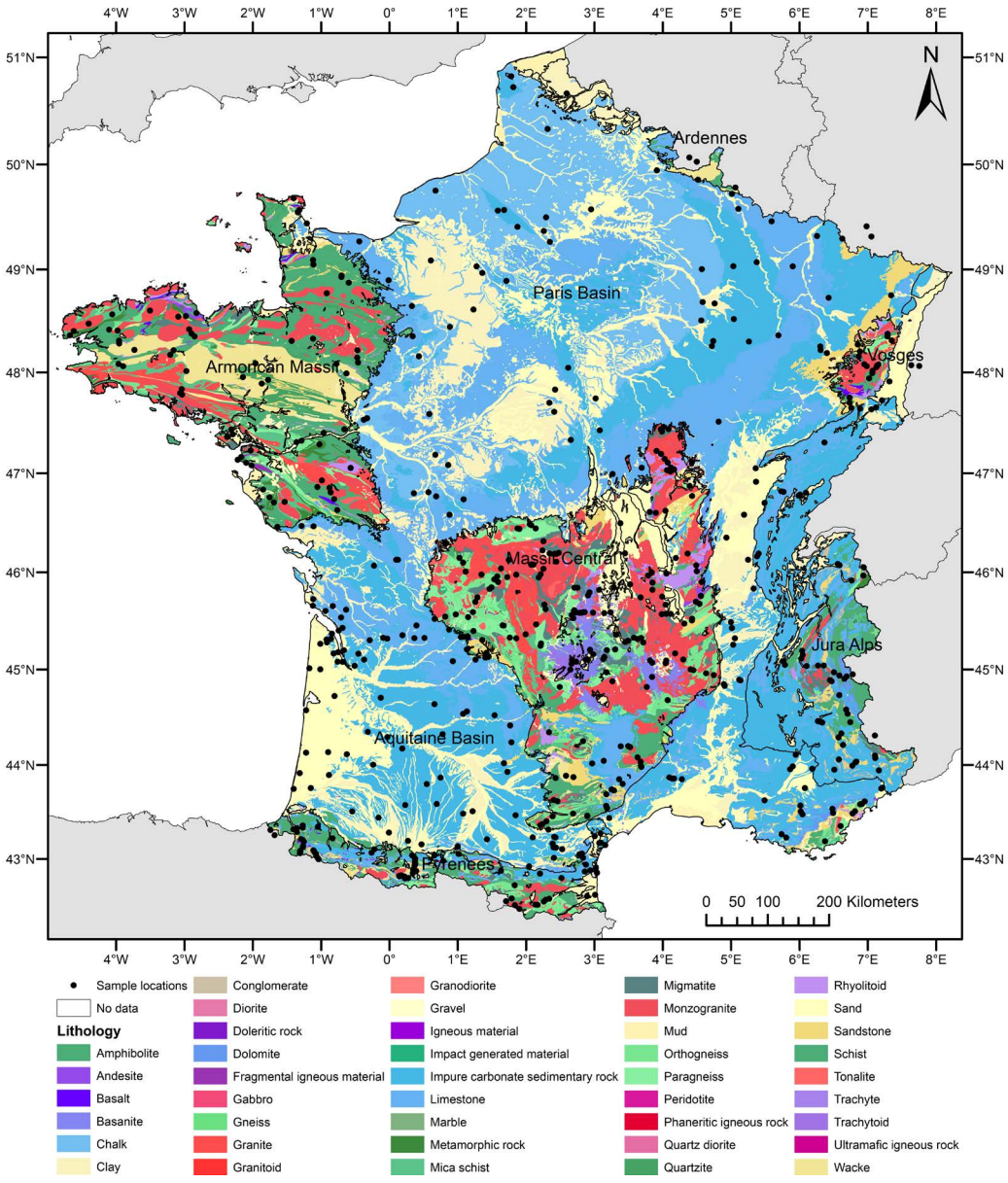

Figure 3-1: Surface geologic map of France (BRGM France) with sample sites from the IRHUM dataset marked as black dots.

3.2.2 Sample preparation and analytical methods

The analytical methods are described in detail in Willmes et al. (2014). In brief, the plant samples analysed in this study were completely ashed at 800°C for 8 hours and a 0.1 g aliquot of each sample was then digested in 1 ml ultrapure concentrated nitric acid (HNO_3). They are considered to represent a direct measure of bioavailable Sr. In contrast, strontium occurs in different parts of the soil, which can be divided into the bioavailable fraction, carbonate fraction and silicate fraction. The soil samples require a leaching process to mimic natural processes and extract the bioavailable part of the bulk Sr concentration (Capo et al., 1998; Sillen et al., 1998; Prohaska et al., 2005). Soil samples were dried, sieved to <2 mm, and a 1 g aliquot was subsampled. A 1M ammonium nitrate (NH_4NO_3) leach to extract the bioavailable Sr component was applied, following the protocol DIN ISO 19730. This leaching technique has been extensively tested (Hall et al., 1998; Gryschko et al., 2005; Meers et al., 2007; Rao et al., 2008) and is considered to produce robust results. Ion exchange chromatography, using two sets of columns in sequence that are filled with Eichrom Sr specific resin (pre-filter and Sr spec resin), was applied to isolate Sr from other interfering elements, in particular ^{87}Rb isobaric interference (Horwitz et al., 1991). Sr concentrations and $^{87}Sr/^{86}Sr$ isotope ratios were measured at the Research School of Earth Sciences (RSES), The Australian National University. Sr concentrations were determined by inductively coupled plasma atomic emission spectroscopy (ICP-AES) and Sr isotope ratios by a Neptune multi-collector inductively coupled plasma mass spectrometry (MC-ICP-MS). Procedural blank levels for plant samples and soil leachates were found to vary between 50-250 pg Sr, which represents an insignificant contribution to the amount of sample Sr measured (i.e. >100 ng). Reproducibility of the analysis was checked by running duplicate and triplicate samples through the entire procedure and differences between $^{87}Sr/^{86}Sr$ ratios measured for the same sample were found to be on average <0.004% (n=42). The Sr carbonate standard SRM987 (National Institute of Standards and Technology) is commonly used as a standard for $^{87}Sr/^{86}Sr$ isotope studies. Direct measurements of SRM987 on the Neptune MC-ICP-MS at RSES gave an average $^{87}Sr/^{86}Sr$ value of 0.71024±0.00001 (n=256, 2σ), which is in agreement with the original certified $^{87}Sr/^{86}Sr$ isotope value of 0.71034±0.00026 (Moore et al., 1982) and the accepted value of 0.71025 (McArthur, 1994).

3.2.3 Spatial and statistical methods

The strontium isotope data from the IRHUM database were spatially joined with the geologic map of France (Chantraine et al., 2005) and the surface geologic map of France (BRGM France) using ESRI ArcGIS™. The definition of the lithological units is taken from OneGeology-Europe (http://www.onegeology-europe.org). The data were then screened to check that the sampled lithology from the IRHUM dataset matches the lithology from the background maps and inconsistencies were manually corrected. Finally, we removed minor lithological units form the map (e.g. impact generated rocks, mud, amphibols, quartzites) and simplified and merged some of the lithological information to achieve uniform descriptions of units across France. For non-parametric statistical analysis Microsoft Excel and the free software environment R (R Core Team, 2013) were used. For the box and whisker

plot the top and bottom of the box are defined as the third and first quartiles. The interquartile range (IQR) is calculated by subtracting the first quartile from the third. The second quartile, which is the median, is shown as a black line. The whiskers are defined as Q1-1.5*IQR for the lower whisker and Q3+1.5*IQR for the upper whisker. Cluster analysis was conducted using R with the cluster (Maechler et al., 2015), fpc (Hennig, 2015), and clValid (Brock et al., 2008) packages.

3.3 Results and Discussion

3.3.1 Comparison of strontium isotope ratios in plant and soil samples

In theory, both soil leachates, which represent the bioavailable Sr of the soil, and plant samples, which are a direct measure of the bioavailable Sr, should give similar $^{87}Sr/^{86}Sr$ isotope ratios at a given sample location (Blum et al., 2000; Hodell et al., 2004). 499 sample locations in this study contain data for both plant samples and soil leachates and thus can be used to investigate potential differences between these sample types. We define the difference between plant samples and soil leachates as $\Delta_{PS} = (^{87}Sr/^{86}Sr_{plant} - ^{87}Sr/^{86}Sr_{soil\ leachate})$. Overall, we find a strong positive correlation between the plant and soil $^{87}Sr/^{86}Sr$ isotope ratios with an r value of 0.94, indicating a good match between different sample materials for large parts of the dataset (Figure 3-2). The average Δ_{PS} value for this dataset, calculated from absolute values, is 0.0008±0.0012 (SD, n=499). However, some sample sites show a significant higher offset between plant and soil samples. The largest Δ_{PS} found in the dataset is -0.0085, which accounts for a large part of the entire $^{87}Sr/^{86}Sr$ isotope ratio variation of France at just one sample location. Sites with large Δ_{PS} values show that soil and plant samples collected even in very close spatial context may sample vastly different strontium isotope reservoirs. This has been observed in previous studies (Blum et al., 2000; Evans and Tatham, 2004; Hodell et al., 2004; Evans et al., 2010; Maurer et al., 2012), and can result from a multitude of different processes.

The primary driver for $^{87}Sr/^{86}Sr$ isotopic variation across a landscape is the underlying geology and thus differences between sample materials may also be related to lithology. Soils and plants in geologically complex areas may form on geochemically highly mixed substrates, caused by the weathering of different rock types and different minerals within the same rock (e.g., Sillen et al., 1998). Thus, lithological units with homogenous geochemical compositions (e.g., limestones) are expected to show smaller average Δ_{PS} values than lithological complex units (gravels, granites, orthogneisses). For example, we find high Δ_{PS} values for gravel units, that could reflect their heterogeneous composition consisting of rock fragments with potentially vastly different $^{87}Sr/^{86}Sr$ isotope ratios placed next to each other. However, in contrast to this hypothesis, the average Δ_{PS} values of limestones and granites are similar (Table 3-1). The vast majority of soils is not only the product of *in situ* weathering but a composite of different processes and strontium sources. Overall, we find high average Δ_{PS} values both in heterogeneous as well as in homogenous geologic substrates, indicating that the underlying geology is not the only driver for the observed difference between soil and plant samples.

The sampling of different soil horizons by different plant root depth can also cause differences in $^{87}Sr/^{86}Sr$ isotope ratios between top soil and plant samples. In addition, atmospheric deposition of strontium will affect shallow rooted plants more than deeply rooted plants. In this study we concentrated on top soil samples and shallow rooted plants (grasses, shrubs). We dissolved the entire plant rather than specific tissues to mitigate this potential source of variability. Grasses should more closely reflect the $^{87}Sr/^{86}Sr$ isotope ratio of the topsoil then other plant species with deeper roots that might sample deeper soil horizons with different $^{87}Sr/^{86}Sr$ isotope ratios (Poszwa et al., 2002, 2004; Drouet et al., 2007; Maurer et al., 2012). However, we observe high Δ_{PS} values for all plant sample types including grass samples (Figure 3-3). There is no significant difference in average Δ_{PS} values for grass samples (0.00082, n=380) compared to tree roots (0.00086, n=35) and other plant sample types (0.00083, n=84). The exception being moss samples that show higher average Δ_{PS} values (0.00107, n=35). Finally, both soil and plant samples have a similar variance of 0.00002, indicating that the variability did not decrease as strontium was moved from the soil into the plant tissue.

External input of strontium, such as precipitation, seaspray, and dust, can potentially create difference between sample materials. As a first order observation we find no direct spatial correlation between the occurrence of Δ_{PS} values and precipitation and land use (appendix Figure 8-3 and Figure 8-4). Dust a major potential source of external strontium could not be investigated in detail because high quality dust distribution data with strontium concentration and $^{87}Sr/^{86}Sr$ isotope ratios do not exist for France. It is possible, that fine dust particles could contaminate plant samples with a foreign strontium isotopic ratio and that this fine dust was not removed in our sample preparation procedure.

Finally, on the scale of France it is likely that at any given sample location a combination of the discussed processes is at work. Identification of the driving process is confounded by the complex interplay between weathering of lithology, soil genesis, plant processes, and external strontium inputs that vary both in absolute strontium concentrations as well as isotope ratios, spatially and with time. Based solely on the strontium isotope ratios it is thus not possible to untangle these processes and quantification of these external strontium inputs was beyond the scope of this work. We intend to revisit a range of sites to conduct detailed sampling to investigate the differences between plant samples and soil leachates. Concerning the aim of this study, which is to create a robust baseline map, we suggest to incorporate the observed local variability but exclude anomalous sites that are not representative of their lithological unit and geographic area. This approach does not favour a specific sample material, taking into account that there are likely multiple processes at work that create the variations in $^{87}Sr/^{86}Sr$ isotope ratios observed at specific sites. Using the top and bottom whisker of the boxplot (Figure 3-2) we can identify outlier Δ_{PS} values as any value above +0.00170 and below -0.00115. In total, 70 sample locations (~14%) have Δ_{PS} values outside of this range (Table 3-1). Removing these sample locations results in a dataset with an average Δ_{PS} value of 0.0004±0.0004 (SD, n=429) and improves the correlation between plant and soil samples to R= 0.99. The danger in removing these sites is that it could potentially lead to an underestimation of the strontium isotopic variability for certain lithological units. We tested this by

comparing the strontium isotope range for each lithological unit from the complete and the outlier removed dataset (appendix Figure 8-5). No significant differences are observed, indicating that removing the outliers did not affect the overall strontium isotopic variability of the different lithological units. The exception from this observation are the gravel and chalk units, which show significantly narrower strontium isotope ranges after outlier removal. However, these lithologies are represented only by a small number of sample locations with 2 for gravel and 4 for chalk. The results for these two units should thus be treated with caution and specifically the gravel samples cannot be considered to represent the full strontium isotopic range of these units for France.

Table 3-1: Summary statistics of the Δ_{PS} values for the different lithological units. Δ_{PS} values are calculated as absolute values to accurately reflect the offset between the sample types.

	$\Delta_{PS(\text{plant sample - soil leachate})}$					Outlier		
Lithologies	Min	Max	Average	Sample pairs [n]	SD	Sample pairs [n]	%	Outlier removed average Δ_{PS}
Volcanics (Basanites, Tephrites, Pyroclastica, Trachytes)	0.00001	0.00065	0.00022	22	0.00017	0	0	0.00022
Chalk	0.00006	0.00563	0.00147	6	0.00213	2	33	0.00034
Dolomite	0.00013	0.00047	0.00028	4	0.00014	0	0	0.00028
Limestone	0.00001	0.00557	0.00066	67	0.00107	6	9	0.00036
Impure carbonate sedimentary rock	0.00001	0.00471	0.00079	95	0.00094	14	15	0.00047
Clay	0.00002	0.00760	0.00096	26	0.00160	5	19	0.00036
Sand	0.00000	0.00774	0.00082	52	0.00132	8	13	0.00041
Gravel	0.00023	0.00531	0.00207	5	0.00217	3	40	0.00023
Conglomerate	0.00006	0.00572	0.00128	15	0.00176	4	27	0.00036
Sandstone	0.00007	0.00429	0.00094	20	0.00111	4	20	0.00047
Wacke	0.00010	0.00066	0.00031	3	0.00031	0	0	0.00031
Granite	0.00001	0.00847	0.00067	64	0.00119	4	5	0.00043
Paragneiss	0.00001	0.00145	0.00048	15	0.00037	0	0	0.00048
Orthogneiss	0.00001	0.00437	0.00096	19	0.00100	3	11	0.00073
Migmatite	0.00005	0.00590	0.00091	15	0.00150	2	13	0.00041
Schist	0.00002	0.00780	0.00113	55	0.00155	12	20	0.00045
Mica schist	0.00006	0.00090	0.00038	5	0.00039	0	0	0.00038
Rhyolitoid	0.00015	0.00375	0.00130	11	0.00133	3	27	0.00055
All lithologies	0.00000	0.00847	0.00082	499	0.00123	70	14	0.00043

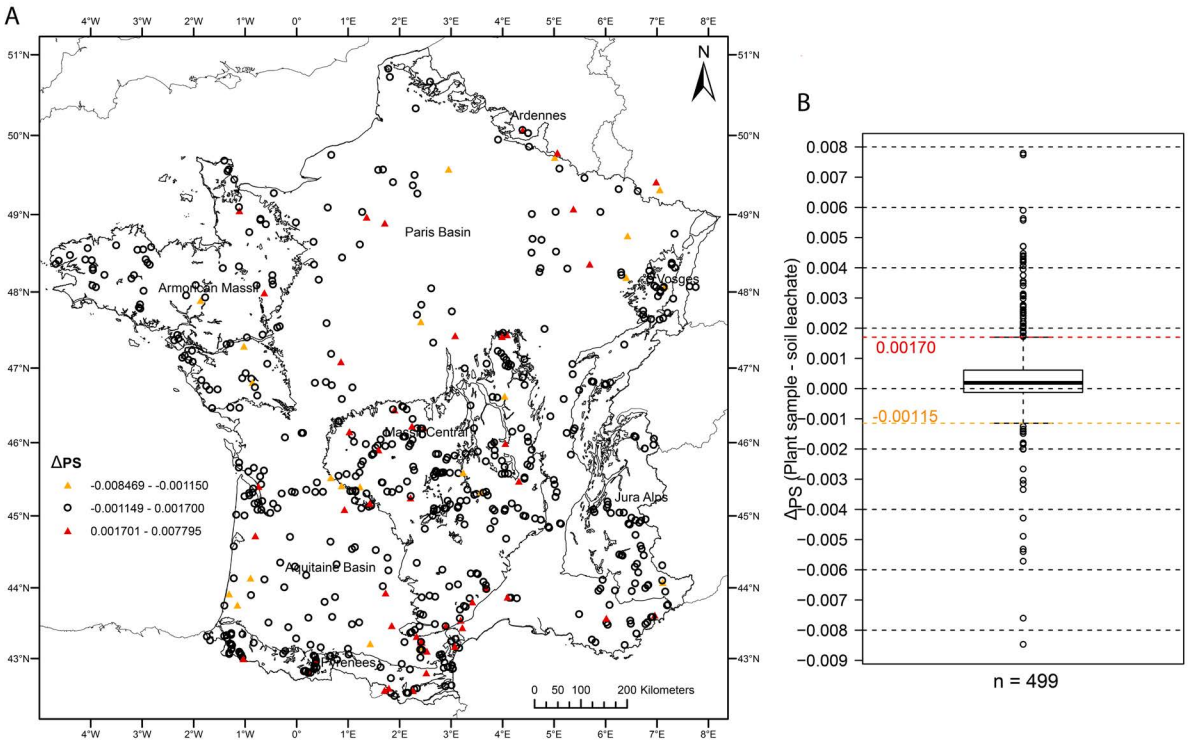

Figure 3-2: A: Geographic distribution of Δ_{PS} values in France and B: Boxplot of the Δ_{PS} values. Outliers are defined by the whiskers, as any value higher than 0.00170 and lower than -0.00115.

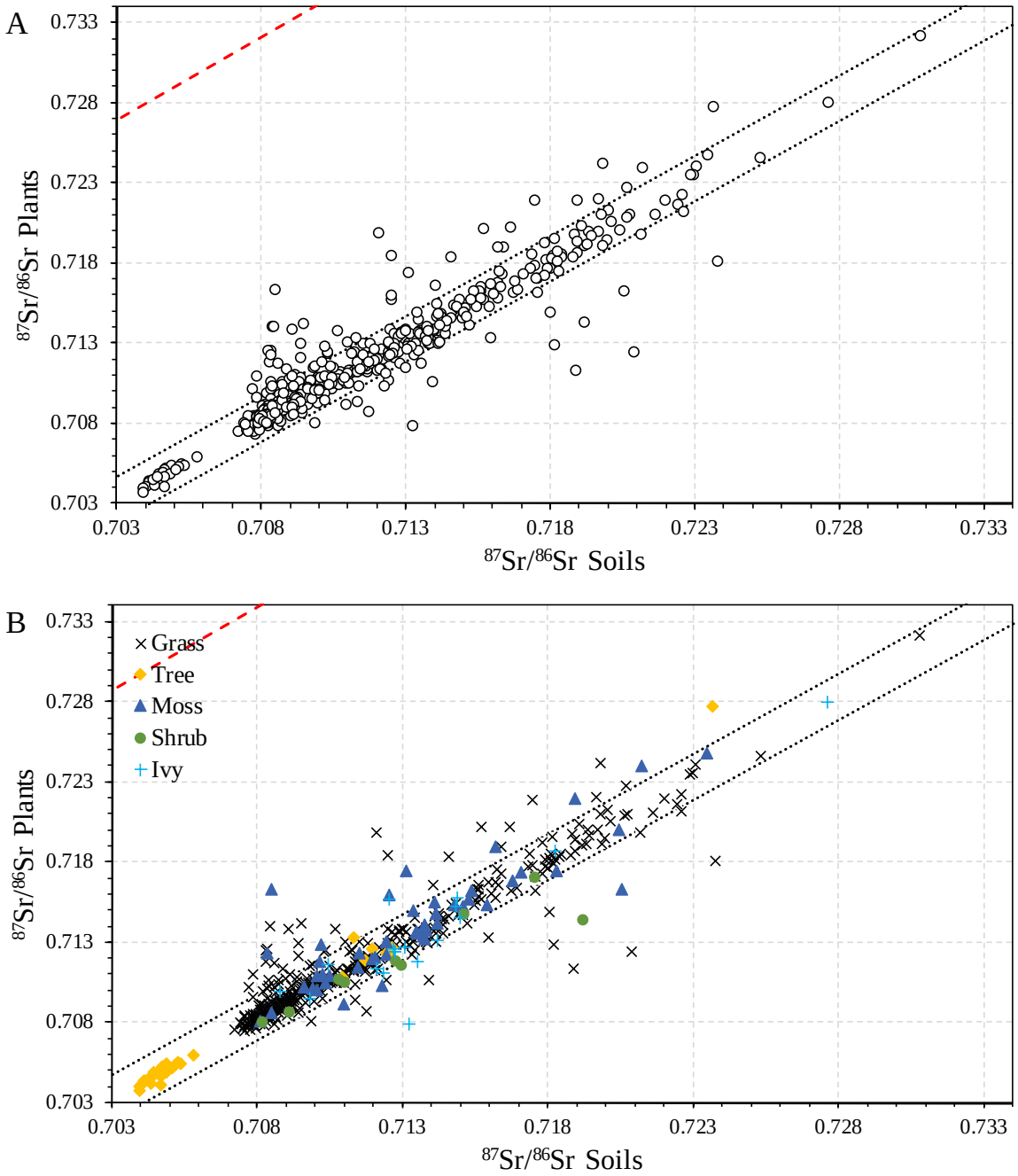

Figure 3-3: $^{87}Sr/^{86}Sr$ isotope ratios of plants plotted against soil leachate values from the same site. A: Plot including all sample pairs, a linear fit is shown in red. Grey lines are the top and bottom whisker from the boxplot of Δ_{PS} values (Figure 3-2), and any data point outside of the grey lines is identified as an outlier. B, same data plotted as in A, classified based on plant type.

3.3.2 Mapping the spatial variability of bioavailable $^{87}Sr/^{86}Sr$ isotope ratios

3.3.2.1 Isotope packages

The dataset presented here consists of 540 sample locations, with a total of 968 individual samples, after outlier removal. The bioavailable $^{87}Sr/^{86}Sr$ isotope ratios for each lithological unit are shown in Figure 3-4, Table 3-2. Significant overlap in $^{87}Sr/^{86}Sr$ isotope ratios exists between different lithological units, showing that the strontium isotope ratios form a continuum rather than specific readily distinguishable groups.

We performed cluster analysis to identify groups of lithological units with minimized internal variance and maximum difference between groups in $^{87}Sr/^{86}Sr$ isotope ratios. Several different clustering techniques (hierarchal, k-means, pam) were tested and k-means clustering set to 5 cluster was found to produce the highest optimized values, as determined by cluster validation (Silhouette, Dunn value). We thus group the lithological units and their strontium isotope ranges into 5 isotope packages, weighted by the area of the lithological unit.

Isotope package 1 (0.7033-0.7059) includes the volcanic units (basanites, tephrites, trachytoids) predominantly found within the Massif Central. Isotope package 2 (0.7072-0.7115) is composed of the carbonaceous sediments (chalk, dolomite, limestone, impure carbonate sedimentary rocks) and is the dominant lithology in the Aquitaine Basin, Paris Basin and Alpine Foreland. Isotope package 3 (0.7076-0.7170) comprises the Clay, Sand, Conglomerate Wacke, Paragneiss, Schist units. The clastic sediments are found within the Basins along rivers intercutting the units of isotope package 2 as well as along the Atlantic coastline. Paragneiss and Schist units are found in the mountainous regions with large outcrops in the Armorican Massif, Massif Central, and in the Pyrenees. Isotope package 4 (0.7084-0.7252) is composed of the Gravel, Sandstone, Granite, Migmatite, Mica schist, and Rhyolitoid units. These units are found dominantly in the mountainous regions of France. The last isotope package 5 (0.7155-0.7213) includes the Orthogneiss units found in the Massif Central and Pyrenees.

The isotope package map (Figure 3-5) is a simplified representation of the bioavailable $^{87}Sr/^{86}Sr$ isotope ranges of the lithological units and first strontium isotope baseline map for France. Since it is based on the surface geologic map it is accurate in displaying the sharp geologic boundaries and their corresponding changes in bioavailable $^{87}Sr/^{86}Sr$ isotope ratios. Limitations of the map are that because lithology was used as classification it does not allow us to investigate isotopic variation within single lithological units. The large strontium isotope ranges and significant overlaps are a direct result of using the broad lithological units as classifiers. For example, granites are represented as one group but different types of granites can have vastly different initial Rb concentrations and resulting $^{87}Sr/^{86}Sr$ isotope ratios. A similar effect can be observed in the clastic sediments, that vary significantly in their $^{87}Sr/^{86}Sr$ isotope ratios depending on their source region (e.g., between mountainous areas and the basins) but are here grouped together increasing their internal variability.

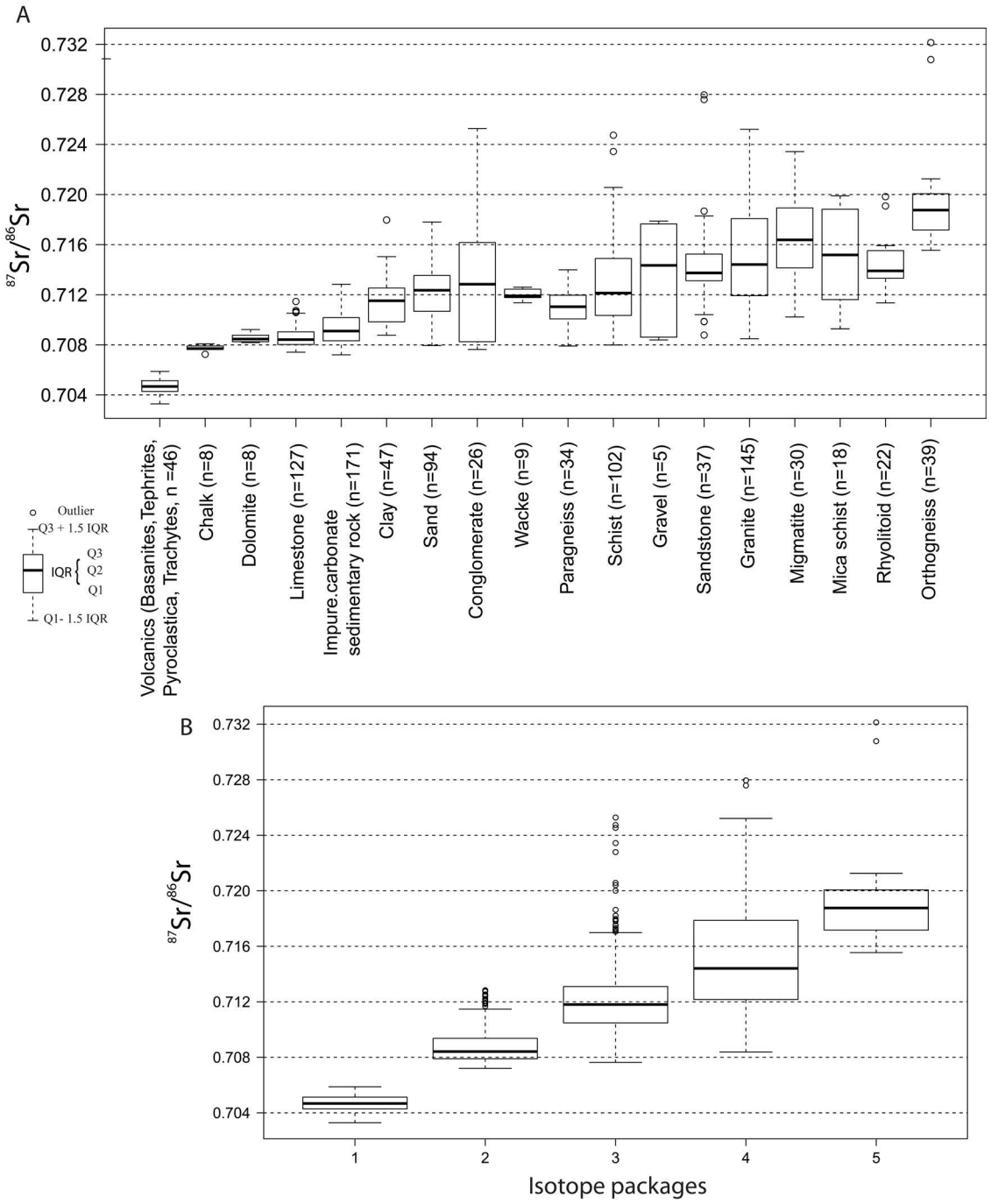

Figure 3-4: Box and whisker plot of the bioavailable $^{87}Sr/^{86}Sr$ isotope range, A for each lithology and B for the 5 isotope packages as determined by cluster analysis. The 5 isotope packages group the lithologies into packages that minimize the internal variance and maximize the difference between groups.

Table 3-2: Summary statistics for the bioavailable $^{87}Sr/^{86}Sr$ isotope range for each lithology and the isotope packages.

Lithologies	Isotope package	Bioavailable $^{87}Sr/^{86}Sr$ Q1-1.5 *IQR	Q1	Q2	Q3	Q3+1.5 *IQR	n	Area [km^2]
Volcanics	1	0.70328	0.70428	0.70468	0.70514	0.70587	46	12693
Chalk	2	0.70764	0.70765	0.70770	0.70790	0.70808	8	100291
Dolomite	2	0.70818	0.70825	0.70846	0.70877	0.70923	8	5772
Limestone	2	0.70741	0.70802	0.70842	0.70904	0.71052	127	172254
Imp. carb. sedi. rock	2	0.70720	0.70832	0.70910	0.71017	0.71284	171	252846
Clay	3	0.70877	0.70983	0.71152	0.71253	0.71504	47	114622
Sand	3	0.70794	0.71067	0.71236	0.71354	0.71781	94	159230
Conglomerate	3	0.70763	0.70825	0.71284	0.71617	0.72528	26	2562
Wacke	3	0.71136	0.71177	0.71191	0.71244	0.71261	9	25385
Paragneiss	3	0.70790	0.71007	0.71104	0.71196	0.71399	34	20603
Schist	3	0.70799	0.71035	0.71214	0.71489	0.72057	102	75615
Gravel	4	0.70839	0.70862	0.71434	0.71766	0.71788	5	1800
Sandstone	4	0.71041	0.71312	0.71374	0.71525	0.71829	37	27438
Granite	4	0.70849	0.71193	0.71441	0.71808	0.72521	145	100313
Migmatite	4	0.71022	0.71414	0.71638	0.71893	0.72343	30	16332
Mica schist	4	0.70928	0.71161	0.71518	0.71883	0.71989	18	14434
Rhyolitoid	4	0.71135	0.71332	0.71390	0.71552	0.71593	22	9635
Orthogneiss	5	0.71555	0.71717	0.71876	0.72007	0.72126	39	18940
Isotope package	1	0.70328	0.70428	0.70468	0.70514	0.70587	46	12693
	2	0.70720	0.70790	0.70842	0.70937	0.71147	314	531163
	3	0.70763	0.71048	0.71180	0.71311	0.71699	312	398017
	4	0.70839	0.71216	0.71441	0.71786	0.72521	257	169952
	5	0.71555	0.71717	0.71876	0.72007	0.72126	39	18940

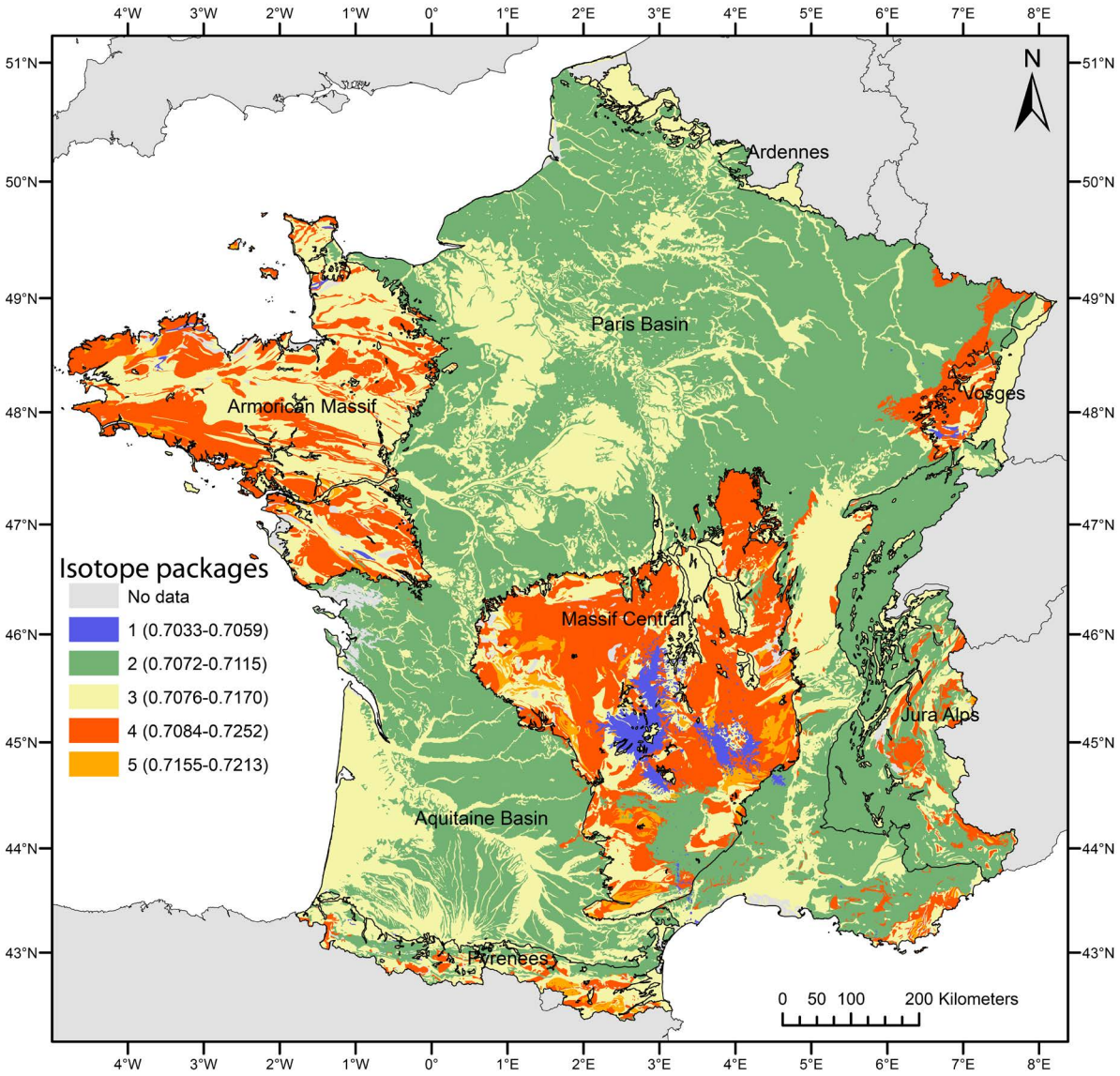

Figure 3-5: Map of the surface geologic lithologies of France, coloured by their classification into the 5 isotope packages. Grey represents no data available in this study. Isotope ranges given represent the interquartile range (Q1 – Q3).

3.3.2.2 Atmospheric deposition of strontium

Atmospheric deposition of strontium through processes such as precipitation, seaspray, and dust can have a significant influence on the bioavailable strontium isotopic $^{87}Sr/^{86}Sr$ isotope ratio. The effect atmospheric deposition of Sr will have on the strontium isotopic composition of a region primarily depends on the concentrations and differences in $^{87}Sr/^{86}Sr$ isotope ratios of the different end members. Evaporated seawater starts with a low strontium concentration and $^{87}Sr/^{86}Sr$ isotope ratio close to modern seawater of 0.70918. The strontium concentration and isotopic ratio is then changed by the addition of terrestrial dust and aerosols (Miller et al., 1993; Åberg, 1995; Capo et al., 1998; Faure and Mensing, 2005). Rainwater $^{87}Sr/^{86}Sr$ isotope ratios measured in France range from 0.709-0.713 (Négrel and Roy, 1998; Probst et al., 2000; Négrel et al., 2001, 2007) show that rainwater $^{87}Sr/^{86}Sr$ can be highly variable.

Due to the generally low Sr concentration in precipitation, in comparison to most soils and plants, only areas with high annual precipitation are expected to show a significant effect. The western part of Britain exhibits high annual precipitation in excess of 2000 mm/a, which results in a pronounced influence on the $^{87}Sr/^{86}Sr$ isotope ratio in the biosphere (Evans et al., 2009, 2010). The island of Bornholm, Denmark, on the other hand, shows low annual precipitation of around ~550 mm, which has only minute effects on the $^{87}Sr/^{86}Sr$ isotope ratio (Frei and Frei, 2013). Areas of high mean annual precipitation (>1000 mm/a) in France are constrained to small parts of the Pyrenees, the Alps, the western Massif Armorican and the south western part of the Aquitaine basin. Predicting the Sr isotope signal of rainfall for a certain area is not simple due to changes in the different sources and mixing of strontium over different timescales. Seaspray can also have a significant effect on the bioavailable $^{87}Sr/^{86}Sr$ isotope ratio in coastal areas (Whipkey et al., 2000; Montgomery et al., 2006; Evans et al., 2009; Frei and Frei, 2013), causing a shift towards marine isotope values. Seaspray affects coastal areas more strongly and the effect decreases further inland. Studies in the Hawaiian rainforest have shown that atmospheric deposition of marine strontium can dominate the $^{87}Sr/^{86}Sr$ ratios of plants on highly weathered surfaces (Chadwick et al., 1999) and even on fresher surfaces may form a significant contribution (Vitousek et al., 1999). Terrestrial dust can also be a major source of strontium in the environment, especially in arid regions (Graustein and Armstrong, 1983; Capo and Chadwick, 1999; Benson et al., 2008). A study on basalt flows in New Mexico observed a pattern where the $^{87}Sr/^{86}Sr$ ratios on young basalt flows was dominated by atmospheric deposition, while older flows were more influenced by bedrock weathering (Reynolds et al., 2012). Saharan dust from Africa is transported across the Atlantic and also north into the Mediterranean and Europe (Goudie and Middleton, 2001; Engelstaedter et al., 2006; Israelevich et al., 2012). Dust from the Sahara region of Africa is considered a significant component of the biogeochemical budget in Europe, and it might have been of even greater importance during the last glacial period. The strontium concentration and isotopic composition of dust may be highly variable since it may come from distant and from local sources and these sources change over time. The lack of average dust distribution maps combined with the lack of Sr isotope data for the dust found in France prohibits the detailed investigation of its potential influence. However, since we find a good correlation between $^{87}Sr/^{86}Sr$ isotope ratios and lithological units, dust from distant sources does not appear to make a significant contribution in this dataset.

In conclusion, the atmospheric deposition of strontium from precipitation, seaspray, and dust can have a significant contribution to the $^{87}Sr/^{86}Sr$ isotope ratios of plants and soils in France. Due to their spatially and temporally complex patterns it was not possible to quantify their contribution to the bioavailable $^{87}Sr/^{86}Sr$ isotope ranges for the lithological units in this study. Thus the $^{87}Sr/^{86}Sr$ isotope ranges established in this map may not adequately reflect times of greatly different climatological and atmospheric regimes in the past.

3.3.2.3 Anthropogenic inputs

Artificial fertilizers are commonly used in Europe and may contribute a significant component to the Sr content in soil and plant material. Only very restricted information is available on the Sr concentration and isotopic composition of artificial fertilizers. A comprehensive study of fertilizers in Spain (Vitòria et al., 2004) found that there is a large variation in $^{87}Sr/^{86}Sr$ isotope ratios for different fertilizers spanning most of the geological materials on Earth. Most fertilizers showed $^{87}Sr/^{86}Sr$ isotope ratios around 0.708-0.709 thus overlapping with modern seawater compositions. However, depending on their source, fertilizers can have highly variable Sr concentrations and $^{87}Sr/^{86}Sr$ isotope ratios. Other anthropogenic sources are urban and industrial wastes ~0.708 and detergents ~0.709-0.710 (Vitòria et al., 2004). A study on Danish surface waters found that unrealistically high amounts of fertilizer input would be needed to change their strontium isotopic composition (Frei and Frei, 2011). A case study investigating the Allanche river watershed in the Massif Central found that while there was a high fertilizer input of dissolved major ions, the Sr source was dominated (~90%) by bedrock weathering (Négrel and Deschamps, 1996). Studies of stream and ground water in the mountainous areas of France such as Armorican Massif and Massif Central have found variable influence of fertilizers and have related generally low $^{87}Sr/^{86}Sr$ isotope ratios to manure from livestock farming (0.7092-0.7109) and fertilizer application (0.7079-0.7095) (Négrel, 1999; Négrel et al., 2004). Data from the GEMAS atlas do not show a systematic and significant difference between the extractable Sr content of agricultural or grazing soils (Reimann et al., 2014), indicating that fertilizer application might not be a major source of Sr for soils in many areas in France. We directly investigated soil and plant samples from 4 fertilized agricultural fields and compared them to soil and plant samples collected in close proximity (<200 m) on grazing land (Table 3-3). We observe small differences between agricultural and grazing samples, but no trend to higher or lower strontium isotope values is detected. This could be the result of the use of different fertilizer with different Sr concentrations or reflect small scale variability caused by the underlying geology. Our data offer no clear indication of wide spread effects on the Sr isotope ratios due to fertilizer use. However, we cannot exclude the possibility that fertilizer use could influence single sample locations and introduce significant shifts, since even small amounts of fertilizer with a very high or low $^{87}Sr/^{86}Sr$ isotope ratio could have a significant effect. New geochemical data on large spatial scales e.g. from the GEMAS atlas (Reimann et al., 2014) may allow to investigate these inputs in more detail in the future.

Table 3-3: Differences in bioavailable $^{87}Sr/^{86}Sr$ isotope ratios between grazing land and agricultural field samples.

	Grazing land $^{87}Sr/^{86}Sr$		**Field sample $^{87}Sr/^{86}Sr$**		**Grazing - Field**	
Sample ID	Soil	Plant	Soil	Plant	Soil	Plant
F12-146	0.7076	0.7077	0.7075	0.7081	0.0002	-0.0004
F12-151	0.7083	0.7084	0.7083	0.7093	0.0000	-0.0009
F13-155	0.7100	0.7109	0.7088	0.7098	0.0012	0.0011
F12-147	0.7086	0.7102	0.7080	0.7111	0.0005	-0.0010

3.3.2.4 Exogenous surface deposits

Exogenous surface deposits such as loess, cover sands, and glacial till, can disconnect the bioavailable $^{87}Sr/^{86}Sr$ isotope ratios from the underlying geology. This can create a problem for mapping $^{87}Sr/^{86}Sr$ isotope ratios in areas where the exogenous surface deposits are patchy and do not represent the larger region. In addition, the timing and occurrence of exogenous surface deposits may be disconnected from the archaeological material in question. Care was taken in areas with exogenous surface deposits before accepting a sample to be representative of the surrounding surface geologic unit. The spatial distribution of exogenous surface deposits (Scheib et al., 2014) does not match any of the observed spatial trends in our dataset and thus does not seem to contribute significantly to our $^{87}Sr/^{86}Sr$ isotope ratio distribution maps. We also collected a loess sample at one location and found $^{87}Sr/^{86}Sr$ isotope ratios of 0.70823±0.00001 and 0.70882±0.00001 for soil leachate and plant, respectively. Samples on loess in south west Saxony-Anhalt, Germany gave a values of 0.7095±0.0010 (Maurer et al., 2012), showing that, as expected loess deposits can have variable $^{87}Sr/^{86}Sr$ isotope ratios.

3.3.3 Application to archaeological provenance studies

France exhibits a significant contrast in $^{87}Sr/^{86}Sr$ isotope ratios making it a suitable area to apply strontium isotopes for archaeological provenance studies. The map produced in this study represents the first attempt to provide bioavailable $^{87}Sr/^{86}Sr$ isotope baseline data for all of France. The previous discussions have shown that more in-depth studies are needed to quantify the spatial and temporal variability of the input from different strontium reservoirs into soils and plants. Nevertheless, this map may still be useful for archaeological province studies, when keeping its limitations in mind.

The main limitation of this map is related to the high variability in $^{87}Sr/^{86}Sr$ isotope ratios observed for many lithological units. This map can thus be used to identify broad geographic patterns of residence change, but may not resolve smaller scale mobility changes within similar $^{87}Sr/^{86}Sr$ isotopic regions. For example, isotope package 1 is constrained to a small area in the Massif Central and thus a sample with a corresponding isotope value could be placed into a tight geographic constrain, while samples with isotope values similar to isotope package 2 could correspond to many areas in the Paris and Aquitaine Basin. This reflects both the high variability found in isotope package 2 as well as the fact that distant geographic locations may exhibit similar $^{87}Sr/^{86}Sr$ isotope ratios based on their similar underlying geology.

In addition, the extend of the strontium baseline map in this study is constrained to present day France, which creates boundaries that have not much meaning for archaeological provenance studies. This can be overcome by including other strontium isotope baseline maps and detailed local studies into the analysis. This is facilitated by founding the baseline map on the surface geologic map of Europe, which uses consistent lithological identifiers across all of Europe and sharing the data on the IRHUM database

(Willmes et al., 2014). The isotope packages established here are in good agreement with the strontium isotopic signatures of natural mineral water samples (Voerkelius et al., 2010) collected at coarse spatial resolution Europe wide. Within France there are a number of detailed studies on $^{87}Sr/^{86}Sr$ isotope ratio variations for different watersheds, ground and river waters (Négrel and Deschamps, 1996; Négrel et al., 1997; Probst et al., 2000; Semhi et al., 2000; Aubert et al., 2002; Négrel and Petelet-Giraud, 2005), as well as a few archaeological provenance studies (Britton et al., 2011; Goude et al., 2012). Overall, the results from these small scale studies fit well within the broad isotope packages established in this study. At the same time these small scale studies show how closer spaced sampling can be used to untangle the $^{87}Sr/^{86}Sr$ isotope ratio variations over small spatial and temporal scales. Rodents and other local animals with small feed ranges from within archaeological sites may be useful to constrain the local $^{87}Sr/^{86}Sr$ isotope ratio at archaeological sites, especially when using rapid analytical techniques to identify potential diagenetic overprints (see chapter 4).

Another limitation of the baseline map presented here is caused by the use of modern environmental samples. For example, the last ice age has significantly influenced the distribution of surface deposits in many parts of Europe and this needs to be taken into account when applying a map like this to trace human mobility in the distant past. The spatial distribution of exogenous surface deposits (Scheib et al., 2014) could be used to identify problematic areas that may have been significantly altered in recent geological time. In addition, climatological and atmospheric conditions change and thus could have a temporally variable effect on the strontium isotope ratios measured in plants and soils. Modern samples that are affected by anthropogenic influences are particular problematic in this regard and need to be avoided for the creation of a baseline map for archaeological provenance studies. Care was taken during the creation of this map to avoid these areas.

Finally, to maximize the use of this map it is best used in combination with detailed strontium isotopic studies around the archaeological site in question. In this capacity is provides a powerful tool to identify possible residence and food source areas for samples that are identified as non-locals to the archaeological site. For the application to provenance human or animal remains we can make use of the fact that they will average their food source over a geographic area and time. Thus more extreme $^{87}Sr/^{86}Sr$ isotope values are less likely to contribute significantly, increasing our ability to identify different regions and thus allowing a more nuanced interpretation of the data. The map is also a useful tool to determine *a prior* where strontium isotopic tracing studies should best be applied and what kind of geographic constrain can be expected. Statistical methods such as linear discriminant function analysis could then be used to determine probable residence or food source areas.

3.4 Conclusions

The map produced in this study represents the first bioavailable $^{87}Sr/^{86}Sr$ isotope baseline map for archaeological provenance studies in France. Significant differences in $^{87}Sr/^{86}Sr$ isotope ratios were observed between plant samples and soil leachates at a number of sample locations. Identification of the driving process behind these differences is confounded by the complex interplay between weathering of lithology, soil genesis, plant processes, and external strontium inputs that vary both in absolute strontium concentrations as well as isotope ratios, spatially and with time. Based solely on the strontium isotope ratios it is thus not possible to untangle these processes and quantification of these external strontium inputs was beyond the scope of this work. To create a robust baseline map, we incorporated the observed local variability but excluded anomalous sites that are not representative of their lithological unit and geographic area. Removing these samples sites did not influence the overall variability of the lithological units, with the exception of gravel and chalk units, and thus represents a viable approach. $^{87}Sr/^{86}Sr$ isotope ranges for all major lithological units were established. These were then grouped into five isotope packages, based on k-means cluster analysis, to achieve minimal internal variability and maximise the difference between the isotope packages.

The large $^{87}Sr/^{86}Sr$ isotope ranges found in many lithological units and isotope packages, and the occurrence of similar lithological units with overlapping $^{87}Sr/^{86}Sr$ isotope ranges at geographically distant areas in France may limit the identification of mobility between those areas. In addition, the use of modern samples to create a map for archaeological provenance studies may not be appropriate if the surface deposits have changed significantly (e.g. deposits from the Ice Ages) or the climatological and atmospheric conditions were different enough to significantly change the $^{87}Sr/^{86}Sr$ isotope ratios in plants and soils. Nevertheless, keeping the limitations of this map in mind, it still provides a useful tool to identify patterns of mobility within France and to identify areas suitable for more in-depth studies of strontium isotopic tracing. Additional archaeological evidence, and isotopic tracers such as oxygen and lead, that are independent of the variability of strontium isotopes, can then be used to further constrain possible mobility patterns and residence areas.

4 Improvement of laser ablation in situ micro-analysis to identify diagenetic alteration and measure strontium isotope ratios in fossil human teeth

This chapter is in review in the Journal of Archaeological Science

M. Willmes, L. Kinsley, M.-H. Moncel, R. A. Armstrong, M. Aubert, S. Eggins, R. Grün (in review), Improvement of laser ablation *in situ* micro-analysis to identify diagenetic alteration and measure strontium isotope ratios in fossil human teeth. Journal of Archaeological Science

The author's contribution to the publication is as follows: The screening for diagenetic overprint has been a continuous development in this research group (Rainer Grün et al., 2008; Boel, 2011) and the new analyses were performed by R. Grün. The investigation of the interferences on strontium isotopes by *in situ* laser ablation ICP-MS was conducted primarily by the author and in collaboration L. Kinsley. Micro-drilling and TIMS analysis were performed by the author and R. A. Armstrong. The manuscript was written jointly by the author and R. Grün.

A part of the data in this chapter has been published in the journal of Archaeological Science.

A. Benson, L. Kinsley, M. Willmes, A. Defleur, H. Kokkonen, M. Mussi, R. Grün (2013), Laser ablation depth profiling of U-series and Sr isotopes in human fossils. Journal of Archaeological Science, 2991–3000. doi: 10.1016/j.jas.2013.02.028

The author's contribution to the publication is as follows: The author conducted the strontium isotope analysis by micro-drilling, contributed to the interpretation of the data and wrote the section on strontium isotope analysis in the article.

Abstract

Strontium isotope ratios measured in fossil human teeth are a powerful tool to investigate past mobility patterns. In order to apply this method, the sample needs to be investigated for possible diagenetic alteration and a least destructive analytical technique needs to be employed for the isotopic analysis. We tested the useability of U, Th, and Zn distribution maps to identify zones of diagenetic overprint in human teeth. Areas with elevated U concentrations in enamel were directly associated with diagenetic alterations in the Sr isotopic composition. Once suitable domains within the tooth are identified, strontium isotope ratios can be determined either with micro-drilling followed by TIMS analysis or *in situ* LA-MC-ICP-MS. Obtaining accurate $^{87}Sr/^{86}Sr$ isotope ratios from LA-MC-ICP-MS is complicated by the occurrence of a significant direct interference on mass 87 from a polyatomic compound in many analytical facilities. We found that this polyatomic compound is present in our analytical setup but is Ar

rather than Ca based, as was previously suggested. The effect of this interference can be significantly reduced by tuning the instrument for reduced oxide levels. We applied this improved analytical protocol to a range of human and animal teeth and compared the results with micro-drilling strontium isotopic analysis using TIMS. Tuning for reduced oxide levels allowed the measurement of accurate strontium isotope ratios from human and animal tooth enamel and dentine, even at low Sr concentrations. The average offset between laser ablation and solution analysis using the improved analytical protocol is 38±394 ppm (n=21, 2σ). LA-MC-ICP-MS thus provides a powerful alternative to micro-drilling TIMS for the analysis of fossil human teeth. This method can be used to untangle diagenetic overprint from the intra-tooth isotopic variability, which results from genuine changes in $^{87}Sr/^{86}Sr$ isotope ratios related to changes in food source, and by extension mobility.

4.1 Introduction

Radiogenic strontium isotope compositions ($^{87}Sr/^{86}Sr$) of human and animal skeletal remains can be used to reconstruct their habitat use and ranging patterns (Price et al., 2002; Bentley, 2006; Slovak and Paytan, 2012). Radiogenic strontium isotope ratios vary between different regions, primarily depending on the age and composition of the underlying geology, augmented by external processes such as precipitation, seaspray, and dust (Capo et al., 1998; Sillen et al., 1998; Bentley, 2006; Montgomery et al., 2007; Evans et al., 2010; Maurer et al., 2012). Strontium enters the body through diet, substitutes for calcium in biological apatite, which is used in the formation of bones and teeth, and serves no metabolic function. Therefore, the $^{87}Sr/^{86}Sr$ isotope ratio measured in skeletal remains will reflect the concentration-weighted average of dietary Sr, that was consumed while the skeletal tissue was formed (Beard and Johnson, 2000; Bentley, 2006). Thus, $^{87}Sr/^{86}Sr$ isotope ratios can be used to reconstruct change in food source and by extension residence area. A common problem when working with fossils remains is that diagenetic processes can change the original isotope compositions, rendering the sample unsuitable for isotopic provenance studies. In addition, isotopic analyses are often destructive, which prohibits their application to valuable fossil remains. Laser-ablation MC-ICP-MS is an analytical method that has the potential to overcome both of these limitations, because it allows for rapid *in situ* screening for diagenetic overprints, and least-destructive strontium isotope analysis of the same sample (Benson et al., 2013; Grün et al., 2014). In this paper, we outline a method to investigate diagenetic overprinting in fossil teeth using U, Th, and Zn concentration distribution maps. We then tested our protocol for $^{87}Sr/^{86}Sr$ isotope analysis in teeth in regard to the current limitations in terms of accuracy and precision, which have been observed in a significant number of analytical facilities, and are hypothesized to be mainly caused by a polyatomic interference on mass 87 (Horstwood et al., 2008; Lewis et al., 2014).

4.1.1 Diagenetic overprint in fossil teeth

The formation of human tooth enamel and dentine of the permanent dentition is a complex process beginning *in utero* (Ash and Nelson, 2003; Nanci, 2012). The mineral component of teeth is bioapatite, which is similar to hydroxyapatite, but affected by numerous substitutions of the Ca, PO_4, and OH

groups with secondary groups, such as Sr, Mg, and Ba. These secondary groups are subject to biological selection and vary in concentration with changes in trophic levels, between different species, and with the element abundance in the underlying substrate (Burton and Wright, 1995; Elliott, 2002). Intra-tooth measurements in mammals may be used to connect the intra tooth isotopic variations to mobility (Balasse et al., 2002; Britton et al., 2009). In human teeth, enamel does not remodel after formation and is closed to chemical exchange (Nanci, 2012). Thus, intra-tooth isotopic variations may relate to the sequential mineralisation of the tooth enamel. However, while the timing of tooth development in humans is well constrained, the complex pattern, timing and rates of mineralisation and maturation of tooth enamel are currently not completely resolved (Suga, 1989; Balasse, 2002; Montgomery et al., 2012).

The preservation of skeletal remains depends on their environmental surroundings. Diagenetic alterations are a common problem for many archaeological samples. To ensure that the isotopic ratios measured in a tooth reflect the original isotopic composition, it is important to identify the domains within the tooth that are least affected by diagenetic alteration (Nelson et al., 1986). For the investigation of diagenetic changes in tooth enamel, a variety of methods have been used, including infra-red (IR) spectroscopy (Sponheimer and Lee-Thorp, 1999) and cathodoluminescence (CL) imaging (Schoeninger et al., 2003). Nearly all of these studies have employed bulk analysis with the aim of testing cleaning techniques (Price et al., 1992; Hoppe et al., 2003; Trickett et al., 2003) or coarse sub-sampling using mineralogical information (e.g. by CL) as a guide. While these approaches provide some information as to the mineralogical state of the hydroxyapatite or functional groups within this mineral (such as hydroxyl or phosphate), any conclusions about sample integrity for isotopic analysis are derived from conjecture. Mapping of element distributions has been used to identify the degree of diagenesis in bones (Trueman et al., 2008; Koenig et al., 2009; Fernandes et al., 2013). In addition, a few studies have investigated the mechanisms of diagenetic alteration using high resolution elemental or isotope analysis (Kohn et al., 1999; Jacques et al., 2008; Martin et al., 2008; McCormack et al., 2015).

Systematic mapping of U, Th, and Zn concentrations may help to qualitatively identify domains of diagenetic alteration in skeletal materials. The basic principle is that modern teeth and bones contain only trace amounts of uranium and thorium and thus their presence in archaeological skeletal remains can be used to identify zones of diagenetic overprinting (Budd et al., 2000; Eggins et al., 2003; Rainer Grün et al., 2008; Koenig et al., 2009; Hinz and Kohn, 2010; Boel, 2011). Uranium is water soluble and highly mobile in skeletal tissues and consequently its concentration and spatial distribution are highly variable and can change on small scales on the order of tens of µm (Rainer Grün et al., 2008; Duval et al., 2011; Grün et al., 2014). Thorium, on the other hand, is water insoluble and represents mechanical overprinting of the sample, for example by clay particles in pores and on the surface. However, there is no linear correlation between uranium and thorium incorporation and the uptake of other elements, such as Sr. This hinders the quantification of possible Sr overprint based on the distributions of U and Th. Nevertheless, zones within a tooth showing high U or Th concentrations can indicate diagenetic overprints, while zones with low U and Th concentrations are more likely to preserve the original Sr

isotope ratio. In mammals, low U zones often occur close to the surface of the tooth enamel, within 200 – 400 µm (Budd et al., 2000; Eggins et al., 2003; Rainer Grün et al., 2008; Boel, 2011). The first aim of this research project is to further test this screening method and to evaluate the usefulness of Zn as an additional tracer to identify zones which have retained the original strontium isotopic compositions.

4.1.2 Strontium isotope analysis of fossil teeth

Strontium isotope ratios from fossil teeth can be analysed either using sample dissolution followed by mass spectrometric measurements (thermal ionisation mass spectrometry (TIMS) or multi-collector inductively coupled plasma mass spectrometry (MC-ICP-MS)), or *in situ* using laser ablation (LA)-MC-ICP-MS. For solution analyses, a micro-drill can be used to extract a small amount of sample, which is then digested in acid and Sr is separated from the matrix elements using ion exchange chromatography. This technique is accurate and reliable, but also time intensive and potentially more destructive to the sample than in situ LA-MC-ICP-MS. The amount of material required varies between a few µg to several tens of mg depending on the Sr concentration, drill setup, and instrument capacity. For samples requiring more than 0.5 mg, drilling causes large destructive marks on the sample, making this technique unsuitable for valuable archaeological materials. Micro-drilling smaller amounts of sample < 0.1 mg is much less destructive, but it is also technically challenging and the equipment is not widely available (e.g., Charlier et al., 2006). LA-MC-ICP-MS allows *in situ* analysis of a sample and has shown great potential in analysing skeletal remains because it is fast, requires minimal sample preparation, and provides high spatial resolution (50-200 µm). Additionally, this method allows for large numbers of measurements on the same skeletal fragment to test for compositional variability within the same specimen. Traditionally, samples were cut to create a flat sample surface for laser ablation analysis which creates significant damage. However, recent studies have shown that accurate data can also be obtained from the outer uncut sample surface (Copeland et al., 2011; Benson et al., 2013; Le Roux et al., 2014).

Problems with laser ablation analysis of the $^{87}Sr/^{86}Sr$ isotope ratios in fossil skeletal material result from molecular interferences from Ca, Kr, Ar, and Rb, that can severely limit the accuracy and precision (Woodhead et al., 2005; Paton et al., 2007; Copeland et al., 2008; Horstwood et al., 2008; Simonetti et al., 2008; Vroon et al., 2008). In particular, the occurrence of a direct interference on mass 87 from a polyatomic compound, possibly $^{40}Ca^{31}P^{16}O$, has been suggested to be the main cause for the consistent positive offsets, observed in a significant number of analytical facilities, between the $^{87}Sr/^{86}Sr$ isotope ratios measured with LA-MC-ICP-MS and with solution methods ($\Delta_{LA\text{-}TIMS}$) on the order of 500 to 1500 ppm (Horstwood et al., 2008; Simonetti et al., 2008; Lewis et al., 2014). The effect of this polyatomic interference on the $^{87}Sr/^{86}Sr$ isotope ratio was found to be highest in samples with low Sr concentration, relative to Ca and P (Horstwood et al., 2008; Simonetti et al., 2008). The Sr/Ca ratio in biogenic apatite is controlled by the Sr concentration, because calcium is a stoichiometric component and can thus be treated as constant. It follows, that under constant laser sampling ablation conditions, the effect of the polyatomic interference on the $^{87}Sr/^{86}Sr$ ratio varies in proportion with changes in Sr concentration (Horstwood et al., 2008). The effect of this interference on samples with high Sr concentration (e.g.

>1500 ppm) is minimal (Simonetti et al., 2008), however, most human tooth samples have much lower Sr concentrations, in the range of 50 ppm to 500 ppm (Bentley, 2006). An isotopically homogenous tooth that has varying Sr concentrations could then show varying $^{87}Sr/^{86}Sr$ isotope ratios when this interference is not corrected for adequately (Horstwood et al., 2008; Simonetti et al., 2008; Nowell and Horstwood, 2009; Richards et al., 2009).

Several methods have been tested to increase the accuracy of LA-MC-ICP-MS analyses on human teeth. Horstwood et al. (2008) used samples with known $^{87}Sr/^{86}Sr$ isotope ratios to calibrate the LA-MC-ICP-MS analyses, but found that this approach limited the precision of the analysis. Tuning for reduced oxide levels has been successful in reducing $\Delta_{LA\text{-}TIMS}$ to 600-100 ±100 ppm (Foster and Vance, 2006; de Jong et al., 2007). A recent study by Lewis et al. (2014) combined tuning for reduced oxide levels with a customized plasma interface. Their setup is similar to a collision cell and allowed for the addition of a variable He flow after the skimmer cone, requiring minimal modification of the mass spectrometer. Using tuning for reduced oxide levels they achieved an accuracy of 100 – 600 ppm in bone and tooth enamel, which improved to 30±50 ppm with the addition of the customized plasma interface. Their analytical setup reduced the signal intensity by only 20-30% and thus is highly applicable to samples with low strontium concentration, such as human teeth. However, modification of the plasma interface is not always possible at an analytical facility with a broad range of applications of different isotopic systems. The second aim of this paper is to further investigate the causes of the polyatomic interference on mass 87 and evaluate our analytical protocol to reduce its effect on the measurement of $^{87}Sr/^{86}Sr$ ratios in fossil human teeth.

4.2 Materials and methods

4.2.1 Sample materials

Diagenetic overprinting was investigated using a modern human tooth, a M3 extracted from R. Grün, and a prehistoric Neanderthal tooth (Payre 1), which is a unerupted molar of an approximately three-year-old child. Detailed U and U-series maps of the Neanderthal tooth were published by Grün et al. (2008). $^{87}Sr/^{86}Sr$ isotope ratios were measured both with solution TIMS and *in situ* LA-MC-ICP-MS. TIMS results are taken here to represent the true value against which the LA-MC-ICP-MS results are compared. Samples were taken from the same locations within each tooth. These samples include eight teeth from Le Tumulus des Sables (Courtaud et al., 2010; Boel, 2011), four Neanderthal teeth from the site of Payre in France, one bovid tooth from Holon, Israel (Porat et al., 1999; Benson et al., 2013) and a diprotodon molar from Camel Swamp, Australia (Benson et al., 2013). We also measured modern marine teeth from a grey nurse shark (*Carcharias taurus*) and a dugong (*Dugong dugon*). In addition, the strontium carbonate standard SRM987 (National Institute of Standards and Technology) was used to mix a series of standard solutions containing varying concentrations of P using the 1000 ppm

Phosphorus AccuTrace Reference Standard. A solution of 2% nitric acid in MilliQ, was mixed with varying concentrations of P and Ca + P (1:1 to 1:0.05) in order to create an additional standard solution.

4.2.2 Thermal ionisation mass spectrometry (TIMS)

After cleaning the surface of the teeth, 0.2-0.5 mg of material was drilled out using a 0.3 mm custom made drill bit at 500 rpm. The samples were then leached in 0.5 ml 1 M ammonium nitrate to remove any residual contamination and digested in 1 ml ultrapure concentrated nitric acid for 1 h. The samples were then evaporated to dryness, redissolved in 2 ml 2 M nitric acid and subjected to ion exchange chromatography using micro-columns with Eichrom Sr specific resin (pre-filter and Sr spec resin) to isolate Sr from other elements (Horwitz et al., 1992). A drop of diluted phosphoric acid was added to each sample before loading onto rhenium filaments with a TaF_5 activator. Samples were measured on a TRITON Plus thermal ionisation mass spectrometer (TIMS) at the Research School of Earth Sciences, ANU. Data reduction procedures include Rb correction ($^{85}Rb/^{87}Rb$=2.591), exponential mass bias correction ($^{86}Sr/^{88}Sr$ ratio of 0.1194), and 2σ outlier rejection. Total procedural blanks were determined by isotope dilution using a ^{84}Sr enriched spike, measured on the TRITON Plus TIMS and are below 100 pg Sr. This blank contribution is insignificant compared to the amount of sample Sr measured (>100ng). Long term measurements of the Sr carbonate standard SRM987 (National Institute of Standards and Technology) gave $^{87}Sr/^{86}Sr$ value of 0.71023±2 (n=99, 2σ) which is in agreement with the original certified $^{87}Sr/^{86}Sr$ isotope value of 0.71034±26 (Moore et al., 1982) as well as the more commonly quoted accepted value of 0.71025±1 (Thirlwall, 1991; McArthur, 1994; Hans et al., 2013).

4.2.3 Laser ablation analysis

Samples were prepared by cutting along the buccal-lingual (cheek to tongue) axis using a fine diamond saw (100 μm) to produce a flat surface exposing both the enamel and dentine. Two of the Neanderthal teeth (Payre 2, 3) and the shark and dugong teeth were analysed from the outside without cutting. The *in situ* elemental and isotopic analyses were carried out using a custom-built laser ablation sampling system (ANU HelEx) interfaced between an ArF Excimer laser (193 nm; Lambda Physik Compex 110) and ICP-MS and MC-ICP-MS. Details of the ANU system and its capabilities have been described in detail previously (Eggins et al., 1998, 2003). In brief, it employs a single long-working distance lens to project and demagnify (by a factor of 20) the image of a laser-illuminated aperture onto the sample surface, which enables a range of geometries to be ablated within bounding dimensions of between about 5 μm and 400 μm. Samples were mounted so that their surface lies in the focal plane of the laser. In this study laser pulse rates of 10 Hz were employed with a fluence of 10 J/cm^2 (power density 0.3 GW/cm^2), the latter resulting in removal of a uniformly thick layer (≈200 nm) from the targeted sample site with each laser pulse. The in-house developed laser ablation cell produces very fast response times, which permits high spatial resolution analysis. Laser ablation was performed under a pure helium atmosphere with a continuous flow of 500 cm^3 min^{-1} through the cell. After the cell, approximately 1 l min^{-1} argon is added to the gas stream and is adjusted to optimise ionisation conditions.

4.2.3.1 Element distributions

Element concentrations were measured with a Varian-820 quadrupole ICP-MS. The maps presented here are part of a larger study that measured 58 elements in fossil and modern human teeth (Grün et al., 2013). Pre-cleaning was performed using a 230 µm spot scanned at 100 µm/s across the sample surface, with the laser operating at 10 pulses per second. For elemental analysis, a track with a spot size of 100 µm with laser pulse rates of 10 Hz was employed. The NIST reference glasses SRM610 and SRM612 were used as calibration standards for element concentration determinations. Data reduction for elemental analysis followed Longerich et al. (1996) and involved the subtraction of interpolated plasma background intensities, measured before and after analysis of the sample. Signal intensities were normalised to ^{43}Ca for each time slice, drift corrected relative to the NIST standard measured before and after the sample sequence, and then calibrated with respect to the known element ratios of the NIST610 and NIST612 standards. Reference data for the NIST standards (Jochum et al., 2011) were taken from the GeoRem database (http://georem.mpch-mainz.gwdg.de).

4.2.3.2 Strontium isotope measurements

For *in situ* Sr isotope analysis, the laser ablation-system was connected to a Neptune MC-ICP-MS with Faraday cup detectors set to measure three different sequences in dynamic mode, thus allowing for monitoring of all potential interferences (Table 4-1,Table 4-2). Only spot sampling measurements were performed for isotope analyses, with a sample ablation time of 60 seconds, using a 180 µm diameter spot and the laser operating with a pulse frequency of 5 Hz. Typical operating conditions are shown in Table 4-3. To remove any surface contamination produced during the sample preparation process, including settled dust and fine particles, the samples were first subjected to a cleaning run using a laser spot of 265 µm for 10 s. Faraday detector integration times were 5 s. An in-house Sr standard, consisting of a piece of modern Giant Clam (*Tridacna gigas)* from the Great Barrier Reef, was measured 3 times before and after each sample analytical sequence. For the modern Giant Clam, we obtained an average Sr isotope composition of 0.70920±6 (n=153, 2σ), which is consistent with present-day values of seawater (McArthur et al., 2001).

4.2.4 Interference correction protocol

A number of methods have been used to account and correct for the different interferences present when analysing strontium isotopes using LA-MC-ICP-MS (Vroon et al., 2008). The relevant interferences on LA-MC-ICP-MS analysis of Sr in skeletal tissue are shown in Table 4-1. The potential isobaric interferences on the ^{87}Sr/^{86}Sr ratio are double charged rare earth elements (REEs), Kr, Rb, Ca dimers, and polyatomic interferences (Woodhead et al., 2005; Paton et al., 2007; Horstwood et al., 2008; Simonetti et al., 2008; Vroon et al., 2008; Müller and Anczkiewicz, 2016). Since some of the corrections required use mass peaks that have pre-existing interferences, the order in which the corrections are applied is important and is discussed below. All isotope ratios used were taken from Rosman and Taylor

(1998). Table 4-4 lists average elemental concentrations in tooth enamel for a variety of elements for the assessment of possible interferences.

Background levels: Background levels were monitored before and after each measurement using the same instrument conditions as during analysis, except without ablating material. Washout times of ~60 s are long enough to ensure that no wash-out effects, e.g. from the previous sample, are present and typical blank levels are shown in Table 4-5.

Rare Earth Elements: Significant interferences from REE elements may occur due to the formation of doubly charged REE species (Paton et al., 2007). REE concentrations in skeletal material are generally low, however, post burial uptake can occur (Trueman and Tuross, 2002; Trueman et al., 2011). The measured intensities at half masses 81.5, 83.5, 85.5 and 86.5 are used to monitor $^{163}Dy^{++}$, $^{167}Er^{++}$, $^{171}Yb^{++}$, $^{173}Yb^{++}$, respectively. The signals could be used to subtract the appropriate amounts of relevant double charged on-peak interferences from all Sr peaks. As can be seem in Table 4-4, these REE are close to background in both the modern and fossil samples. Should significant REE signals occur, this would be a sign of either diagenetic alteration or incomplete cleaning (some polishing pastes contain high REE and W concentrations). Such samples should be checked and rerun or removed from further analysis. ^{89}Y was used as the primary indicator for the presence of REE in the teeth. ^{89}Y is a sensitive indicator of potential REE interference because it is chemically similar to the lanthanide REEs, and is generally concentrated in minerals that contain REEs. In addition, doubly charged REE would be several orders of magnitude lower than the single charged species.

Ca dimers and argides: Samples with high Ca concentrations may produce calcium dimers and calcium argides in the plasma. $^{40}Ca^{44}Ca$, $^{40}Ca^{46}Ca$ and $^{40}Ca^{48}Ca$ dimers interfere with the ^{84}Sr, ^{86}Sr and ^{88}Sr, respectively. To correct for these the Ca dimer intensity on mass 82 was measured. However, on this mass there is a ^{82}Kr interference, which is monitored on mass 83 and calculated using the known $^{83}Kr/^{82}Kr$ ratio. ^{82}Kr was then subtracted from the total intensity at mass 82, leaving the $^{40}Ca^{42}Ca$ or $^{40}Ar^{42}Ca$ interferences. Using the known isotopic ratio for $^{42}Ca/^{44}Ca$, $^{42}Ca/^{46}Ca$, and $^{42}Ca/^{48}Ca$ all dimer and argide interferences could be corrected. We did not observe any Ca dimers or argides.

Polyatomic interferences: Both $^{40}Ca^{31}P^{16}O$ and $^{40}Ar^{31}P^{16}O$ may interfere on mass 87 when measuring calcium phosphate matrices. This interference is investigated in this study and discussed in detail in the results and discussion section.

Mass bias: The isotopic fractionation induced from the laser and the instrument mass discrimination are corrected during Sr isotope analyses by using the stable $^{86}Sr/^{88}Sr$ ratio of 0.1194 and an exponential correction.

Krypton: Kr occurs as an impurity in the Ar gas and interferes with masses ^{84}Sr and ^{86}Sr. The amount of Kr varies depending on the gas supplier, between different batches, and also with time from a single vessel, as the Ar is used up (Woodhead et al., 2005). A standard method to correct for Kr is using a gas blank correction, measured before and after each sample and to subtract the intensities (Woodhead et

al., 2005; Vroon et al., 2008). A problem with this correction is the assumption that the measured Kr intensity stays the same whether or not sample material is being ablated. This is not necessarily correct, as the presence of ablated material changes the plasma loading and consequently the percentage of ionisation of atoms in the plasma. Correcting for the Kr interference using peak stripping is further complicated by the uncertainty surrounding the Kr mass bias (Jackson and Hart, 2006; Vroon et al., 2008). We used a similar approach to Jackson and Hart (2006) and corrected for the Kr interference by subtracting ^{84}Kr from mass 84 until the $^{84}Sr/^{88}Sr$ ratio reaches the known value of 0.00672, see also Konter and Storm (2014). Iterations are used for the mass bias correction, substituting the Kr number in the $^{86}Sr/^{88}Sr$ ratio and repeating the calculations until there is no more change in the calculated isotope ratios (often less than 2 iterations). Using this correction method means that the $^{84}Sr/^{86}Sr$ ratio as data quality control is lost. The $^{84}Sr/^{86}Sr$ isotope ratio, while useful as a general monitor of the correction procedures, is problematic because of the very small intensities at these masses. The precision of the $^{84}Sr/^{86}Sr$ does not necessarily reflect that of the $^{87}Sr/^{86}Sr$ ratios (Copeland et al., 2010).

Rubidium: The direct interference of ^{87}Rb on the $^{87}Sr/^{86}Sr$ is corrected by monitoring ^{85}Rb and subtracting the appropriate amount from the signal at mass 87 assuming the natural $^{85}Rb/^{87}Rb$ ratio. The $^{85}Rb/^{87}Rb$ ratio is then reversely corrected for mass bias, using the Sr mass bias. This correction method is limited because it assumes that the mass bias for Rb and Sr are the same, which is not necessarily true. Generally, in teeth the Rb/Sr ratio is low (see Table 4-4), thus this correction has only a negligible effect. However, in samples with higher Rb/Sr ratio the possible difference between the Rb mass bias and Sr mass bias would have to be considered and this correction method could have a significant effect. A recent study by Müller and Anczkiewicz (2015) was able to accurately constrain the mass bias corrected $^{85}Rb/^{87}Rb$ ratio, allowing for accurate measurements of tooth enamel with high Rb/Sr ratio.

Table 4-1: Summary of relevant isotopes of this study and their interferences (adapted from Horstwood et al., 2008).

89	**88**	**87.5**	**87**	**86.5**	**86**	**85.5**	**85**	**84.5**	**84**	**83.5**	**83**	**82.5**	**82**	**81.5**	**81**
	Sr		Sr		Sr				Sr						
			Rb				Rb								
					Kr				Kr		Kr		Kr		
Y	Lu^{2+}	Lu^{2+}	Yb^{2+}	Yb^{2+}	Yb^{2+}	Yb^{2+}	Yb^{2+} Er^{2+}	Tm^{2+}	Yb^{2+} Er^{2+}	Er^{2+}	Er^{2+}	Ho^{2+}	Er^{2+} Dy^{2+}	Dy^{2+}	Ar_2H
	^{40}Ca ^{48}Ca				^{40}Ca ^{46}Ca				^{40}Ca ^{44}Ca				^{40}Ca ^{42}Ca		
			$^{40}Ca^{31}P^{16}O$												
			$^{40}Ar^{31}P^{16}O$												

Table 4-2: Cup configuration of the LA-MC-ICP-MS for strontium isotope measurements of skeletal remains at RSES.

	L4	L3	L2	L1	C	H1	H2	H3	H4	Integration time [s]
Seq. 1	-	82	83	84	85	86	87	88	89	5
Seq. 2	-	81.5	82.5	83.5	84.5	85.5	86.5	87.5	88.5	5
Seq. 3					71					3
Seq. 4					103.9					3

Table 4-3: Instrument operating conditions for *in situ* Sr isotope measurements.

Neptune MC-ICP-MS	
Forward power	1200 W
Extraction voltage	-2000 V
Analyser pressure	< 5e-8 mbar
Cones	Jet sampler
	+ standard skimmer
	(both Nickel)
Gas flows	
Plasma gas	17 l/min
Auxiliary gas	1 l/min
Nebuliser gas	~ 1 l/min
HelEx laser ablation system	
ArF Excimer laser, Lambda Physik Compex 110	193 nm
Laser fluence	~ 10 J/cm^2
Repetition rate	5 Hz
He gas to cell	500 ml/min

Table 4-4: Average elemental concentrations measured in the enamel of a modern tooth (RG) and a Neanderthal tooth from Payre (from Grün et al. 2013). DL stands for detection limit.

	Sr (ppm)	Rb (ppb)	Y (ppb)	Dy (ppb)	Ho (ppb)	Er (ppb)	Tm (ppb)	Yb (ppb)	Lu (ppb)	U (ppb)
RG	100.0±0.2	299±1.0	15±2	1.4±0.2	0.20±0.04	0.7±0.1	0.11±0.03	9.7±0.1	0.15±0.02	1.0±0.1
Neanderthal	151.3±3.6	232±1.8	19±1	2.2±0.3	0.41±0.08	<DL	0.22±0.06	1.8±0.3	0.20±0.08	625±7.8

Table 4-5: Typical blank levels after 60 s washout time.

Mass	Isotopes/polyatomic compounds	Average V (n=30)	2se
89	^{89}Y	4.2E-06	9.2E-07
82	$^{82}Kr+^{40}Ca^{42}Ca$	1.3E-04	1.2E-05
83	^{83}Kr	8.1E-05	5.7E-06
84	$^{84}Sr+^{84}Kr+^{40}Ca^{44}Ca$	3.6E-04	2.8E-05
85	^{85}Rb	2.0E-05	1.3E-06
86	$^{86}Sr+^{86}Kr+^{40}Ca^{46}Ca$	1.5E-04	1.1E-05
87	$^{87}Sr+^{87}Rb+^{40}Ca^{31}P^{16}O,^{40}Ar^{31}P^{16}O$	4.0E-05	4.1E-06
88	$^{40}Ca^{31}P$, $^{40}Ar^{31}P$	1.7E-04	6.9E-06
71	$^{88}Sr+^{40}Ca^{48}Ca$	3.2E-04	2.9E-05
104	$^{88}Sr+^{16}O$	4.6E-05	4.0E-06

4.3 Results and discussion

4.3.1 Identifying diagenetic alteration in fossil human teeth using element distribution maps

The results of the systematic mapping of elemental distribution in a Neanderthal tooth (Payre 1) and a modern human tooth (RG) and are shown in Figure 4-1and Figure 4-2, respectively. Since the resolution along a laser ablation track is greater (500 data points) than in the perpendicular direction (up to 35 data points from the parallel tracks, see lowest profiles in B, C), we carried out two maps focusing on the enamel with horizontal and vertical track directions. In the modern sample (RG) the Sr concentrations throughout the tooth are relatively uniform with little contrast between enamel and dentine, the dentine-enamel junction (DEJ) is barely identifiable in the Sr maps. Towards the buccal enamel boundary (BEB) there is a moderate decrease in the Sr concentrations. The U and Th concentrations are all close to the detection limit of 0.1 ppb for our particular analytical setup. The Zn distribution shows a clear contrast between enamel and dentine, but also an outer rim in the enamel with high concentrations (D). Where the occlusal surface of the tooth is worn this is also evident by the absence of the Zn rim (vertical tracks 8 to 16, cycles 100 to 200). The Zn rim in the enamel can be geochemically used to identify erosion of the enamel surface, which would facilitate diagenetic alteration (Eggins et al., 2003).

The U and Th distribution in the Neanderthal tooth (Payre 1) has previously been mapped by Grün et al., (2008). Figure 4-1 shows maps of Sr (Figure 4-1B, C) and U concentration (Figure 4-1D, E). In contrast to the modern sample (Figure 4-2), Sr concentrations vary significantly between dentine and enamel. In dentine they are between 150 to 250 ppm, whereas in enamel, they are around 60 to 110 ppm. The Sr concentrations also show a clear separation at the DEJ. There is a gradient in Sr concentration from the dentine that is not covered with enamel towards the interior of the tooth (see arrow in Figure 4-1C). The enamel has somewhat elevated Sr concentrations near the base (solid ellipse in Figure 4-1C) and low concentrations near the outer surface (e.g. area of the dotted ellipse in Figure 4-1C). The general concentration gradients of Sr and U are similar, and even smaller features of concentration changes are reproduced (compare circled sections in track 3, or details in track 6). Since virtually all measured U is

the result of post depositional U-uptake, we interpret the co-varying distribution of Sr in dentine to reflect post depositional Sr uptake as well.

In contrast to dentine, there are both similarities as well as clear differences between the U and Sr distributions in the enamel. Both Sr and U are enriched at the base of the enamel (solid ellipses in Figure 4-1C and E), and depleted close to the outer surface (dotted ellipses in Figure 4-1C and E). However, U is enriched along lineaments, and in a central patch (see rectangle in Figure 4-1D and track 13), while Sr does not show any apparent concentration changes in these areas (Figure 4-1C and track 13). Furthermore, U concentrations drop by a factor of 25 to 100 at the DEJ while the Sr concentrations drop by a factor of 2 to 3. The Sr concentrations in the detrital material on the outside of the enamel are less than twice the Sr inside the enamel while the U contrast is in the range of 100. Figure 4-3 shows the Zn and Th maps for the Neanderthal tooth. The Zn rim is completely intact for the tooth (Figure 4-3A) showing that no abrasion or material removal through weathering has taken place. Th only occurs within a very small volume on the surface of the tooth and is an indicator of remaining sediment and other surface contaminations (Figure 4-3B). Figure 4-4 details the relationship between Sr and U concentrations in the different enamel domains. While the U concentrations vary over 5 orders of magnitude, Sr varies only by a factor of 2 to 4. The enamel was subdivided into four different domains. The outside domain is the volume of enamel immediately on the interior of the Th peaks to a depth of about 50 μm (see Figure 4-3B, track 4 and track 12). The BEB domain corresponds to the volume with increased Zn concentrations (Figure 4-3A, track 4 and track 12). The base domain relates to the area with increased Sr and U concentrations (solid circles in Figure 4-1C and E), and the DEJ domain contains the remaining data points. It can be seen that all high U and Sr concentrations occur in the surface veneer (Figure 4-4B) and are the result of diffusion from the outside. The base domain (Figure 4-4C) has the highest Sr concentrations in the enamel, followed by the DEJ domain (Figure 4-4D). The BEB domain has the lowest U and Sr concentrations and is thus least influenced by diagenesis (Figure 4-4E). This means that on the one hand, U can be used to identify domains that contain original Sr isotope signatures, on the other hand, if no such low U domains can be identified, it will be impossible to ascertain whether any Sr analysis provided non-contaminated results. As soon as the outer surface of the enamel is weathered, U-migration proceeds from the outside (Eggins et al., 2003). Such teeth will be rendered unsuitable for Sr isotope analysis. The effect of diagenetic overprint is illustrated in Figure 4-5. $^{87}Sr/^{86}Sr$ isotope ratio analysis using micro-drilling TIMS yielded a value of 0.7087 for the dentine. Three of the enamel $^{87}Sr/^{86}Sr$ ratios are closely similar, around 0.7108, while the forth is significantly lower at 0.7097. The latter was drilled from the domain with highly elevated U-concentrations (rectangle in Figure 4-1E), and shows a diagenetic overprint from the dentine, lowering the $^{87}Sr/^{86}Sr$ ratio by around 0.0011.

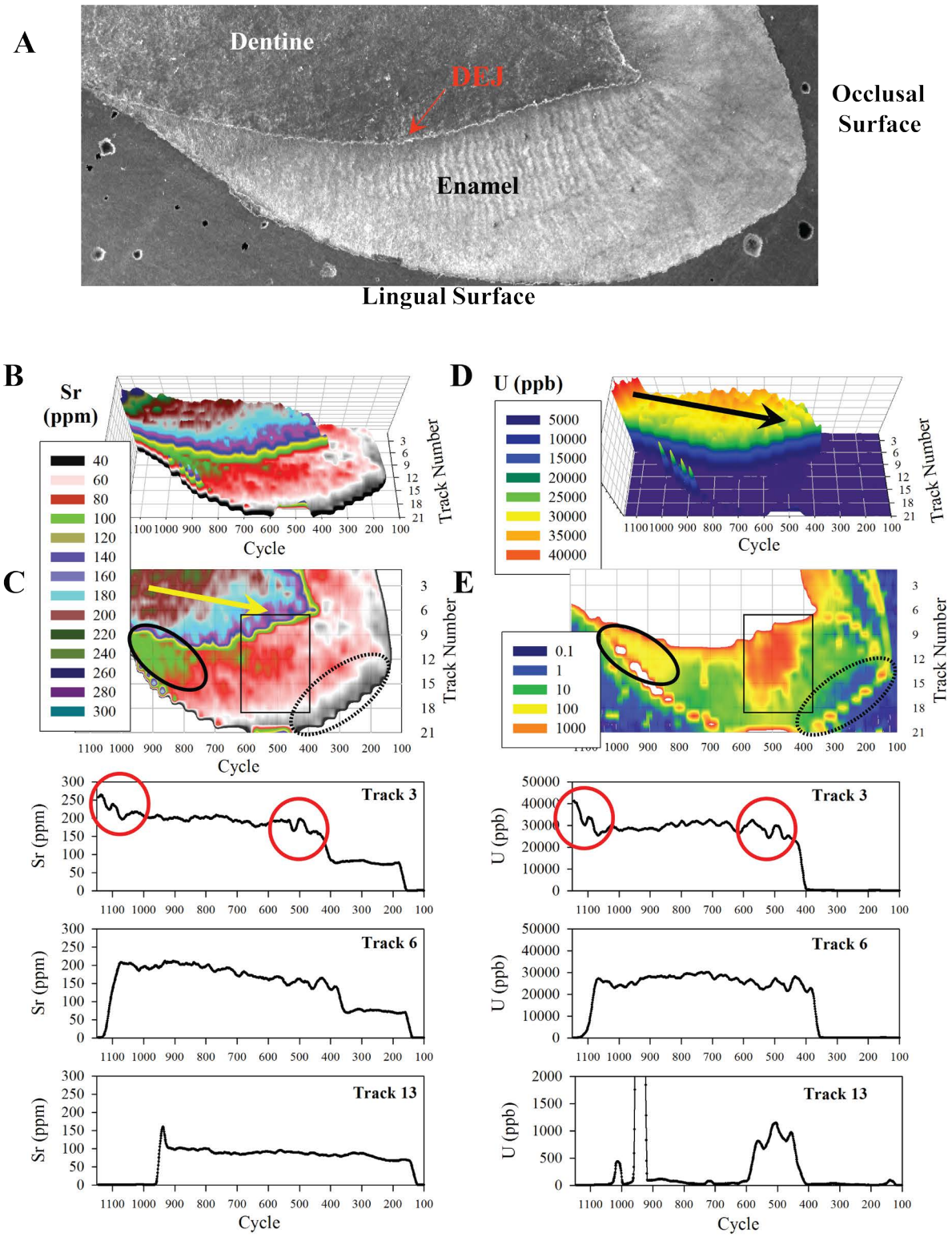

Figure 4-1: Elemental distribution maps of the Neanderthal tooth (Payre 1). A: Scanning electron microscope (SEM) image of the tooth, B, C: Sr concentration maps (oblique and planar view) and selected tracks D, E: U concentration maps oblique and planar view and selected tracks. The arrow indicates a general concentration gradient. The sections indicated by circles, ellipses and rectangles are discussed in the text.

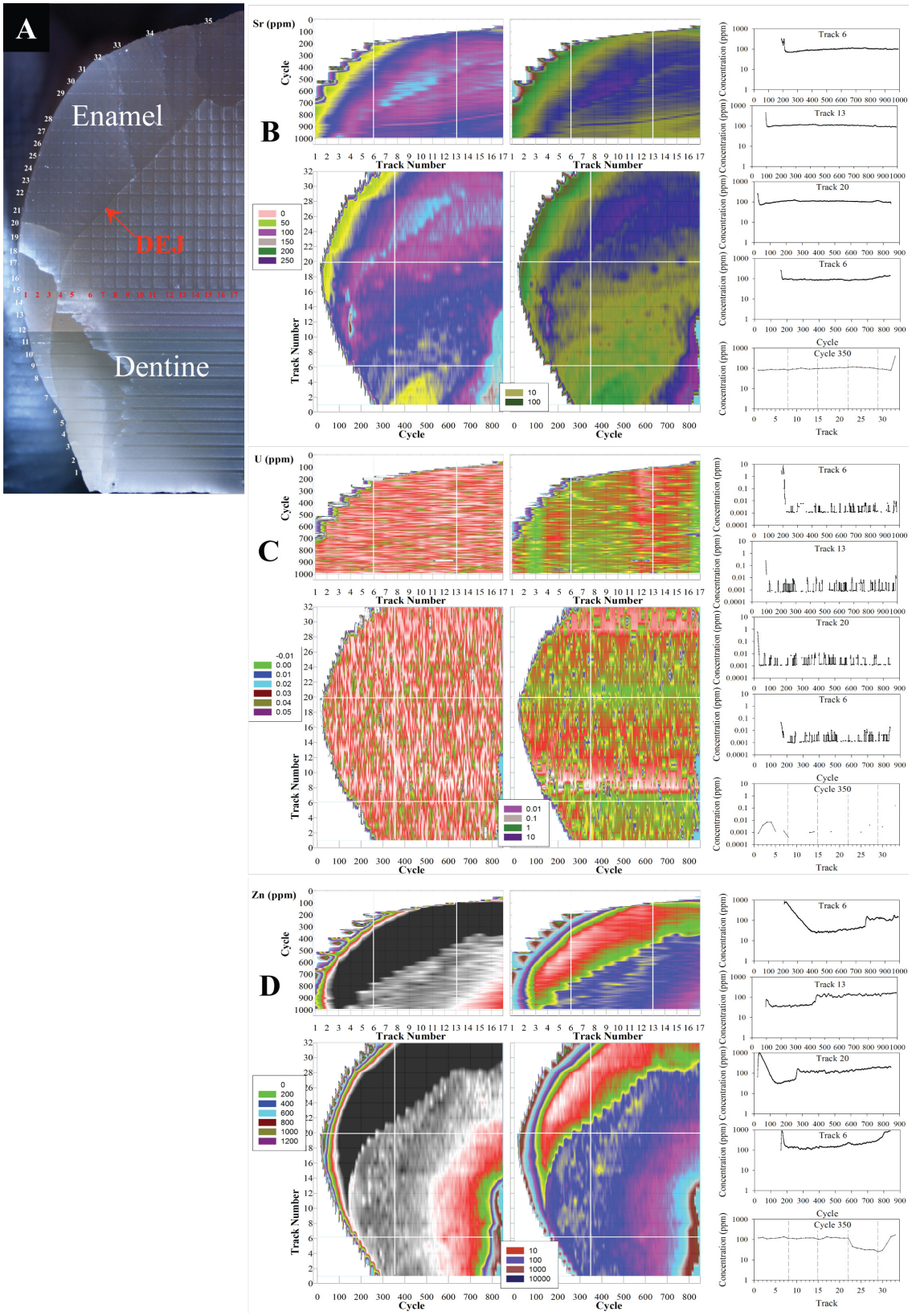

Figure 4-2: Elemental distribution maps of a modern human tooth (RG), A: location of tracks, B-C: Sr, U and Zn element distribution maps (top maps: vertical tracks, below: horizontal tracks; left maps: linear scale, right maps logarithmic scale). Right hand diagrams: selected tracks indicated with the white lines in the respective maps.

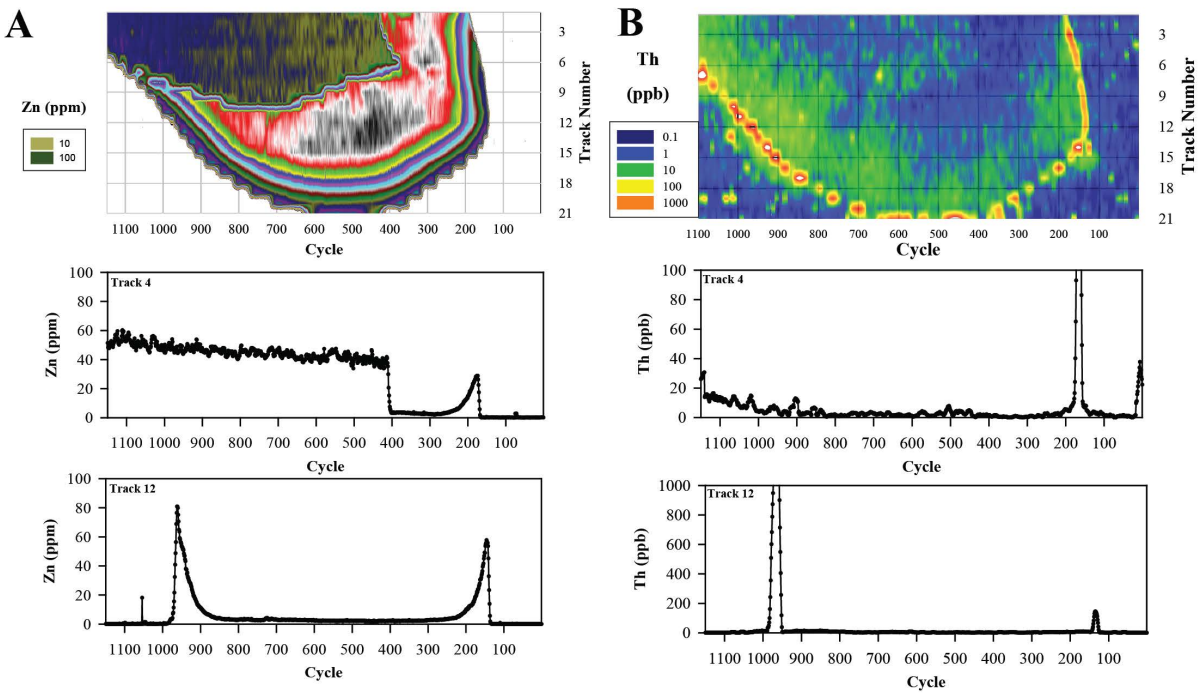

Figure 4-3: A: Zn distribution map (planar view) and selected tracks, B: Th distribution map (planar view) and selected tracks, of the Neanderthal tooth (Payre 1).

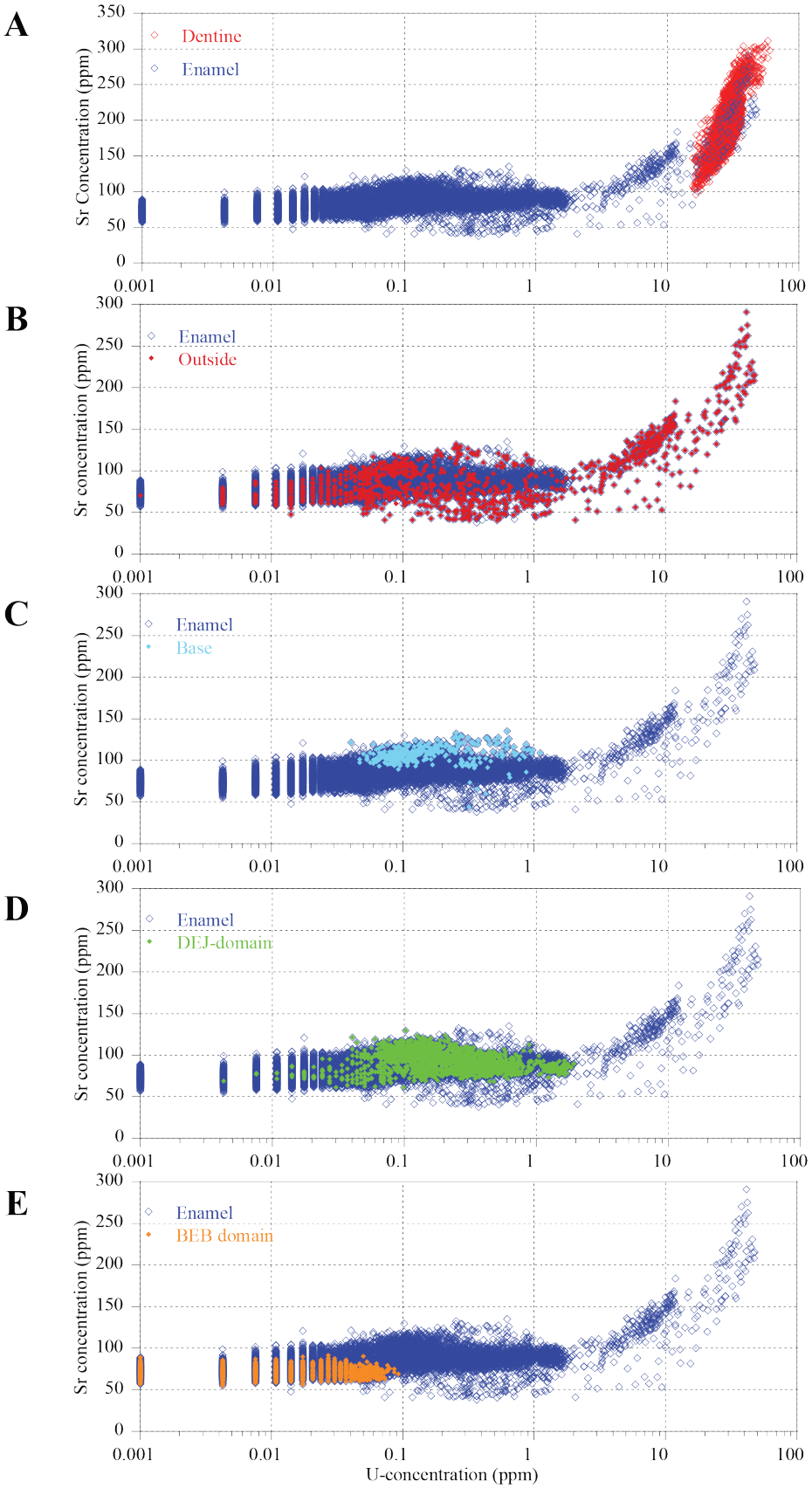

Figure 4-4: Relationship of Sr and U concentrations in different domains of a modern human tooth (RG); Enamel, Dentine, Base, Dentine-enamel junction (DEJ), buccal enamel boundary (BEB).

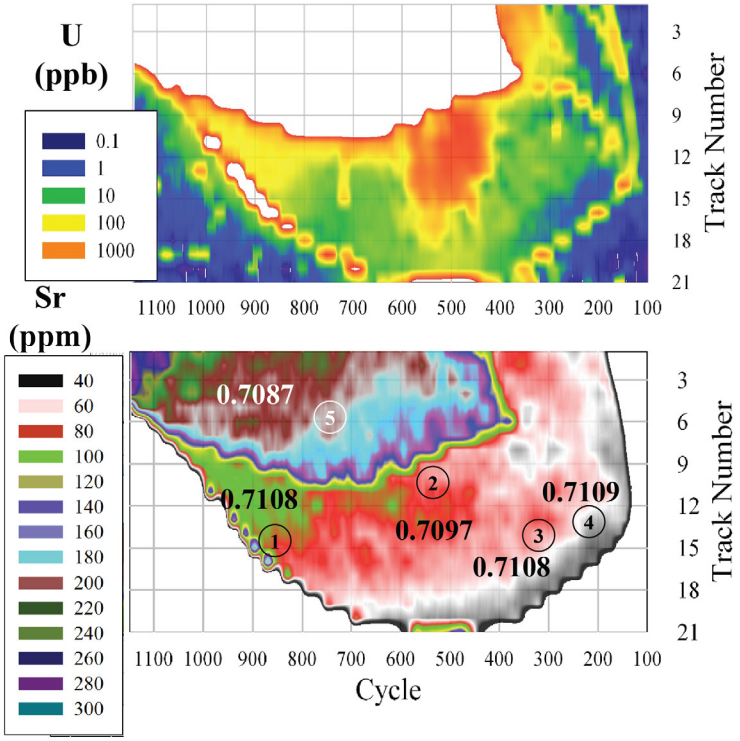

Figure 4-5: U and Sr elemental concentration map and $^{87}Sr/^{86}Sr$ isotopic composition at 5 locations determined by TIMS analysis from the Neanderthal tooth Payre 1. There is a direct relationship between diagenetic overprint as indicated by elevated U concentrations at location 2 and variation in $^{87}Sr/^{86}Sr$ isotopic composition.

4.3.2 Investigating the accuracy of strontium isotope measurements by LA-MC-ICP-MS

In 2007, we created a distribution map of $^{87}Sr/^{86}Sr$ ratios with the aim of resolving the changes of the strontium isotope ratios caused by changes in diet and mobility from the diagenetic overprint. We found a large range of $^{87}Sr/^{86}Sr$ ratios of 0.707 to 0.710 for dentine and 0.712 to 0.718 for enamel (Figure 4-6). Initially, this was interpreted as diagenetic overprint with the end members reflecting the $^{87}Sr/^{86}Sr$ composition of the Jurassic limestone, the bedrock where the tooth was found, and a $^{87}Sr/^{86}Sr$ ratio of around 0.718, thought to be the isotopic signature of the region of origin of this individual (Figure 4-6D). However, further investigations showed that these LA-MC-ICP-MS results, especially in the enamel, are much higher than the $^{87}Sr/^{86}Sr$ ratios determined by micro-drilling TIMS. In conjunction with the observed correlation between increasing $^{87}Sr/^{86}Sr$ ratios and decreasing Sr concentrations (Figure 4-6D) this points to a bias stemming from analytical interferences, most likely the previously identified polyatomic interference on mass 87 (Horstwood et al., 2008; Simonetti et al., 2008; Lewis et al., 2014). This example illustrates that monitoring and, if necessary correcting for this analytical bias, is critical for any interpretation of strontium isotope ratios from teeth in terms of diagenetic overprint or mobility.

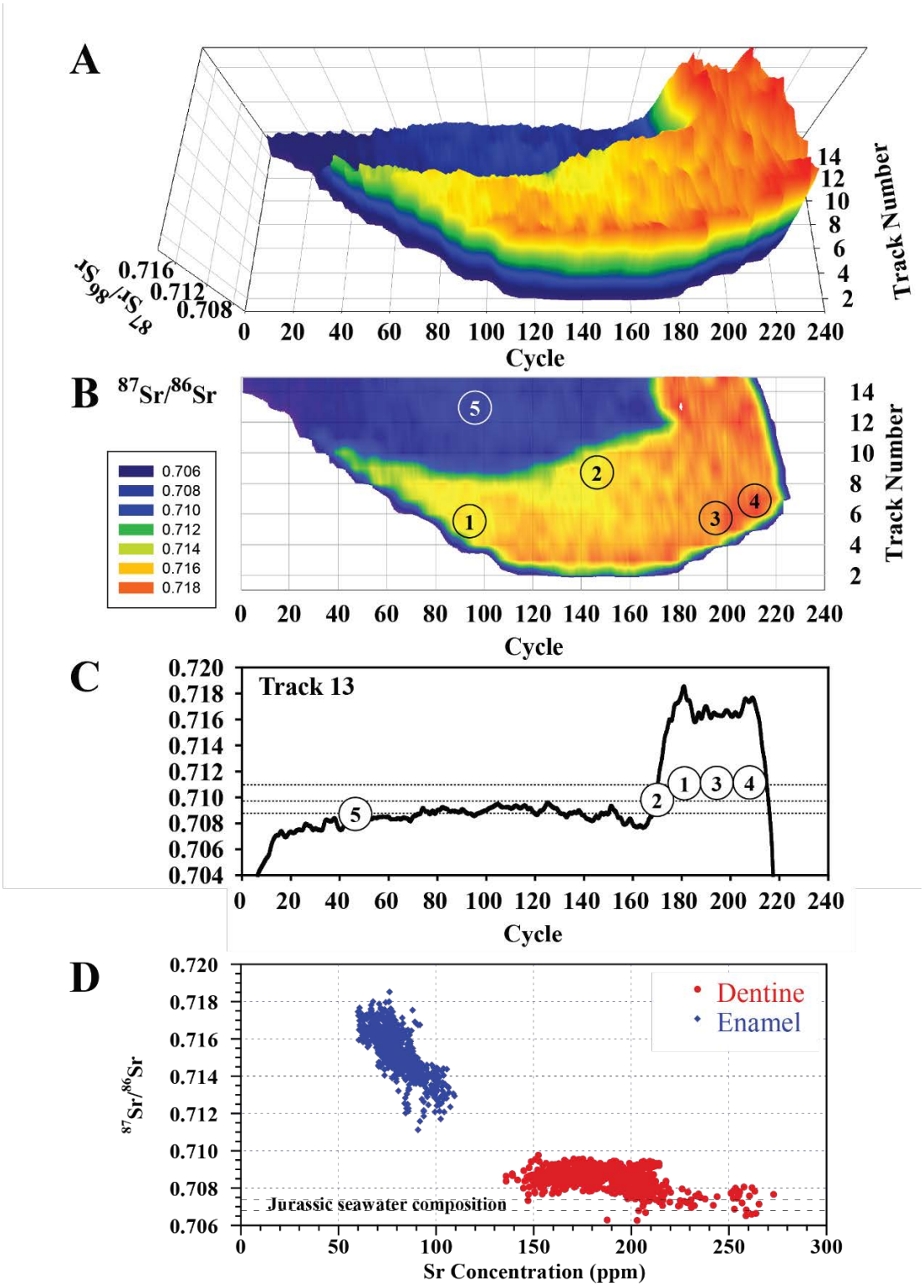

Figure 4-6: A, B: Distribution map of the $^{87}Sr/^{86}Sr$ ratios of the Neanderthal tooth (Payre 1) in oblique and planar view, circles show the positions of the solution TIMS analyses. C: Track 13 with a projection of the TIMS analysis spots and their corresponding $^{87}Sr/^{86}Sr$ ratios. D: Differences between Sr concentrations and $^{87}Sr/^{86}Sr$ ratios in the enamel and dentine.

4.3.2.1 The polyatomic interference on mass 87

A polyatomic interference on mass 87 is suggested to be the main cause of observed offsets between solution and *in situ* analyses of $^{87}Sr/^{86}Sr$ isotope ratios in teeth, observed in many analytical facilities. This interference has been described in the literature as $^{40}Ca^{31}P^{16}O$ (Horstwood et al., 2008; Simonetti et al., 2008). However, a $^{40}Ar^{31}P\ ^{16}O$ interference is also possible as Ar is always present in analysis on a MC-ICP-MS. In order to determine whether this interference originates from Ca or Ar we used solutions of ultra-clean nitric acid mixed with Ca and P in varying concentrations and monitored masses 71 (^{40}Ca or ^{40}Ar, ^{31}P) and 87 (^{40}Ca or ^{40}Ar, $^{31}P^{16}O$). Figure 4-7A, B show that there is a positive correlation between P concentration and the voltage produced on mass 71 and 87. No difference was observed, whether the solutions contained Ca or not (Figure 4-7). This indicates that the polyatomic interference is related to Ar rather than Ca and provides direct evidence of the $^{40}Ar^{31}P^{16}O$ polyatomic compound. Figure 4-7C shows the effect on the measured Sr isotope ratio of the standard solution SRM987, with increasing P concentrations. We observe increasing deviations from the accepted value of this standard, and in the absence of other interferences, are directly attributable to the $^{40}Ar^{31}P^{16}O$ polyatomic compound. Furthermore, in solution analysis, there is a direct relationship between increasing 71/88 ($^{40}Ar^{31}P$), as a measure of relative P to Sr concentration, and the deviation from the accepted $^{87}Sr/^{86}Sr$ isotope ratio of SRM987. This suggests that mass 71 could be used to monitor and correct the polyatomic interference on 87. At 71/88 ratios of >0.05, significant offsets are observed. As the 71/88 voltage increases, this offset becomes larger reaching values of 0.03, dominating the $^{87}Sr/^{86}Sr$ ratio at high P concentrations (Figure 4-7C). The effect of the interference on the $^{87}Sr/^{86}Sr$ ratio is hypothesised to be essentially controlled by the Sr concentration and oxide production rate, which in turn depends on the specific analytical facility used and the instrument conditions during analysis. Both Ca and P are stoichiometric components in bioapatite, and Ar is always present in the plasma, and thus can be assumed to be constant.

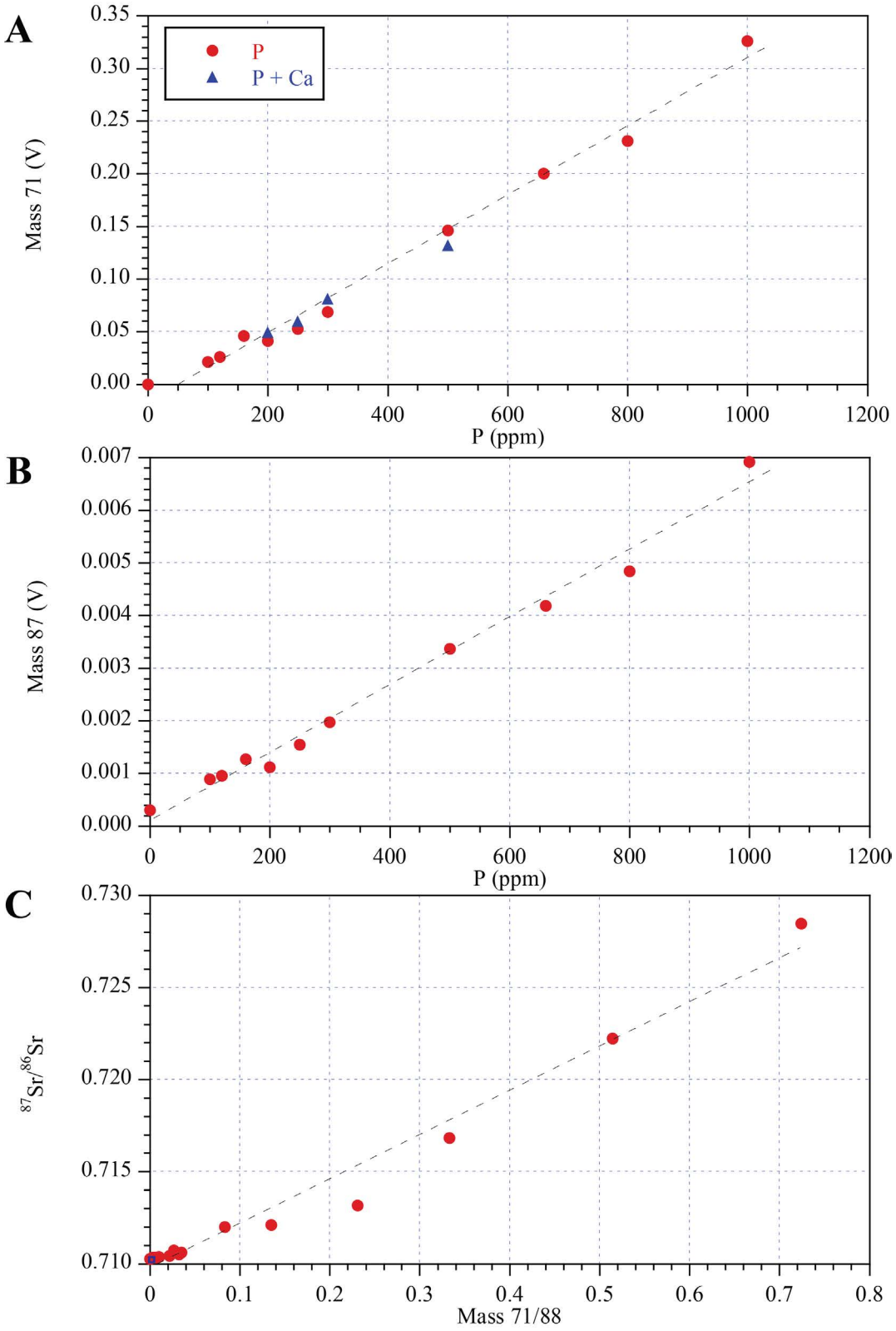

Figure 4-7: A: Signal intensity of Mass 71 (V) plotted against P concentration, B: Signal intensity of Mass 87 (V) caused by the interference plotted against P concentration. P + Ca not shown because the Ca standard contains traces of Sr. C: SRM987 mixed with various P concentrations. Blue square indicates the value of SRM987 without any added P measured during this analytical session 0.71024±2 (n=8, 2σ).

4.3.2.2 *Correcting for the polyatomic interference*

To mitigate the bias arising from the polyatomic interference it is necessary to either reduce the oxide production rate (Foster and Vance, 2006; Lewis et al., 2014), to apply a correction for the interference by using a suitable proxy, or a calibration with known sample materials (Horstwood et al., 2008).

The oxide production rate during laser-ablation MC-ICP-MS analysis depends on the instrument tuning conditions, and the material and element being analysed (i.e. on the metal - oxide bond strength). Changes in oxide production rates caused by the different tuning of the instrument can be monitored for example by measuring UO^+/U^+, in NIST 610 or in a U bearing solution. Horstwood et al. (2008) found an UO^+/U^+ production rate of 0.25% to 1% using a U-solution and oxide production rates of 2.8% during laser-ablation analysis. The oxide production rate is different for solution and laser ablation MC-ICP-MS analyses and is not directly transferable between different analytical setups. It varies greatly between different instruments and analytical facilities. Assuming that the blank corrected voltage on mass 87 in the ultra-clean nitric acid solution is solely caused by the oxide, it is possible to calculate an average oxide production rate from mass 71 ($^{40}Ar+^{31}P$) to mass 87 ($^{40}Ar+^{31}P+^{16}O$) of 2.2±0.56% (n=10, 2σ). We find no positive linear correlation (r=-0.64) between the increase in P concentration and changes in oxide production rate in our solution analysis (Figure 4-8).

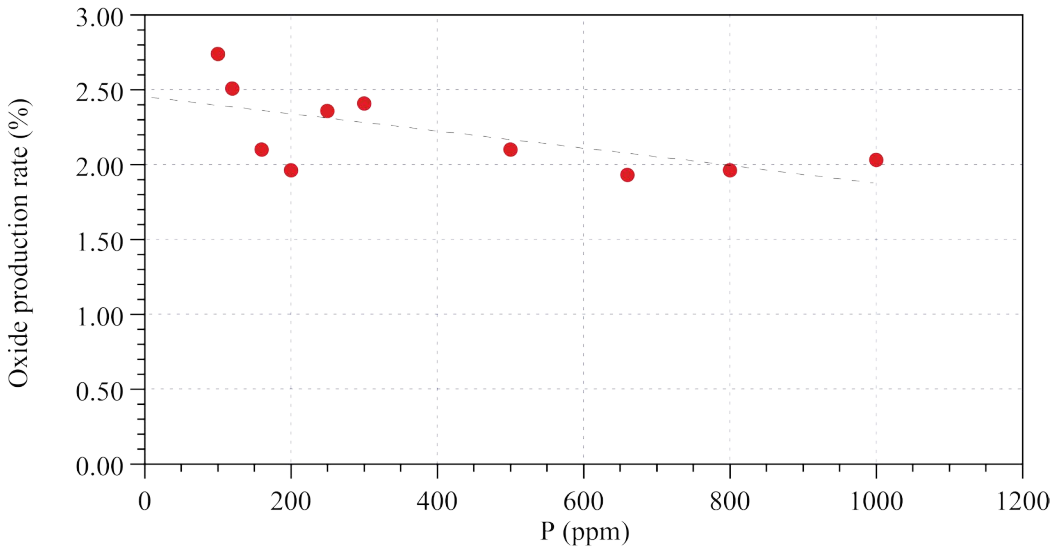

Figure 4-8: Relationship between P concentration and oxide production rate during solution analysis using 2% nitric acid (r= -0.64).

LA-MC-ICP-MS analysis of NIST 610 and monitoring of UO^+/U^+ shows that the oxide production rate is highly dependent on the tuning. Tuning for maximum signal intensity of ^{88}Sr showed UO^+/U^+ production rates of ~1%, but depending on the tuning, rates of up to 7.5% were possible. The oxide production depends on the residence time of the particles in the plasma and thus sample gas flow and position of the torch are hypothesised to be the most sensitive tuning parameter. A low sample gas flow allows the plasma to break down oxides more efficiently, but comes at the expense of decreased signal

intensity. This can be countered by adding nitrogen to the plasma, which increases the energy distribution into the central channel, resulting in a higher signal intensity. Adding 8cc/min nitrogen allows the reduction of the sample gas flow by ~50%, significantly increasing the residence time of the particulates in the plasma. This reduces oxide production rates by 2 orders of magnitude while decreasing the ^{88}Sr intensity by only a factor of 2-3. Possible nitrogen based interferences were checked by running mass scans across the full Sr isotope mass range and none were found.

However, while the tuning of the LA-MC-ICP-MS can be kept the same between a series of analyses, the conditions in the plasma may change due to different loading conditions when analysing different samples. This means that the residual oxide production rate cannot assumed to be constant and may change between samples and should ideally be monitored independently. Since it is not possible to monitor $^{40}Ar+^{31}P+^{16}O$ directly, a proxy for the oxide production rate needs to be used, perhaps mass 89 ($^{40}Ar+^{31}P+^{18}O$), but this has a potential REE interference. In addition, the error magnification from the $^{18}O/^{16}O$ ratio would make this correction problematic. Mass 103.9 ($^{88}Sr^{16}O$) could be used to determine the residual oxide production during each analysis but the production of this oxide is extremely low and very close to the background level of $4.6x10^{-5}$, at Sr concentrations of ~300 ppm. Since the oxide production rates cannot assumed to be constant, and no adequate independent monitor was found, it was not possible to correct for the residual oxide production rate using our analytical setup.

4.3.2.3 Improvement in accuracy

Tuning the instrument for reduced oxide production resulted in an average $\Delta_{LA\text{-}TIMS}$ value of 38±394 ppm (n=21, 2σ) for the human and animal teeth (Figure 4-9 and Table 4-6). This is a significant improvement over our previously obtained data which had an average $\Delta_{LA\text{-}TIMS}$ value of ~3700 ppm. In absolute terms we reduced the average $\Delta_{LA\text{-}TIMS}$ value and now achieve an accuracy of 0.00003±0.00028 (n=21, 2σ). Without tuning for reduced oxide production, the strontium isotope ratios acquired by *in situ* LA-MC-ICP-MS in our laboratory were dominated by the interference of the polyatomic compound. The analyses of the shark and dugong teeth show only slight differences between the different tuning protocols. This is because shark and dugong teeth have much higher Sr concentrations (>1000 ppm) than the human and terrestrial animal teeth (~100s of ppm) and were thus not significantly influenced by the polyatomic interference in the first place. Applying the improved analytical protocol to the Neanderthal tooth (Payre 1) resulted in $^{87}Sr/^{86}Sr$ ratios of 0.70885±10 (±2se) and 0.71084±9 (±2se) for the dentine and enamel (next to spot 3), respectively. These new values are in agreement with the solution TIMS analysis with $^{87}Sr/^{86}Sr$ ratios of 0.70871±8 (±2se) for the dentine, and 0.71094±11 (±2se), 0.71080±5 (±2se), 0.71081±6 (±2se) for the enamel. This indicates that our improved analytical technique now allows the investigation of changes in $^{87}Sr/^{86}Sr$ ratios within a tooth. In terms of mobility, the original LA-MC-ICP-MS values of the enamel would have indicated a vastly different geologic substrate than those obtained by the new analytical protocol or with TIMS

With the new protocol our laser ablation data show both positive and negative offsets from the TIMS value. Figure 4-10 shows increased $\Delta_{LA\text{-}TIMS}$ values at low 88 signal intensities, the result of less precise measurements at low signal intensities. There is a residual positive offset to higher $^{87}Sr/^{86}Sr$ ratios at high 88 signal intensities, indicating a residual production of the polyatomic interference of ~ 59 ppm, for samples > 1V ^{88}Sr. The effect of the polyatomic compound does not correlate with the 71/88 ratio, which could have been a useful monitor as indicated by the solution analysis of SRM987 + P (comparison of Figure 4-7C and Figure 4-10). This is likely because P is a stoichiometric component of the bioapatite in teeth, and thus like Ca, and Ar from the gas, not limited during the analysis on a MC-ICP-MS. Since the isotopic composition in teeth may vary spatially, one expects to find both positive and negative $\Delta_{LA\text{-}TIMS}$ values because it was assumed that a single TIMS values was representative for that part of the tooth. Finally, the $\Delta_{LA\text{-}TIMS}$ values now achieved in our lab (38±394 ppm) are comparable to the results of Lewis et al. (2014), without the need of a customized plasma interface, though at a greater loss of signal intensity.

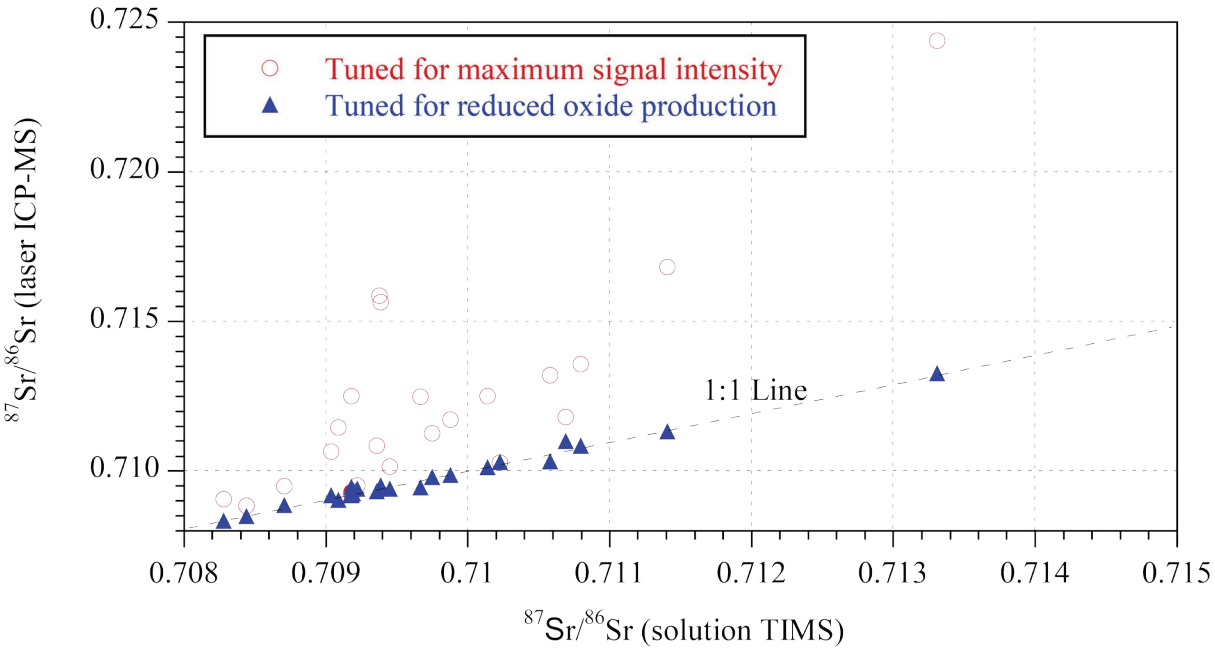

Figure 4-9: Enamel and dentine samples analysed using LA-MC-ICP-MS with tuning for maximum signal intensity (circles) compared to tuning for reduced oxide production (diamonds). Spots for each analysis were directly bordering the TIMS drill spot of each samples used to determine the correct $^{87}Sr/^{86}Sr$ isotope ratio. Analytical errors are smaller than the size of the symbols.

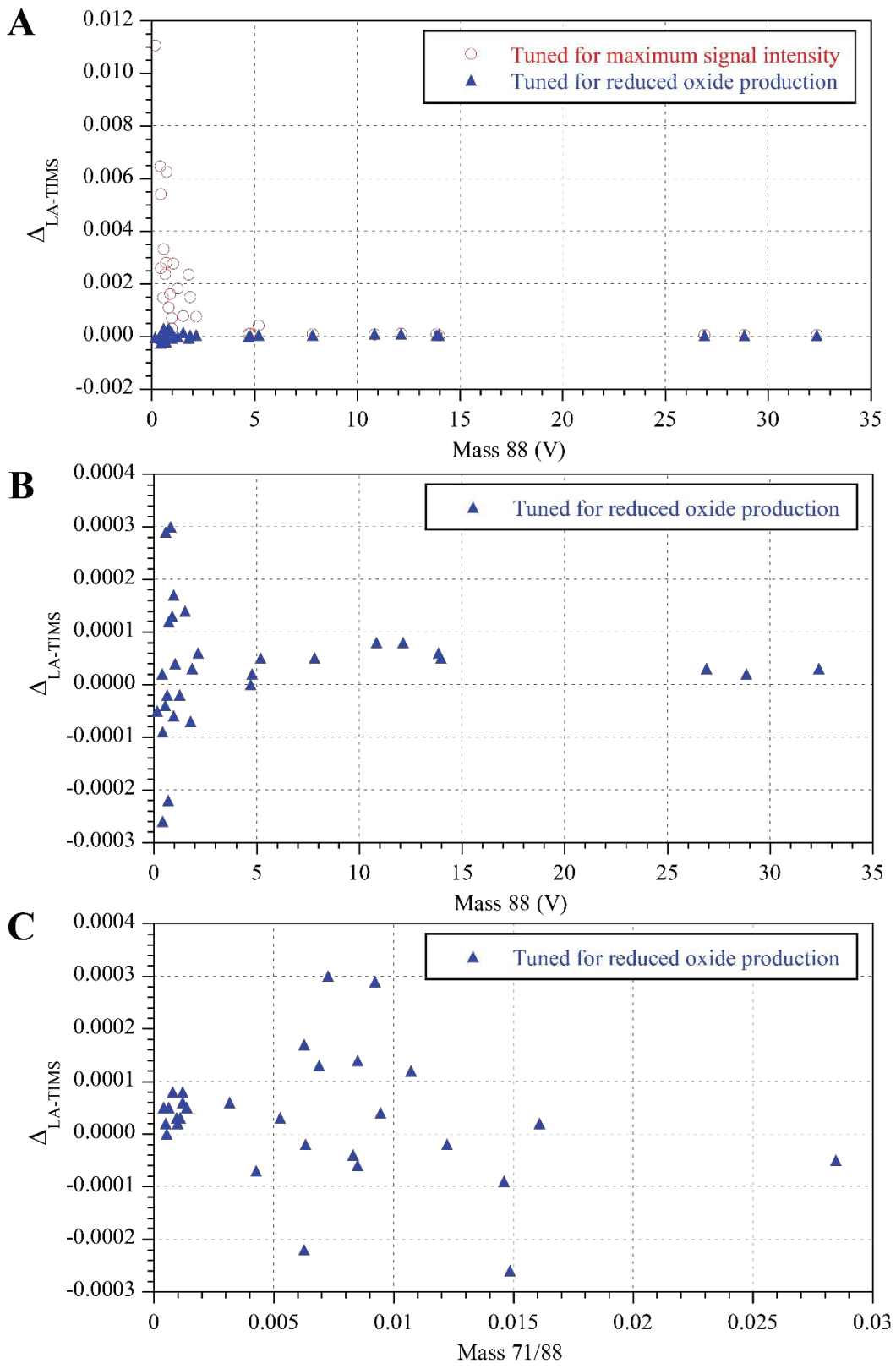

Figure 4-10: A: $\Delta_{LA\text{-}TIMS}{}^{87}Sr/^{86}Sr$ values for the complete dataset plotted against 88 V, B: Expanded $\Delta_{LA\text{-}TIMS}$ values of the dataset tuned for reduced oxide production plotted against 88 V, and C: plotted against 71/88.

Table 4-6: Summary of the TIMS and LA-MC-ICP-MS strontium isotope data for the human and animal tooth samples.

Sample details		TIMS		LA-MC-ICP-MS						LA-MC-ICP-MS 8cc N		Absolute difference		Relative difference (ppm)	
Sample	Sample type	$^{87}Sr/^{86}Sr$	2se	Spot size (µm)	$^{87}Sr/^{86}Sr$	2se	88 (V)	71 (V)	104 (V)	$^{87}Sr/^{86}Sr$	2se	$\Delta_{LA\text{-}TIMS}$	$\Delta_{LA\text{-}TIMS}$ 8cc N	$\Delta_{LA\text{-}TIMS}$	$\Delta_{LA\text{-}TIMS}$ 8cc N
Tum SLM EM 263	dentine	0.70967	0.00003	265	0.71248	0.00013	0.70	0.00440	0.00004	0.70945	0.00010	0.00281	-0.00022	3957	-313
Tum SLM EM 466	dentine	0.71058	0.00004	265	0.71318	0.00020	0.45	0.00675	0.00005	0.71032	0.00021	0.00259	-0.00026	3650	-367
Tum SLM EM 308	dentine	0.70918	0.00002	265	0.71249	0.00030	0.58	0.00534	0.00006	0.70947	0.00011	0.00332	0.00029	4676	407
Tum SLM EM 308	enamel	0.70939	0.00001	265	0.71564	0.00029	0.72	0.00775	0.00003	0.70951	0.00010	0.00625	0.00012	8815	167
Tum SLM EM 282	dentine	0.71014	0.00003	265	0.71249	0.00034	0.65	0.00799	0.00007	0.71012	0.00008	0.00236	-0.00002	3316	-23
Tum SLM EM 282	enamel	0.71141	0.00001	265	0.71682	0.00059	0.44	0.00638	0.00007	0.71132	0.00017	0.00541	-0.00009	7609	-122
Tum SLM EM 432	dentine	0.70936	0.00003	265	0.71083	0.00031	0.56	0.00464	0.00006	0.70932	0.00021	0.00147	-0.00004	2073	-58
Tum SLM EM 432	enamel	0.70938	0.00008	265	0.71584	0.00054	0.42	0.00678	0.00003	0.70940	0.00009	0.00646	0.00002	9104	22
Tum SLM EM 861	dentine	0.70988	0.00002	265	0.71170	0.00016	1.25	0.00791	0.00015	0.70986	0.00006	0.00182	-0.00002	2559	-31
Tum SLM EM 1007	enamel	0.71331	0.00007	265	0.72437	0.00047	0.18	0.00524	0.00004	0.71326	0.00071	0.01106	-0.00005	15505	-76
Tum SLM EM 1251	dentine	0.70904	0.00016	265	0.71064	0.00031	0.90	0.00618	0.00005	0.70918	0.00008	0.00160	0.00013	2251	186
Bovid (1557)	enamel	0.70828	0.00002	265	0.70904	0.00015	2.15	0.00682	0.00016	0.70834	0.00005	0.00076	0.00006	1073	80
Bovid (1557)	dentine	0.70844	0.00002	265	0.70884	0.00008	5.21	0.00714	0.00016	0.70849	0.00002	0.00040	0.00005	566	68
Diprotodon (2104) molar	dentine	0.71023	0.00001	265	0.71026	0.00005	13.99	0.00572	0.00026	0.71029	0.00001	0.00003	0.00005	41	77
Neanderthal Payre 1	dentine	0.70871	0.00008	265	0.70948	0.00019	1.53	0.00959	0.00010	0.70885	0.00010	0.00077	0.00014	1083	204
Neanderthal Payre 1	enamel	0.71080	0.00005	265	0.71356	0.00020	1.05	0.00763	0.00010	0.71084	0.00009	0.00276	0.00004	3880	52
Neanderthal Payre 2	dentine	0.70945	0.00006	265	0.71015	0.00104	0.96	0.00818	0.00009	0.70939	0.00012	0.00070	-0.00006	988	-82
Neanderthal Payre 2	enamel	0.70909	0.00003	265	0.71144	0.00083	1.79	0.00764	0.00011	0.70902	0.00005	0.00235	-0.00007	3307	-101
Neanderthal Payre 3	dentine	0.70975	0.00002	265	0.71125	0.00033	1.86	0.00979	0.00012	0.70978	0.00006	0.00150	0.00003	2107	47
Neanderthal Payre 5	dentine	0.70922	0.00043	265	0.70951	0.00013	0.96	0.00818	0.00009	0.70939	0.00012	0.00029	0.00017	413	242
Neanderthal Payre 5	enamel	0.71069	0.00028	265	0.71179	0.00015	0.82	0.00772	0.00010	0.71099	0.00011	0.00110	0.00030	1543	425
Modern human (RG)	enamel			265	0.71280	0.00020	0.74	0.00826	0.00010	0.70987	0.00004				
Modern human (RG)	dentine			265	0.71091	0.00029	0.67	0.00760	0.00008	0.70995	0.00020				
											Mean	**0.00266**	**0.00003**	**3739**	**38**
Grey nurse shark		0.70918	0.00001	160	0.70927	0.00001	4.73	0.00258	0.00015	0.70918	0.00003	0.00009	0.00000	132	4
				160	0.70929	0.00002	4.78	0.00243	0.00014	0.70920	0.00004	0.00011	0.00002	158	32
				205	0.70926	0.00001	7.83	0.00485	0.00016	0.70922	0.00002	0.00008	0.00005	114	64
				205	0.70925	0.00001	10.85	0.00848	0.00031	0.70926	0.00001	0.00007	0.00008	105	108
Dugong		0.70918	0.00004	265	0.70923	0.00001	32.38	0.03099		0.70921	0.00001	0.00006	0.00003	78	49
				265	0.70922	0.00001	28.86	0.02882		0.70920	0.00001	0.00004	0.00002	57	30
				265	0.70923	0.00002	26.91	0.02951		0.70921	0.00001	0.00005	0.00003	76	47
Dugong		0.70919	0.00004	160	0.70927	0.00001	13.87	0.01665	0.00256	0.70925	0.00001	0.00008	0.00006	113	84
				160	0.70930	0.00002	12.14	0.01468	0.00211	0.70927	0.00002	0.00011	0.00008	157	112
											Mean	**0.00008**	**0.00004**	**110**	**59**

4.3.3 Analytical sampling strategies for fossil human teeth

The recent advancements of *in situ* laser ablation micro-analytical techniques made by a number of studies (Benson et al., 2013; Le Roux et al., 2014; Lewis et al., 2014) and in this research project significantly improve the application of this technique to fossil human teeth.

Scanning for diagenetic overprint can be rapidly applied to a large number of samples to identify teeth that have most likely preserved the original isotopic signatures. In an earlier paper we suggested to use laser ablation drilling for U-series micro-sampling (Benson et al., 2013). Figure 4-11 shows how the laser can be used to probe the enamel BEB domain. The laser holes are 85 µm in diameter and cannot be seen with the naked eye (Figure 4-11A). The uranium profiles can be used to identify the best locations for isotope analysis. From our study, we can develop the following sampling strategies for human teeth that keep any destruction to an absolute minimum. Firstly, the enamel is probed with an 85 µm laser for U, Th and Zn to estimate the depth of surface contamination (Th), to locate the BEB domain (Zn) and to evaluate diagenetic contamination (U). Intra-tooth isotopic variation can be investigated either along already broken surfaces, or possibly by sequential laser drilling similar to the U-series analysis (Benson et al., 2013). Once a suitable sample has been selected, different analytical methods can be applied to analyse its strontium isotopic composition.

In situ spot analysis for LA-MC-ICP-MS and micro-drilling for TIMS cause comparable damage (Figure 4-11B), on the same scale as most surface impurities such as scratches, cracks and dirt. However, for the study of intra-tooth isotopic variations, and a large number of samples, TIMS analysis can be prohibitively labour intensive and time consuming. In addition, TIMS analysis may average intra-tooth isotopic variation depending on the amount of material required and the size of the micro-drill. LA-MC-ICP-MS presents a valuable alternative because it allows for a high sample throughput, requires minimal sample preparation, and enables the investigation of intra-tooth isotopic variability at high spatial resolution. Intra-tooth isotopic variation can be investigated either along already broken surfaces, or possibly by sequential laser drilling similar to the U-series analysis (Benson et al., 2013).

The potential of the polyatomic interference on mass 87 during LA-MC-ICP-MS analysis varies between different analytical facilities. Changes in instrument conditions (laser cell design, gas sources, cones and torch design) can have a significant effect, and thus this interference should be monitored during each study. If present, tuning to minimise the oxide levels, is currently the most promising way for achieving accurate $^{87}Sr/^{86}Sr$ isotope ratio measurements from teeth using LA-MC-ICP-MS (this study, de Jong et al., 2007; Lewis et al., 2014). Monitoring and tuning to minimise $\Delta_{LA\text{-}TIMS}$ should be performed on a well characterised tooth standard with low Sr concentration (~100-300 ppm), in the same range as the unknown samples (e.g., Copeland et al., 2010, 2008; Le Roux et al., 2014).

Finally, the level of precision required to relate human samples to strontium isotope regions in the landscape will vary considerably between different geologic terrains. LA-MC-ICP-MS analysis with

the accuracy range obtained here is sufficient for human mobility studies between most geologic terrains (e.g., Hodell et al., 2004; Evans et al., 2010; Frei and Frei, 2011; Bataille and Bowen, 2012; Willmes et al., 2014) and thus offers an alternative to solution analysis. This allows the application of this method to a large range of archaeological samples, which in turn will significantly improve our understanding of human and animal mobility and ranging patterns in the past.

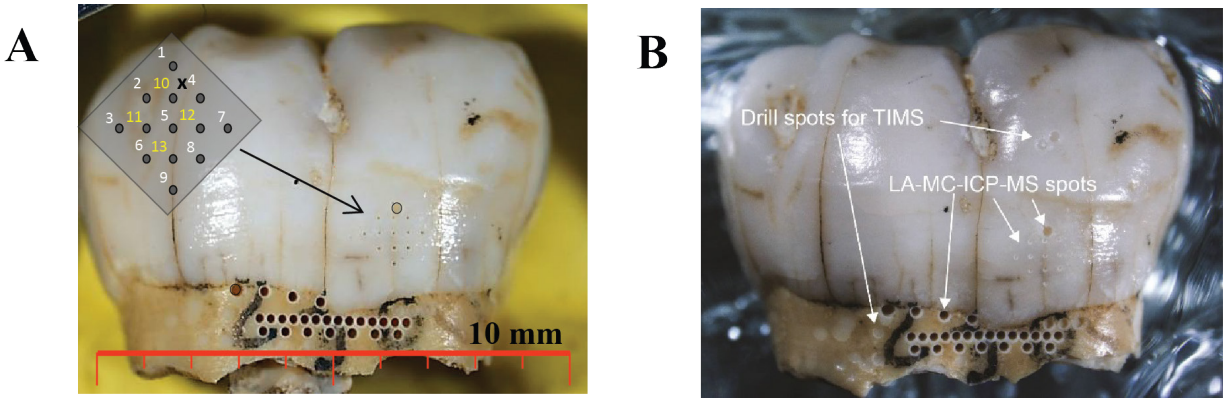

Figure 4-11: Neanderthal tooth from Moula-Guercy (Benson et al., 2013) as an example of the overall damage done to a tooth for isotopic analysis. A before and B after strontium isotope analysis by LA-MC-ICP-MS and drilling for solution TIMS. The row of holes in the dentine were used for U-series dating and are not related to the strontium isotope analysis.

4.4 Conclusions

The main conclusions from this project are:

(1) Using *in situ* LA-ICP-MS for U, Th, Sr and Zn concentrations in fossil teeth allows for rapid screening to identify zones of least diagenetic overprint. This method limits damage to the sample and ensures that only suitable samples are further processed for isotopic analysis.

(2) The polyatomic interference on mass 87 is the principal cause for the offset between solution and LA-MC-ICP-MS strontium isotope analysis observed in a significant number of analytical facilities. We found direct evidence that this interference originates from Ar, rather than Ca compounds. The effect of the interference on the $^{87}Sr/^{86}Sr$ isotope ratio is essential controlled by the Sr concentration and oxide production rate, because both Ca and P are stoichiometric components in bioapatite, and Ar is always present in the plasma.

(3) The oxide production rate in LA-MC-ICP-MS analysis varies between different analytical facilities, analytical conditions of the instrument, and the sample being analysed. No suitable proxy was found in this study to determine the oxide production rate during the analysis of a tooth independently, prohibiting online correction of potential oxide related interferences.

(4) Monitoring for this interference, and if present, tuning for reduced oxide levels is currently the most promising way to obtain accurate $^{87}Sr/^{86}Sr$ isotope ratio measurements from teeth using LA-MC-ICP-MS. We achieved $\Delta_{LA\text{-}TIMS}$ values of 38±394 ppm (n=21, 2σ). This analytical offset is small, particularly when considering the variability of $^{87}Sr/^{86}Sr$ isotope ratios in the environment.

(5) LA-MC-ICP-MS analysis of fossil human teeth can be used to investigate intra-tooth strontium isotopic variability and relate it to diagenetic alteration or changes in food source, thus providing a powerful technique to investigate diet and mobility patterns in archaeology.

5 Archaeological case studies

5.1 Introduction

The archaeological sites investigated in this research project are not connected through their time period or geographic location (Figure 5-1). They represent case studies to test the application of strontium isotopic tracing under a variety of different archaeological contexts and geologic settings. The strontium isotope tracing conducted at the archaeological sites is part of larger projects including dating and dietary reconstruction. At the Neanderthal site of Moula-Guercy we established a robust chronology of the site and used strontium isotopes to reconstruct the mobility of two Neanderthal individuals and one Neolithic individual. The Neolithic site of Le Tumulus des Sables was subject to a large project including new radiocarbon dating, and combined multi-isotope reconstruction of diet and mobility using strontium, oxygen (James et al., 2013), nitrogen and carbon isotopes. Finally, the study at La Grotte des Perrats is an ongoing investigation and only the newly obtained strontium isotope data on human remains is presented here.

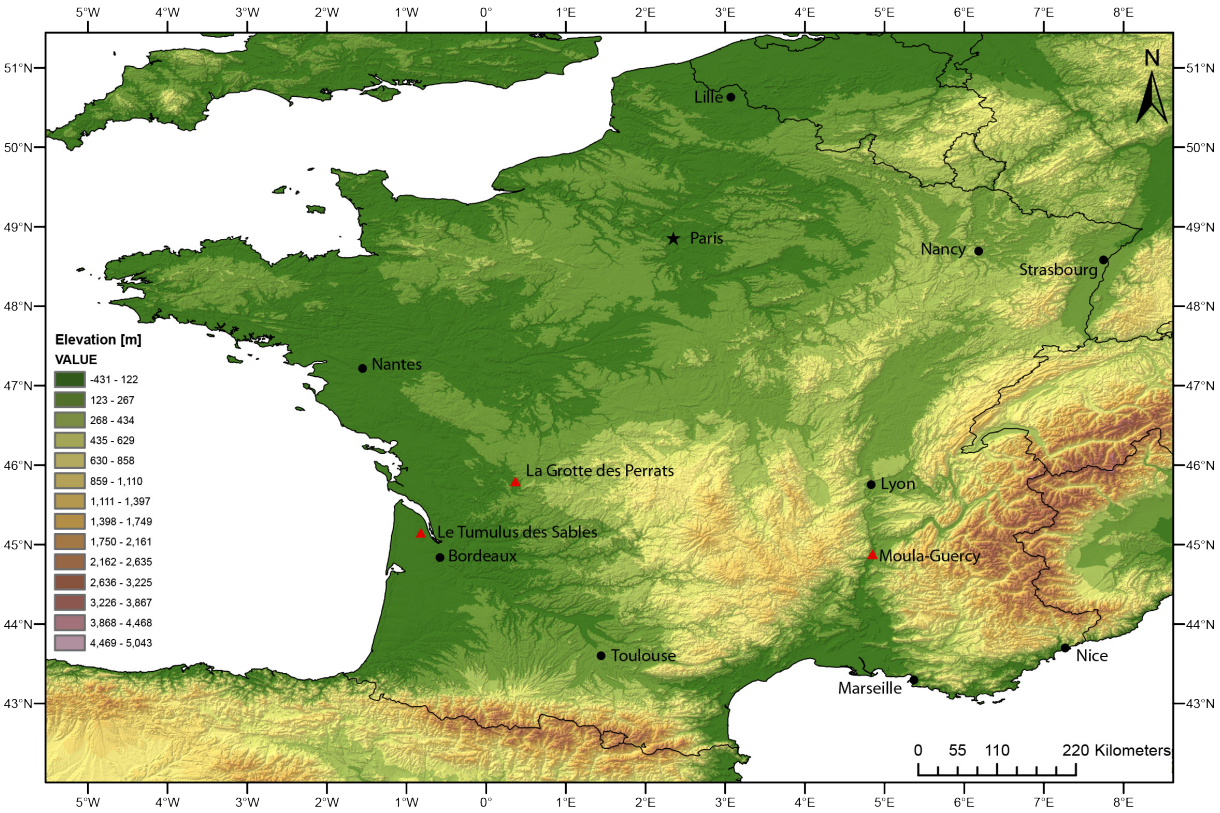

Figure 5-1: Location of the archaeological sites investigated in this research project. Elevation map for France created from data of worldclim.org (Hijmans et al., 2005).

5.2 Moula-Guercy

This chapter is in preparation to be submitted to PLOS ONE

M. Willmes, R. Grün, K. Douka, V. Michel, R. A. Armstrong, A. Benson, E. Crégut-Bonnoure, E. Desclaux, F. Fang, L. Kinsley, T. Saos, A. R. Defleur (in preparation), Chronology and human mobility at the Neanderthal site of Moula-Guercy (Ardèche, France). PLOS ONE

The author's contribution to the publications is as follows: The author conducted the strontium isotope analysis. The chronology studies were conducted in collaboration with all co-authors under the direction of R. Grün. The article was written jointly by the author and R. Grün with suggestions and corrections from all co-authors.

Abstract

The Baume (cave) Moula-Guercy, in southeast France, contains an important sedimentary sequence, which includes the remains of a cannibalised group of Neanderthals. For the upper layers of the cave a tephra deposit (layer VI) has been dated to 72±12 ka using thermoluminescence. The middle and lower layers of the cave have been constrained by biostratigraphy, pointing towards MIS 5.5 for the Neanderthal bearing layer XV. In order to refine the chronology of the site, we applied radiocarbon, $^{40}Ar/^{39}Ar$, U-series and ESR dating analyses. Radiocarbon dates on bone samples from the upper layer (IV) showed ages older than 50 ka. $^{40}Ar/^{39}Ar$ dating on sanidines reveals, that these volcanic minerals derived probably from the Hercynian basement, and thus provided no tangible chronological constrain. Combined US-ESR results on faunal teeth place layer IV at 61±8.5 ka, layer VIII at 66 ±4 ka, layer XIV at 83.5 ±20 ka, and layer XV at 119±13 ka. Direct U-series analyses on two Neanderthal teeth shows, that U-mobilisation even into small teeth is highly complex, but nevertheless indicates that the Neanderthals could correlate to MIS 5.5. In addition, we carried out strontium isotopic analysis ($^{87}Sr/^{86}Sr$) on two Neanderthal and one Neolithic teeth to investigate childhood residence and mobility. Strontium isotope ratios of two the Neanderthal teeth suggest a childhood food source within the Rhône valley and exclude the Massif Central. This provides direct support for the archaeological evidence, which suggests that Moula-Guercy was used by mobile hunter-gathers as a specialised hunting site for the gregarious herbivores of the Rhône valley, when they were seasonally abundant in this area. The Neolithic individual, with a strontium isotope ratio indicative of young volcanic units, presents a strong case for mobility. The closest volcanic units occur ~30 km south east of Moula-Guercy, another possible childhood residence area for this individual are the larger occurrences of these units in the Massif Central ~50-80 km to the west of the cave. In either case this individual experienced significant mobility in its lifetime.

5.2.1 Introduction

The Baume (cave) Moula-Guercy is located 80 m above the west bank of the Rhône River near the city of Valence, southeastern France, in the parish of Soyons, Ardèche (Figure 5-2). The archaeological site was discovered in 1970 and excavated in two phases: between 1975 and 1982 by an amateur archaeologist. After a 1 m^2 test pit was dug in 1991, systematic excavations were carried out between 1993 and 1999 by A.R. Defleur.

The earlier excavation from 1975 to 1982 removed about 100 m^3 of Mousterian sediments, destroying much of the upper section of the sequence, and reached down to the mid of layer XIV (the stratigraphy is shown in Figure 5-3). This campaign yielded only two Neanderthal teeth that cannot be attributed with certainty to any level. The 1991 test pit, starting at the base of the previous excavation more than 5 m below the surface, yielded 13 Neanderthal remains, some of which showed cut marks and evidence of fractures of fresh bones (Defleur et al., 1993). The follow-up excavations yielded 119 human remains from layer XV representing at least six individuals: two adults - a large older male individual and a smaller one, possibly a female, two adolescents most likely female and two children aged between four and seven years (Defleur et al., 1999). DNA analyses of the material did not yield any results due to the difficulty in extracting any organic material from the examined fossils (pers. comm. S. Pääbo to A.R. Defleur, 15 August 2013).

Anatomical studies on the crania and mandibles (Guipert and Defleur, n.d.), teeth (Hlusko et al., 2013) and postcranial remains (Mersey et al., 2013a, 2013b), identified characteristic Neanderthal traits, while no evidence for the presence of any of other hominid taxa was found. Detailed forensic examinations on the human remains showed that all individuals, including a 4 year old child, had been cannibalised. The skulls had been skinned and the pericranium removed before fracturing. All muscles from the crania, mandibles, limbs were removed. Shoulders, elbows, feet and hands were disarticulated and all bones with marrow were systematically fragmented, while those without marrow were not (Defleur et al., 1999, 2014). Human remains were only found in Layer XV, apart from Neolithic graves dug into upper layers, and the two Neanderthal teeth uncovered during the initial excavation.

Thermoluminescence dating on quartz from layer VI provided an age of 72±12 ka (Sanzelle et al., 2000). This was used to correlate this tephra layer with two other volcanos in the Ardèche: le Ray-Pic with TL dating on plagioclases: 77±10 ka and/or le Pic de l'Etoile with TL dating on plagioclases: 83±9 ka (Guérin, 1983; Guérin and Gillot, 2007). The first one is characterised by abundant mineral of basement olivines and shows a strong mineralogical similarity with those found at Moula-Guercy (Debard and Pastre, 2008). Using studies of large mammals, rodents, reptiles and amphibians the remainder of the layers are placed in the general biochronology of Europe. In order to corroborate the existing chronological framework of the whole sedimentary sequence, in particular the crucial layer XV, we carried out a range of radiometric dating analyses. In the following sections we first give a brief description of the stratigraphy, lithics, biostratigraphy, followed by our new dating and isotope analyses.

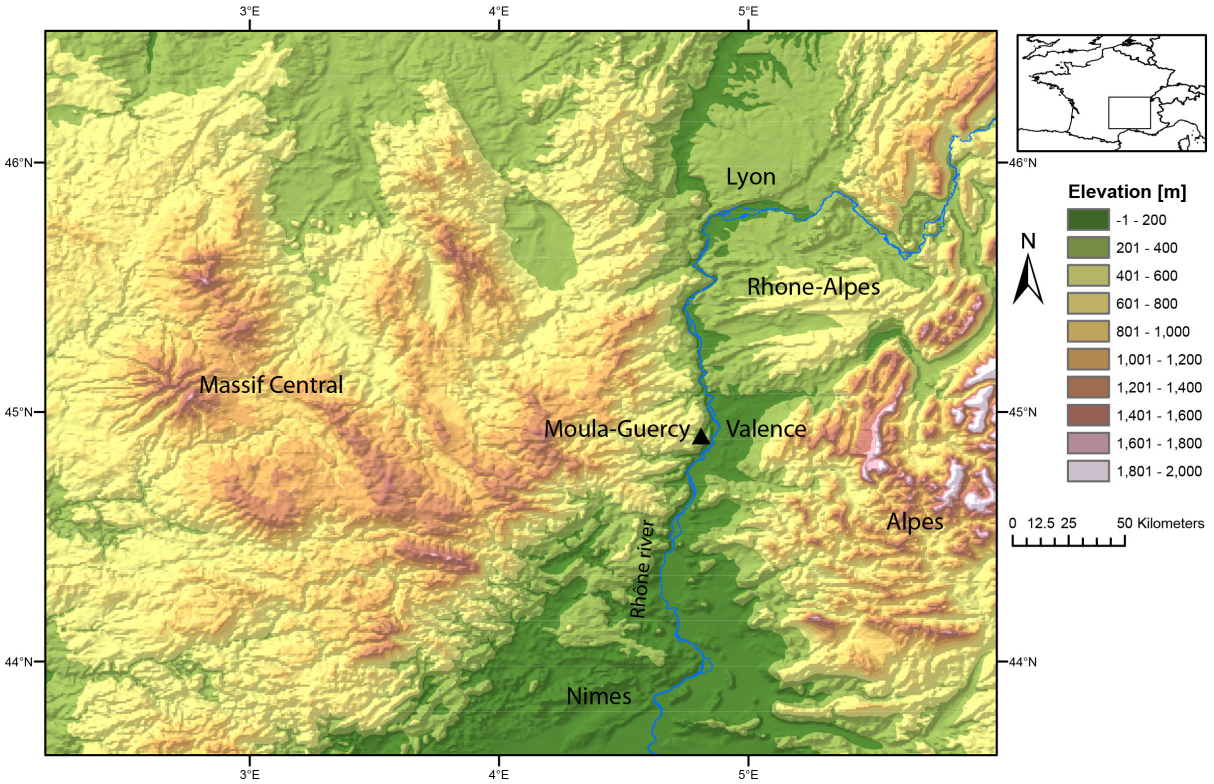

Figure 5-2: Geographical location of the Moula-Guercy Cave. Elevation data from worldclim.org (Hijmans et al., 2005).

5.2.2 The site of Moula-Guercy

5.2.2.1 Stratigraphy

The stratigraphy of Moula-Guercy has been investigated in detail by Saos et al. (2014) and an overview is shown in Figure 5-3. All depths refer to below datum and the bedrock has not been reached during the excavations. The description of the excavated sections and the sedimentological analysis of the cave infilling (Saos, 2003; Saos et al., 2014) allow the distinction of three major depositional complexes, which are further subdivided into layers, some of which include archaeological levels. The lower stratigraphic complex comprises of layers XIX to XVI from the base to 610 cm below datum, and is only exposed in the pit near the west wall (see inset in Figure 5-3). The sediments are mainly sandy with limestone blocks. The middle stratigraphic complex (from 610 cm to about 400 cm) begins with layer XV, which yielded numerous human remains, and ends with layer XI. All layers are sloped (up to 30º) towards the north. The upper stratigraphic complex (from 400 cm to 0 cm) is only exposed at the entrance of the cavity, since it was strongly affected by previous excavations. The sedimentological sequence can be interpreted as follows: the lower complex represents an active karst system with alluvial deposits from sands to small limestone pebbles. The sediments indicate a cold climate (Saos et al., 2014). With the onset of the deposition of the middle stratigraphic complex, the cave opened to the outside.

During this time the cave dried out and the infill is characterised by cave wall fragments and the matrix is dominated by windblown sediments. Importantly, the cave becomes inhabited by animals and men. The sediments indicate a warmer climatic phase. Finally, the upper sedimentological complex shows solifluction in a periglacial environment (Saos et al., 2014).

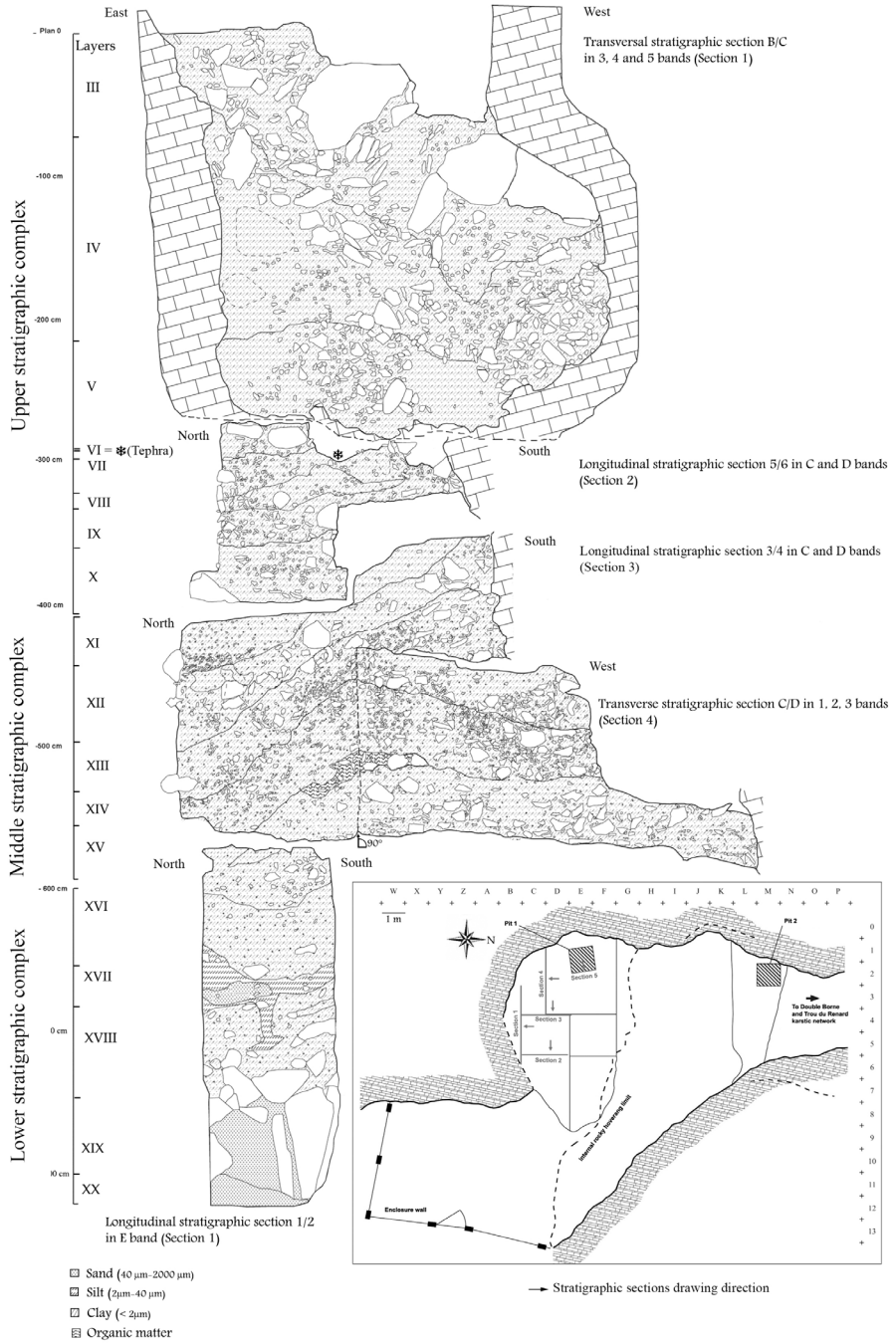

Figure 5-3: Cave plan and locations of the cross sections (Saos et al., 2014).

5.2.2.2 Lithics

The more recent excavations yielded a total of 2595 lithic artefacts from 11 layers, 1294 of which were larger than 25 mm (Defleur, 2015). The vast majority of the lithics, 92.3 %, were found in four layers (IV, VIII, XIV and XV). The lithics of layers IV and VIII are technologically and typologically distinct from those of XIV and XV. 225 chips larger than 25 mm and 57 retouched tools were found in layer XV. The débitage belongs to the same family of Levallois/discoidal technology (Bordes, 1961). Over 30 % of the lithic materials have been identified to come from ~40 km south of the Rhône River between the municipalities of Meysse and Rochemaure), which contains high quality flint (Defleur, 2015). Due to the significant distance of these sources and the use of small flint pebbles and siliceous limestone from the alluvium of the Rhône river, Levallois débitage is low, but of good quality. The few tools are dominated by simple, transverse and convergent scrapers.

5.2.2.3 Biostratigraphy

Based on the detailed paleontological studies of macrofauna, microfauna, reptiles and amphibians (Desclaux and Defleur, 1997; Defleur et al., 2001, 2014; Cregut-Bonnoure et al., 2010) the stratigraphic layers can be divided into three major climatic phases.

The lower stratigraphic complex does not contain any macrofauna, but a large number of micromammal remains (*Dicrostonyx torquatus*, *Microtus gregalis*, *Sicista betulina*), indicating cold, steppe environmental conditions.

The middle stratigraphic complex is a thick homogenous deposit and contains diverse faunal remains. Layers XIV and XV contain cultural remains including a lithic assemblage, fireplaces, charcoal and abundant fauna such as red deer (*Cervus elaphus)*, alpine ibex (*Capra ibex),* gazelle (*Dama* sp.), straight-tusked elephant (*Palaeoloxodon antiquus*,) rhinoceros (*Dicerorhinus hemitoechus)* and many carnivores. Layers XIV to XII contain wolf (*Canis lupus*) remains that are intermediate between Late and Middle Pleistocene. Furthermore, the bear lineage *deningeri-spelaeus* is dominated by the more primitive character of *Ursus deningeri*, the presence of *Ursus thibetanus* in association with brown bear (*Ursus arctos*), badger (*Meles meles*) and wildcat (*Felis silvestris*) is similar to other interglacial sites (Cregut-Bonnoure et al., 2010).

The upper stratigraphic complex contains *Mammuthus primigenius*, *Rangifer tarandus*, *Dicrostonyx torquatus*, *Microtus* (*Stenocranius*) *gregalis* which is also indicating a cold phase. In addition, these layers contain wolf remains whose evolutionary stage is typical for the Upper Pleistocene, bear and hyena species typical for European Würm cave sites, as well as red deer (*Cervus elaphus)* similar to species during the Würm in the southwest France.

The cenogram method (Legendre, 1986, 1988), has been successfully applied to southern France Pleistocene communities (Montuire and Desclaux, 2008) and can be used to investigate the nature of the environment. For Moula-Guercy, the results of the cenogram method are summarised in Table 5-1

and Figure 5-4. We find an opening of the environment from the basis (level XV) to the top (level IV) of the sedimentary sequence. With a regular and continuous slope and no important gap in body mass, the cenogram obtained for the level XV indicates a closed and humid environment, which is representative of a temperate forest and characteristic of an interglacial period in Europe, indicating MIS 5.5. Layers XIV and XIII show similar cenograms, but with a smaller number of species, indicating more arid conditions. This trend continuous in Layer XII. Overall, there is a trend towards an open landscape from layer XI-X to IV, where based on the scarcity of medium-weight species, the environment is interpreted to be open and the climate more arid and cold. These levels may be assigned to earlier stages of MIS 5 or to MIS 4 (Montuire and Desclaux, 2008).

The chronological and environmental deductions from the sedimentology, microfauna and macrofauna are in agreement. They allow a preliminary association of the lower stratigraphic complex to MIS 6, the middle stratigraphic complex MIS 5 and the upper stratigraphic complex MIS 4. Apart from the Neolithic human graves at the top of the sequence, all other human remains from the site come from layer XV in the middle stratigraphic complex. The fauna of layer XV shows the first occurrence of fallow deer and its other faunal elements can be correlated to MIS 5.5 interglacial sites in the Mediterranean area. Similar results were suggested by the study of rodent remains. The presence of *Hystrix vinogradovi*, in association with three species typical of the Middle Pleistocene (*Allocricetus bursae*, *Pliomys lenki* and *Microtus* (*Iberomys brecciensis*) not encountered in association with any late Pleistocene levels in Mediterranean Europe so far, further point towards MIS 5.5. A recent study on amphibians and reptiles provide additional support to this chronological attribution (Manzano, 2015). Furthermore, the marked persistence of taxa characteristics of a continental climate and an open environment, such as *Marmota marmota*, *Microtus* (*Stenocranius*) *gregalis* and *Spermophilus citellus*, suggests that this level is contemporary of the start of the early late Pleistocene temperate climatic oscillation. A detailed taphonomic analysis of the larger mammals from Layer XV (Valensi et al., 2012) concluded that many animal remains were brought to the site for consumption. The faunal remains were processed in the same way as the human remains for food extraction (Defleur et al. 1999, Defleur et al., 2014).

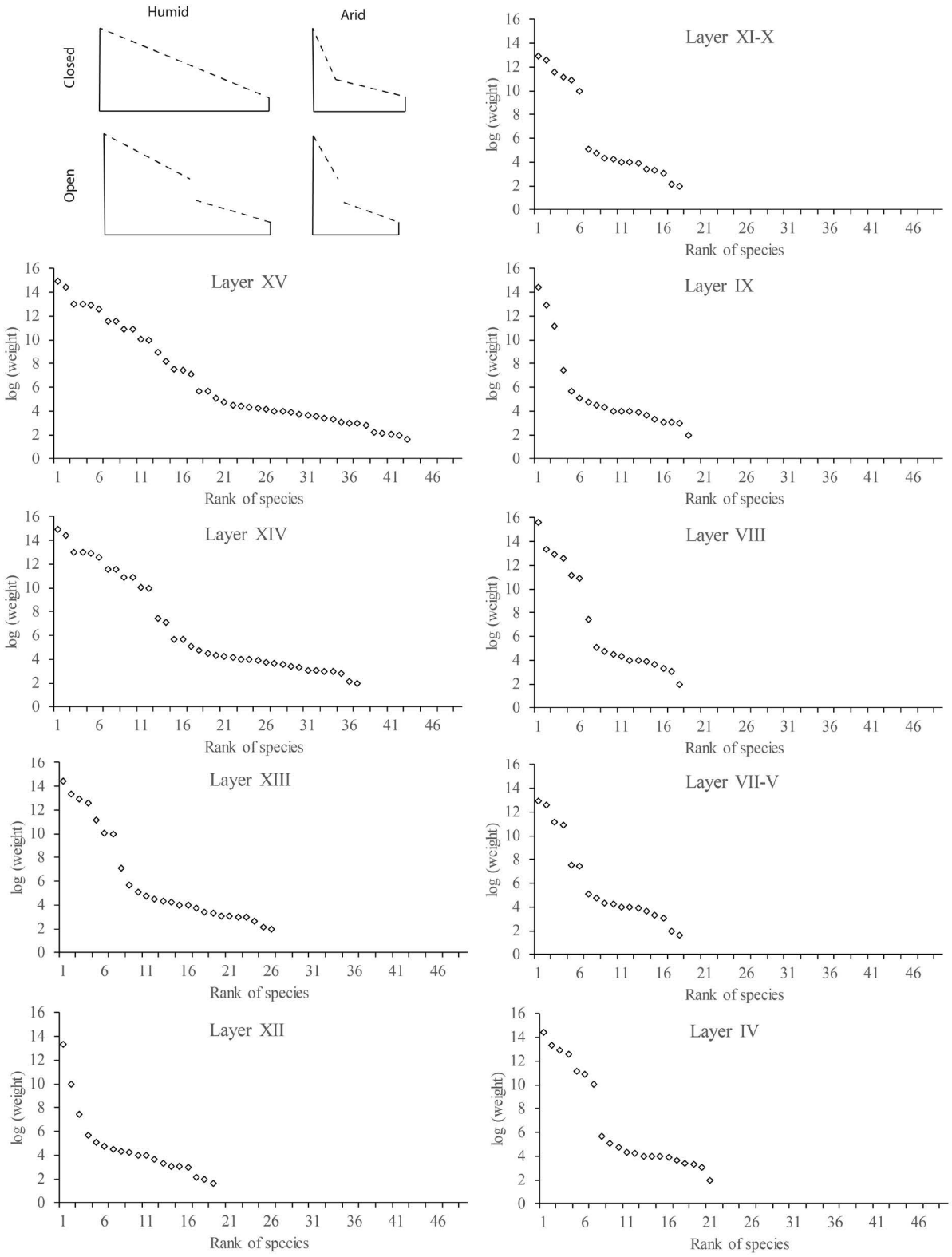

Figure 5-4: Cenograms of the layers of Moula-Guercy.

Table 5-1: Cenogram method results.

Species	Log (weight)	XV	XIV	XIII	XII	XI-X	IX	VIII	VII-V	IV
Mammuthus primigenius	15.61							+		
Palaeoloxodon antiquus	14.95	+	+							
Dicerorhinus hemitoechus	14.43	+	+	+			+			+
Equus caballus	12.88	+	+	+		+	+	+	+	+
Sus scrofa	11.55	+	+			+				
Bos/Bison	13.30			+	+			+		+
Bos primigenius	13.01	+	+							
Megaloceros giganteus	13.00	+	+							
Cervus elaphus	12.59	+	+	+		+		+	+	+
Rangifer tarandus	11.56	+	+	+		+	+	+	+	+
Capra caucasica	10.90	+								
Dama sp.	10.88	+	+							
Capra ibex	10.86		+			+		+	+	+
Rupicapra sp.	10.03	+	+	+						+
Capreolus capreolus	9.99	+	+	+	+	+				
Hystrix cf. *vinogradovi*	8.99	+								
Lepus sp.	8.16	+								
Marmota marmota	7.55	+							+	
Oryctolagus cuniculus	7.47	+	+		+		+	+	+	
Erinaceus europaeus	7.08	+	+	+						
Sciurus vulgaris	5.70	+	+	+	+					+
Citellus citellus	5.67	+	+				+			
Arvicola sapidus	5.08	+	+	+	+	+	+	+	+	+
Arvicola terrestris	4.79	+	+	+	+	+	+	+	+	+
Glis glis	4.53	+	+	+	+		+	+		
Pliomys lenki	4.38	+								
Eliomys quercinus	4.28	+	+	+	+	+			+	+
Talpa europeaa	4.31	+	+	+	+	+	+	+	+	+
Microtus (I.) brecciensis	4.19	+	+							
Microtus agrestis	3.97	+	+	+	+	+	+	+	+	+
Microtus oeconomus	3.96	+	+	+	+	+	+	+	+	+
Dicrostonyx torquatus	3.95						+			+
Microtus (S.) gregalis	3.91	+	+			+	+	+	+	+
Microtus (T.) pyrenaicus	3.74	+	+	+						
Microtus (C.) nivalis	3.66	+	+		+		+	+	+	+
Allocricetus bursae	3.60	+	+							
Microtus (T.) duodecimcostatus	3.40	+	+	+		+				+
Microtus arvalis	3.35	+	+	+	+	+	+	+	+	+
Microtus (T.) subterraneus	3.09		+	+	+		+			
Apodemus sylvaticus	3.08	+	+	+	+	+	+	+	+	+
Microtus (T.) multiplex	3.01	+	+	+	+					
Muscardinus avellanarius	3.00	+	+	+			+			
Crocidura leucodon	2.77	+	+							
Neomys fodiens	2.65			+						
Crocidura russula	2.26	+								
Sorex araneus	2.12	+	+	+	+	+				
Crocidura suaveolens	2.01	+								
Myodes glareolus	1.99	+	+	+	+	+	+	+	+	+
Sorex minutus	1.63	+			+				+	

5.2.3 Strontium isotope analysis and the reconstruction of human mobility

Strontium isotope ratios ($^{87}Sr/^{86}Sr$) measured in skeletal remains can be used to directly investigate past mobility (Capo et al., 1998; Bentley, 2006; Slovak and Paytan, 2012). The fundamental principal is that $^{87}Sr/^{86}Sr$ isotope ratios vary between different geologic regions depending on their age and composition, due to the radioactive decay of ^{87}Rb by emission of a negative β-particle with a half-life of ~4.88×10^{10} years to ^{87}Sr. Weathering releases Sr into the soil, where it can be taken up by plants and enters the food cycle. The $^{87}Sr/^{86}Sr$ isotope ratio is mainly controlled by weathering of the underlying geology, but can be augmented by additional sources of Sr, such as atmospheric deposition (Price et al., 2002; Bentley, 2006; Evans et al., 2009, 2010; Frei and Frei, 2011, 2013; Maurer et al., 2012; Slovak and Paytan, 2012). Humans incorporate Sr from their diet into their dental and skeletal tissues (Beard and Johnson, 2000), where it substitutes for calcium and serves no metabolic function. $^{87}Sr/^{86}Sr$ isotope ratios of dental remains reflect the average isotope ratios of food intake and to a lesser extent drinking water, during childhood when the teeth were formed. Archaeological dental remains can be affected by both physical and chemical changes after deposition, potentially leading to the loss of the original isotope composition. The degree of subsequent diagenetic overprinting can be different from sample to sample and depends on a large number of factors, including the length of burial, the hydro-geochemical environment, and the type of dental material (e.g., Bentley, 2006; Slovak and Paytan, 2011). Tooth dentine is prone to diagenetic overprinting because it contains pores ~ 1 µm diameter, which are larger than its phosphate crystals (Kohn et al., 1999). Tooth enamel, on the other hand consists of ~ 96 wt.% Ca phosphate, has phosphate crystals larger than 1 µm, a compact structure, little pore space and is thus much denser and more inert. Several studies have shown that tooth enamel is much more resistant than bone or dentine to post-burial diagenesis and more likely to retain its original isotopic signature (Budd et al., 2000; Hoppe et al., 2003; Bentley, 2006; Slovak and Paytan, 2012). Finally, to investigate mobility the $^{87}Sr/^{86}Sr$ isotopes measured in the human remains can be compared to the bioavailable $^{87}Sr/^{86}Sr$ isotope range of the surrounding environment to identify potential childhood residence areas. A limitation of this method is that geographically distant areas can have similar or overlapping isotope ratio compositions, depending on their geologic substrate. $^{87}Sr/^{86}Sr$ isotope ratios can thus be used to exclude areas, but cannot provide a definite childhood residence area. Isotopically "local" therefore only means indistinguishable from the local isotopic signature. In order to investigate mobility, the source of diet intake also needs to be considered. For farming communities this correlation is relatively straight forward, as long as exotic food sources can be excluded, and is tied to the residence area. However, in the case of a largely hunting based diet it is possible that even a relatively stationary individual could acquire a non-local isotopic signature related to the movement of the prey.

5.2.4 Neanderthal mobility

The extent of Neanderthal mobility is currently not well understood. Lithic raw materials found at Neanderthal sites are often local, with only a small percentage coming from sites > 5 km away, suggesting limited mobility (Féblot-Augustins, 1993; Mellars, 1996). Some exotic materials do occur at Mousterian sites, suggesting that substantial mobility of Neanderthals may have occurred sometimes (Mellars, 1996). However, lithic materials can travel by barter and thus are not a direct measure of mobility. Faunal remains at Palaeolithic sites show that Neanderthals in central and northern Europe were hunting large, gregarious herbivores and may have tracked the seasonal migrations of these herds (Patou-Mathis, 2000). Zooarchaeological evidence from the Quina Mousterian deposits from the site of Jonzac (Charente-Maritime, France) indicate that Neanderthals were hunting reindeer when it was seasonally abundant in that area. This would support the idea of Neanderthals as highly mobile hunter-gathers and the use of Jonzac as a frequent, but short-term hunting camp (Niven et al., 2012). Strontium isotopic investigation of these reindeer by Britton et al. (2011) further support this interpretation, in showing that these reindeer were most likely killed during the same hunting event. Migrating gregarious herbivores, can be considered an important prey species for Neanderthals and potentially exhibit complex and changing mobility patterns. This adds another layer of complexity when trying to infer Neanderthal childhood origin using strontium isotopes because a change in strontium isotope ratio might simply reflect the changing mobility pattern of the food source. Richards et al. (2008) first applied strontium isotope tracing to directly investigate the mobility of a Neanderthal individual from the site of Lakonis, Greece. They argued, that this individual had spent its childhood in an area at least 20 km away from the site. However, due to potential problems with the analytical technique they used, as well as the lack of a strontium isotope baseline map for the area their interpretation of the data has been disputed by Nowell and Horstwood, (2009), but see also Richards et al. (2009) for further discussion.

5.2.5 Materials and methods

5.2.5.1 Samples

Accelerator Mass Spectrometry (AMS) radiocarbon dating of five bone samples [M93-C4-IV 21, 22, 26, 32 and M93-C3-IV 28] from layer IV was carried out at the Oxford Radiocarbon Accelerator Unit (ORAU), University of Oxford (Table 5-2). A sample from the tephra, layer VI, was collected for $^{40}Ar/^{39}Ar$ dating. In addition, we applied U-series and electron spin resonance (ESR) dating on a range of teeth. Teeth were selected by A.R. Defleur from the collection in the Musée Archéologique de Soyons. All samples were originally collected *in situ* and were completely cleaned. Combined U-series/ESR dating was carried out on 14 faunal teeth (Figure 5-5,) sample layers are given in Table 5-3 and Table 5-4. U-series dating was carried out on Neanderthal teeth from layer XV. Tooth 3524 (M-D1-230), Figure 5-6A, was intact, while sample 3525 (M-H3-73), Figure 5-7A, was a tooth fragment. In addition, we analysed one intact tooth (3526) of a Neolithic individual from a grave dug into the uppermost layer, Figure 5-8A. For the reconstruction of human mobility, we applied $^{87}Sr/^{86}Sr$ isotope analysis to three human dental remains. The bioavailable $^{87}Sr/^{86}Sr$ isotope range for Moula-Guercy was determined by analysing 11 soil samples collected from different layers within the cave and just outside of the present day cave entrance.

5.2.5.2 Radiocarbon analysis

Prior to dating, the material was subjected to %N testing as a way of assessing the preservation of protein in the bone (Brock et al., 2010b). Two of the Moula-Guercy bones (21 and 28) failed to provide N above the cut-off limit of the ORAU and were not treated further. Three samples were dated using the latest preparation protocol for bone collagen, which includes an ultrafiltration step (Higham et al., 2006; Brock et al., 2010a). About 600 mg of bone powder was drilled from each sample, and collagen was extracted using a series of chemical steps. These included immersion in HCl and NaOH for the demineralization and removal of humic acids, respectively, interspersed with cleaning in ultrapure MilliQ water. The extracted collagen was gelatinised and underwent ultrafiltration, after which ~1 ml of >30 kD gelatin was lyophilised. About 5 mg of dried collagen was combusted using a GC-MS system and the CO_2 generated via this process was purified, graphitised, and pressed into target holders prior to its introduction to the AMS system for ^{14}C measurement.

5.2.5.3 $^{40}Ar/^{39}Ar$ dating

The $^{40}Ar/^{39}Ar$ dating for sanidine grains followed the protocol of Michel et al. (2013). The largest possible well-preserved sanidine grains (500 µm) were extracted using standard heavy liquid methods and then hand-picked under a binocular microscope. Grains were treated with HNO_3 and HF for 10 minutes, followed by deionised water for 10 minutes in an ultrasonic bath. Their chemical composition

was estimated using scanning electron microscopy with Energy Dispersive X-ray Spectroscopy (EDS) in order to check the homogeneous presence of potassium (Ecole des Mines, Sophia Antipolis, Valbonne, France). The samples were irradiated for one hour with Cd shielding in 5C position at McMaster University Reactor (Hamilton, Canada). The sanidine grains were subsequently loaded onto a copper plate by sets of about 50-100 grains per hole for multigrain aliquot analyses. Gas was extracted with an infrared continuous laser and purified in stainless and glass extraction line using two Al-Zr getters and a N_2 cold trap. System blanks were run for every two or three analysed samples. The mass spectrometer is a VG3600 with a Daly detector. Mass discrimination was monitored by regularly analysing one air pipette volume. The ultimate accuracy of the $^{40}Ar/^{39}Ar$ method depends on well-dated homogeneous standards (Nomade et al., 2005).

5.2.5.4 U-series analysis

The laser ablation U-series analysis was carried out at the Research School of Earth Sciences (RSES), using a custom-built laser ablation sampling system (ANU HelEx) interfaced between an ArF Excimer laser (193 nm; Lambda Physik Compex 110) and a Neptune MC-ICP-MS. Details of the laser ablation system including detailed description of the equipment, sampling strategies, and data reduction, has been given by Grün et al. (2014). U-series analysis on the Neanderthal tooth 3524 and of the Neolithic tooth utilised laser drilling (Benson et al., 2013). Neanderthal tooth 3525 was already broken and analyses were carried out on cross section through the dentine. The faunal samples were cut and analysed along cross sections using laser spot analysis (e.g., Storm et al., 2013). The U concentrations in enamel were too low for U-series isotopic analysis.

5.2.5.5 ESR analysis

In order to obtain external dose rate data, *in situ* gamma spectrometric measurements were carried out at the site and representative sediment samples were collected and analysed for U, Th, and K by solution ICP-MS/OES (Genalysis, Perth).

The dating procedures followed those routinely applied in the ANU ESR dating laboratory (R. Grün et al., 2008). From each tooth, an enamel fragment was removed and powdered. The sample was then successively irradiated in 9 steps to 810 Gy using an X-ray source, which was calibrated using secondary standards (samples that had previously been irradiated with a calibrated gamma source).

For the calculation of the internal dose rate values we used beta attenuation values of Marsh (1999) and an alpha efficiency of 0.13±0.02 (Grün and Katzenberger-Apel, 1994). Dose rates were calculated with the conversion factors of Guérin et al. (2011) and for the estimation cosmic dose rate (Prescott and Hutton, 1988) an average depth of 10±5 m was assumed. For layer XV, gamma dose rate measurements were also carried out by thermoluminescent dosimeters (TLDs) by Helene Valladas in 1993. For this

layer all measurements were averaged. A time averaged water content of 10±5 % was assumed for the sediments and dentine. The U concentrations in enamel are too low for U-series isotopic analysis. For the calculation of the enamel dose rates the dentine U-series values were used. Age calculations were carried out with the ESR-DATA program (Grün, 2009) for combined U-series/ESR (Grün et al., 1988) and the closed system U-series (CSUS) ESR system (Grün, 2000).

5.2.5.6 $^{87}Sr/^{86}Sr$ isotope analysis at Moula-Guercy

The analysis of the sediment samples followed standard protocols to extract the bioavailable Sr (DIN ISO 19730) and chemical separation was performed using ion exchange chromatography with Eichrom Sr specific resin. The Neptune multi-collector inductively coupled plasma mass spectrometer (MC-ICP-MS) at the Research School of Earth Sciences was used for measurement. The blank contribution for the analysis of soil samples varied between 50-250 pg Sr, which is negligible compared to the amount of sample (>100 ng). For the analysis of the human remains micro-drilling followed by thermal ionisation mass spectrometry (TIMS) was used. A custom made 0.3 mm drill bit was used to extract ~0.5 mg of sample material and a 1M acetic acid leach was performed to remove possible residual contamination. The samples underwent ion exchange chromatography to isolate Sr from other elements using a micro column set filled with the Eichrom Sr specific resin. A drop of dilute phosphoric acid was added to each sample before loading onto rhenium filaments with a tantalum fluoride activator. Samples were measured on the TRITON *Plus* thermal ionisation mass spectrometer (TIMS) at RSES. Data reduction includes an isobaric Rb interference correction, exponential mass bias correction (using the internal $^{86}Sr/^{88}Sr$ ratio of 0.1194) and 2σ outlier rejection. Total procedural blank levels for the human samples are below 100 pg Sr. Long term measurements of the Sr carbonate standard SRM987 (National Institute of Standards and Technology) on the Neptune MC-ICP-MS gave an average $^{87}Sr/^{86}Sr$ value of 0.71024±3 (n=256, 2σ) and 0.71023±2 (n=99, 2σ) on the TIMS. This is in agreement with the original certified $^{87}Sr/^{86}Sr$ isotope value of 0.71034±26 (Moore et al., 1982) and the more commonly quoted value of 0.71025±1 (Thirlwall, 1991; McArthur, 1994; Hans et al., 2013).

5.2.5.7 $^{87}Sr/^{86}Sr$ regional isotope baseline data

In order to create baseline bioavailable $^{87}Sr/^{86}Sr$ isotope data for the region surrounding Moula-Guercy soil leachates and plant samples from the IRHUM (isotopic reconstruction of human migration) database (Willmes et al., 2014) were used. A box and whisker plot was created in R (R Core Team, 2013) to compare the different lithological units. The top and bottom of the box are the third and first quartiles. The interquartile range (IQR) is calculated by subtracting the first quartile from the third. The second quartile, which is the median, is shown as a black line. The whiskers are defined as Q1-1.5*IQR for the lower whisker and Q3+1.5*IQR for the upper whisker.

5.2.6 Results and discussion

5.2.6.1 Radiometric dating

Radiocarbon dating The dating results are summarised in Table 5-2. One bone sample (26) was dated twice (OxA-28094 & OxA-28095) as a routine internal laboratory check. Both results were infinite - greater than our background ages, as were the two further determinations (OxA-28093 & OxA-28096). These ages provide a minimum age for the formation of layer IV, which seems to predate 50 ka BP.

Table 5-2: Radiocarbon results.

Sample	Material	OxA	^{14}C age BP	Chemistry parameters of dated samples					
				Used bone mg	Collagen yield, mg	Collagen yield, %	$\delta^{13}C$	$\delta^{15}N$	C:N
M93 C4 IV 21	bone	*Failed*							
M93 C4 IV 22	bone	28093	>47000	610	29.69	4.9	-21.2	2.35	3.38
M93 C4 IV 26	bone	28094	>48500	600	16.8	2.8	-20.0	5.91	3.38
M93 C4 IV 26	bone	28095	>48000	600	17.93	3.0	-20.0	5.78	3.34
M93 C4 IV 32	bone	28096	>49400	600	19.99	3.3	-20.6	1.72	3.32
M93 C3 IV 28	bone	*Failed*							

$^{40}Ar/^{39}Ar$ dating Each laser step-heating experiment of the multigrain aliquots provided an extremely high ^{40}Ar signal (> 6 V) whereas the ^{39}Ar signal was very low (under 15 mV), suggesting that these sanidines are not of Quaternary age. The estimated ages are older than 200 Ma. The new $^{40}Ar/^{39}Ar$ dating results unfortunately did not provide any tangible chronological information and are thus excluded from the discussion on the chronology of Moula-Guercy.

U-series on faunal teeth For the interpretation of the U-series data one has to keep in mind that the U-series ages are indications of when uranium migrated into the skeletal tissue. Firstly, there can be a long delay between the deposition of a bone or tooth and the U-uptake. Secondly, there may be several consecutive overprinting uptake phases in the skeletal tissue (see e.g., Grün et al. (2014), and sample 3525, below). Thus, apparent U-series ages have generally to be regarded as minimum age estimates. However, U migration processes can be highly complex and U-leaching can also occur, leading to older apparent ages. Leaching is usually associated with lower U-concentrations in the effected domains compared to their surroundings.

The U-series results on the faunal teeth are given in Table 5-3 and shown in Figure 5-5. For layer IV, all apparent U-series determinations are of Holocene age, whereas for layer VIII, of late Pleistocene to early Holocene age. The results from layer XIV vary between around 14 and 70 ka and those of layer XV between 9 and 104 ka. Since the sedimentological and biochronological data of this cave indicate that these layers are in stratigraphic order (Defleur et al., 2014; Saos et al., 2014) we attribute the huge spread in U-series age results from the faunal teeth to be caused by complex U-migration on small scales. In an intact sample the $^{234}U/^{238}U$ ratios change little within a tooth and are an indication of the U source. As it

can be seen, layer IV has very similar $^{234}U/^{238}U$ ratios, but with the increase in age spread in the lower layers the spread in $^{234}U/^{238}U$ ratios also increase. That is a sign that the U sources for the different teeth were different, most probably by the position within a given layer. Samples 3040 and 3041 have clearly distinct $^{234}U/^{238}U$ ratios from all other samples. It is important to note that in spite of having very different U-series isotopic compositions, none of the samples show any indication of U-leaching.

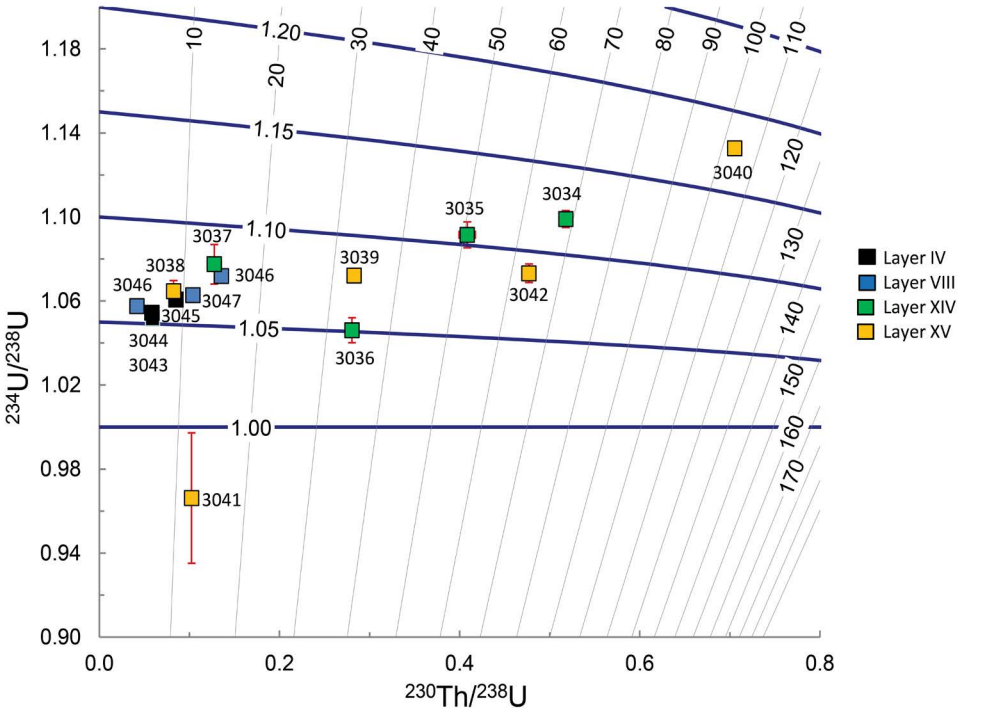

Figure 5-5: U-series results of the faunal teeth. Errors are 2σ, plot created using Isoplot (Ludwig, 2003). Solid purple lines highlight the different $^{234}U/^{238}U$ ratios.

U-series on human teeth Figure 5-6A shows the Neanderthal tooth 3524 and the laser ablation scans of the 14 holes (Figure 5-6B) and the 1500s hole (Figure 5-6E). The results of the 14 holes (Figure 5-6D) yield an average age of 91.8±0.9 ka, each age estimation has an average error of 0.55 ka. This shows that there is some inhomogeneity in the U-series composition within the range of the 14 holes. The 1500s scan was binned into 30 sections with a length of 40 cycles. It is clearly visible that the errors in the isotope ratios (Figure 5-6F) and consequently the calculated ages (Figure 5-6G) increase as the isotope intensities decrease (Figure 5-6E). Nevertheless, the average of the 30 age calculations along the depth probing 92.8±6.3 ka is indistinguishable from the previous measurements. The average errors increased nearly tenfold to 4.9 ka. Using the continuous diffusion model for uranium acquisition of Sambridge et al. (2012), the ages become slightly older, but only by about 1.8 ka (see Figure 5-6D,G).

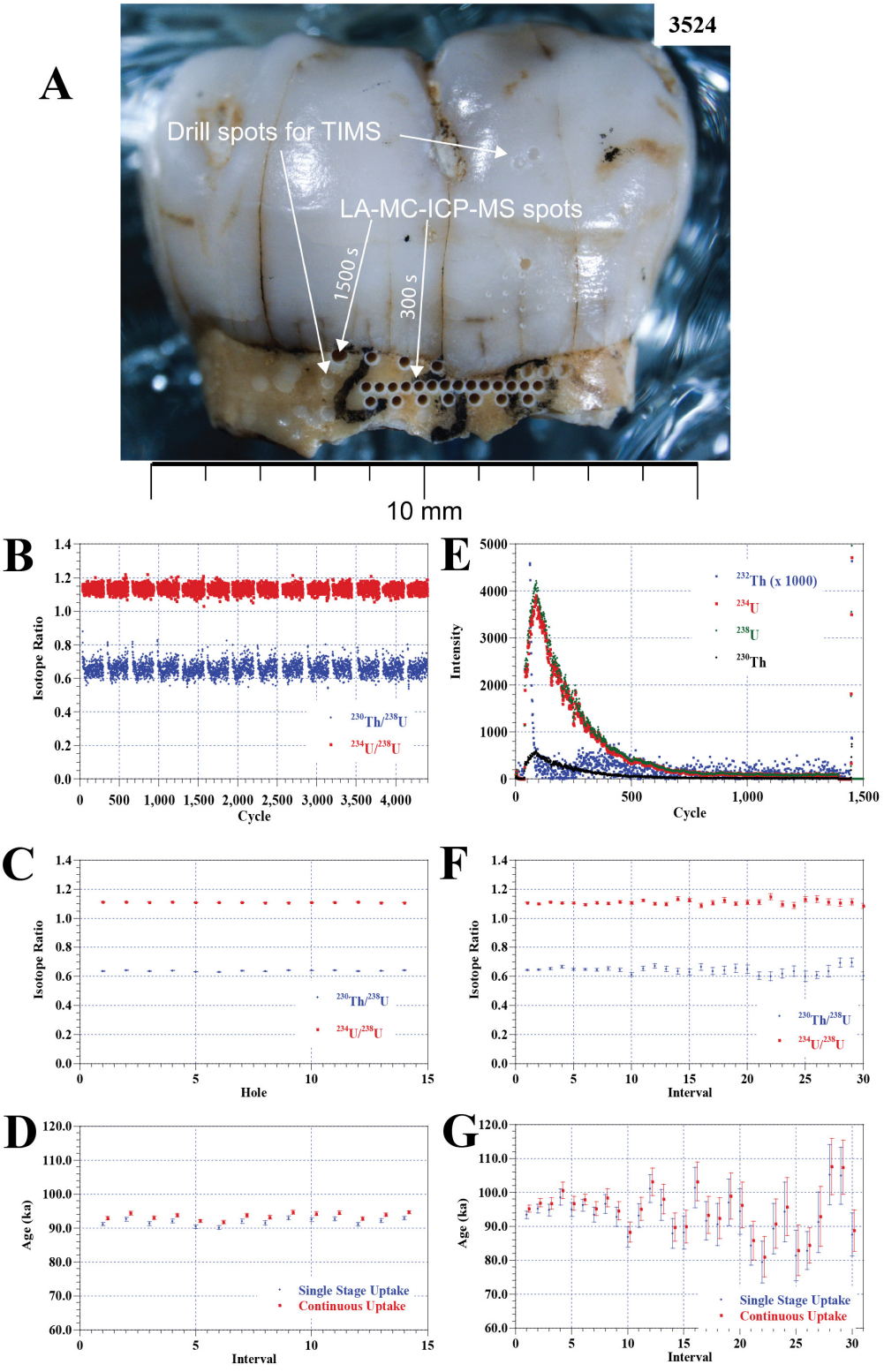

Figure 5-6: U-series results of Neanderthal tooth 3524. (A) Photo and location of the sampling spots from LA-MC-ICP-MS (Benson et al., 2013) and drilling spots for TIMS analysis. (B) U-series isotope ratios along the 300 s drill holes. (C) Binned data of B. (D) Apparent U-series ages for closed system (single stage uptake) and continuous diffusion from B. (E) Isotope measurements along the 1500 s drill hole. (F) Binned isotope ratios. (G) Apparent U-series ages for closed system (single stage uptake) and continuous diffusion from E.

The results of sample 3525 show the full complexity of U-migration into teeth (Figure 5-7). As it was a broken specimen, we could measure several traverses through various dentine sections. The results of all three sections are different. Transect I (Figure 5-7B) yielded ages between 90 and 120 ka, and it is possible to calculate an age using the diffusion-adsorption-decay (DAD) model of Sambridge et al. (2012), yielding an age of 118±15 ka (2σ). The first two spots of transect II (Figure 5-7C) yielded younger ages of around 70 ka while the rest yielded ages of around 86 ka. Transect III (Figure 5-7D) starts with ages of around 95 ka, increasing to around 130 ka (spots 5 to 7) then decreasing back to around 82 ka towards the outside of the tooth. This shows that even small teeth may experience complex U-uptake histories. Contrary to expectations, the high age values in transect C are associated with higher U-concentrations, i.e. it is unlikely that the older ages were the result of U-leaching. It seems that there is an earlier U-uptake phase from the base of the tooth, perhaps around 120 to 130 ka migrating from the lower end into the dentine as well as from the left side (as in the photo) followed by diffusion from the right side and somewhat later overprinted near the pulp cavity.

The U-series analyses of the two Neanderthal teeth clearly demonstrate that layer XV at least corresponds to MIS 5 *sensu lato*. As all results still have to be regarded as minimum age estimates, any older age cannot be excluded: the results of the faunal teeth of layer IV indicate a delay in U-uptake of at least 45 ka.

The tooth of the Neolithic individual yielded only one analysis that could be evaluated (Figure 5-8). Cycles 1 to 20 and 21 to 40 yield ages of 4.8±1.4 ka and 3.6±1.6 ka, respectively. However, the average ^{230}Th is on average only 1.1 and 0.6 counts above background, which was 1.4 counts per cycle, i.e., any age results are critically dependent on the accurate assessment of the background levels. The very low U-concentrations in this tooth may be taken as indication that U-accumulation was delayed in the other human teeth as well.

In conclusion, the U-uptake into skeletal elements recovered from the sediments of Moula-Guercy involves complex processes. Even small human teeth are subject to complicated U-migration histories. If layer XV was accumulated within a reasonably short time range, its minimum age would be given by the U-series results from 3524 and the upper age range from transect III in 3525, i.e. around 120-130 ka. However, it would be difficult to assess a maximum age, because U-series results on faunal material are always a minimum age. This is best illustrated by the Neolithic tooth, where large domains did not experience any U-uptake.

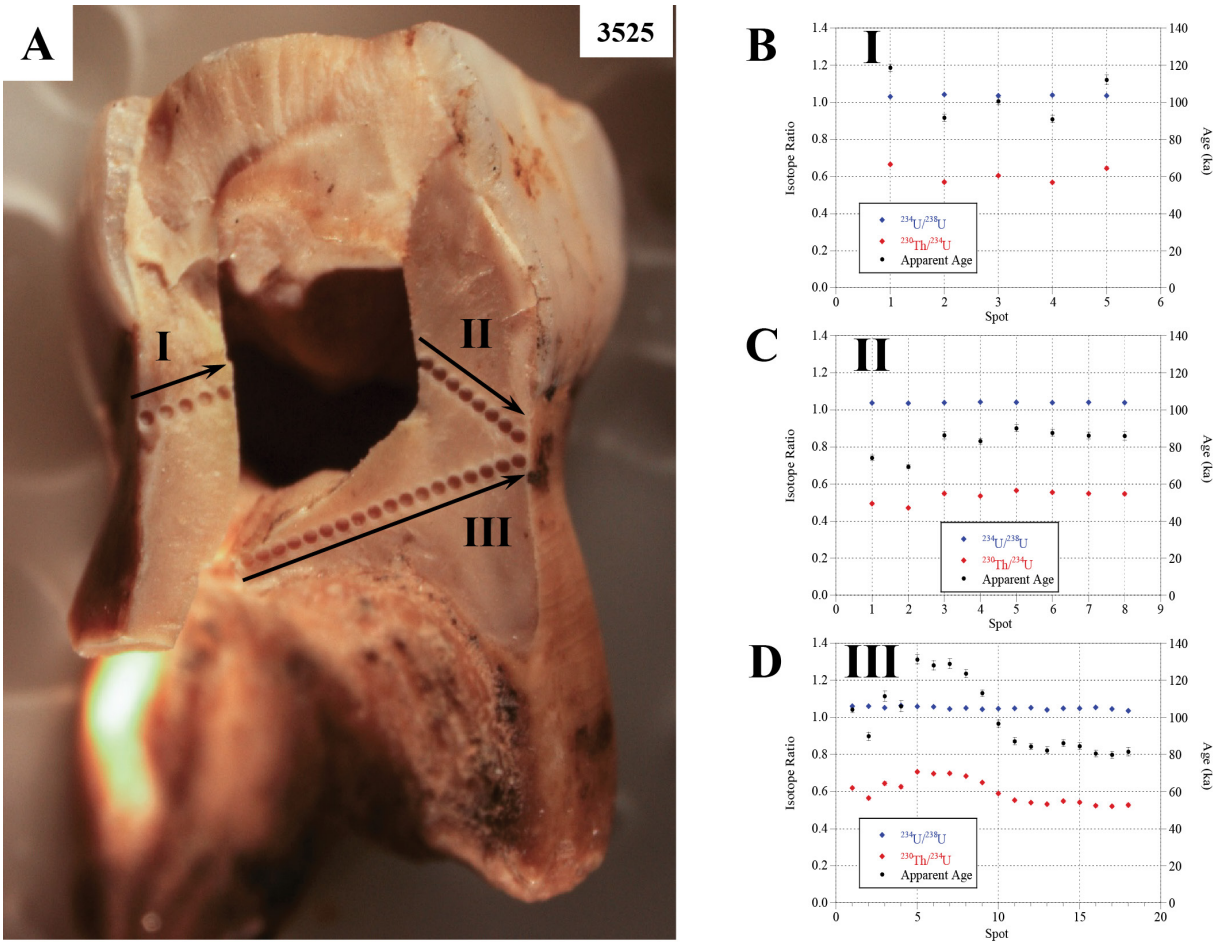

Figure 5-7: U-series results of Neanderthal tooth 3525. (A) Photo and location of the transects. (B) Isotope ratios and apparent U-series age estimates along transect I. (C) Isotope ratios and apparent U-series age estimates along transect II. (D) Isotope ratios, U-concentrations and apparent U-series age estimates along transect III.

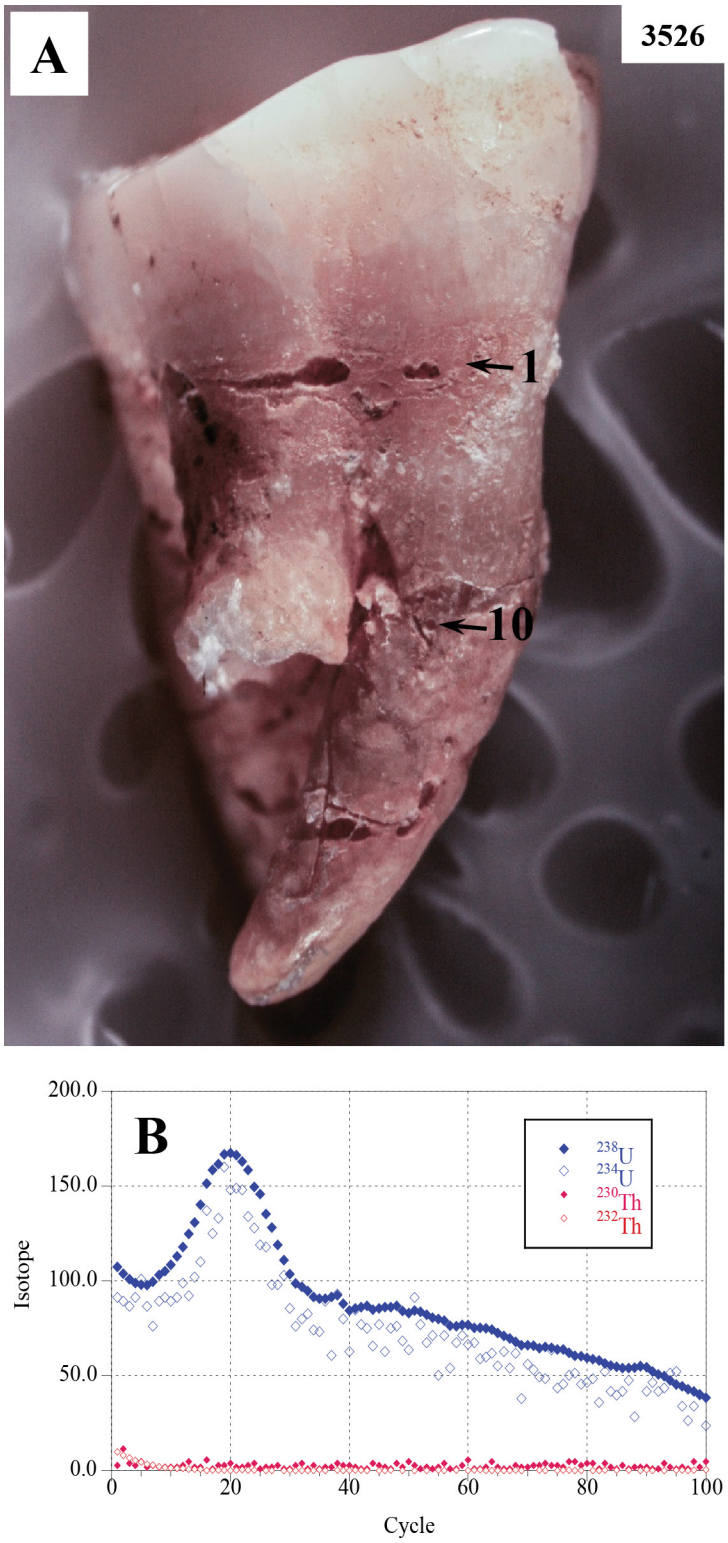

Figure 5-8: U-series results of the Neolithic tooth (3526). (A) Photo and location of the laser ablation drill holes. (B) Isotope measurements of the first 100 cycles of hole one.

ESR dating on faunal teeth For ESR dating of teeth an assessment of the dose rates of the surrounding sediments is critical. All samples had been cleaned long before the measurement of the dose rates of the sediment layers. The sediments give reasonably similar geochemical results, the dose rates in layer XV, where six independent measurements were carried out, vary between 500 μGy/a, and 733 μGy/a. This implies that the actual external dose rate (beta and gamma) at a given place within a layer could vary by as much 20-40 %.

Table 5-3: U-series results on the faunal teeth from Moula-Guercy. EN stands for enamel and DE for dentine.

Lab Number	Field Number	Layer	U(EN) (ppm)	U(DE) (ppm)	U(CE) (ppm)	$^{234}U/^{238}U$ (DE)	$^{230}Th/^{234}U$ (DE)	Apparent Age (ka)
3043	M93-F4-29	IV	0.05	33.0		1.0517±0.0022	0.0561±0.0012	6.3±0.1
3044	M93-F5-17	IV	0.15	21.5		1.0544±0.0028	0.0553±0.0015	6.2±0.2
3045	M93-C3-M1	IV	0.09	58.1		1.0607±0.0018	0.0802±0.0010	9.1±0.1
3046	M94-D4-23	VIII	0.75	41.9		1.0576±0.0025	0.0394±0.0009	4.4±0.1
3046					70.0	1.0719±0.0018	0.1265±0.0011	14.7±0.1
3047	M94-C3-222	VIII	0.10	55.1		1.0628±0.0023	0.0977±0.0013	11.2±0.2
3034	M95-D2-154	XIV	0.10	13.8		1.0990±0.0040	0.4712±0.0060	68.8±1.3
3035	M95-D2-287	XIV	0.05	6.1		1.0915±0.0062	0.3742±0.0080	50.8±1.5
3036	M95-G2-46	XIV	0.05	8.6		1.0461±0.0060	0.2681±0.0069	34.0±0.9
3037	M95-G2-83	XIV	0.07	2.2		1.0775±0.0094	0.1184±0.0071	13.7±0.9
3038	M95-F3-217	XV	0.03	7.6		1.0647±0.0051	0.0774±0.0036	8.8±0.4
3039	M97-784	XV	0.14	22.5		1.0721±0.0030	0.2638±0.0037	33.3±0.6
3040	M95-F2	XV	0.18	25.3		1.1327±0.0023	0.6227±0.0042	103.7±1.4
3041	M97-F1-398	XV	0.30	57.2		0.9662±0.0310	0.1060±0.0015	12.2±0.2
3042	M06-96-E1-177	XV	0.01	9.6		1.0732±0.0044	0.4444±0.0059	63.7±1.1

The sediment data are shown in Table 5-4 and the results of the ESR measurements and age calculation in Table 5-5. Since all teeth were analysed for U-series, we present only combined US-ESR (Grün et al., 1988) and CSUS-ESR (Grün, 2000) age calculations. The difference between the models is that the former assumes a continuous U uptake while the latter assumes a single short phase uptake at a time that corresponds to the closed system U-series age. The two models encompass all possible U-uptake scenarios (except for leaching). As it can be seen in Table 5-5, there is only one sample (3039) where the CSUS-ESR model yielded an 11 ka older age, however, still within overlapping errors. All other results are indistinguishable.

Three teeth (3046, 3037 and 3038) returned much younger ages than the other samples from the same layers. Surprisingly, all samples have closely similar dose values between 33.7 to 36 Gy. None of the other samples have such low dose values. This may indicate either that they were located in unexpectedly low dose rate environments (e.g. surrounded by large limestone blocks) or that these teeth

were incorporated from higher levels. However, incorporation from higher levels is deemed very unlikely based on the known stratigraphy of the site (Defleur et al., 2014; Saos et al., 2014).

The age estimates are calculated as averages and their errors as the root of sum of squares for standard deviation of the ages and their average error. The age estimate for layer IV is 61±8.5 ka (n=3). The age estimate for layer VIII is presented by a single sample (3047) with an age of 66±4 ka (n=1). This overlaps with the thermoluminescence result on layer VI (Sanzelle et al., 2000) on a 1σ basis. The age estimates for layers XIV and XV yield values of 83.5±20 ka (n=2) and 119±13 ka (n=2), respectively**.** Detailed studies on the composition of the ESR signals in teeth show that gamma irradiation induced large amounts of unstable components (Joannes-Boyau and Grün, 2011). A sample from Broken Hill in Zambia yielded a 30 % higher dose value once the dose response curve was corrected for these unstable components. However, the teeth from Moula-Guercy were irradiated with an X-ray source, which induced significantly less unstable signals, in the range of 6 % more than the natural, (Grün et al., 2012b). In contrast to the U-series results, it is not possible to assume that the oldest ESR results come closest to the age of deposition. The scatter in the ESR ages is in the first instance caused by our inability to accurately reconstruct the external dose rate for a given tooth. It seems that ESR, in spite of all its conceived failings, is essential for reconstructing chronologies for complex sites, such as Moula-Guercy. The newly developed dating procedures using laser ablation drilling will help to tighten the ages of human fossils, however, additional analyses seem essential to move from minimum U-series age estimates to more constrained age assessments. It has to be noted that nearly non-destructive ESR analysis, which also allows the quantification of thermally unstable components, is a highly work intensive process (Joannes-Boyau and Grün, 2011, and references therein). Furthermore, the tendency of palaeoanthropologists to CT scan everything that comes out of excavations will make direct ESR dating of human teeth virtually impossible (Grün et al., 2012a).

Table 5-4: Sediment data for ESR dating.

Layer	U (ppm)	Th (ppm)	K (ppm)	External Gamma dose rate (μGy/a)	Cosmic dose rate (μGy/a)
IV	3.53±0.18	9.80±0.49	8904±1000	581±25	63±23
VIII	3.46±0.17	9.13±0.46	11800±1000	546±25	63±23
XIX	3.68±0.18	10.70±0.54	14800±1000	709±41	63±23
XV	4.55±0.22	9.39±0.47	16700±1000	642±98	63±23

Table 5-5: ESR results, EN stands for enamel and DE for dentine. Samples in parentheses were not used for the average age calculation for that layer.

Lab Number	Layer	D_e (Gy)	TT (µm)	EN+DE DR (µGy/a)	Beta SED (µGy/a)	Total DR (µGy/a)	p-value (DE)	US-ESR Age (ka)	CSUS-ESR Age (ka)
3043	IV	44.7±0.8	900	31±5	180±25	856±41	6.08±0.45	52±2	52±2
3044	IV	50.9±0.8	1050	16±2	157±21	817±39	7.77±0.58	62±3	62±3
3045	IV	60.3±1.1	1000	58±10	164±22	867±40	5.36±0.41	69±4	69±3
3046	VIII	36.0±0.6		32±3		787±43	8.22±0.70	45±3	(46±2)
3047	VIII	56.4±1.0	1100	68±11	170±22	847±41	3.70±0.32	66±4	66±4
3034	XIV	n/a							
3035	XIV	98.1±2.1	1100	35±6	201±36	1008±59	0.23±0.11	97±7	97±6
3036	XIV	73.9±1.4	950	42±9	230±46	1045±64	0.04±0.13	70±5	70±4
3037	XIV	33.7±0.8	1350	9±2	165±24	946±52	0.51±0.21	35±2	(35±2)
3038	XV	34.7±0.6	1200	13±3	226±40	944±107	2.07±0.55	36±5	(36±4)
3039	XV	109.8±2.5	1050	72±14	236±30	1013±105	0.98±0.35	108+15/-11	119±13
3040	XV	109.1±2.1	1000	no US-ESR	calculation	possible	U-series	too old	(103.7±1.4)
3041	XV	120.8±3.0	950	52±11	259±34	1016±106	7.26±1.14	118+16/-12	119±13
3042	XV	101.2±2.1	900	71±14	272±37	1049±110	0.58±.015	96+13/-9	(97±10)

5.2.6.2 Radiometric chronology of Moula-Guercy

The radiometric chronology of the site is summarised in Figure 5-9. The radiocarbon dating results on bone samples show that layer IV is older than 50 ka. Combined US-ESR results on faunal teeth place layer IV at 61±8.5 ka, layer VIII at 66±4 ka, layer XIV at 83.5±20 ka, and layer XV at 119±13 ka. All results for layer IV fall within 62 to 69 ka, fitting well with the infinite radiocarbon dates of the same layer and the previously obtained thermoluminescence result on layer VI of 72±12 ka (Sanzelle et al., 2000). The single date on layer VIII most likely underestimates the age of the layer and more analysis are needed to resolve this discrepancy. Taking the uncertainties into account the remaining results are in stratigraphical order. The U-series results on faunal materials from various layers demonstrate a greatly delayed U-uptake yielding results which are significantly younger than the expected ages from biostratigraphy. The data on the faunal teeth show that U-series on bones and teeth alone can lead to considerable age underestimations. Direct U-series analyses on two Neanderthal teeth indicate an age for the crucial layer XV corresponding to MIS 5 *sensu lato*. The U-series analyses of both human teeth from layer XV fall within the ESR age range. The U-series results on the Neanderthal tooth 3525 show that U-mobilisation even into small teeth is highly complex, but nevertheless give an indication that the Neanderthals could correlate to MIS 5.5**.** The difference in age estimates for layers XIV and XV are unexpected, since these layers are only distinguished by the presence of human remains. Micro and macro fauna, as well as lithics are similar in these layers (Defleur, 2015).

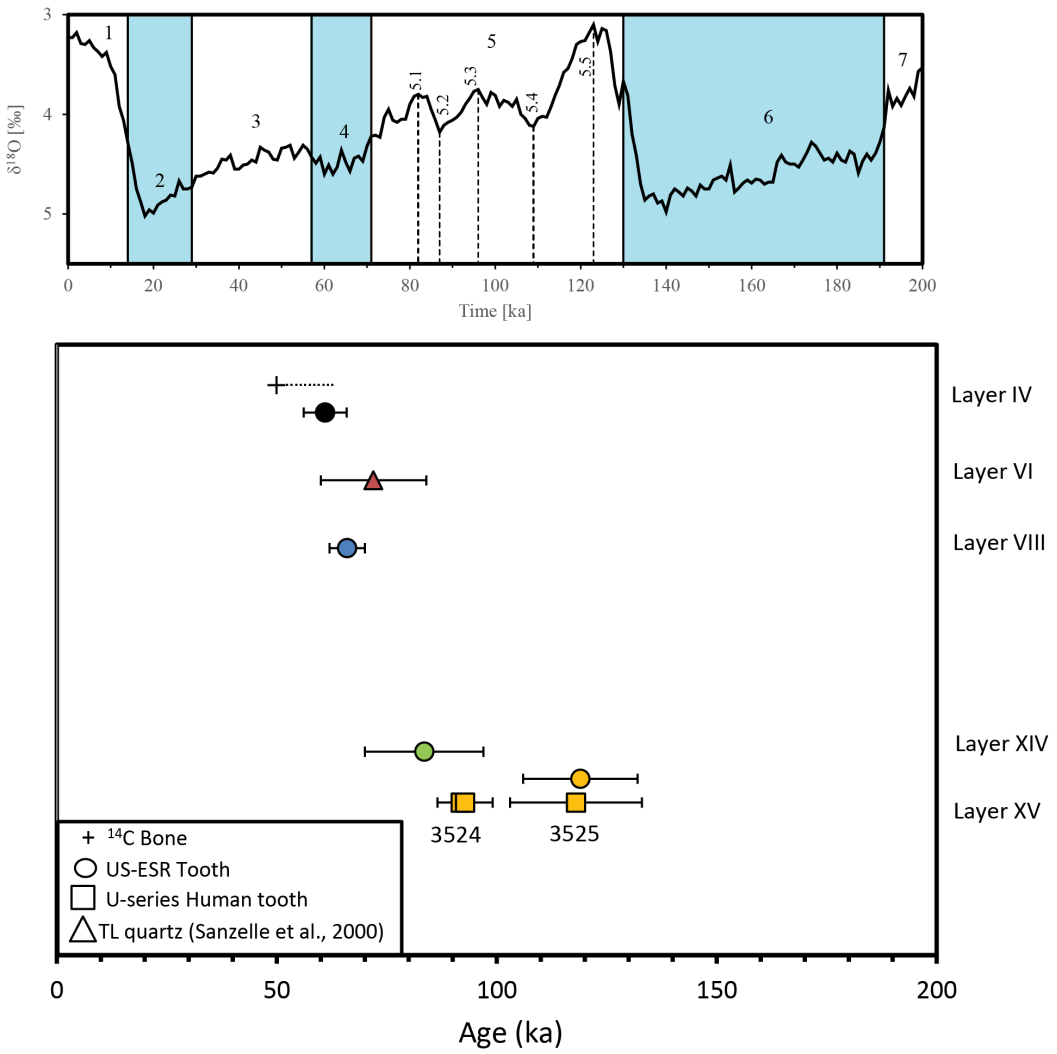

Figure 5-9: Summary of the refined chronology of Moula-Guercy. Marine isotope stage data and boundaries taken from Lisiecki and Raymo, (2005).

5.2.6.3 Isotope tracing of mobility

$^{87}Sr/^{86}Sr$ isotope baseline data The cave of Moula-Guercy is situated on a narrow cliff consisting of Upper Jurassic limestone and dolomite on the west bank of the Rhône River (Figure 5-2). The isotopic variation in bioavailable $^{87}Sr/^{86}Sr$ of the cave sediment is shown in Table 5-6. Within the cave the bioavailable strontium isotope values range between 0.70844-0.70886. The Neanderthal bearing layer XV has an average value of 0.70851 (n=2). The two soil samples collected directly outside of the present day cave entrance exhibit values of 0.70809 and 0.70815, lower than the cave deposits themselves. These two samples were collected from soils and plants sitting directly on top of the limestone, while the cave deposits consist of limestone and dolomite fragments mixed in with sand, silt and clay deposits, which could explain the higher strontium isotope values found within the cave. The bioavailable $^{87}Sr/^{86}Sr$ isotope range of the different lithological units of France, taken from Willmes et al. (2014), is shown in Figure 5-10. Note that only sample locations within the study area were chosen from the IRHUM dataset and not all sample sites from across France as in chapter 3. The clastic and carbonaceous

units found within the Rhône valley have a bioavailable $^{87}Sr/^{86}Sr$ isotope range of 0.7064-0.7139. The igneous and metamorphic units of the Massif Central to the west of the cave consist of granites, gneisses, schists, mica schists, migmatites and amphibolites. The soils and plants on these units show a large range of bioavailable $^{87}Sr/^{86}Sr$ ratios of 0.7086-0.7234, reflecting the heterogeneous geology that changes over short distances. Finally, the young volcanic units found in the Massif Central and south of Moula-Guercy range between 0.7037-0.7053. The bioavailable $^{87}Sr/^{86}Sr$ isotope range of Moula-Guercy, taking both the cave deposits and samples outside of the cave (blue shaded area in Figure 5-10) overlaps with some of the clastic and carbonaceous units of the Rhône valley, but is distinct from most of the igneous and metamorphic units of the Massif Central and from all of the young volcanic units of the Massif Central. This broad scale classification of the landscape into three isotope regions forms the underlying framework for the investigation of human mobility.

Table 5-6: $^{87}Sr/^{86}Sr$ isotope results for the soil samples and human remains from Moula-Guercy.

Soil samples	**$^{87}Sr/^{86}Sr$**	**±2se**	**Human remains**	**sample**	**$^{87}Sr/^{86}Sr$**	**±2se**
Cave entrance west	0.70809	0.000003	Neanderthal (3524)	Enamel	0.71014	0.00010
Cave entrance east	0.70815	0.000004		Dentine	0.70891	0.00005
IV	0.70865	0.000003	Neanderthal (3525)	Enamel	0.71036	0.00002
IV	0.70886	0.000006		Dentine	0.70882	0.00003
VIII	0.70857	0.000003	Neolithic (3526)	Enamel	0.70547	0.00001
VIII	0.70859	0.000004		Dentine	0.70962	0.00040
XIV	0.70848	0.000004				
XIV	0.70844	0.000003				
XIV	0.70849	0.000004				
XV	0.70849	0.000004				
XV	0.70853	0.000005				

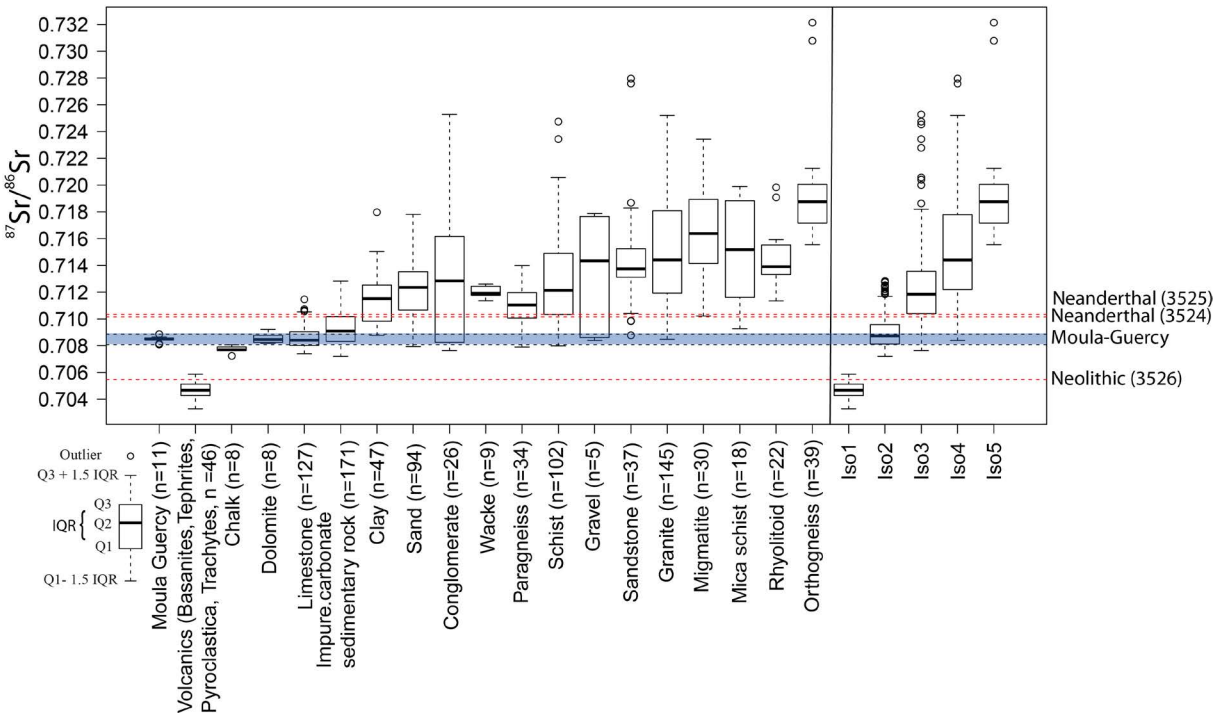

Figure 5-10: Boxplot of the bioavailable $^{87}Sr/^{86}Sr$ isotope ratios lithological units of France. Data are taken from the IRHUM database (Willmes et al., 2014). Isotope packages are taken from chapter 3. The $^{87}Sr/^{86}Sr$ isotope range of Moula-Guercy cave is shown as a shaded area and the values ratios for the enamel samples from the human remains are shown as red dashed lines.

Neanderthal mobility at Moula-Guercy The $^{87}Sr/^{86}Sr$ isotope results of the Neanderthal teeth are shown in Table 5-6. The two Neanderthals (3524, 3525) show dentine $^{87}Sr/^{86}Sr$ isotope values of 0.70891±5 and 0.70882±3 and enamel values of 0.71014±10 and 0.71036±2, respectively. Dentine and enamel form at the same time and thus should exhibit the same strontium isotope ratio. However, dentine is much more susceptible to digenetic alteration and was not well preserved in these samples. We observe that the dentine strontium isotope values are lower than the enamel value and approach the isotope ratios of layer XV of 0.70851, an indication for diagenetic overprint. The enamel values on the other hand, are outside of the strontium isotope range of the cave, and the material was better preserved, indicating no significant diagenetic alteration. See also Benson et al. (2013) for a more detailed study on sample 3524. Using our established isotope baseline, it is apparent that the strontium isotope values of the enamel samples from the Neanderthals are overlapping with many lithological units across France (Figure 5-10). Based on the surface geologic map of France (Figure 5-11A) it is possible to map all lithologic units that are an isotopic match for the enamel Neanderthal values (Figure 5-11B). Using only the IQR of the strontium isotope ratios for the different lithological units shows gravel, sand and clay units within the Rhone Valley as the closet match, while using the full range (IQR+whiskers) includes a significant area of south east France. Even at this broad scale the Massif Central can be excluded as the major childhood food source region of the Neanderthals. The clastic and carbonaceous sediment units of the Rhône valley

represent the spatially closest match for the enamel values of both Neanderthals. We can thus consider them as isotopically local to the larger Rhône Valley, with their food source possibly constrained to come from the clastic lithological units north and east of Moula-Guercy. However, isotopically local does not have to equate to stationary. A detailed study on the Middle Palaeolithic assemblages of the Rhône valley has shown different types of occupation, ranging from long-term residential camps to short-term hunting and stopover camps (Daujeard and Moncel, 2010). Based on the small amount of lithic material and based on the animal remains found at Moula-Guercy this site is considered to have been a used as specialized, short-term hunting camp (Daujeard and Moncel, 2010; Valensi et al., 2012; Saos et al., 2014). Our isotopic analysis provides further evidence that the Neanderthals were mobile hunter-gathers, using Moula-Guercy when their prey animals, such as red deer, were seasonally abundant in this area. Determining a mobility range of the Neanderthals, with a certain number of kms, is complicated by a number of factors, including the large strontium isotope ranges found in many lithological units, and more importantly, the fact that the composition and spatial distribution of the surface geologic features has likely changed since MIS 5. Nevertheless, the new strontium isotope measurements shown here provide direct evidence for Neanderthal mobility within the Rhône Valley.

Mobility of the Neolithic individual The Neolithic individual (3526) shows $^{87}Sr/^{86}Sr$ isotope values of 0.70962±40 for dentine and 0.70547±1 for enamel (Table 5-6). The dentine was poorly preserved and shows $^{87}Sr/^{86}Sr$ isotope values that fall outside of the $^{87}Sr/^{86}Sr$ isotope range of the sediments we collected from the cave. This may indicate that there is variability in the upper layers of the cave that we did not sample, perhaps caused by mixing with loess, dust, or clay rich deposits that shifted the diagenetic overprint in this sample. However, due to the poor preservation of this sample and associated large analytical uncertainties this result should be regarded with great caution. The enamel on the other hand is well preserved and shows an $^{87}Sr/^{86}Sr$ isotope ratio outside the local bioavailable $^{87}Sr/^{86}Sr$ isotope range of the cave. It is consistent with the strontium isotope range of young volcanic units (purple colour in Figure 5-11B) in central and southern France. A small Palaeogene basanite volcanic outcrop occurs ~30 km south east of Moula-Guercy. Another possible region is ~50-80 km to the west of the cave, where volcanic deposits of Palaeogene to Quaternary age occur over a large area in the Massif Central. It follows, that this individual did not grow up on food from the Rhône valley, but grew up on food from an area of young volcanic units, possibly within the Massif Central. The Neolithic individual is thus interpreted as a non-local with significant mobility (>30 km) in its lifetime.

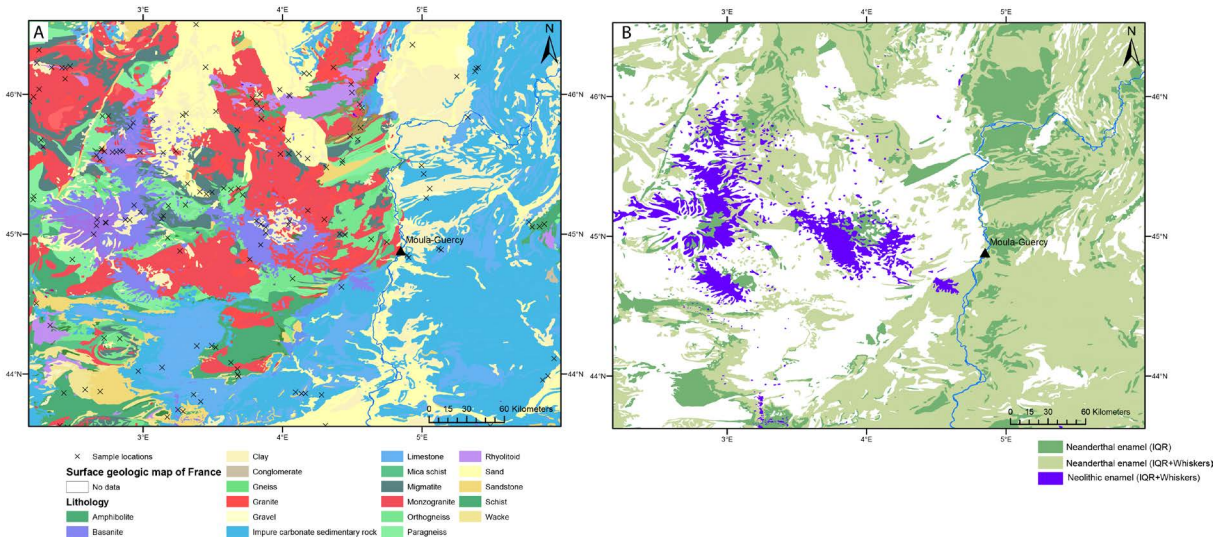

Figure 5-11: A: Surface geologic map of France (BRGM) with the colours representing the lithological units. B: Strontium isotope overlap between the IQR and IQR+whisker range of the different lithological units for the Neanderthal samples (green) and the Neolithic individual (purple).

5.2.7 Conclusions

This study provides the first comprehensive radiometric chronology of Moula-Guercy. It places the layers IV to XV between 60 ka to 120 ka, between MIS 4 and MIS 5 and using combined U-series/ESR dating, indicates that the crucial layer XV, which contains the Neanderthal remains, could correspond to MIS 5.5, and is younger than MIS 6. These results agree with the biostratigraphy at the site, which places layer XV to MIS 5.5. The combined U-series/ESR dating results for layer XIV are younger and do not agree with the biostratigraphy of the site. More dating of material from this layer is needed to resolve these discrepancies. Direct U-series analyses of the two Neanderthal teeth also demonstrate that layer XV at least corresponds to MIS 5 sensu lato, and sample 3525 likely corresponds to MIS 5.5. From the strontium isotope analysis of the two Neanderthal teeth we can infer the Rhône valley as the childhood food source region and exclude the Massif Central. The isotopic evidence is consistent with the archaeological data and shows that the Neanderthals were mobile within the Rhône Valley and used Moula-Guercy as specialized, short-term hunting camp, when their prey animals, such as red deer, were seasonally abundant in this area. Care should be taken to extrapolate from this small (n=2) dataset to any interpretation of Neanderthal mobility overall and more direct investigations of Neanderthal mobility are certainly needed. The Neolithic individual, with a strontium isotope ratios indicative of young volcanic units, presents a strong case for childhood mobility. The closest volcanic units occur ~30 km south east of Moula-Guercy, another possible childhood residence area for this individual are the much larger occurrences of these units in the Massif Central ~50-80 km to the west of the cave. In either case this individual experienced significant mobility in its lifetime.

5.3 Le Tumulus des Sables

This chapter has been submitted to the Journal of Archaeological Science: Reports

M. Willmes, H. F. James, C. A. Boel, P. Courtaud, A. Chancerel, R. Wood, S. Fallon, L. McMorrow, R. A. Armstrong, I. S. Williams, L. Kinsley, M. Aubert, S. Eggins, I. Moffat, R. Grün (in preparation), Radiocarbon dating and isotopic tracing of human diet and mobility at the collective burial site, Le Tumulus des Sables, France. Journal of Archaeological Science: Reports.

The author's contribution to the publications is as follows: The author conducted the strontium isotope study, and in collaboration with R. Wood performed the radiocarbon dating and carbon and nitrogen isotope analysis. The oxygen isotope data was collected and interpreted by H. F. James (James et al., 2013) as part of her Master thesis. The article was written together with H. F. James and suggestions from all co-authors.

Abstract

Radiocarbon dating and multi-isotope analysis ($\delta^{13}C$, $\delta^{15}N$, $\delta^{18}O$, $^{87}Sr/^{86}Sr$) were used to investigate the human remains found at the collective burial site Le Tumulus des Sables, southwest France. The burial is heavily disturbed, and the radiocarbon dates reveal a long use of the burial site spanning from the Neolithic into the Iron Age, consistent with the associated archaeological material. The wide age range of the site and the disturbed stratigraphy, prevent the definite identification of a particular sample as belonging to a certain time period without individually dating it. $\delta^{13}C$ and $\delta^{15}N$ in tooth collagen samples indicate a dominantly terrestrial diet, in agreement with data from other Neolithic sites in Europe. K-means cluster analysis of combined $\delta^{18}O$ and $^{87}Sr/^{86}Sr$ of tooth enamel from 22 individuals suggests 5 distinct groupings within this dataset. Interpreting these isotopic differences in terms of human mobility is limited, due to the uncertainties associated with the *in situ* $\delta^{18}O$ analysis and the difficulty of relating $\delta^{18}O$ and $^{87}Sr/^{86}Sr$ values in tooth enamel to prehistoric geographic location. Nevertheless, for three of the five groups some inferences about childhood residence area were possible, placing group 1 as locals to the site and individuals from group 2 and 3 as possible short-distance migrants from the surrounding Aquitaine basin.

5.3.1 Introduction

5.3.1.1 The site of Le Tumulus des Sables

The collective burial site of Le Tumulus des Sables is located in the town of Saint-Laurent-Médoc, in the Gironde department, about 40 km north-west of Bordeaux, southwest France (Figure 5-12). It was discovered in 2006 when human remains were accidentally uncovered by school children. The site was excavated until 2010 (Chancerel and Courtaud, 2006; Courtaud et al., 2010). The collective burial was

contained within a roughly circular raised mound, 7 x 8 m in diameter and 0.5 m high at its peak (Figure 5-13). It is believed that this mound is natural and that the burials were placed within it.

The human remains found at the site are highly disarticulated and fragmented. No individual burials could be identified. The remains of at least 30 individuals were identified—20 adults and 10 juveniles. The archaeological deposit associated with the burial area is irregular in shape and extends well beyond the mound itself (Figure 5-13). Distinctive pottery, arrow heads and bone buttons discovered within the burial area suggest use of the site by people of the Bell Beaker Phenomenon (BBP) (Chancerel and Courtaud, 2006). A radiocarbon date previously measured on a human bone from within the collective burial yielded an age of 2485-2290 cal. BC (Table 5-7), supporting this conclusion. However, ceramic finds at the site suggest activity extending from the Early Neolithic, through the Bell Beaker period, and into protohistoric and Iron Age periods (Chancerel and Courtaud, 2006; Courtaud et al., 2010). Radiocarbon dates also suggest the mound was used over a significant period of time. A date on a juvenile vertebra yielded an age of 3650-3375 cal. BC. Two radiocarbon dates on charcoal from the top and bottom of the burial mound gave dates of 1395-1215 cal. BC and 6090-5925 cal. BC, respectively. However, there is no archaeological evidence to link these charcoal dates to the funeral use of the site. The purpose of the present study was to investigate the chronology of the site in more detail using radiocarbon dating and to apply multi-isotope techniques to determine the diet and mobility of the individuals.

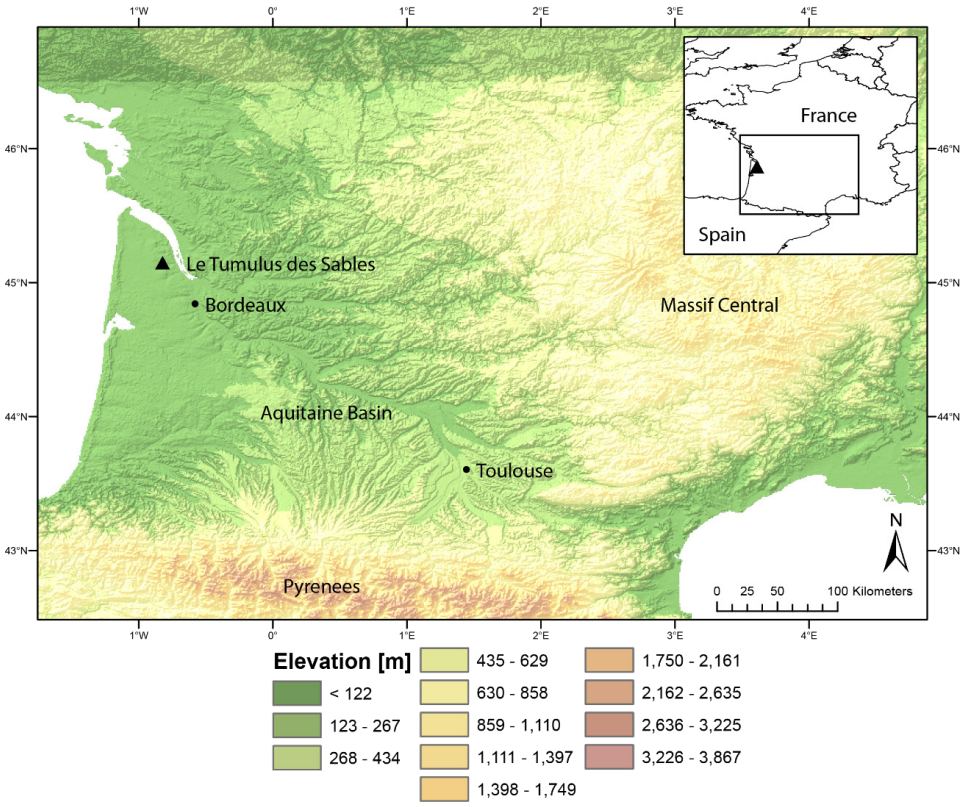

Figure 5-12: Regional setting of the collective burial at Le Tumulus des Sables, southwest France. Elevation data taken from worldclim.org (Hijmans et al., 2005).

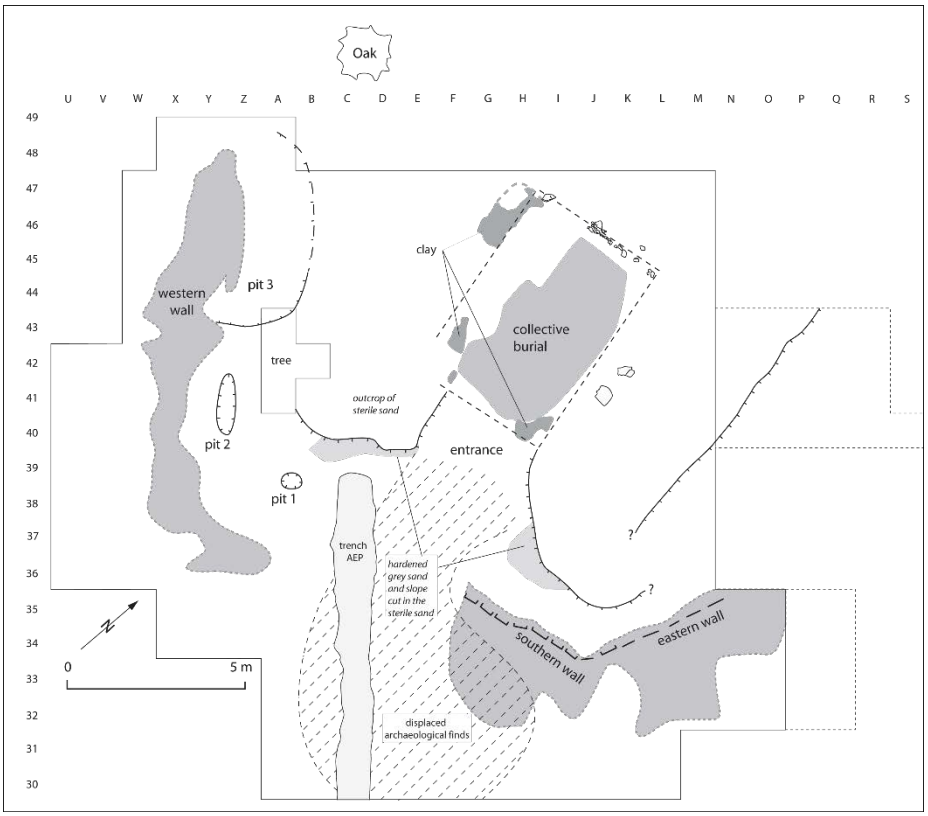

Figure 5-13: Sketch map of the site of Le Tumulus des Sables, showing collective burial and remains of the mound.

5.3.1.2 The Bell Beaker Phenomenon

The term Bell Beaker initially referred to a distinctive type of ceramic ware (inverted-bell shaped beakers), but has since come to describe an artefact assemblage, a cultural complex, a group of people, and time period (Benz and van Willigen, 1998; Price et al., 1998; Vander Linden, 2006; Desideri and Besse, 2010). The Bell Beaker Phenomenon (BBP) was widespread across Europe, from Central Europe to the Atlantic Ocean and from Scandinavia to the North Africa. It appears at the transition from the Neolithic to the Bronze Age about 3000 BC and persisting until about 1800 BC. The BPP appears at different times in different areas, was established on very different preceding local substrates, and in some cases coexisted with local cultures (Desideri and Besse, 2010). Numerous types of artefact have come to be recognised as part of a Bell Beaker assemblage, including some of the first gold and copper objects in Europe, jet, amber and obsidian ornaments, V-perforated bone buttons, tanged daggers, and archery equipment including projectile points and stone wrist guards (Price et al., 1998, 2004; Vander Linden, 2006). While this artefact assemblage unites this widespread phenomenon, the funerary and domestic structures vary greatly. Funerary practices ranged from individual graves (predominantly in Eastern Europe) to re-use of graves, collective tombs and mass inhumations (predominantly in Western Europe) (Benz and van Willigen, 1998; Price et al., 1998, 2004; Besse and Desideri, 2004; Vander Linden, 2007; Desideri and Besse, 2010).

The wide geographic distribution of the BBP has been interpreted in a number of different ways. These include migration of a unique population into Europe, long distance exchange of prestige goods, and diffusion of the cultural components of the BBP without movement of people. The appearance sequence of sites attributed to the BBP suggests a southwest to northeast trend originating on the Iberian Peninsula (Desideri and Besse, 2010; Fokkens and Nicolis, 2012; Czebreszuk, 2014) and movement along the Atlantic coastline (Prieto Martínez and Salanova, 2009). Direct evidence for high mobility during the Bell Beaker period comes from Sr isotope studies of Bell Beaker sites in Germany, Hungary, Austria and the Czech Republic (Grupe et al., 1997; Price et al., 2002, 2004). Price et al. (2004) found no difference in $^{87}Sr/^{86}Sr$ derived mobility between sex and age, and between early and late Bell Beaker people. In that study 51 out of 81 individuals were classified as non-locals. Direct investigation of mobility at the site Le Tumulus des Sables in south-western France fills an important geographic gap and can offer new insights into the distribution and mobility patterns of the BBP in western in Europe.

5.3.2 Isotopic analysis of human remains

Through radiocarbon dating and multi-isotope studies it is possible to reconstruct the age, diet and mobility pattern of an individual using a single tooth fragment.

5.3.2.1 Reconstructing diet

Carbon ($\delta^{13}C$) and nitrogen ($\delta^{15}N$) isotopic compositions can be used to reconstruct diet in archaeological populations due to isotopic differences between food types and trophic levels (Richards and Hedges, 1999; Privat et al., 2002; Richards, 2002; Schulting et al., 2008). The $\delta^{13}C$ and $\delta^{15}N$ of collagen, the main organic component of dentine, reflect the average protein components of the childhood diet. This means it will reflect the diet of food eaten over a long period of time and will average out individual potentially isotopically different food sources.

The isotopic composition of plant C ($\delta^{13}C$) is determined by the photosynthetic pathway utilised by the plant during photosynthesis to fix carbon from the atmosphere. Three pathways, C3, C4 and Crassulacean Acid Metabolism (CAM) lead to different average $\delta^{13}C$ values of -26.5, -12.5 and -19‰, respectively (Deines, 1980). However, geographic, temporal and plant specific differences exist (Heaton, 1999). Most C4 plants (e.g. grasses and sedges) are dominantly found in dry or arid environments, so in temperate climatic regions $\delta^{13}C$ can be used to distinguish between terrestrial and marine diet sources. The source of C in these two systems differs; atmospheric C (-7‰) being the main source in terrestrial systems and dissolved carbonate (0‰) being the main source in marine systems (Katzenberg, 2008). Fractionation occurs between the C in plant and herbivore animal tissue, decreasing $\delta^{13}C$ by 5‰ in bone collagen, and 10‰ in tooth enamel and bone collagen of carnivores exhibits an additional decrease of 1.5‰ (Schoeninger and DeNiro, 1984). Thus the $\delta^{13}C$ measured in human bone collagen will reflect the full range of isotopic variability of the food source caused by environmental, physiological and dietary processes. Generally, in human populations, an exclusively marine diet leads

to a bone collagen $\delta^{13}C$ of about -13‰ and an exclusively terrestrial C3 diet to a bone collagen $\delta^{13}C$ of about -20‰ (Chisholm et al., 1982).

In archaeological research $\delta^{15}N$ can be used to assess the amount and tropic level from which the food originated (Schoeninger et al., 1983; Sealy et al., 1987; Hedges and Reynard, 2007; Richards and Trinkaus, 2009). Nitrogen is incorporated into the food chain through plants by adsorbed soil compounds or from the atmosphere. ^{14}N is excreted by the body in preference to the heavier ^{15}N. Generally, an herbivore would have higher $\delta^{15}N$ than the plant source and a carnivore that fed on the herbivore would have another step higher than the herbivore. In the same area omnivores (such as humans) would fall in between those values. Typically, an increase in trophic level within a given environment is expected to lead to an increase in $\delta^{15}N$ of 1.3–5.3‰ per level (Schoeninger and DeNiro, 1984). However, a higher increase of ~6‰ from $\delta^{15}N$ from the diet to human bone collagen has also been observed (O'Connell et al., 2012). The greater number of trophic levels found in marine ecosystems result in higher $\delta^{15}N$ values, compared to terrestrial environments, resulting. Animals whose diet consisted entirely of marine resources have a $\delta^{15}N$ on average 9‰ higher (14.8±2.5‰) than those with an entirely terrestrial diet (5.9±2.2‰) while those with a mixed diet have intermediate values (Schoeninger and DeNiro, 1984).

5.3.2.2 Reconstructing mobility

Strontium ($^{87}Sr/^{86}Sr$) and O ($\delta^{18}O$) are two independent isotope systems that have been used together in various recent studies to investigate past mobility in Europe (Bentley and Knipper, 2005; Evans et al., 2006; White et al., 2007; Eckardt et al., 2009; Chenery et al., 2010; Hemer et al., 2013, 2014; Buckberry et al., 2014; Lamb et al., 2014). The basic principle is that the $^{87}Sr/^{86}Sr$ and $\delta^{18}O$ of teeth reflect the average isotopic composition of food and drinking water consumed during childhood, when the teeth were forming. By comparing the isotopic composition of a tooth with isotopic baseline maps it can be possible to identify mobility between different terrains and environments. A fundamental limitation of this method, however, is that geographically distant areas can have similar or overlapping isotopic compositions. Thus 'local' in this context means that it is not possible to distinguish between the isotopic composition of the skeletal remains and the surrounding environment. It remains possible that the individual came from a distant area of similar isotopic composition, however the use of multiple isotope systems reduces this possibility.

The isotopic composition of bioavailable Sr differs depending on the age, composition and weathering regime of the local rocks (Capo et al., 1998; Bentley, 2006; Slovak and Paytan, 2012). The $^{87}Sr/^{86}Sr$ signature in archaeological human remains is mainly controlled by the underlying geology, but can be modified by additional sources of Sr from atmospheric deposition (precipitation, seaspray, dust) and, in a modern context, fertiliser use (Price et al., 2002; Bentley, 2006; Evans et al., 2010; Voerkelius et al., 2010; Maurer et al., 2012; Slovak and Paytan, 2012; Frei and Frei, 2013). In regions with exogenic surface deposits (loess, glacial deposits, peat), the local bioavailable $^{87}Sr/^{86}Sr$ can be completely disconnected from the underlying bedrock geology. These complexities hinder inferring the range of

bioavailable $^{87}Sr/^{86}Sr$ from the bedrock geology, making it necessary to either measure or model that compositional range for a specific area. Humans and animals incorporate Sr from their diet into their dental and skeletal tissues (Beard and Johnson, 2000) where it substitutes for Ca and serves no metabolic function.

The oxygen isotopic composition of meteoric water is a function of geographic location and climate (Gat, 1996). $\delta^{18}O$ changes with the water source, temperature, elevation and quantity of precipitation, which creates a distinctive geographic profile (Dansgaard, 1964; Bowen and Wilkinson, 2002). However, this geographic profile will exhibit seasonal and annual variability as the climatological and atmospheric conditions change. The $\delta^{18}O$ of skeletal and dental remains is related to the composition of body water, which in turn is influenced by diet, physiology and climate. Most of the water consumed by humans comes from drinking water, typically sourced locally. The constant body temperature of mammals means the $\delta^{18}O$ is not influenced by environmental temperature, changing only with the composition of the ingested water (Longinelli, 1984; Luz et al., 1984). Seasonal changes in drinking water $\delta^{18}O$ cause fluctuations in $\delta^{18}O$ in a sedentary population. Seasonal changes in diet and behaviour can also add to this pattern (Balasse, 2003).

5.3.3 Materials and Methods

5.3.3.1 Human dental remains

Twenty five teeth (18 permanent, 7 deciduous) from Le Tumulus des Sables were selected for this study. The left maxillary second molar (LM2) was chosen for the adult samples and the left deciduous maxillary second incisor (LdI2) for juveniles, thus ensuring that each tooth came from a different individual. The permanent teeth represent individuals over 14 years of age, and the deciduous teeth represent individuals younger than 8 years of age.

Archaeological dental and skeletal material are affected by both physical and chemical changes after deposition, potentially leading to the loss of the original isotope composition. The degree of subsequent diagenetic overprinting can be different from sample to sample and depends on a large number of factors, including the length of burial, the hydro-geochemical environment, and the type of dental material (e.g., Bentley, 2006; Slovak and Paytan, 2011). Tooth dentine is prone to diagenetic overprinting because it contains pores ~ 1 µm diameter, which are larger than its phosphate crystals (Kohn et al., 1999). With time, elements from soil and water can move into the pore spaces of bones and dentine where dissolution and recrystallisation can occur. Tooth enamel, on the other hand, has phosphate crystals larger than 1 µm, a compact structure, and little pore space. It consists of ~ 96 wt.% Ca phosphate and is much denser, harder and more inert than bone and dentine. Several studies have shown that tooth enamel is much more resistant than bone or dentine to post-burial diagenesis and more likely to retain its original isotopic signature (Bentley, 2006; Slovak and Paytan, 2011; and references therein). The samples for the present study were checked for diagenetic overprint using *in situ* mapping of U, Th and Sr concentrations (Boel,

2011), and only samples that contained enamel areas likely to have preserved their original isotopic signatures were chosen for analysis. Due to the limited amount of material available, not all analytical techniques were applied to all samples. Of the 25 teeth selected, eight (7 permanent, 1 deciduous) were chosen for radiocarbon dating as well as C and N isotope analysis, and 22 (17 permanent, 5 deciduous) were chosen for O isotope analysis. All 25 (enamel and dentine) were analysed for Sr isotopes.

5.3.3.2 Radiocarbon dating

The discoloured surface of the dentine was removed with a tungsten carbide drill and the sample either drilled or cut and crushed in a pestle and mortar. Collagen was extracted and purified using an ultrafiltration protocol similar to that described by Brock et al. (2010). Briefly, the powdered sample was demineralised (HCl, 0.5M, 5°C, overnight), washed in NaOH (0.1M, room temperature, 30 minutes) and HCl (0.5M, room temperature, 1 hour), with thorough rinsing in MilliQ water between each treatment. Subsequently the sample was gelatinised (0.001 M HCl, 70°C, 20 hours), filtered (~ 90 μm Ezee™ filter) and ultrafiltered (Vivaspin™ VS15 30 kDa MWCO ultrafilter). The freeze-dried collagen was combusted in an evacuated sealed quartz tube in the presence of CuO wire and Ag foil. The CO_2 generated was cryogenically collected and purified prior to reduction to graphite over an Fe catalyst in the presence of H for measurement in a NEC single stage accelerator mass spectrometer at the ANU (Fallon et al., 2010). A sample size dependant background subtraction derived from repeat measurements of > 50 ka bone (from Latton, UK) and young bone (from the Batavia and Vergulde Draeck shipwrecks, Australia) was subtracted from each sample following the method of Wood et al., (2010). Calibration was carried out in OxCal v4.2 (Bronk Ramsey, 2009) against IntCal13 (Reimer, 2013).

5.3.3.3 Carbon and nitrogen isotope analysis

A second aliquot was taken from the collagen extracted for radiocarbon dating for C and N stable isotope analysis. $\delta^{13}C$ and $\delta^{15}N$ were measured in a Sercon 20-22 isotope ratio mass spectrometer coupled to an ANCA GSL elemental analyser operating in continuous flow mode. Samples were referenced to an in-house gelatin standard and corrected against USGS-40 and USGS-41.

5.3.3.4 Strontium isotope analysis

After the tooth surface was cleaned, 0.2–0.5 mg of enamel and dentine were drilled out using a custom made drill bit at 500 rpm. The tooth powder was then leached in 0.5 ml 1 M NH_4NO_3 to remove any residual contamination and digested in 1 ml ultrapure concentrated HNO_3 for 1 h. The samples were then evaporated to dryness, redissolved in 2 ml 2 M HNO_3 and subjected to ion exchange chromatography using micro columns with Eichrom Sr specific resin (pre-filter and Sr spec resin) to isolate Sr from other elements. A drop of dilute H_3PO_4 was added to each sample before loading onto Re filaments with a TaF_5 activator. Samples were analysed on the TRITON Plus thermal ionisation mass spectrometer (TIMS) at the Research School of Earth Sciences, ANU. Data were evaluated using a Rb

correction, exponential mass bias correction ($^{86}Sr/^{88}Sr$ = 0.1194) and 2σ outlier rejection. Total procedural blanks were determined by isotope dilution using an ^{84}Sr enriched spike, measured on the TRITON Plus TIMS and were below 100 pg Sr. Long term measurements of the Sr carbonate standard SRM987 gave $^{87}Sr/^{86}Sr$ = 0.71023±0.00002 (n = 99, 2σ) which is in agreement with the most precise of modern measurements (0.710250±0.000003: Hans et al., 2013) and within uncertainty of the original certified value of 0.71034±0.00026 (Moore et al., 1982).

5.3.3.5 Oxygen isotope analysis

A cross section of tooth enamel was cut using a dental drill fitted with a fine diamond saw blade. The samples were then mounted around crystals of Durango 3 mineral apatite standard (Rigo et al., 2012), cast in epoxy and polished to expose the enamel in cross section. After washing with petroleum spirit, RBS solution and Millipore H_2O the mounts were dried for at least 24 h in a 60˚C vacuum oven, then coated with high purity Al prior to analysis using the Sensitive High Resolution Ion MicroProbe (SHRIMP II) at the Research School of Earth Sciences. Analytical and instrumental conditions are described in detail by Trotter et al. (2008) and Ickert et al. (2008). Archaeological applications of SHRIMP II are outlined in Aubert et al. (2012). Durango 3 was analysed first and then after every five enamel measurements. The $\delta^{18}O$ of Durango apatite was 9.4‰ relative to VSMOW. Each tooth traverse consisted of a line of between 3 and 17 spots, working from the enamel layer closest to the dentine outward to the tooth surface. The number of spots was determined primarily by the thickness of the enamel. Three samples (A4, J4, J5) did not contain enough enamel for analysis. The standard deviations of the SHRIMP $\delta^{18}O$ apatite analyses of Durango 3 from the six sample mounts ranged from 0.12 to 0.39‰.

The incorporation of O isotopes into skeletal tissues involves physiological mass fractionation. The isotopic offset between structural carbonates and body water is ~ 27‰; the phosphate to body water offset is smaller ~18‰ (Kohn and Cerling, 2002; France and Owsley, 2015). To compare the $\delta^{18}O$ measured *in situ* ($\delta^{18}O_{IS}$) in tooth enamel with that in the environment, it is necessary to estimate the contribution of carbonates to the measurement and then apply a conversion equation from phosphate ($\delta^{18}O_p$) to water ($\delta^{18}O_w$).

Approximately 12% of the tooth O analysed by *in situ* techniques is not derived from the phosphate fraction (Kohn and Cerling, 2002). Most of that 12% is carbonate bound. The difference in $\delta^{18}O$ between co-existing carbonate and phosphate is 7.8±1.5‰ (France and Owsley, 2015). Correcting for the contribution of carbonate to the $\delta^{18}O_{IS}$ measured *in situ* decreases the $\delta^{18}O_p$ by ~ 0.9‰. The conversion of $\delta^{18}O_p$ to $\delta^{18}O_w$ has been outlined in several equations (Longinelli, 1984; Luz et al., 1984; Levinson et al., 1987; Daux et al., 2008; Chenery et al., 2010). The multiple sources of uncertainty associated with the *in situ* measurement of $\delta^{18}O$ and with the conversion to $\delta^{18}O_W$ have led many researchers to suggest that it is better to rely on direct comparisons to the $\delta^{18}O$ of skeletal material from local fauna (e.g., rodents), not to measured drinking water compositions (Pollard et al., 2011; Laffoon et al., 2013). There

is a scarcity of data on $\delta^{18}O$ in skeletal material from Le Tumulus des Sables, however, so for this study the estimation of $\delta^{18}O_W$ from measured tooth $\delta^{18}O_{IS}$ has been necessary. For the human teeth we used equation (6) in Daux et al. (2008) where $\delta^{18}O_w = 1.54(\pm 0.09)\ \delta^{18}O_p - 33.72(\pm 1.51)$. We have accounted for the uncertainties in the conversion from $\delta^{18}O_{IS}$ to $\delta^{18}O_w$ by increasing the error envelope around each analysis to ± 1.9‰ (2σ).

5.3.3.6 Baseline Sr and O isotope maps

To determine the local range of bioavailable $^{87}Sr/^{86}Sr$ at Le Tumulus des Sables soil samples and associated fauna samples (*Microtus*. sp. teeth) were collected from several sediment layers from within and around the burial. The faunal teeth were crushed using a mortar and pestle and then subject to the same analytical procedure as the human teeth. The soil samples were pre-treated for Sr isotope analysis following the protocol DIN ISO 19730. Strontium was isolated from other elements using ion exchange chromatography using Eichrom Sr specific resin (pre-filter and Sr spec resin). Strontium isotope ratios were measured using a Thermo Finnigan Neptune multi-collector inductively coupled plasma mass spectrometer (MC-ICP-MS) equipped with a quartz dual cyclonic spray chamber, PFA 100 µl nebuliser and standard Ni cones at the Environmental Geochemistry and Geochronology Laboratory at the Research School of Earth Sciences, ANU. Data reduction included a correction for Kr and Rb isobaric interferences, exponential mass bias correction ($^{86}Sr/^{88}Sr = 0.1194$) and 2σ outlier rejection. Long term measurements of the Sr carbonate standard SRM987 (National Institute of Standards and Technology) on the Neptune MC-ICP-MS gave an average $^{87}Sr/^{86}Sr$ value of 0.71023±0.00001 (n = 167, 2σ).

Plant samples and soil leachates from the Isotopic Reconstruction of Human Migration (IRHUM) database (Willmes et al., 2014) were used to infer the regional range of bioavailable $^{87}Sr/^{86}Sr$ for the major geologic units of southern France, including the Aquitaine Basin, the Pyrenees and Massif Central. These sample types were chosen because they provide a good estimate of the differences in bioavailable $^{87}Sr/^{86}Sr$. A map of bioavailable $^{87}Sr/^{86}Sr$ for all of France, including a detailed overview of our mapping procedures can be found in chapter 3.

A subset of the global dataset of gridded maps of the isotopic composition of meteoric waters (Bowen and Revenaugh, 2003; Bowen, 2015) was used to determine the range of $\delta^{18}O$ in the surrounding environment. Local modern weather station data from the International Atomic Energy Agency (IAEA) Global Network of Isotopes in Precipitation (GNIP) database from France and northern Spain were also used, the closest station to the site being Cestas-Pierroton (44°44'17"N, 00°46'29"W). The data were processed in ESRI ArcGIS™ and statistical analysis was carried out using R (R Core Team, 2013).

5.3.4 Results and discussion

5.3.4.1 Chronology of the site

The new radiocarbon results from eight teeth, in combination with the two human bone and two charcoal dates from previous studies, illustrate the complex chronology of the site (Table 5-7, Figure 5-14). The two charcoal dates from the top and bottom of the burial are 1395–1215 cal. BC and 6090–5925 cal. BC, respectively, bracketing the teeth and bone ages from the site. However, the charcoal dates may not directly relate to the funeral use of the site, and charcoal can easily move within the sediments. One bone date and six of the teeth dates fall within the range of the Bell Beaker period in France: 2900–1800 BC (Champion et al., 2009). One tooth (A4-SLMEM466) and the juvenile vertebra are significantly older, 3650–3520 cal. BC and 3650–3375 cal. BC, respectively. One tooth (A3-SLMEM454) was much younger, 1275–1120 cal. BC, close to the age of the charcoal sample from the top of the burial. These dates show that Le Tumulus des Sables is a highly mixed site that was used across multiple time periods. The collective burial was built during the Neolithic and reused during the Bell Beaker Period, during the second half of the third millennium BC. The discovery of many broken and dislocated bones outside of the burial the chamber, near the entrance (Figure 5-13) indicate a partial emptying of the burial, before its use by the Bell Beaker. According to one radiocarbon date, the use of the burial continued during the Early Bronze Age indicating a re-occupation of this space, without direct relation with the collective burial. This conclusion is in agreement with the archaeological material found at the site that indicates use during multiple time periods. The large number of artefacts associated with the BBP found at the site, and the fact that six of the eight randomly selected individuals are from the BBP period, suggests that most of the individuals found at this site belong to the BBP. The wide age range of the site and the disturbed stratigraphy, however, prevent the definite identification of a particular sample as belonging to a certain time period without individually dating it. When using isotope analysis to determine diet and mobility it cannot be assumed *a priori* that the samples represent a single population.

Table 5-7: Details of ^{14}C dating samples. The bone and charcoal dates are summarised in the excavation reports (Courtaud et al., 2009, 2010). $\delta^{13}C$ is measured on the AMS and used during date calculation. It is not equivalent to IRMS $\delta^{13}C$ values. For reliable stable isotope and radiocarbon analysis, % collagen yield should be >1%, C:N ratio between 2.9-3.4 and %C >30% (van Klinken, 1999).

Sample Name	Laboratory code	Sample material	$\delta^{13}C$	±	Collagen yield [%]	C:N	% C	^{14}C age [BP]	±	^{14}C age [calBC, 95.4% range]	
A01 - SLMEM263	SANU 39010	Tooth	-21	1	2.8	3.2	46.7	3570	25	2017	1784
A02 - SLMEM900	SANU 38939	Tooth	-15	1	9.1	3.2	46.2	3950	25	2566	2347
A03 - SLMEM454	SANU 38938	Tooth	-15	1	7.6	3.2	46.0	2980	25	1277	1121
A04- SLMEM466	SANU 39009	Tooth	-22	1	6.9	3.2	45.0	4800	30	3650	3522
A06 - SLMEM282	SANU 39005	Tooth	-19	1	5.9	3.2	46.0	4030	25	2620	2475
A08 - SLMEM432	SANU 39006	Tooth	-20	1	9.3	3.2	45.3	4045	25	2831	2480
A12 - SLMEM1007	SANU 39007	Tooth	-19	1	5.9	3.2	45.5	3850	25	2458	2207
J02 - SLMEM66	SANU 38901	Tooth	-20	1	6.0	3.2	46.3	3815	25	2345	2146
Bone SLMEM07	Poz 23194	Bone						3915	35	2487	2291
Bone St. Laurent 02/07-1	Erl 10575	Bone						4755	35	3648	3374
Charcoal Lyon-6217	SacA 16631	Charcoal						3040	30	1397	1216
Charcoal Lyon-6216	SacA 16630	Charcoal						7160	40	6092	5927

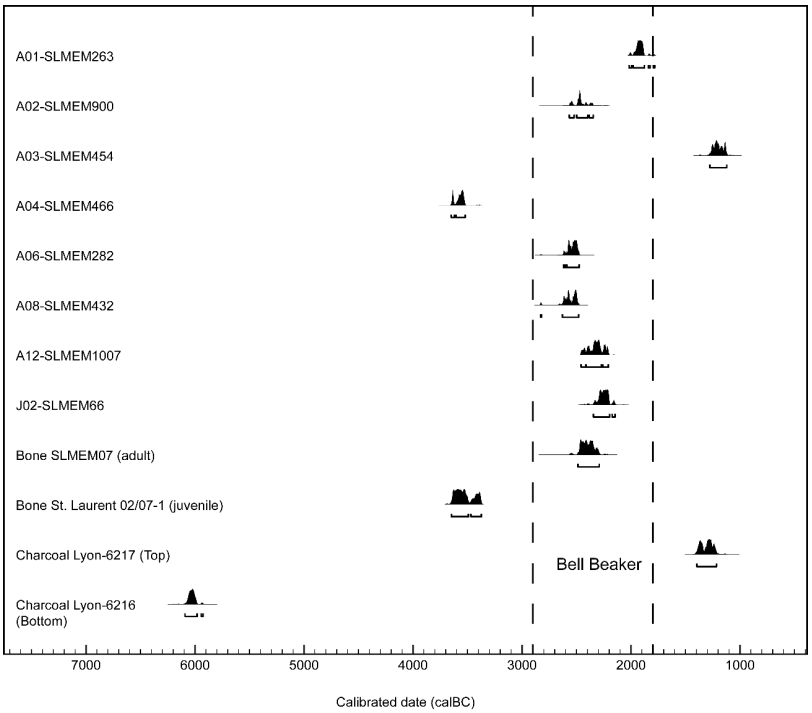

Figure 5-14: Radiocarbon results of the eight teeth analysed in this study, as well as the two bone and two charcoal dates previously obtained from this site (Courtaud et al., 2010). Bell Beaker time period estimates (Champion et al., 2009) are shown as dashed lines.

5.3.4.2 Diet

The eight individuals analysed have $\delta^{13}C$ between -19.6 and -20.6‰ and $\delta^{15}N$ between 9.4 and 11.4‰. These are narrow ranges, despite the very different ages of the individuals, and suggest a predominantly terrestrial diet consistent with isotopic compositions found at other European Neolithic sites (Figure 5-15). It appears that diet remained relatively terrestrial throughout the extended lifetime of the site, despite its close proximity to the Gironde Estuary and the Atlantic Ocean.

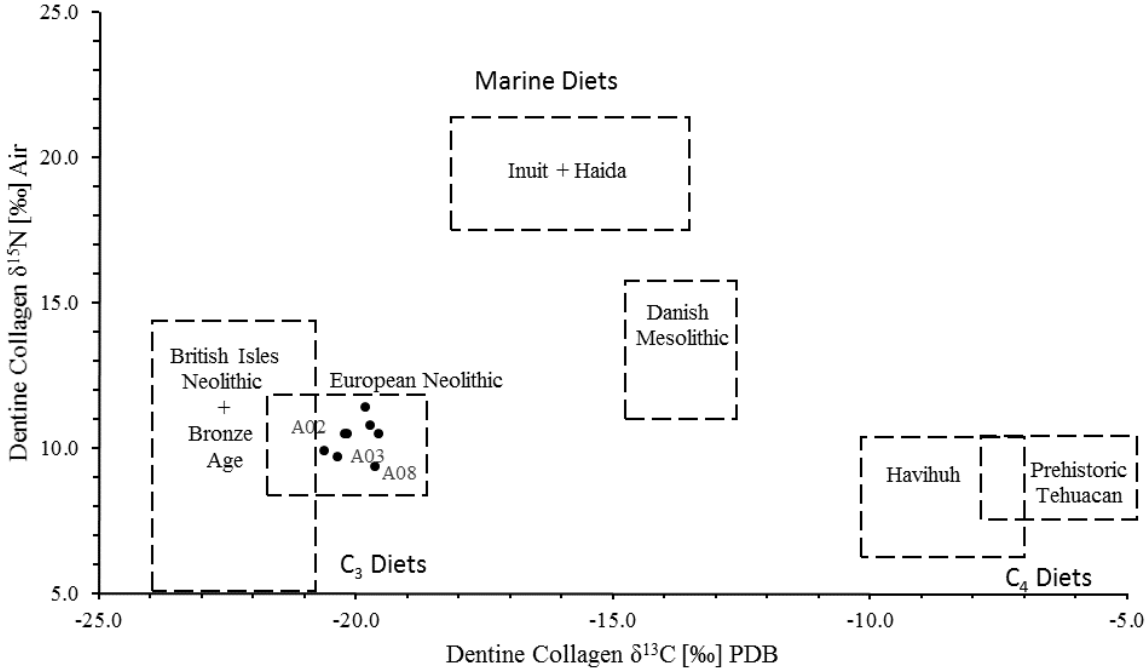

Figure 5-15: Carbon and nitrogen isotope results for eight individuals in this study with approximate dietary groups as dashed boxes (Schoeninger et al., 1983; Pollard, 1993).

5.3.4.3 Human mobility

$^{87}Sr/^{86}Sr$ and $\delta^{18}O$ baseline data

Le Tumulus des Sables is situated on the Médoc peninsula, a flat, low lying region situated between the Atlantic coast and the Gironde Estuary, dominated by unconsolidated Quaternary and Neogene sediments. The site lies within Pliocene sand, clay and gravel, with a band of Holocene sands, clays, pebbles and gravel along the shorelines to the north and east. There are small patches of Eocene and Oligocene limestone, conglomerate and sandstone towards the eastern edge in close proximity to the site (Figure 5-16). The range of bioavailable $^{87}Sr/^{86}Sr$ at Le Tumulus des Sables is 0.7081–0.7102, as determined from soil leachates (0.7088–0.7099) and faunal samples (0.7081–0.7102), with average differences between the sample types of 0.0007 (Table 5-8). This intra site variation is large and most likely reflects the variability of the sand and clay sedimentary units within the site and the mixing caused by repeated burials in this location.

Table 5-8: Bioavailable $^{87}Sr/^{86}Sr$ at Le Tumulus des Sables determined by soil leachates and faunal samples (*Microtus*. sp. teeth).

Grid reference	Location	Soil $^{87}Sr/^{86}Sr$	±2se	Faunal $^{87}Sr/^{86}Sr$	±2se
H43	Within the burial	0.70893	0.00001	0.70827	0.00003
I43	Within the burial	0.70973	0.00002	0.70909	0.00002
H42	Within the burial	0.70963	0.00002		
H45	Within the burial	0.70910	0.00004		
J44	Within the burial	0.70883	0.00002	0.70808	0.00005
G40	Within the burial	0.70879	0.00002	0.70906	0.00017
G44	Within the burial	0.70876	0.00002	0.70904	0.00015
E30	Outside the burial	0.70949	0.00004	0.71016	0.00006
E34	Outside the burial	0.70920	0.00002	0.70906	0.00009
H36	Outside the burial	0.70991	0.00002	0.70961	0.00003
H38	Outside the burial	0.70887	0.00001	0.70827	0.00008
$^{87}Sr/^{86}Sr$ range in the burial		0.7088-0.7097		0.7081-0.7091	
$^{87}Sr/^{86}Sr$ range adjacent to the burial		0.7089-0.7099		0.7083-0.7102	
Local $^{87}Sr/^{86}Sr$ range combined		**0.7081-0.7102**			

The range of bioavailable $^{87}Sr/^{86}Sr$ from different geologic units in France is based on plant and soil leachate data from the IRHUM database (Willmes et al., 2014). There are significant differences between different lithological units both in terms of average bioavailable $^{87}Sr/^{86}Sr$ and the range of bioavailable $^{87}Sr/^{86}Sr$ within the lithological unit (Figure 5-16A). The isotope packages (Figure 5-16B) encompass all lithological units and group them to reduce internal variability while maximising the difference between groups. The local range of bioavailable $^{87}Sr/^{86}Sr$ at Le Tumulus des Sables is distinct from the isotopic compositions of volcanic, igneous and metamorphic rocks mainly found in the Massif Central, Armorican Massif and Pyrenees, but overlaps with those of carbonaceous sediment units of the Aquitaine Basin. Although there is significant overlap in bioavailable $^{87}Sr/^{86}Sr$ between the lithological units of southern France, the different areas of the study region can be broadly distinguished (Figure 5-17).

The annual average $\delta^{18}O$ of precipitation ($\delta^{18}O_W$) exhibits a distinct geographic profile across Western Europe and Northern Africa. The $\delta^{18}O_W$ is highest in Africa, becoming progressively lower northwards into Spain and southwest France (Figure 5-18). There is a strong trend to more negative $\delta^{18}O_W$ across Europe from southwest to east. Lower $\delta^{18}O_W$ is also found in areas of higher elevation, such as the Pyrenees and the Alps. The global dataset of gridded maps of the isotopic composition of meteoric waters (waterisotopes.org; Bowen and Revenaugh 2003) provides an estimated $\delta^{18}O_W$ for Le Tumulus des Sables (45°8'44" N, 00°49'37" W, elevation 20 m) of -6.4±0.3‰.

These predicted compositions are close to those of modern precipitation in the area (Daux et al., 2008). Modern weather station data from the IAEA-GNIP database for the closest station (Cestas-Pierroton: 44°44'17" N, 00°46'29" W, elevation 59 m) 50 km south of Le Tumulus des Sables, shows an average annual $\delta^{18}O_W$ of -5.72±1.57‰. IAEA modern weather station data from France and northern Spain shows an average shift of 3‰ between winter and summer meteoric water $\delta^{18}O_W$. The seasonal averages

for $\delta^{18}O_W$ at Cestas-Pierroton are winter: -6.59±1.17‰, spring: -5.79±1.36‰, summer: -4.75±1.07‰, autumn: -5.85±2.23‰. A conservative estimate of the modern range in $\delta^{18}O_W$ for Le Tumulus des Sables and the western Aquitaine Basin is therefore -4.15 to -6.7‰. The baseline map presented here can only serve as a guideline to predict the variation of $\delta^{18}O$ across the landscape, because significant variation in $\delta^{18}O$ is expected between different seasons and subtle changes from year to year in atmospheric patterns can have a significant effect on $\delta^{18}O$ in rainwater. Finally, how $\delta^{18}O_W$ has changed through time is not well understood, both the magnitude and geographic distribution of $\delta^{18}O_W$ might have been quite different ~ 4 ka ago.

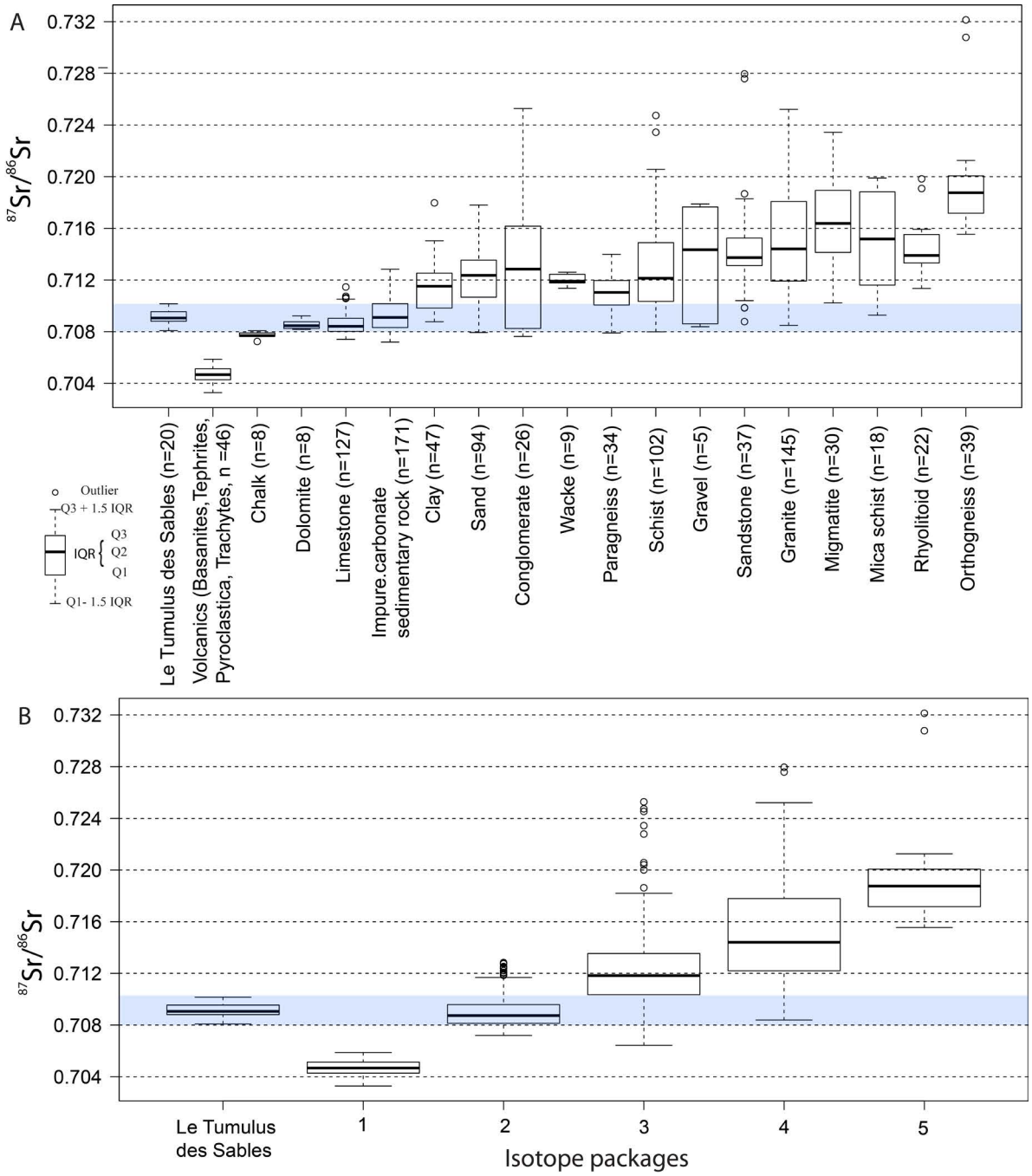

Figure 5-16: A: Box plots of bioavailable $^{87}Sr/^{86}Sr$ isotope ranges for the different lithological units of France based on soil leachate and plant data from the IRHUM database (Willmes et al., 2014). B: Box plots of the bioavailable $^{87}Sr/^{86}Sr$ isotope packages. The shaded bar shows the $^{87}Sr/^{86}Sr$ range at the site of Le Tumulus des Sables.

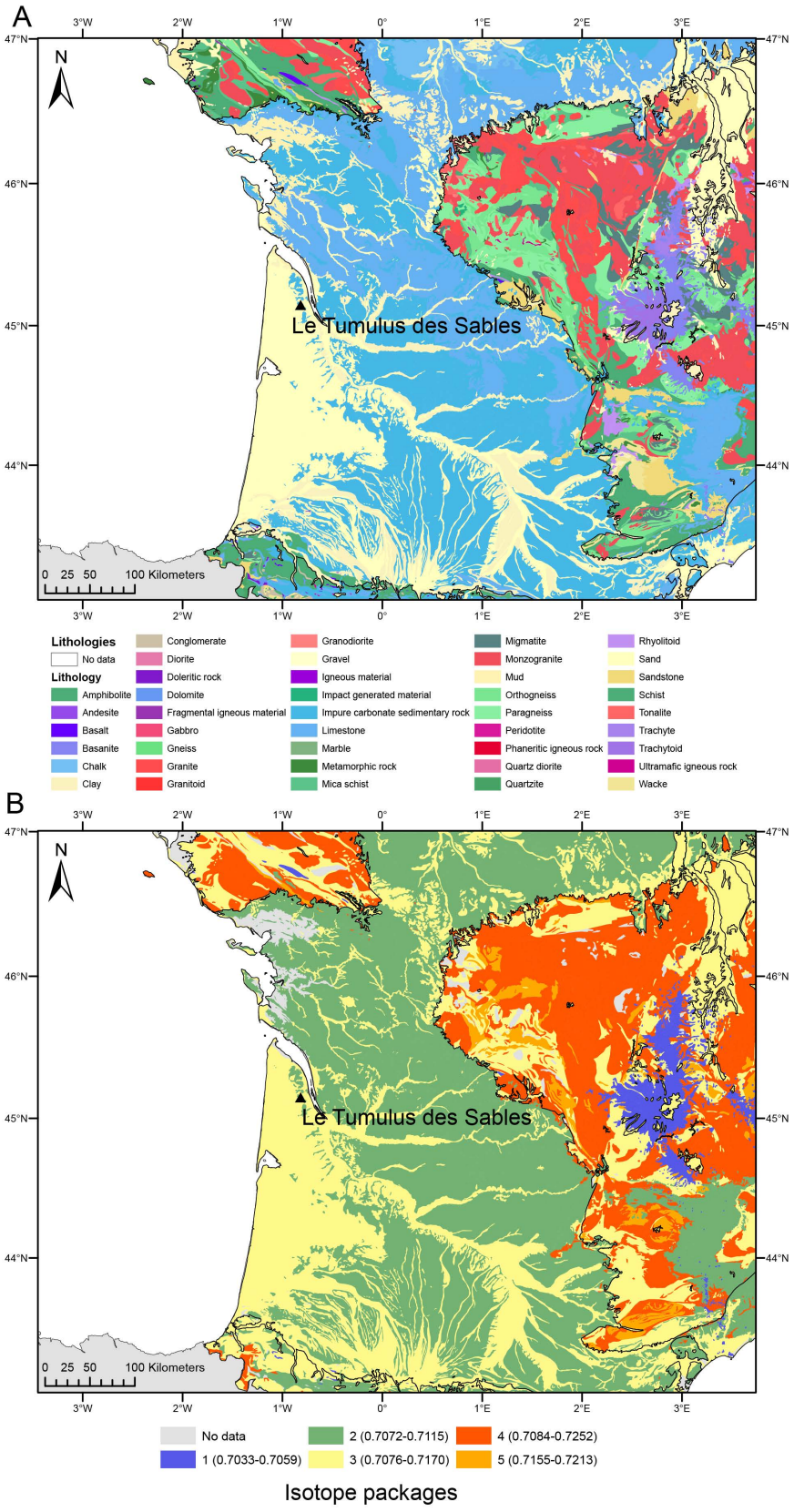

Figure 5-17: A: Surface geologic map of France (BRGM). B: Isotope package map of bioavailable $^{87}Sr/^{86}Sr$ in southern France based on the IRHUM database (Willmes et al., 2014).

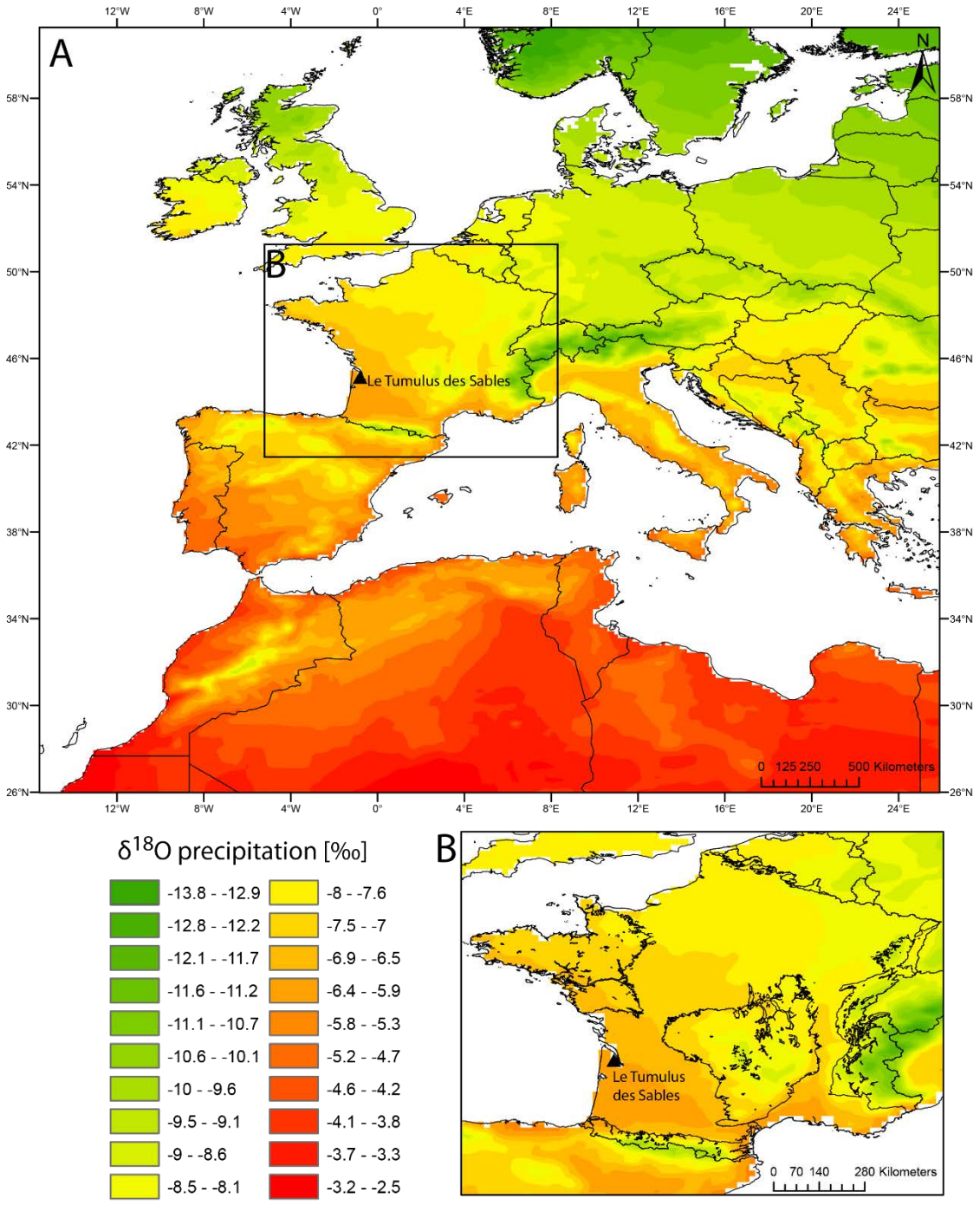

Figure 5-18: A: Annual average $\delta^{18}O_w$ of precipitation across Europe and part of northern Africa. B: Average $\delta^{18}O_w$ of precipitation in France. Data from waterisotopes.org (Bowen and Revenaugh, 2003; Bowen, 2015).

Intra-tooth differences in $\delta^{18}O$

In situ analysis of tooth enamel, which allows for multiple measurements across the enamel thickness, can be used to investigate intra-tooth differences in $\delta^{18}O$ (Figure 5-19, Table 5-9). Intra-tooth compositional heterogeneity appears to be a remnant of the two-stage enamel formation process, amelogenesis. The initial phase, matrix production, results in the creation of successive organic-rich layers that become highly mineralised during the second phase of maturation (Butler, 1978; Hillson, 2005). Changes in the $\delta^{18}O$ of ingested water during this formation process, due to seasonal influences of rainwater, physiological changes, geographical movement or cultural changes, may produce changes in $\delta^{18}O$ within the enamel. Intra-tooth heterogeneity has previously been found in hypsodont and continuously growing teeth, and has been used to assess climate, seasonality and migration (Fricke and O'Neil, 1996; Balasse, 2002; Zazzo et al., 2005; Bernard et al., 2009; Stevens et al., 2011). The present study is one of the first to assess intra-tooth $\delta^{18}O$ variation across the enamel in human teeth.

The teeth analysed had intra-tooth ranges in $\delta^{18}O$ of between 1.1 and 3.1‰. The first analysis in two of the samples (A11, A15), that closest to the enamel-dentine boundary, was more than 2‰ different from the next spot in the profile, accounting for most of the isotopic range in those teeth. Studies of diagenetic overprint in human tooth enamel have shown that areas closest to the enamel-dentine boundary commonly have higher levels of diagenetic overprint (Rainer Grün et al., 2008). In contrast, some studies of herbivore teeth have shown the opposite (e.g., Müller et al., 2013). It is possible that a diagenetic overprint has influenced the first spot analyses from samples A11 and A15, so the compositions of those spots have been omitted from further consideration. This reduces the intra-tooth heterogeneity in A11 from 3.5 to 1.7‰, and in A15 from 3.2 to 2.8‰. One sample (A16) shows an overall rise in $\delta^{18}O$ of 3.1‰ along the measured profile, a compositional range that is probably an original feature.

Considering the seasonal variation in the $\delta^{18}O$ of modern precipitation, it is likely that the intra-tooth heterogeneity in $\delta^{18}O$ in the analysed samples records seasonal changes in the $\delta^{18}O$ of water ingested during the period of tooth formation/mineralisation. However, due to the complex spatial and temporal patterning of human enamel mineralisation (Suga, 1989) this is unlikely to represent a simple time series record. As all samples appear to be influenced by the same agent (seasonality), the median $\delta^{18}O$ for each profile can be used to assess human mobility.

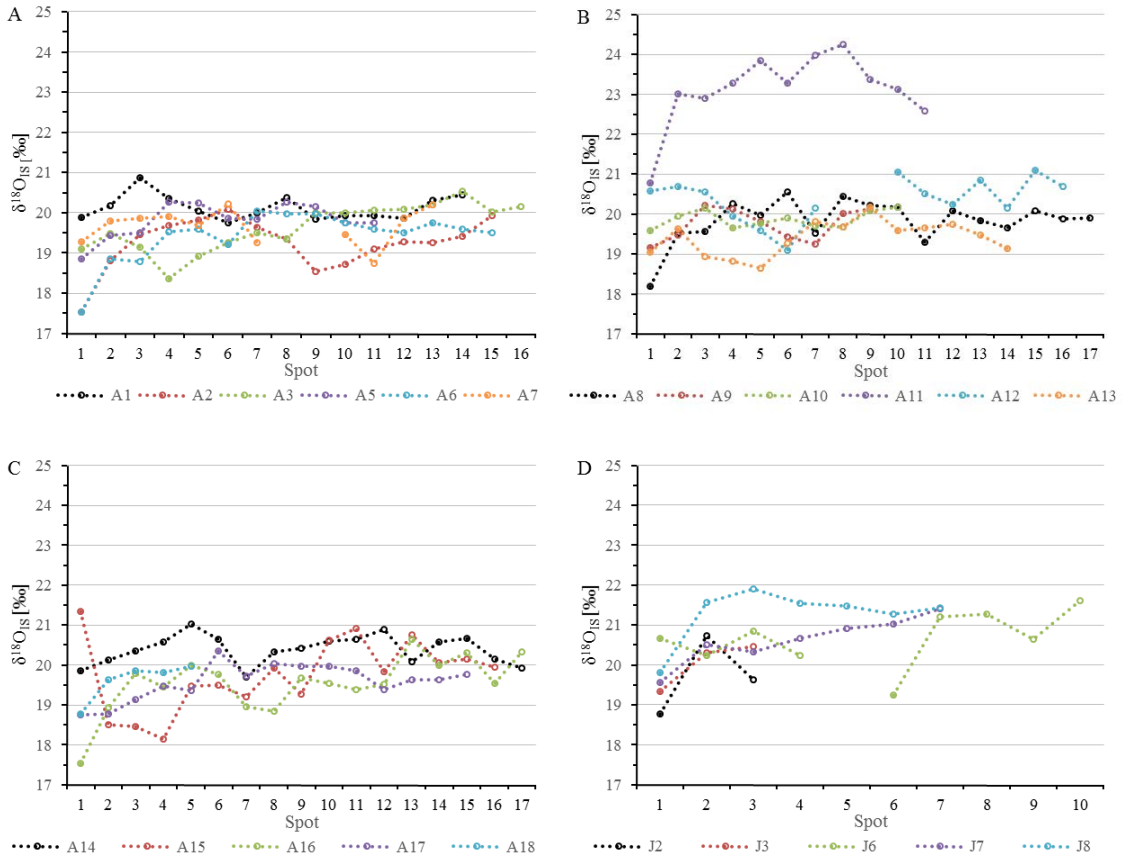

Figure 5-19: Intra-tooth profiles of enamel $\delta^{18}O$. All profiles are plotted running outwards from close to the enamel-dentine boundary to the tooth's outer surface.

Table 5-9: $\delta^{18}O$ of human teeth from Le Tumulus des Sables.

Sample ID	Tooth	$\delta^{18}O_{IS}$ Average [‰]	±2σ	N	Intra tooth range ‰	$Enamel_p$ [‰]	±2σ	$Enamel_w$ [‰]	±2σ
A01 - SLMEM263	Permanent	20.1	0.6	14	1.1	19.2	1.6	-4.2	2.2
A02 - SLMEM900	Permanent	19.2	1.3	15	2.5	18.3	2.0	-5.5	2.5
A03 - SLMEM454	Permanent	19.6	1.2	16	2.2	18.7	1.9	-4.9	2.4
A04- SLMEM466	Permanent								
A05 - SLMEM308	Permanent	19.8	0.9	11	1.4	18.9	1.7	-4.7	2.3
A06 - SLMEM282	Permanent	19.4	1.3	15	2.5	18.5	2.0	-5.3	2.5
A07 - SLMEM1157	Permanent	19.7	0.9	11	1.5	18.7	1.8	-4.9	2.3
A08 - SLMEM432	Permanent	19.8	1.1	17	2.4	18.9	1.9	-4.6	2.4
A09 - SLMEM112	Permanent	19.7	0.8	9	1.1	18.8	1.7	-4.8	2.3
A10 - SLMEM813	Permanent	19.9	0.5	10	0.6	18.9	1.6	-4.6	2.2
A11- SLMEM861	Permanent	23.4	1.1	10	1.7	22.4	1.8	0.8	2.4
A12 - SLMEM1007	Permanent	20.4	1.1	14	2.0	19.4	1.9	-3.8	2.4
A13 - SLMEM1094	Permanent	19.4	0.9	14	1.5	18.5	1.8	-5.3	2.3
A14 - SLMEM1289	Permanent	20.4	0.8	17	1.3	19.5	1.7	-3.8	2.3
A15 - SLMEM491	Permanent	19.7	1.7	15	2.8	18.7	2.3	-4.9	2.7
A16 - SLMEM298	Permanent	19.5	1.4	17	3.1	18.6	2.1	-5.1	2.6
A17 - SLMEM509	Permanent	19.6	0.9	15	1.6	18.7	1.8	-5.0	2.3
A18 - SLMEM5	Permanent	19.6	1.0	5	1.2	18.7	1.8	-5.0	2.4
J02 - SLMEM66	Deciduous	19.7	2.0	3	2.0	18.8	2.5	-4.8	2.9
J03 - SLMEM1251	Deciduous	20.0	1.2	3	1.1	19.1	1.9	-4.3	2.5
J04 - SLMEM119	Deciduous								
J05 - SLMEM102	Deciduous								
J06 - SLMEM1192	Deciduous	20.7	1.4	9	2.4	19.7	2.1	-3.3	2.6
J07 - SLMEM86	Deciduous	20.6	1.2	7	1.8	19.7	1.9	-3.4	2.4
J08 - SLMEM276	Deciduous	21.3	1.4	7	2.1	20.4	2.0	-2.4	2.5

$^{87}Sr/^{86}Sr$ and $\delta^{18}O$ in the human remains

The $^{87}Sr/^{86}Sr$ of enamel and dentine from the 25 individuals is in the ranges 0.70904–0.71331 and 0.70904–0.71187, respectively (Table 5-10). Nine individuals have significant differences in $^{87}Sr/^{86}Sr$ (> 0.00050) between dentine and enamel, the ratio being lower in dentine (Figure 5-20A). Dentine and enamel should have similar $^{87}Sr/^{86}Sr$, but as discussed above, dentine is the more susceptible to diagenetic alteration that can shift its isotopic composition towards the local range. It is likely, therefore, that the nine samples with Sr isotopic differences between enamel and dentine have been affected by diagenesis. The $^{87}Sr/^{86}Sr$ in two other samples is higher in dentine than in the enamel, again indicative of alteration, but possibly under different conditions. These inconsistencies between dentine and enamel compositions show that, at this site, dentine has not preserved its original $^{87}Sr/^{86}Sr$, leaving enamel compositions as the more reliable tracer of human mobility. Enamel $\delta^{18}O_p$ from the 22 analysed individuals ranged from 18.3 to 22.4‰, equivalent to $\delta^{18}O_W$ of approximately -5.5 to 0.8‰ (Table 5-10). The conversion from $\delta^{18}O_p$ to $\delta^{18}O_w$ is subject to several sources of uncertainty in the equations (Daux et al., 2008), leading to large uncertainties of ~ 2.5‰ in each calculated value (Figure 5-20B). Some of the larger uncertainties apply equally to all analyses, however, so differences between individuals may still be observed.

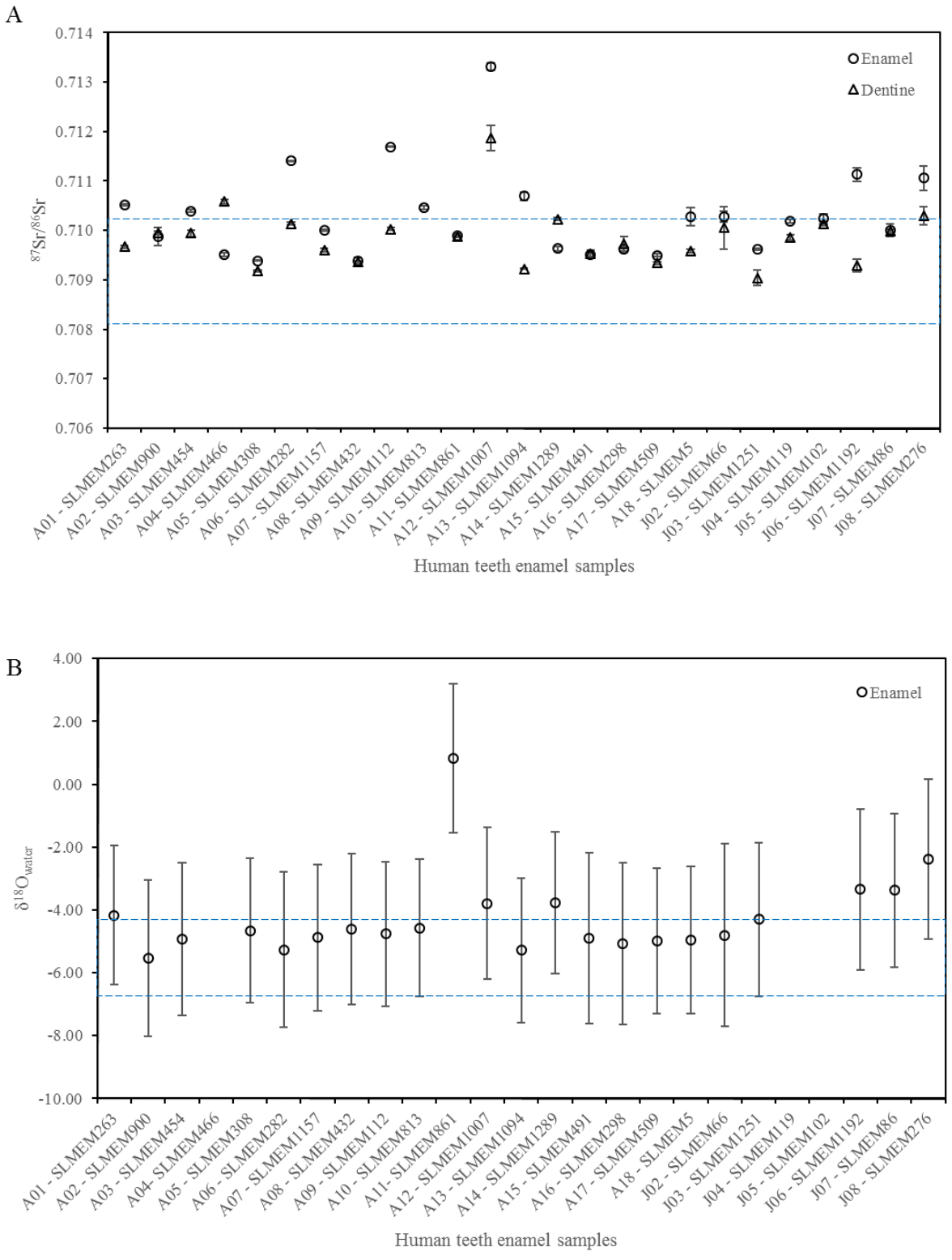

Figure 5-20: A: $^{87}Sr/^{86}Sr$ in tooth enamel and dentine. Uncertainties are 2se. B: $\delta^{18}O_w$ calculated from the $\delta^{18}O_p$ of enamel. Uncertainties are 2σ. Dashed lines indicate the local isotope range at the site of Le Tumulus des Sables.

Human mobility

K-means cluster analysis was applied to the tooth enamel isotopic compositions. The number of clusters was varied to achieve the best fit using clValid (Brock et al., 2008). Five statistically distinct groups of individuals (Figure 5-21) were identified. The median compositions of the defined clusters can be compared to the isotope baseline maps (Figure 5-17, Figure 5-18) to assess the regions from which those people might have originated. No systematic differences were found between the isotopic compositions of adults and juveniles. The wide range of isotopic composition in the bioavailable Sr within the burial site and the immediately surrounding Aquitaine Basin, as well as the large uncertainties associated with the calculation of $\delta^{18}O_w$ from the $\delta^{18}O_p$ analyses, and uncertainties associated with predicting the geographic variations of $\delta^{18}O_w$ back in time limit the interpretation of the data in terms of human mobility. Nevertheless, some careful observations can be made about the different groups. The individuals in Group 1 (n = 8) have isotopic compositions ($^{87}Sr/^{86}Sr$: 0.70938–0.71001, $\delta^{18}O_w$: -5.1 – 3.4) consistent with the modern range of Sr compositions at the burial site, and O isotopic compositions of precipitation in the western Aquitaine Basin. The individuals in Groups 2 (n = 8) and 3 (n = 3) have more radiogenic $^{87}Sr/^{86}Sr$ isotope ratios than those in Group 1 (0.70988–0.71069 and 0.71141–0.71331 respectively), but similar $\delta^{18}O_w$. Isotopically the closest fit for Group 2 is isotope package 2, and for Group 3 isotope package 3. The geographically closest fit for the Sr isotope ratios in Group 2 are the carbonaceous sedimentary units < 5 km south of Le Tumulus des Sables. Large areas of the Aquitaine Basin have $^{87}Sr/^{86}Sr$ consistent with Group 3. The individuals in Group 4 (n = 2) and a single individual Group 5 (A11) have $\delta^{18}O_w$ (-3.3 – -2.4‰), and (0.8±2.4‰), respectively. These $\delta^{18}O_w$ compositions are outside the range of the modern $\delta^{18}O_w$ in the Aquitaine Basin. The $^{87}Sr/^{86}Sr$ isotope ratios of Group 4 fall into isotope package 3 and Group 5 to isotope package 1 within the $^{87}Sr/^{86}Sr$ isotope range of the burial. Using the current dataset, it is not possible to determine if these higher $\delta^{18}O_w$ values are an indication of a different childhood residence area or if they represent local and or seasonal variations in the drinking water supply, or water use practices (e.g. boiling) of these individuals. This reflects both the high analytical uncertainties when converting *in situ* $\delta^{18}O_p$ to $\delta^{18}O_w$ values, as well as the problem of comparing modern day precipitation water values to the hydrological environment several thousand years ago. Drinking water intake of prehistoric populations is likely to reflect a mixture of precipitation input and other surface and ground water inputs that could result in significantly different $\delta^{18}O$ values. In regards to human mobility we can interpret Group 1 to contain individuals who spent their childhood in the area of Le Tumulus des Sables. Groups 2 and 3 contain individuals who spent their childhood not directly at the site but in close proximity elsewhere in the Aquitaine Basin. No further interpretation is currently possible for Group 4 and 5. Finally, any interpretation of the individuals from Le Tumulus des Sables in regards to mobility within the Bell Beaker period is further limited because only eight of the teeth collected were of sufficient size and quality for ^{14}C dating. While six of these did fall into the Bell Beaker period the burial is too disturbed to assume any individual belonging to a certain period without individually dating it.

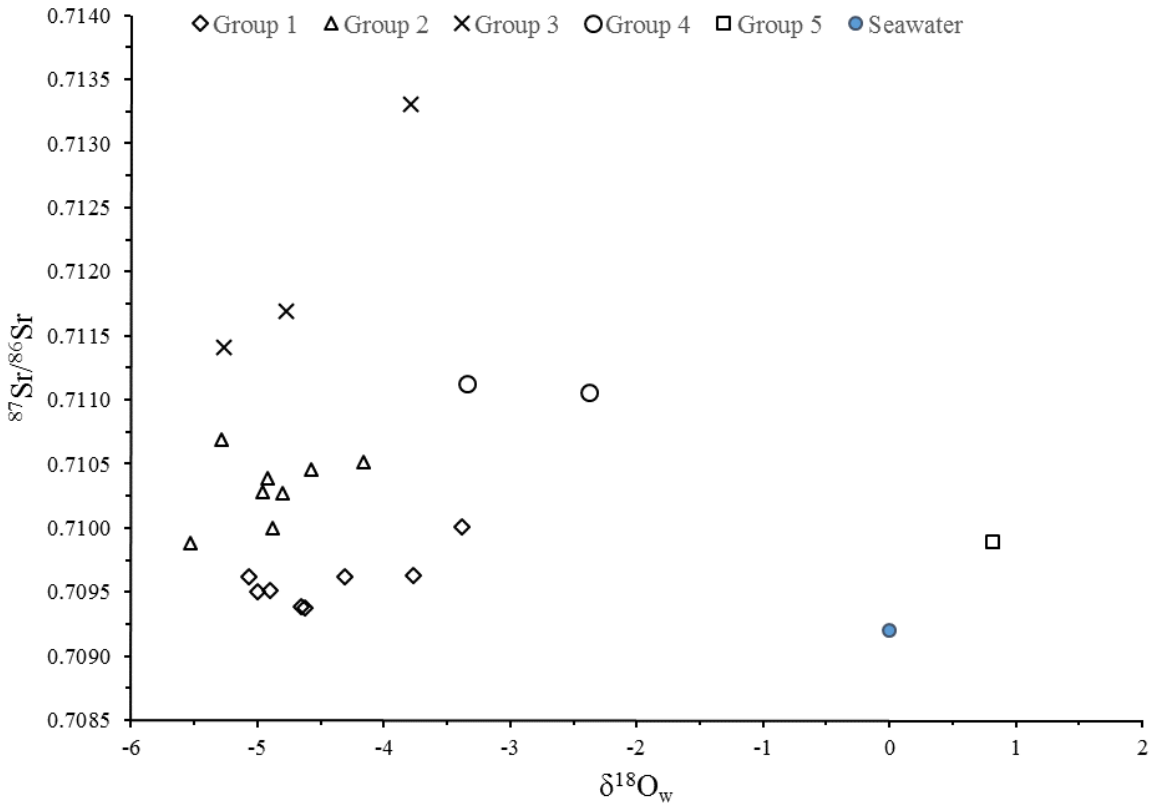

Figure 5-21: Strontium and oxygen isotope compositions of tooth enamel from the individuals buried at Le Tumulus des Sables. Groups determined by K-means cluster analysis using R (R Core Team, 2013).

Table 5-10: Summary of isotopic data for the individuals from Le Tumulus des Sables.

Sample			$^{87}Sr/^{86}Sr$				$\delta^{18}O$				$\delta^{13}C$	$\delta^{15}N$	
ID		Tooth	Enamel	±2se	Dentine	±2se	$Enamel_p$ ‰	±2σ	$Enamel_w$ ‰	±2σ	Dentine (PDB) ‰	Dentine (AIR) ‰	Group
A01	A01 - SLMEM263	Permanent	0.71051	2	0.70967	3	19.19	1.63	-4.16	2.22	-20.2	10.5	2
A02	A02 - SLMEM900	Permanent	0.70988	18	0.70995	4	18.31	1.98	-5.53	2.49	-19.81	11.41	2
A03	A03 - SLMEM454	Permanent	0.71039	3	0.70994	7	18.70	1.90	-4.92	2.43	-20.21	10.51	2
A04	A04- SLMEM466	Permanent	0.70951	3	0.71058	4					-19.6	10.5	
A05	A05 - SLMEM308	Permanent	0.70939	1	0.70918	2	18.87	1.74	-4.65	2.31			1
A06	A06 - SLMEM282	Permanent	0.71141	1	0.71014	3	18.48	1.97	-5.26	2.48	-19.7	10.8	3
A07	A07 - SLMEM1157	Permanent	0.71000	2	0.70960	4	18.72	1.76	-4.88	2.32			2
A08	A08 - SLMEM432	Permanent	0.70938	8	0.70936	3	18.90	1.87	-4.62	2.40	-19.6	9.4	1
A09	A09 - SLMEM112	Permanent	0.71169	1	0.71003	2	18.80	1.72	-4.77	2.29			3
A10	A10 - SLMEM813	Permanent	0.71046	4			18.93	1.57	-4.57	2.18			2
A11	A11- SLMEM861	Permanent	0.70989	4	0.70988	2	22.43	1.83	0.82	2.38			5
A12	A12 - SLMEM1007	Permanent	0.71331	7	0.71187	26	19.44	1.88	-3.79	2.41	-20.3	9.7	3
A13	A13 - SLMEM1094	Permanent	0.71069	9	0.70922	1	18.46	1.75	-5.29	2.31			2
A14	A14 - SLMEM1289	Permanent	0.70963	4	0.71023	2	19.45	1.68	-3.77	2.26			1
A15	A15 - SLMEM491	Permanent	0.70951	3	0.70953	7	18.71	2.25	-4.90	2.71			1
A16	A16 - SLMEM298	Permanent	0.70962	3	0.70972	16	18.61	2.08	-5.06	2.57			1
A17	A17 - SLMEM509	Permanent	0.70950	2	0.70934	3	18.65	1.76	-5.00	2.32			1
A18	A18 - SLMEM5	Permanent	0.71028	18	0.70958	3	18.67	1.80	-4.96	2.35			2
J02	J02 - SLMEM66	Deciduous	0.71027	11	0.71005	43	18.78	2.48	-4.81	2.90	-20.62	9.89	2
J03	J03 - SLMEM1251	Deciduous	0.70962	2	0.70904	16	19.10	1.94	-4.31	2.46			1
J04	J04 - SLMEM119	Deciduous	0.71019	4	0.70986	6							
J05	J05 - SLMEM102	Deciduous	0.71024	1	0.71014	4							
J06	J06 - SLMEM1192	Deciduous	0.71113	14	0.70929	13	19.73	2.07	-3.34	2.56			4
J07	J07 - SLMEM86	Deciduous	0.71001	13	0.70999	4	19.70	1.91	-3.38	2.44			1
J08	J08 - SLMEM276	Deciduous	0.71106	25	0.71030	18	20.35	2.03	-2.38	2.53			4

5.3.5 Conclusions

The results of this study of the chronology, diet, and mobility of individuals from the collective burial Le Tumulus des Sables lead to the following conclusions:

(1) The site was used for burials over a much longer period than previously thought. Initially classified as an early Bell Beaker site, the radiocarbon chronology and artefacts associated with the burials instead document occupation over a period of ~ 2.5 ka. Given the tendency of the BBP people to re-use collective tombs of preceding cultures, and considering the relatively large quantity of Bell Beaker material exhumed (especially ceramic finds), it is possible that most of the human remains found at this site represent the deceased of the BBP. However, without dating each individual the disturbed condition of the burial does not allow the secure identification of a specific individual to the BBP.

(2) The remains of eight individuals analysed to determine diet had a narrow range of isotopic compositions ($\delta^{13}C$ = -19.6 to -20.6‰, $\delta^{15}N$ = 9.4 to 11.4‰). This suggests, in combination with the radiocarbon dates, that the diet of the inhabitants remained terrestrial throughout the lifetime of the site, despite its close proximity to the Gironde Estuary and the Atlantic Ocean. A similar result has been found at other Neolithic sites in Europe.

(3) Assuming a local, terrestrial diet, the geographic differences in bioavailable $^{87}Sr/^{86}Sr$ and precipitation $\delta^{18}O$ within southern France make it possible to infer the regions in which the individuals spent their childhood. Five groups were identified that represent statistically different isotopic compositions of their food and drinking water source. Interpreting these isotopic differences in terms of human mobility is limited due to the large range of bioavailable $^{87}Sr/^{86}Sr$ near Le Tumulus des Sables and in the surrounding Aquitaine Basin and the uncertainties associated with interpreting the $\delta^{18}O_W$ values. Nevertheless, for three of the five groups some inferences about childhood residence area were possible, placing group 1 as locals to the site and individuals from group 2 and 3 as possible short-distance migrants from the surrounding Aquitaine Basin.

5.4 La Grotte des Perrats

This chapter has been submitted as part of an archaeological report about this site.

M. Willmes, L. Kinsley, R. Grün (submitted), Strontium isotope tracing of human mobility at la Grotte des Perrats, Charente, France.

The author's contribution to the publications is as follows: The author conducted the strontium isotope analysis, evaluated the data and wrote the article including suggestions from all co-authors. This study represents the first direct application of the improved LA-MC-ICP-MS analytical protocol at RSES.

5.4.1 Introduction

Strontium isotope ratios ($^{87}Sr/^{86}Sr$) can be used to reconstruct human and animal mobility across geologically different terrains (e.g., Bentley, 2006; Capo et al., 1998; Price et al., 2002; Slovak and Paytan, 2011). The underlying principal is, that $^{87}Sr/^{86}Sr$ isotope ratios vary between different geologic regions depending on their age and composition, due to the radioactive decay of ^{87}Rb by emission of a negative β-particle with a half-life of ~4.88 x 10^{10} years to ^{87}Sr (e.g., Faure and Mensing, 2005). The $^{87}Sr/^{86}Sr$ isotope signature of a region is mainly controlled by the underlying geology, but can be augmented by additional sources of strontium from atmospheric deposition (precipitation, seaspray, dust) and exogenic surface deposits (loess, peat) (Price et al., 2002; Bentley, 2006; Montgomery et al., 2007; Evans et al., 2010; Maurer et al., 2012; Slovak and Paytan, 2012; Frei and Frei, 2013). Humans and animals incorporate strontium from their diet into their dental and skeletal tissues (Beard and Johnson, 2000), where it substitutes for calcium and serves no metabolic function. $^{87}Sr/^{86}Sr$ isotope ratios of dental remains reflect the average isotope ratios of food intake and drinking water, during childhood when the teeth were formed. In order to investigate mobility, the $^{87}Sr/^{86}Sr$ isotope ratios measured in the human remains are compared to the bioavailable $^{87}Sr/^{86}Sr$ isotope range of the surrounding region. A limitation of this method is that geographically distant areas can have similar or overlapping isotope ratio compositions.

5.4.2 The site of la Grotte des Perrats

La Grotte des Perrats is located in Charente, southwest France near the town of Agris, 23 km northeast of Angouleme. It is one of many karst cavities found in this area within the Jurassic limestone of the northern Aquitaine Basin. The cave opens to the steep side of a hill bordering the north Bellonne valley, a tributary of the river Tardoire. The site was discovered in 1981 and excavated until 1994 under the direction of J. Gomez de Soto. New excavations under the direction of B. Boulestin from 2002 until 2008 focused on the entrance of the cave, which had not been studied in the previous exactions. This site contains one of the most important post Palaeolithic sequences in western France. The oldest known occupation of the cave is in the Mesolithic but different layers of occupation continue into the High Middle Ages. 8 individuals, consisting of 5 adults and 3 children (age 2-10), were found in the Mesolithic

sequence at the entrance of the cave. Radiocarbon dating on two human bones show ages of 7345-6704 (GifA-95476) and 7308-7069 cal. BC (Lyon-5914(GrA)). They are associated with a number of animal remains, including aurochs, boars, deer, roe deer, dog and wildcat. The human and animal remains are mixed, possibly due to post depositional processes. Both the animal and human remains show characteristic scraping and cut marks linked to anthropogenic origin. Many bones are broken to extract bone marrow, the skulls are cracked open, and specific bones are missing indicating preferential removal. This indicates that the remains found at this site are the product of food preparation techniques from humans, and therefore indicate cannibalism at this site. Cannibalism in human groups can take many forms. It can be related to food shortages, can be part of a ritual or common way of dealing with the dead within a group, or related to cannibalism of rivals during conflicts. This is a complex subject and our understanding of what drove cannibalism at this site is only in its beginning. As a small case study we investigated the mobility of 2 of the Mesolithic adults and 4 bovid to test if they were locals to this area. This could have implications for the form of cannibalism practiced at this site.

5.4.3 Materials and Methods

Two human teeth and four bovid teeth were chosen for strontium isotope analysis. Samples were prepared by cutting along the long axis using a fine diamond saw to produce a flat surface exposing both the enamel and dentine. The *in situ* isotopic analyses were carried out using a custom-built laser ablation sampling system (ANU HelEx) interfaced between an ArF Excimer laser (193 nm; Lambda Physik Compex 110) and Finnigan MAT Neptune MC-ICP-MS using Faraday cup detectors. Details of the ANU system and its capabilities have been described in detail previously (Eggins et al., 1998, 2003). Spot measurements were performed with a sample ablation time of 60 seconds, using a 233 µm diameter spot and the laser operating at 5 pulses per second. To remove any surface contamination received during the preparation process, such as dust and fine particles, the samples were first subjected to a cleaning run using the laser with a 233 µm spot at 10 Hz for 5s. There are a number of interferences that have to be corrected when using LA-MC-ICP-MS to measure strontium isotopes of dental material (Woodhead et al., 2005; Horstwood et al., 2008; Simonetti et al., 2008; Vroon et al., 2008). Data were corrected offline for Ca-dimers, polyatomic interferences ($^{40}Ca^{+31}P^{+16}O$, $^{40}Ar^{+31}P^{+16}O$), Krypton, Rubidium, and Mass bias, in this order. The data were then subject to a 2σ outlier rejection. Double charged rare earth elements (REE), which can cause interferences on the $^{87}Sr/^{86}Sr$ ratio were monitored but their contribution was negligible. A strontium standard, consisting of a piece of *Tridacna gigas*, with modern seawater Sr isotopic composition was measured and we obtained an average value of 0.70920±6 (n=6, 2σ), which is consistent with present-day values of marine taxa 0.7090-0.7092 (Burke et al., 1982; Hodell et al., 1990). In addition, we measured a modern shark and dugong tooth and obtained an average value of 0.70919±2 (n=4, 2σ).

5.4.4 Bioavailable strontium isotope range around la Grotte des Perrats

The variability of bioavailable $^{87}Sr/^{86}Sr$ isotope ratios for the different geologic units around the site was inferred from plant and soil leachate data from the IRHUM database, for details see Willmes et al. (2014). The site is situated within the carbonaceous units of the Aquitaine Basin, which are intercut by clastic sediments of varying compositions, coming from the near-by Massif Central (Figure 5-22A). Lacking direct samples from the excavation we use the isotope packages (see Chapter 3) to characterise the $^{87}Sr/^{86}Sr$ isotope ranges of the surrounding area. The carbonaceous sediments (isotope package 2) have an $^{87}Sr/^{86}Sr$ isotope range of 0.7072-0.7115 (Figure 5-22B). The clastic sediments of the Aquitaine and Paris Basin (isotope package 3) are highly variable and have $^{87}Sr/^{86}Sr$ isotope values of 0.7076-0.7170. The igneous and metamorphic units of the Massif Central and the Armorican Massif belong to isotope package 4 and 5. Isotope package 4 (0.7084-0.7252) is composed of the Gravel, Sandstone, Granite, Migmatite, Mica schist, and Rhyolitoid units and isotope package 5 (0.7155-0.7213) includes the Orthogneiss units found in the Massif central. The $^{87}Sr/^{86}Sr$ isotope range of la Grotte des Perrats is similar to many areas within the Aquitaine and Paris Basins (Figure 5-22B), but significantly lower than the Massif Central and Armorican Massif, allowing us to identify possible mobility between these regions.

5.4.5 Human and animal mobility

The results for the two human and four bovid teeth are shown in Figure 5-23 and Table 5-11. Since dentine and enamel form at the same time, we would expect them to show the same $^{87}Sr/^{86}Sr$ isotope ratio. The observation that all samples show lowered $^{87}Sr/^{86}Sr$ isotope ratios in their dentine compared to the enamel indicates, that the dentine has been partially overprinted with the $^{87}Sr/^{86}Sr$ isotope range of the site.

The bovid enamel samples show $^{87}Sr/^{86}Sr$ isotope ratios of 0.71152±17, 0.71197±14, 0.71169±74 and 0.71092±22. These values are on the upper limit of isotope package 2 and fit well within the highly variable clastic sediment units of the Aquitaine and Paris Basin as defined by isotope package 3. They are below the $^{87}Sr/^{86}Sr$ isotope ratios expected from many units within the Massif Central and the Armorican Massif. This indicates that the movement of the bovids was constrained to areas dominated by carbonaceous and clastic sediments in the Aquitaine and Paris Basin (Figure 5-22B). The lower $^{87}Sr/^{86}Sr$ isotope ratios of 0.71092±22 suggest that this bovid had a different feeding area than the other three, most likely within the Basins.

The human enamel $^{87}Sr/^{86}Sr$ isotope ratios are 0.71351±41 and 0.71332±14 for sample 3455 and 3456, respectively. These values are higher than the carbonaceous and clastic sediments of the Aquitaine and Paris Basins, excluding these regions as possible childhood residence areas. They are also lower than isotope package 5 (orthogneiss) units. The closest fit for their $^{87}Sr/^{86}Sr$ isotope ratios are the schist units and clastic sediment units that occur as patches in the western part of the Massif Central. The closest of

these units is 12 km to the east of the site (Figure 5-22B). The granites and metamorphic rocks of that dominate the Massif Central and Armorican Massif are highly variable in their $^{87}Sr/^{86}Sr$ isotope ratios (isotope package 4) and are thus also possible childhood residence areas. In conclusion, the two individuals did not spend their childhood in the immediate vicinity of the burial site but come from an area with higher $^{87}Sr/^{86}Sr$ isotope ratios. In terms of distance the closet possibly match is the western part of the Massif Central. Additional tracers such as oxygen and lead isotopes could be used to further constrain the childhood residence area for these individuals.

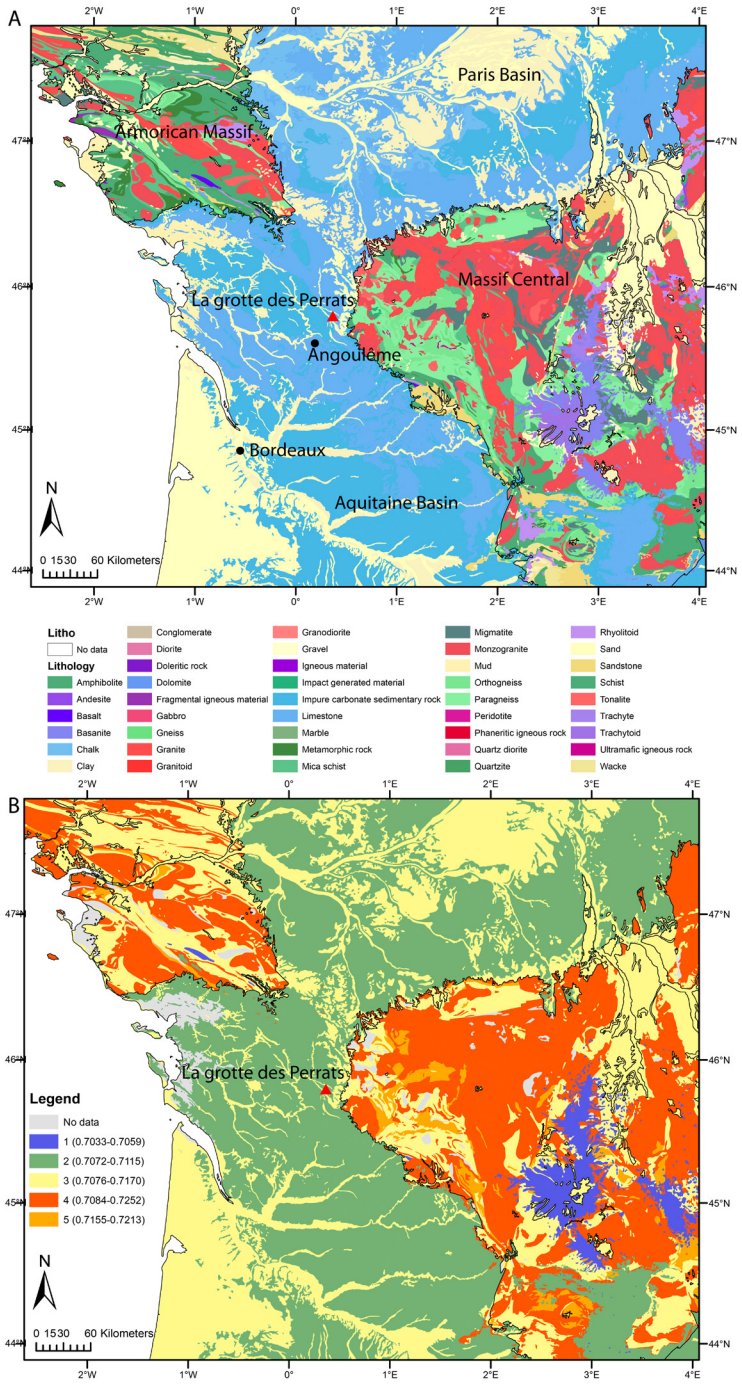

Figure 5-22: A: Surface geologic map of France (BRGM). B: $^{87}Sr/^{86}Sr$ isotope packages, data taken from the IRHUM dataset (Willmes et al., 2014) and chapter 3 of this thesis.

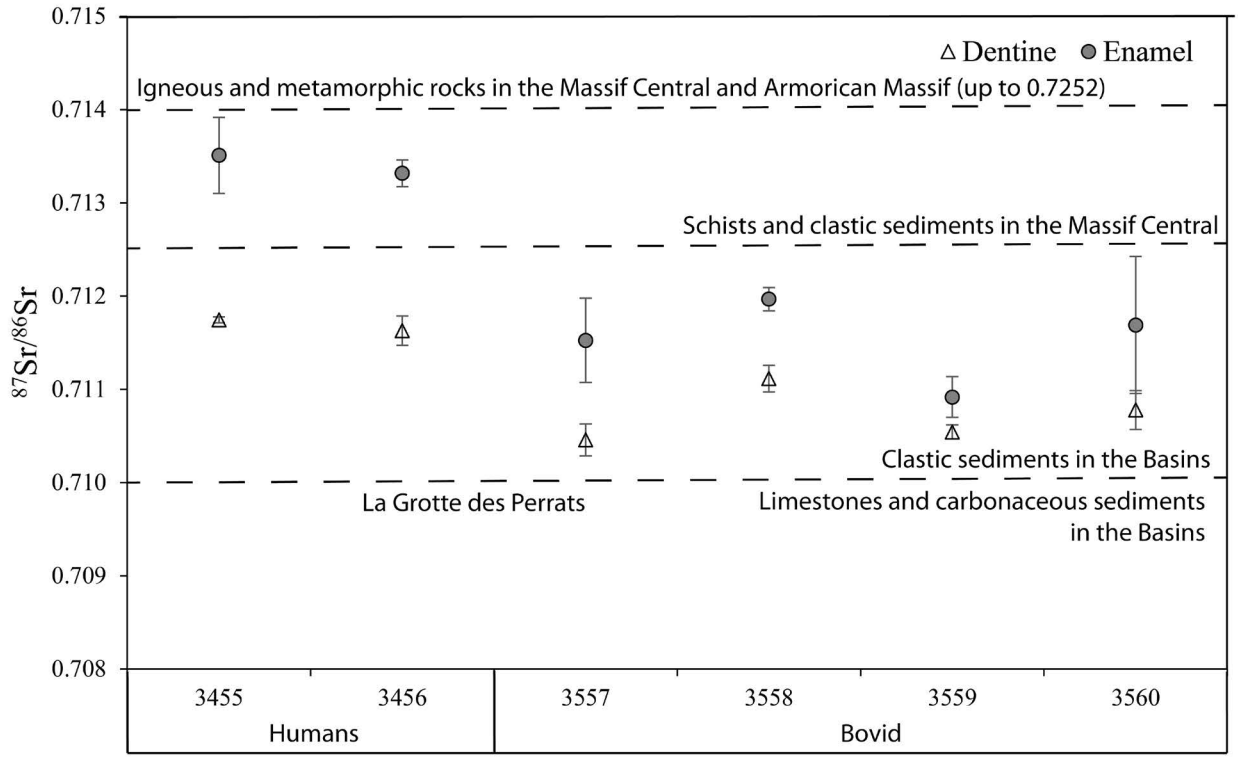

Figure 5-23: $^{87}Sr/^{86}Sr$ isotope ratios for the human and bovid samples from la Grotte des Perrats. The dashed lines indicate the $^{87}Sr/^{86}Sr$ isotope range for the lithological units. In addition to the isotope packages we added a further subdivision to distinguish between clastic sediments in the basins, and clastic sediments in the Massif Central.

Table 5-11: Results for the human and bovid samples from la Grotte des Perrats.

	Sample	ID	^{88}Sr Volts	$^{87}Sr/^{86}Sr$	±2se
Human	3455	Dentine	2.85	0.71174	0.00003
		Enamel	1.85	0.71351	0.00041
	3456	Dentine	1.16	0.71163	0.00016
		Enamel	0.97	0.71332	0.00014
Bovid	3557	Dentine	0.81	0.71046	0.00017
		Enamel	0.29	0.71152	0.00045
	3558	Dentine	1.39	0.71112	0.00014
		Enamel	1.19	0.71197	0.00012
	3559	Dentine	1.06	0.71054	0.00008
		Enamel	0.75	0.71092	0.00022
	3560	Dentine	0.51	0.71078	0.00021
		Enamel	0.23	0.71169	0.00074
Marine		Dugong	16.73	0.70920	0.00001
		Dugong	21.78	0.70919	0.00001
		Shark	17.46	0.70918	0.00002
		Shark	13.99	0.70921	0.00002

6 Conclusions and future directions

The aim of the research project was to (i) define the bioavailable strontium isotope range of France, (ii) develop least-destructive analytical techniques to screen for diagenetic overprint and to perform strontium isotope analysis of fossil human teeth, and (iii) to apply isotopic tracing to key archaeological sites in France. The main research outcomes and future directions for each of these aims is discussed below.

(i) The IRHUM database (Willmes et al., 2014) and the new baseline map of the spatial variability of bioavailable strontium isotopes for France (Willmes et al., in review), provide a powerful tool for archaeological provenance studies. This database and map are also potentially suitable for other applications such as food provenance studies and forensics. The database (www.irhumdatabase.com) and its associated dataset are both open access. Usage of the open source software GeoNode (Boundless) for the database and storage of the dataset in the Pangea data repository (doi:10.1594/PANGAEA.819142) proved to be a fundamental advantage, by allowing for easy access and future developments from the scientific community.

(ii) Using the plant and soil samples from the IRHUM database we produced the first bioavailable $^{87}Sr/^{86}Sr$ isotope baseline map for archaeological provenance studies in France. Significant differences in $^{87}Sr/^{86}Sr$ isotope ratios were observed between plant samples and soil leachates at a number of sample locations. Identification of the driving process behind these differences is confounded by the complex interplay between weathering of lithology, soil genesis, plant processes, and external strontium inputs that vary both in absolute strontium concentrations as well as isotope ratios, spatially and with time. Based solely on the strontium isotope ratios it is thus not possible to untangle these processes and quantification of these external strontium inputs was beyond the scope of this work. For future sampling campaigns, it would be beneficial to collect a number of soil and plant samples from a single site to investigate the full range of the different Sr fluxes between soil horizons, plant types, and external Sr inputs, over multiple seasons.

To create a robust baseline map, we incorporated the observed local variability but excluded anomalous sites that are not representative of their lithological unit and geographic area. Removing these samples sites did not influence the overall variability of the lithological units, with the exception of gravel and chalk units, and thus represents a viable approach. $^{87}Sr/^{86}Sr$ isotope ranges for all major lithological units were established. These were then grouped into five isotope packages, based on k-means cluster analysis, to achieve minimal internal variability and maximise the difference between the isotope packages. The large $^{87}Sr/^{86}Sr$ isotope ranges found in many lithological units and isotope packages, and the occurrence of similar lithological units with overlapping $^{87}Sr/^{86}Sr$ isotope ranges at geographically distant areas in France may limit the identification of mobility between those

areas. In addition, the use of modern samples to create a map for archaeological provenance studies may not be appropriate if the surface deposits have changed significantly (e.g. deposits from the Ice Ages) or if the climatological and atmospheric conditions were different enough to significantly change the $^{87}Sr/^{86}Sr$ isotope ratios in plants and soils. Nevertheless, keeping the limitations of this map in mind it still provides a useful tool to identify patterns of mobility within France and to identify areas suitable for more in-depth studies of strontium isotopic tracing. A logical next step is to create isotope variability maps for additional isotopic tracers such as oxygen and lead. Combining multiple independent proxies would greatly improve the ability to discriminate different geographic regions. In addition, strontium isotope maps of the Iberian Peninsula and Italy would greatly enhance the current capabilities of strontium isotope tracing in Europe.

(iii) The isotopic analysis of valuable fossil human remains requires the use of least destructive analytical techniques. Systematic mapping of U, Th, Zn, and Sr element distributions can detect diagenetic overprint in fossil teeth, which is a common problem in archaeological studies. Comparison of a modern human tooth and a Neanderthal tooth showed the full potential of these chemical tracers to detect zones within a tooth, which are least affected by diagenetic overprint. This nearly destruction free screening method ensures that only suitable samples are further processes for either micro-drilling TIMS or *in situ* LA-MC-ICP-MS analysis.

The polyatomic interference on mass 87 is the principal cause of the offsets between solution and LA-MC-ICP-MS strontium isotope analyses observed in a significant number of analytical facilities. We found direct evidence that this interference originates from Ar, rather than Ca. The effect of the interference on the $^{87}Sr/^{86}Sr$ isotope ratio is essentially controlled by the Sr concentration and oxide production rate. This is because both Ca and P are stoichiometric components in bioapatite, and Ar is always present in the plasma. Currently, monitoring for this interference and, if present, reducing the oxide production rate is the most promising approach to minimise the effect of this interference. The improved analytical protocol significantly reduced the effect of the polyatomic interference on the $^{87}Sr/^{86}Sr$ isotope ratio to 38±394 ppm (n=21, 1σ). In terms of mobility studies, the analytical uncertainties of LA-MC-ICP-MS analysis are now significantly smaller than the variability in $^{87}Sr/^{86}Sr$ isotope ratios in the environment, thus allowing the use of *in situ* LA-MC-ICP-MS as an alternative to micro-drilling TIMS.

(iv) Combining rapid screening for diagenetic overprint and least destructive strontium isotope analysis, either by *in situ* LA-MC-ICP-MS, or micro-drilling TIMS, has opened the door to previously unavailable human fossil samples.

The study at Moula-Guercy of 2 Neanderthal individuals and one Neolithic individual was part of a larger effort to investigate the chronology and mobility of this important

Neanderthal site. The radiometric chronology for Moula-Guercy, provided by combined U-series/ESR dating, indicated that the crucial layer XV, corresponds to MIS 5 *sensu lato*, and is younger than MIS 6. These results agree with the biostratigraphy at the site, which places layer XV to MIS 5e. Strontium isotopic tracing on two Neanderthal individuals provided consistent results with the archaeological data. This shows that the Neanderthals were mobile within the Rhône Valley and used Moula-Guercy as specialized, short-term hunting camp, when their prey animals, such as red deer, were seasonally abundant in this area. Care should be taken to extrapolate from this small (n=2) dataset to any interpretation of Neanderthal mobility overall and more direct investigations of Neanderthal mobility are certainly needed. In contrast, the Neolithic individual showed strontium isotope ratios indicative of young volcanic units. The closest volcanic units occur ~30 km south east of Moula-Guercy, but a more likely residence area for this individual are the much larger occurrences of these units in the Massif Central ~50-80 km to the west of the cave. In either case, this individual experienced significant mobility in its lifetime. To gain a better understanding of Neanderthal mobility as a whole, least destructive strontium and oxygen isotope studies could be carried out on a range of Neanderthal samples across France.

The study at Le Tumulus des Sables, an important Neolithic site near Bordeaux, was the focus of a new radiocarbon dating campaign combined with multi-isotope study to reconstruct mobility and diet using strontium, oxygen (James et al., 2013), nitrogen and carbon isotopes. We found that the site was used for burials over a much longer period than previously thought. Initially classified as an early Bell Beaker site, the radiocarbon chronology and artefacts associated with the burials instead document occupation over a period of ~ 2.5 ka. Given the tendency of the BBP people to re-use collective tombs of preceding cultures, and considering the relatively large quantity of Bell Beaker material exhumed (especially ceramic finds), it is possible that most of the human remains found at this site represent the deceased of the BBP. However, without dating each individual the disturbed condition of the burial does not allow the secure identification of a specific individual to the BBP. The remains of eight individuals had narrow C and N isotopic ranges, suggesting that the diet of the inhabitants remained terrestrial throughout the lifetime of the site, despite its close proximity to the Gironde Estuary and the Atlantic Ocean. Assuming a local, terrestrial diet, the geographic differences in bioavailable $^{87}Sr/^{86}Sr$ and precipitation $\delta^{18}O$ within southern France make it possible to infer the regions in which the individuals spent their childhood. Five groups were identified that represent statistically different isotopic compositions of their food and drinking water source. Interpreting these isotopic differences in terms of human mobility is limited due to the large range of bioavailable $^{87}Sr/^{86}Sr$ near Le Tumulus des Sables and in the surrounding Aquitaine Basin and the uncertainties associated with interpreting the $\delta^{18}O_W$ values. Nevertheless, for three of the five groups some inferences about childhood residence area were possible, placing group 1

as locals to the site and individuals from group 2 and 3 as possible short-distance migrants from the surrounding Aquitaine basin. The study at La Grotte des Perrats provided evidence that the individuals found at this site may have come from the Massif Central. This could have implications for the interpretation of cannibalism at this site, but only presents one line of evidence and needs to be substantiated with more archaeological and geochemical datasets. The different archaeological case studies illustrate the potentials and pitfalls of strontium isotope tracing, and offer new insights into these renowned archaeological sites. Especially when multiple isotopic tracers are used in conjunction with archaeological evidence, detailed insights about the mobility patterns of our ancestors can be gained from minute amounts of sample material.

7 References

Åberg, G., 1995. The Use of Natural Strontium Isotopes as Tracers in Environmental-Studies. Water Air and Soil Pollution. 79, 309–322.

Ash, M.M., Nelson, S.J., 2003. Wheeler's dental anatomy, physiology, and occlusion, 8th ed. W.B. Saunders, Philadelphia.

Aubert, D., Probst, A., Stille, P., Viville, D., 2002. Evidence of hydrological control of Sr behavior in stream water (Strengbach catchment, Vosges mountains, France). Applied Geochemistry. 17, 285–300.

Aubert, M., Williams, I.S., Boljkovac, K., Moffat, I., Moncel, M.-H.H., Dufour, E., Grün, R., 2012. In situ oxygen isotope micro-analysis of faunal material and human teeth using a SHRIMP II: a new tool for palaeo-ecology and archaeology. Journal of Archaeological Science. 39, 3184–3194.

Balasse, M., 2002. Reconstructing dietary and environmental history from enamel isotopic analysis: Time resolution of intra-tooth sequential sampling. International Journal of Osteoarchaeology. 12, 155–165.

Balasse, M., 2003. Potential biases in sampling design and interpretation of intra-tooth isotope analysis. International Journal of Osteoarchaeology. 13, 3–10.

Balasse, M., Ambrose, S.H., Smith, A.B., Price, T.D., 2002. The Seasonal Mobility Model for Prehistoric Herders in the South-western Cape of South Africa Assessed by Isotopic Analysis of Sheep Tooth Enamel. Journal of Archaeological Science. 29, 917–932.

Bashkin, V.N., Howarth, R.W., 2002. Modern biogeochemistry. Springer Science & Business Media.

Bataille, C.P., Bowen, G.J., 2012. Mapping 87Sr/86Sr variations in bedrock and water for large scale provenance studies. Chemical Geology. 304-305, 39–52.

Bataille, C.P., Laffoon, J., Bowen, G.J., 2012. Mapping multiple source effects on the strontium isotopic signatures of ecosystems from the circum-Caribbean region. Ecosphere. 3, 1–24.

Beard, B.L., Johnson, C.M., 2000. Strontium isotope composition of skeletal material can determine the birth place and geographic mobility of humans and animals. Journal of Forensic Sciences. 45, 1049–61.

Beaumont, J., Gledhill, A., Lee-Thorp, J.A., Montgomery, J., 2013. Childhood diet: a closer examination of the evidence from dental tissues using stable isotope analysis of incremental human dentine. Archaeometry. 55, 277–295.

Benson, A., Kinsley, L., Willmes, M., Defleur, A., Kokkonen, H., Mussi, M., Grün, R., 2013. Laser ablation depth profiling of U-series and Sr isotopes in human fossils. Journal of Archaeological Science. 40, 2991–3000.

Benson, L.V., Taylor, H.E., Peterson, K.A., Shattuck, B.D., Ramotnik, C.A., Stein, J.R., 2008. Development and evaluation of geochemical methods for the sourcing of archaeological maize. Journal of Archaeological Science. 35, 912–921.

Bentley, R.A., 2006. Strontium Isotopes from the Earth to the Archaeological Skeleton: A Review. Journal of Archaeological Method and Theory. 13, 135–187.

Bentley, R.A., Knipper, C., 2005. Geographical patterns in biologically available strontium, carbon and oxygen isotope signatures in prehistoric SW Germany. Archaeometry. 47, 629–644.

Bentley, R.A., Price, T.D., Stephan, E., 2004. Determining the "local" 87Sr/86Sr range for archaeological skeletons: A case study from Neolithic Europe. Journal of Archaeological Science. 31, 365–375.

Benz, M., van Willigen, S., 1998. Some new approaches to the Bell Beaker phenomenon. Lost paradise...?: proceedings of the 2nd Meeting of the "Association Archâeologie et Gobelets" Feldberg, Germany, 18th-20th April 1997, Vol. 690. British Archaeological Reports Ltd.

Bern, C.R., Townsend, A.R., Farmer, G.L., 2005. Unexpected dominance of parent-material strontium in a tropical forest on highly weathered soils. Ecology. 86, 626–632.

Bernard, A., Daux, V., Lécuyer, C., Brugal, J.P., Genty, D., Wainer, K., Gardien, V., Fourel, F., Jaubert, J., 2009. Pleistocene seasonal temperature variations recorded in the δ18O of Bison priscus teeth. Earth and Planetary Science Letters. 283, 133–143.

Besse, M., Desideri, J., 2004. Graves and funerary rituals during the Late Neolithic and Early Bronze Age in Europe (2700-2000 BC): proceedings of the International Conference held at the Cantonal Archaeological Museum, Sion (Switzerland) October 4th-7th 2001, British archaeological Reports - International Series S. Vol. 1284. Archaeopress.

Blum, J.D., Erel, Y., Brown, K., 1993. 87Sr/86Sr ratios of sierra nevada stream waters: Implications for relative mineral weathering rates. Geochimica et Cosmochimica Acta. 57, 5019–5025.

Blum, J.D., Taliaferro, E.H., Weisse, M.T., Holmes, R.T., 2000. Changes in Sr/Ca, Ba/Ca and 87Sr/86Sr ratios between trophic levels in two forest ecosystems in the northeastern U.S.A. Biogeochemistry. 49, 87–101.

Boel, C.A., 2011. Identifying Migration : Strontium Isotope Studies on an Early Bell Beaker Population from Le Tumulus des Sables, France. B.Sc. (Hons) Thesis. The Australian National University.

Bordes, F., 1961. Typologie du paléolithique ancien et moyen. Publications de l'Institut de Préhistoire de l'Université de Bordeaux. Bordeaux. Delmas. 2.

Bowen, G.J., 2015. Gridded maps of the isotopic composition of meteoric waters. http://www.waterisotopes.org.

Bowen, G.J., Revenaugh, J., 2003. Interpolating the isotopic composition of modern meteoric precipitation. Water Resources Research. 39.

Bowen, G.J., Wilkinson, B., 2002. Spatial distribution of δ18O in meteoric precipitation. Geology. 30, 315–318.

BRGM, n.d. Geology of France at 1:1million scale (6th edition) - OneGeology-Europe project - WP6.

Britton, K., Grimes, V., Dau, J., Richards, M.P., 2009. Reconstructing faunal migrations using intra-tooth sampling and strontium and oxygen isotope analyses: a case study of modern caribou (Rangifer tarandus granti). Journal of Archaeological Science. 36, 1163–1172.

Britton, K., Grimes, V., Niven, L., Steele, T.E., McPherron, S., Soressi, M., Kelly, T.E., Jaubert, J., Hublin, J.J., Richards, M.P., 2011. Strontium isotope evidence for migration in late Pleistocene Rangifer: Implications for Neanderthal hunting strategies at the Middle Palaeolithic site of Jonzac, France. Journal of Human Evolution. 61, 176–185.

Brock, F., Higham, T., Ditchfield, P., Ramsey, C.B., 2010a. Current Pretreatment Methods for AMS Radiocarbon Dating at the Oxford Radiocarbon Accelerator Unit (ORAU). Radiocarbon. 52, 103–112.

Brock, F., Higham, T., Ramsey, C.B., 2010b. Pre-screening techniques for identification of samples suitable for radiocarbon dating of poorly preserved bones. Journal of Archaeological Science. 37, 855–865.

Brock, G., Pihur, V., Datta, S., Datta, S., 2008. clValid: An R Package for Cluster Validation. Journal of Statistical Software,. 25, 1–22.

Bronk Ramsey, C., 2009. Bayesian Analysis of Radiocarbon Dates. Radiocarbon. 51, 337–360.

Buckberry, J.O., Montgomery, J., Towers, J., Müldner, G., Holst, M., Evans, J.A., Gledhill, A., Neale, N., Lee-Thorp, J.A., 2014. Finding Vikings in the Danelaw. Oxford Journal of Archaeology. 33, 413–434.

Budd, P., Montgomery, J., Barreiro, B., Thomas, R.G., 2000. Differential diagenesis of strontium in archaeological human dental tissues. Applied Geochemistry. 15, 687–694.

Burke, W.H., Denison, R.E., Hetherington, E.A., Koepnick, R.B., Nelson, H.F., Otto, J.B., 1982. Variation of seawater 87Sr/86 Sr throughout Phanerozoic time. Geology. 10, 516–519.

Burton, J.H., Price, T.D., Middleton, W.D., 1999. Purification of Calcium. Journal of Archaeological Science. 26, 609–616.

Burton, J.H., Wright, L.E., 1995. Nonlinearity in the relationship between bone Sr/Ca and diet:

Paleodietary implications. American Journal of Physical Anthropology. 96, 273–282.

Butler, P.M., 1978. The ontogeny of mammalian heterodonty. Journal de biologie buccale. 6, 217–28.

Capo, R.C., Chadwick, O.A., 1999. Sources of strontium and calcium in desert soil and calcrete. Earth and Planetary Science Letters. 170, 61–72.

Capo, R.C., Stewart, B.W., Chadwick, O.A., 1998. Strontium isotopes as tracers of ecosystem processes: theory and methods. Geoderma. 82, 197–225.

Chadwick, O.A., Derry, L.A., Vitousek, P.M., Huebert, B.J., Hedin, L.O., 1999. Changing sources of nutrients during four million years of ecosystem development. Nature. 397, 491–497.

Champion, T., Gamble, C., Shennan, S., Whittle, A., 2009. Prehistoric Europe. Left Coast Press.

Chancerel, A., Courtaud, P., 2006. Le tumulus des Sables: Rapport de fouille programmée. Direction Régionale Commune de St-Laurent-Médoc. Les Affaires Culturelles d'Aquitaine Service Régional de l'Archéologie.

Chantraine, J., Chêne, F., Nehlig, P., Rabu, D., 2005. Carte géologique de la France à 1/1 000 000 6e édition révisée 2003. BRGM.

Charlier, B.L.A., Ginibre, C., Morgan, D., Nowell, G.M., Pearson, D.G., Davidson, J.P., Ottley, C.J., 2006. Methods for the microsampling and high-precision analysis of strontium and rubidium isotopes at single crystal scale for petrological and geochronological applications. Chemical Geology. 232, 114–133.

Chenery, C., Müldner, G., Evans, J.A., Eckardt, H., Lewis, M., 2010. Strontium and stable isotope evidence for diet and mobility in Roman Gloucester, UK. Journal of Archaeological Science. 37, 150–163.

Chisholm, B.S., Nelson, D.E., Schwarcz, H.P., 1982. Stable-Carbon Isotope Ratios as a Measure of Marine Versus Terrestrial Protein in Ancient Diets. Science. 216, 1131–1132.

Copeland, S.R., Sponheimer, M., de Ruiter, D.J., Lee-Thorp, J.A., Codron, D., le Roux, P.J., Grimes, V., Richards, M.P., 2011. Strontium isotope evidence for landscape use by early hominins - Supplementary Information. Nature. 474, 76–8.

Copeland, S.R., Sponheimer, M., le Roux, P.J., Grimes, V., Lee-Thorp, J.A., de Ruiter, D.J., Richards, M.P., 2008. Strontium isotope ratios (87Sr/86Sr) of tooth enamel: a comparison of solution and laser ablation multicollector inductively coupled plasma mass spectrometry methods. Rapid Communications in Mass Spectrometry. 22, 3187–3194.

Copeland, S.R., Sponheimer, M., Lee-Thorp, J.A., le Roux, P.J., de Ruiter, D.J., Richards, M.P., 2010. Strontium isotope ratios in fossil teeth from South Africa: Assessing laser ablation MC-ICP-MS analysis and the extent of diagenesis. Journal of Archaeological Science. 37, 1437–1446.

Courtaud, P., Chancerel, A., Cieselski, E., 2009. Le tumulus des Sables: Commune de St-Laurent-Médoc.

Courtaud, P., Chancerel, A., Cieselski, E., 2010. Le tumulus des Sables: Rapport de fouille programmée. Direction Régionale Commune de St-Laurent-Médoc. Les Affaires Culturelles d'Aquitaine Service Régional de l'Archéologie.

Cox, G., Sealy, J., 1997. Investigating Identity and Life Histories: Isotopic Analysis and Historical Documentation of Slave Skeletons Found on the Cape Town Foreshore, South Africa. International Journal of Historical Archaeology. 1, 207–224.

Cregut-Bonnoure, É., Boulbes, N., Daujeard, C., Fernandez, P., Valensi, P., 2010. Nouvelles données sur la grande faune de l'Éemien dans le Sud-Est de la France. Quaternaire. 227–248.

Czebreszuk, J., 2014. Similar but Different: Bell Beakers in Europe. Sidestone Press.

Dansgaard, W., 1964. Stable isotopes in precipitation. Tellus. 16, 463–468.

Daujeard, C., Moncel, M.-H., 2010. On Neanderthal subsistence strategies and land use: A regional focus on the Rhone Valley area in southeastern France. Journal of Anthropological Archaeology. 29, 368–391.

Daux, V., Lécuyer, C., Héran, M.A., Amiot, R., Simon, L., Fourel, F., Martineau, F., Lynnerup, N., Reychler, H., Escarguel, G., 2008. Oxygen isotope fractionation between human phosphate and water revisited. Journal of Human Evolution. 55, 1138–1147.

de Jong, H.N., Foster, G.L., Hawkesworth, C., Pike, A.W.G., 2007. LA-MC-ICPMS 87Sr/86Sr on tooth enamel—pitfalls and problems. Geochimica et Cosmochimica Acta. A212.

de Laeter, J.R., Böhlke, J.K., De Bièvre, P., Hidaka, H., Peiser, H.S., Rosman, K.J.R., Taylor, P.D.P., 2003. Atomic weights of the elements. Review 2000 (IUPAC Technical Report). Pure and Applied Chemistry. 75, 683–800.

Debard, É., Pastre, J.-F., 2008. Nouvelles données sur les téphras pléistocènes piégés dans les remplissages karstiques ardéchois (SE France). Quaternaire. 107–116.

Defleur, A., 2015. Les industries lithiques moustériennes de la Baume Moula-Guercy (Soyons, Ardèche). Fouilles 1993–1999. L'Anthropologie. 119, 170–253.

Defleur, A., Crégut-Bonnoure, É., Desclaux, E., Thinon, M., 2001. Présentation paléo-environnementale du remplissage de la Baume Moula-Guercy à Soyons (Ardèche): implications paléoclimatiques et chronologiques. L'Anthropologie. 105, 369–408.

Defleur, A., Dutour, O., Valladas, H., Vandermeersch, B., 1993. Cannibals among the Neanderthals? Nature. 362, 214.

Defleur, A., White, T., Valensi, P., Slimak, L., Crégut-bonnoure, E., 1999. Neanderthal cannibalism at Moula-Guercy, Ardèche, France. Science. 286, 128–131.

Defleur, A.R., Baillon, S., Black, M.T., Brudvik, K., Carlson, J.P., Condemi, S., Crégut-Bonnoure, E., Desclaux, E., Djerrab, A., Douka, K., Guatelli-Steinberg, D., Guipert, G., Hlusko, L.J., Jabbour, R.S., Krueger, K.L., Longo, L., Manzano, A., Mersey, B., Michel, V., Saos, T., Thinon, M., Ungar, P.S., Valensi, P., J.-L, V., 2014. La Baume Moula-Guercy, Soyons, Ardèche, Ministère de la Culture, Lyon, 545p.

Deines, P., 1980. The isotopic composition of reduced organic carbon. Handbook of Environmental Isotope Geochemistry. 1 - Terres, 329–406.

Desclaux, E., Defleur, A., 1997. Étude préliminaire des micromammifères de la Baume Moula-Guercy à Soyons (Ardèche, France). Systématique, biostratigraphie et paléoécologie. Quaternaire. 8, 213–223.

Desideri, J., Besse, M., 2010. Swiss Bell Beaker population dynamics: Eastern or southern influences? Archaeological and Anthropological Sciences. 2, 157–173.

Din, 2009. ISO 19730 (2009-07) Soil quality - Extraction of trace elements from soil using ammonium nitrate solution (ISO 19730:2008). DIN.

Drouet, T., Herbauts, J., Gruber, W., Demaiffe, D., 2007. Natural strontium isotope composition as a tracer of weathering patterns and of exchangeable calcium sources in acid leached soils developed on loess of central Belgium. European Journal of Soil Science. 58, 302–319.

Duval, M., Aubert, M., Hellstrom, J., Grün, R., 2011. High resolution LA-ICP-MS mapping of U and Th isotopes in an early Pleistocene equid tooth from Fuente Nueva-3 (Orce, Andalusia, Spain). Quaternary Geochronology. 6, 458–467.

Eckardt, H., Chenery, C., Booth, P., Evans, J.A., Lamb, A., Müldner, G., 2009. Oxygen and strontium isotope evidence for mobility in Roman Winchester. Journal of Archaeological Science. 36, 2816–2825.

Eerkens, J.W., Barfod, G.H., Jorgenson, G. a., Peske, C., 2014. Tracing the mobility of individuals using stable isotope signatures in biological tissues: "locals" and "non-locals" in an ancient case of violent death from Central California. Journal of Archaeological Science. 41, 474–481.

Eerkens, J.W., Berget, A.G., Bartelink, E.J., 2011. Estimating weaning and early childhood diet from serial micro-samples of dentin collagen. Journal of Archaeological Science. 38, 3101–3111.

Eggins, S., Grün, R., Pike, A.W.G., Shelley, M., Taylor, L., 2003. 238U, 232Th profiling and U-series isotope analysis of fossil teeth by laser ablation-ICPMS. Quaternary Science Reviews. 22, 1373–1382.

Eggins, S., Kinsley, L., Shelley, J.M.G., 1998. Deposition and element fractionation processes during atmospheric pressure laser sampling for analysis by ICP-MS. Applied Surface Science. 127-129, 278–286.

Elias, R.W., Hirao, Y., Patterson, C.C., 1982. The circumvention of the natural biopurification of calcium along nutrient pathways by atmospheric inputs of industrial lead. Geochimica et Cosmochimica Acta. 46, 2561–2580.

Elliott, J.C., 2002. Calcium Phosphate Biominerals. Reviews in Mineralogy and Geochemistry. 48, 427–453.

Engelstaedter, S., Tegen, I., Washington, R., 2006. North African dust emissions and transport. Earth-Science Reviews. 79, 73–100.

Ericson, J.E., 1985. Strontium isotope characterization in the study of prehistoric human ecology. Journal of Human Evolution. 14, 503–514.

European Environment Agency (EEA), 2009. Corine land cover.

Evans, J.A., Montgomery, J., Wildman, G., 2009. Isotope domain mapping of 87Sr/86Sr biosphere variation on the Isle of Skye, Scotland. Journal of the Geological Society. 166, 617–631.

Evans, J.A., Montgomery, J., Wildman, G., Boulton, N., 2010. Spatial variations in biosphere 87Sr/86Sr in Britain. Journal of the Geological Society. 167, 1–4.

Evans, J.A., Stoodley, N., Chenery, C., 2006. A strontium and oxygen isotope assessment of a possible fourth century immigrant population in a Hampshire cemetery, southern England. Journal of Archaeological Science. 33, 265–272.

Evans, J.A., Tatham, S., 2004. Defining "local signature" in terms of Sr isotope composition using a tenth- to twelfth-century Anglo-Saxon population living on a Jurassic clay-carbonate terrain, Rutland, UK. Geological Society, London, Special Publications. 232, 237–248.

Fallon, S.J., Fifield, L.K., Chappell, J.M., 2010. The next chapter in radiocarbon dating at the Australian National University: Status report on the single stage AMS. Nuclear Instruments and Methods in Physics Research, Section B: Beam Interactions with Materials and Atoms. 268, 898–901.

Faure, G., Mensing, T.M., 2005. Isotopes: Principles and Applications, 3rd ed. John Wiley and Sons Inc., Hoboken, New Jersey.

Féblot-Augustins, J., 1993. Mobility Strategies in the Late Middle Palaeolithic of Central Europe and Western Europe: Elements of Stability and Variability. Journal of Anthropological Archaeology.

Fernandes, R., Hüls, M., Nadeau, M.-J., Grootes, P.M., Garbe-Schönberg, C.-D., Hollund, H.I., Lotnyk, A., Kienle, L., 2013. Assessing screening criteria for the radiocarbon dating of bone mineral. Nuclear Instruments and Methods in Physics Research Section B: Beam Interactions with Materials and Atoms. 294, 226–232.

Fietzke, J., Eisenhauer, A., 2006. Determination of temperature-dependent stable strontium isotope (88Sr/86Sr) fractionation via bracketing standard MC-ICP-MS. Geochemistry, Geophysics, Geosystems. 7.

Fokkens, H., Nicolis, F., 2012. Background to Beakers: Inquiries Into the Regional Cultural Background to the Bell Beaker Complex. Sidestone Press, Leiden.

Foster, G.L., Vance, D., 2006. In situ Nd isotopic analysis of geological materials by laser ablation MC-ICP-MS. Journal of Analytical Atomic Spectrometry. 21, 288.

France, C.A.M., Owsley, D.W., 2015. Stable Carbon and Oxygen Isotope Spacing Between Bone and Tooth Collagen and Hydroxyapatite in Human Archaeological Remains. International Journal of Osteoarchaeology. 25, 299–312.

Frei, K.M., Frei, R., 2011. The geographic distribution of strontium isotopes in Danish surface waters – A base for provenance studies in archaeology, hydrology and agriculture. Applied Geochemistry. 26, 326–340.

Frei, R., Frei, K.M., 2013. The geographic distribution of Sr isotopes from surface waters and soil extracts over the island of Bornholm (Denmark) - A base for provenance studies in archaeology

and agriculture. Applied Geochemistry. 38, 147–160.

Fricke, H.C., O'Neil, J.R., 1996. Inter- and intra-tooth variation in the oxygen isotope composition of mammalian tooth enamel phosphate: Implications for palaeoclimatological and palaeobiological research. Palaeogeography, Palaeoclimatology, Palaeoecology. 126, 91–99.

Gat, J.R., 1996. Oxygen and hydrogen isotopes in the hydrological cycle. Annual Review of Earth and Planetary Sciences. 24, 225–262.

Gosz, J.R., Moore, D.I., 1989. Strontium isotope studies of atmospheric inputs to forested watersheds in New Mexico. Biogeochemistry. 8, 115–134.

Goude, G., Castorina, F., Herrscher, E., Cabut, S., Tafuri, M.A., 2012. First Strontium Isotope Evidence of Mobility in the Neolithic of Southern France. European Journal of Archaeology. 15, 421–439.

Goudie, A.S., Middleton, N.J., 2001. Saharan dust storms: Nature and consequences. Earth-Science Reviews. 56, 179–204.

Graustein, W.C., Armstrong, R.L., 1983. The Use of Strontium-87/Strontium-86 Ratios to Measure Atmospheric Transport into Forested Watersheds. Science. 219, 289–292.

Grün, R., 2000. An alternative for model for open system U-series/ESR age calculations: (closed system U-series)-ESR, CSUS-ESR. Ancient TL. 18, 1–4.

Grün, R., 2009. The DATA program for the calculation of ESR age estimates on tooth enamel. Quaternary Geochronology. 4, 231–232.

Grün, R., Athreya, S., Raj, R., Patnaik, R., 2012a. ESR response in tooth enamel to high-resolution CT scanning. Archaeological and Anthropological Sciences. 4, 25–28.

Grün, R., Aubert, M., Joannes-Boyau, R., Moncel, M.-H.H., 2008. High resolution analysis of uranium and thorium concentration as well as U-series isotope distributions in a Neanderthal tooth from Payre (Ardèche, France) using laser ablation ICP-MS. Geochimica et Cosmochimica Acta. 72, 5278–5290.

Grün, R., Eggins, S., Kinsley, L., Moseley, H., Sambridge, M., 2014. Laser ablation U-series analysis of fossil bones and teeth. Palaeogeography, Palaeoclimatology, Palaeoecology. 416, 150–167.

Grün, R., Katzenberger-Apel, O., 1994. An alpha irradiator for ESR dating. Ancient TL. 12, 35–38.

Grün, R., Kinsley, L., Eggins, S., 2013. Maps of elemental distributions in modern and fossil human teeth. In: 7th Bone Diagenesis Meeting. pp. 22–25.

Grün, R., Mahat, R., Joannes-Boyau, R., 2012b. Ionization efficiencies of alanine dosimeters and tooth enamel irradiated by gamma and X-ray sources. Radiation Measurements. 47, 665–668.

Grün, R., Schwarcz, H.P., Chadam, J., 1988. ESR dating of tooth enamel: Coupled correction for U-uptake and U-series disequilibrium. International Journal of Radiation Applications and Instrumentation. Part D. Nuclear Tracks and Radiation Measurements. 14, 237–241.

Grün, R., Wells, R., Eggins, S., Spooner, N., Aubert, M., Brown, L., Rhodes, E., 2008. Electron spin resonance dating of South Australian megafauna sites. Australian Journal of Earth Sciences. 55, 917–935.

Grupe, G., Price, T.D., Schroter, P., Soellner, F., Johnson, C.M., Beard, B.L., 1997. Mobility of Bell Beaker people revealed by Sr isotope ratios of tooth and bone: a study of southern Bavarian skeletal remains. Applied Geochemistry. 12, 517–525.

Gryschko, R., Kuhnle, R., Terytze, K., Breuer, J., Stahr, K., 2005. Research Articles Soil Extraction of Readily Soluble Heavy Metals and As with 1 M NH4NO3-Solution. Journal of Soils & Sediments. 5, 101–106.

Guérin, G., 1983. La thermoluminescence des plagioclases, méthode de datation du volcanisme. Application au domaine volcanique français: chaîne des Puys, Mont-Dore et Césallier, Bas-Vivarais. Paris VI University.

Guérin, G., Gillot, P.Y., 2007. Nouveaux éléments de chronologie du volcanisme Pléistocène du bas Vivarais (Ardèche, France) par thermoluminescence. Comptes Rendus - Geoscience. 339, 40–49.

Guérin, G., Mercier, N., Adamiec, G., 2011. Dose-rate conversion factors: update. Ancient TL.

Guipert, G., Defleur, A.R., n.d. The Neanderthal Human Cranial Remains of Moula-Guercy, France. submitted to Journal of Human Evolution.

Halicz, L., Segal, I., Fruchter, N., Stein, M., Lazar, B., 2008. Strontium stable isotopes fractionate in the soil environments? Earth and Planetary Science Letters. 272, 406–411.

Hall, G.E.M., Maclaurin, A.I., Garrett, R.G., 1998. Assessment of the 1 M NH 4 NO 3 extraction protocol to identify mobile forms of Cd in soils. Journal of Geochemical Exploration. 64, 153–159.

Hans, U., Kleine, T., Bourdon, B., 2013. Rb–Sr chronology of volatile depletion in differentiated protoplanets: BABI, ADOR and ALL revisited. Earth and Planetary Science Letters. 374, 204–214.

Hartman, G., Richards, M., 2014. Mapping and defining sources of variability in bioavailable strontium isotope ratios in the Eastern Mediterranean. Geochimica et Cosmochimica Acta. 126, 250–264.

Heaton, T.H.E., 1999. Spatial, Species, and Temporal Variations in the13C/12C Ratios of C3Plants: Implications for Palaeodiet Studies. Journal of Archaeological Science. 26, 637–649.

Hedges, R.E.M., Reynard, L.M., 2007. Nitrogen isotopes and the trophic level of humans in archaeology. Journal of Archaeological Science. 34, 1240–1251.

Hemer, K.A., Evans, J.A., Chenery, C.A., Lamb, A.L., 2013. Evidence of early medieval trade and migration between Wales and the Mediterranean Sea region. Journal of Archaeological Science. 40, 2352–2359.

Hemer, K.A., Evans, J.A., Chenery, C.A., Lamb, A.L., 2014. No Man is an island: evidence of pre-Viking Age migration to the Isle of Man. Journal of Archaeological Science. 52, 242–249.

Hennig, C., 2015. fpc: Flexible Procedures for Clustering. R package version 2.1-10.

Higham, T., Jacobi, R., Ramsey, C., 2006. AMS radiocarbon dating of ancient bone using ultrafiltration. Radiocarbon.

Hijmans, R.J., Cameron, S.E., Parra, J.L., Jones, P.G., Jarvis, A., 2005. Very high resolution interpolated climate surfaces for global land areas. International Journal of Climatology. 25, 1965–1978.

Hillson, S., 2005. Teeth, second edi. ed. Cambridge University Press, New York.

Hinz, E.A., Kohn, M.J., 2010. The effect of tissue structure and soil chemistry on trace element uptake in fossils. Geochimica et Cosmochimica Acta. 74, 3213–3231.

Hlusko, L.J., Carlson, J., Guatelli-Steinberg, D., Krueger, K.L., Mersey, B., Ungar, P.S., Defleur, A., 2013. Neanderthal teeth from Moula-Guercy, Ardeche, France. American Journal of Physical Anthropology. 151, 477–491.

Hobbs, J.A., Yin, Q.Z., Burton, J., Bennett, W.A., 2005. Retrospective determination of natal habitats for an estuarine fish with otolith strontium isotope ratios. Marine and Freshwater Research. 56, 655–660.

Hodell, D.A., Mead, G.A., Mueller, P.A., 1990. Variation in the strontium isotopic composition of seawater (8 Ma to present) : Implications for chemical weathering rates and dissolved fluxes to the oceans. Chemical Geology: Isotope Geoscience section. 80, 291–307.

Hodell, D.A., Quinn, R.L., Brenner, M., Kamenov, G., 2004. Spatial variation of strontium isotopes (87Sr/86Sr) in the Maya region: A tool for tracking ancient human migration. Journal of Archaeological Science. 31, 585–601.

Hoogewerff, J., Papesch, W., Kralik, M., Berner, M., Vroon, P., Miesbauer, H., Gaber, O., Künzel, K.-H., Kleinjans, J., 2001. The Last Domicile of the Iceman from Hauslabjoch: A Geochemical Approach Using Sr, C and O Isotopes and Trace Element Signatures. Journal of Archaeological Science. 28, 983–989.

Hoppe, K.A., Koch, P.L., Furutani, T.T., 2003. Assessing the preservation of biogenic strontium in fossil bones and tooth enamel. International Journal of Osteoarchaeology. 13, 20–28.

Horstwood, M.S.A., Evans, J.A., Montgomery, J., 2008. Determination of Sr isotopes in calcium phosphates using laser ablation inductively coupled plasma mass spectrometry and their application to archaeological tooth enamel. Geochimica et Cosmochimica Acta. 72, 5659–5674.

Horwitz, E.P., Chiarizia, R., Dietz, M.L., 1992. A novel Strontium-Selective Extraction Chromatographic Resin*. Solvent Extraction and Ion Exchange. 10, 313–336.

Horwitz, E.P., Dietz, M.L., Fisher, D.E., 1991. Separation and preconcentration of strontium from biological, environmental, and nuclear waste samples by extraction chromatography using a crown ether. Analytical Chemistry. 63, 522–525.

Hosono, T., Nakano, T., Igeta, A., Tayasu, I., Tanaka, T., Yachi, S., 2007. Impact of fertilizer on a small watershed of Lake Biwa: Use of sulfur and strontium isotopes in environmental diagnosis. Science of the Total Environment. 384, 342–354.

Ickert, R.B., Hiess, J., Williams, I.S., Holden, P., Ireland, T.R., Lanc, P., Schram, N., Foster, J.J., Clement, S.W., 2008. Determining high precision, in situ, oxygen isotope ratios with a SHRIMP II: Analyses of MPI-DING silicate-glass reference materials and zircon from contrasting granites. Chemical Geology. 257, 114–128.

Israelevich, P., Ganor, E., Alpert, P., Kishcha, P., Stupp, A., 2012. Predominant transport paths of Saharan dust over the Mediterranean Sea to Europe. Journal of Geophysical Research. 117, D02205.

Jackson, M., Hart, S.R., 2006. Strontium isotopes in melt inclusions from Samoan basalts: Implications for heterogeneity in the Samoan plume. Earth and Planetary Science Letters. 245, 260–277.

Jacobson, A.D., Blum, J.D., Chamberlain, C.P., Poage, M.A., Sloan, V.F., 2002. Ca/Sr and Sr isotope systematics of a Himalayan glacial chronosequence: carbonate versus silicate weathering rates as a function of landscape surface age. Geochimica et Cosmochimica Acta. 66, 13–27.

Jacques, L., Ogle, N., Moussa, I., Kalin, R., Vignaud, P., Brunet, M., Bocherens, H., 2008. Implications of diagenesis for the isotopic analysis of Upper Miocene large mammalian herbivore tooth enamel from Chad. Palaeogeography, Palaeoclimatology, Palaeoecology. 266, 200–210.

James, H., Williams, I.S., Willmes, M., Coutaud, P., Grün, R., 2013. Tracing human migration at a Bell Beaker site, Le Tumulus des Sables (Saint-Laurent-Médoc, France), by in situ δ18O analyses of tooth enamel. Master Thesis. The Australian National University.

Joannes-Boyau, R., Grün, R., 2011. A comprehensive model for CO_2^- radicals in fossil tooth enamel: Implications for ESR dating. Quaternary Geochronology. 6, 82–97.

Jochum, K.P., Weis, U., Stoll, B., Kuzmin, D., Yang, Q., Raczek, I., Jacob, D.E., Stracke, A., Birbaum, K., Frick, D.A., Günther, D., Enzweiler, J., 2011. Determination of reference values for NIST SRM 610-617 glasses following ISO guidelines. Geostandards and Geoanalytical Research. 35, 397–429.

Katzenberg, M.A., 2008. Stable Isotope Analysis: A Tool for Studying Past Diet, Demography, and Life History. In: Biological Anthropology of the Human Skeleton. pp. 413–442.

Kelly, S., Heaton, K., Hoogewerff, J., 2005. Tracing the geographical origin of food: The application of multi-element and multi-isotope analysis. Trends in Food Science and Technology. 16, 555–567.

Knudson, K.J., Williams, H.M., Buikstra, J.E., Tomczak, P.D., Gordon, G.W., Anbar, A.D., 2010. Introducing δ88/86Sr analysis in archaeology: A demonstration of the utility of strontium isotope fractionation in paleodietary studies. Journal of Archaeological Science. 37, 2352–2364.

Koch, P.L., Tuross, N., Fogel, M.L., 1997. The Effects of Sample Treatment and Diagenesis on the Isotopic Integrity of Carbonate in Biogenic Hydroxylapatite. Journal of Archaeological Science. 24, 417–429.

Koenig, A.E., Rogers, R.R., Trueman, C.N., 2009. Visualizing fossilization using laser ablation-inductively coupled plasma-mass spectrometry maps of trace elements in Late Cretaceous bones. Geology. 37, 511–514.

Kohn, M.J., Cerling, T.E., 2002. Stable Isotope Compositions of Biological Apatite. Reviews in Mineralogy and Geochemistry. 48, 455–488.

Kohn, M.J., Schoeninger, M.J., Barker, W.W., 1999. Altered states: Effects of diagenesis on fossil tooth chemistry. Geochimica et Cosmochimica Acta. 63, 2737–2747.

Konter, J.G., Storm, L.P., 2014. High precision 87Sr/86Sr measurements by MC-ICP-MS, simultaneously solving for Kr interferences and mass-based fractionation. Chemical Geology. 385, 26–34.

Krabbenhöft, A., Fietzke, J., Eisenhauer, A., Liebetrau, V., Böhm, F., Vollstaedt, H., 2009. Determination of radiogenic and stable strontium isotope ratios (87Sr/86Sr; δ88/86Sr) by thermal ionization mass spectrometry applying an 87Sr/84Sr double spike. Journal of Analytical Atomic Spectrometry. 24, 1267.

Laffoon, J.E., Davies, G.R., Hoogland, M.L.P., Hofman, C.L., 2012. Spatial variation of biologically available strontium isotopes (87Sr/86Sr) in an archipelagic setting: a case study from the Caribbean. Journal of Archaeological Science. 39, 2371–2384.

Laffoon, J.E., Rojas, R.V., Hofman, C.L., 2013. Oxygen and carbon isotope analysis of human dental enamel from the caribbean: Implications for investigating individual origins. Archaeometry. 55, 742–765.

Lamb, A.L., Evans, J.E., Buckley, R., Appleby, J., 2014. Multi-isotope analysis demonstrates significant lifestyle changes in King Richard III. Journal of Archaeological Science. 50, 559–565.

Le Roux, P.J., Lee-Thorp, J.A., Copeland, S.R., Sponheimer, M., de Ruiter, D.J., 2014. Strontium isotope analysis of curved tooth enamel surfaces by laser-ablation multi-collector ICP-MS. Palaeogeography, Palaeoclimatology, Palaeoecology.

Lee-Thorp, J., 2002. Two decades of progress towards understanding fossilization processes and isotopic signals in calcified tissue minerals. Archaeometry. 44, 435–446.

Lee-Thorp, J. a., 2008. On isotopes and old bones. Archaeometry. 50, 925–950.

Legendre, S., 1986. Analysis of mammalian communities from the late Eocene and Oligocene of Southern France. Palaeovertebrata. 191–217.

Legendre, S., 1988. Les communautés de mammifères du paléogène (éocène supérieur et oligocène) d'Europe occidentale : structures, milieux et évolution. Münchner geowissenschaftliche Abhandlungen (A). Geologie und Palaeontologie,.

Levinson, A.A.A., Luz, B., Kolodny, Y., 1987. Variations in oxygen isotopic compositions of human teeth and urinary stones. Applied Geochemistry. 2, 367–371.

Lewis, J., Coath, C.D., Pike, A.W.G., 2014. An improved protocol for 87Sr/86Sr by laser ablation multi-collector inductively coupled plasma mass spectrometry using oxide reduction and a customised plasma interface. Chemical Geology. 390, 173–181.

Lisiecki, L.E., Raymo, M.E., 2005. A Pliocene-Pleistocene stack of 57 globally distributed benthic δ 18 O records. Paleoceanography. 20.

Longerich, H.P., Jackson, S.E., Günther, D., 1996. Laser ablation inductively coupled plasma mass spectrometric transient signal data acquisition and analyte concentration calculation. Journal of Analytical Atomic Spectrometry. 11, 899–904.

Longinelli, A., 1984. Oxygen isotopes in mammal bone phosphate: A new tool for paleohydrological and paleoclimatological research? Geochimica et Cosmochimica Acta. 48, 385–390.

Ludwig, K.R., 2003. A Geochronological Toolkit for Microsoft Excel: Berkeley Geochronology Center Special Publication.

Luz, B., Kolodny, Y., Horowitz, M., 1984. Fractionation of oxygen isotopes between mammalian bone-phosphate and environmental drinking water. Geochimica et Cosmochimica Acta. 48, 1689–1693.

Maechler, M., Rousseeuw, P., Struyf, A., Hubert, M., Hornik, K., 2015. cluster: Cluster Analysis Basics and Extensions. R package version 2.0.3.

Manzano, A., 2015. Les amphibiens et les reptiles des sites Pléistocène moyen de la France méditerranéenne (Caune de l'Arago, grotte du Lazaret et Baume Moula-Guercy). Etude systématique, reconstitutions paléoclimatiques et paléoenvironnementales. niversité de Perpignan

Via Domitia, Perpignan, France.

Marsh, R.E., 1999. Beta-gradient isochrons using electron paramagnetic resonance: towards a new dating method in archaeology. McMaster University, Hamilton.

Martin, C., Bentaleb, I., Kaandorp, R., Iacumin, P., Chatri, K., 2008. Intra-tooth study of modern rhinoceros enamel δ18O: Is the difference between phosphate and carbonate δ18O a sound diagenetic test? Palaeogeography, Palaeoclimatology, Palaeoecology. 266, 183–189.

Maurer, A.F., Galer, S.J.G., Knipper, C., Beierlein, L., Nunn, E. V., Peters, D., Tütken, T., Alt, K.W., Schöne, B.R., 2012. Bioavailable 87Sr/ 86Sr in different environmental samples - Effects of anthropogenic contamination and implications for isoscapes in past migration studies. Science of the Total Environment. 433, 216–229.

McArthur, J.M., 1994. Recent trends in strontium isotope stratigraphy. Terra Nova. 6, 331–358.

McArthur, J.M., Howarth, R.J., Bailey, T.R., 2001. Strontium Isotope Stratigraphy: LOWESS Version 3: Best Fit to the Marine Sr-Isotope Curve for 0–509 Ma and Accompanying Look-up Table for Deriving Numerical Age. The Journal of Geology. 109, 155–170.

McCormack, J.M., Bahr, A., Gerdes, A., Tütken, T., Prinz-Grimm, P., 2015. Preservation of successive diagenetic stages in Middle Triassic bonebeds: Evidence from in situ trace element and strontium isotope analysis of vertebrate fossils. Chemical Geology. 410, 108–123.

Meers, E., Du Laing, G., Unamuno, V., Ruttens, A., Vangronsveld, J., Tack, F.M.G., Verloo, M.G., 2007. Comparison of cadmium extractability from soils by commonly used single extraction protocols. Geoderma. 141, 247–259.

Mellars, P., 1996. The Neanderthal Legacy: An Archaeological Perspective of Western Europe. Princeton University Press.

Mersey, B., Brudvik, K., Black, M.T., Defleur, A., 2013a. Neanderthal axial and appendicular remains from Moula-Guercy, Ardèche, France. American Journal of Physical Anthropology. 152, 530–42.

Mersey, B., Jabbour, R.S., Brudvik, K., Defleur, A., 2013b. Neanderthal hand and foot remains from Moula-Guercy, Ardèche, France. American Journal of Physical Anthropology. 152, 516–29.

Michel, V., Shen, G., Shen, C.-C., Wu, C.-C., Vérati, C., Gallet, S., Moncel, M.-H., Combier, J., Khatib, S., Manetti, M., 2013. Application of U/Th and 40Ar/39Ar Dating to Orgnac 3, a Late Acheulean and Early Middle Palaeolithic Site in Ardèche, France. PLoS ONE. 8, e82394.

Miller, E.K., Blum, J.D., Friedland, A.J., 1993. Determination of soil exchangeable-cation loss and weathering rates using Sr isotopes. Nature. 362, 438–441.

Montgomery, J., Beaumont, J., Mackenzie, K., Gledhill, A., Shore, R., Brookes, S., Salmon, P., Lynnerup, N., 2012. Timelines in teeth: using micro-CT scans of partially mineralized human teeth to develop a new isotope sampling strategy. In: The 81st Annual Meeting of the American Association of Physical Anthropologists, Portland, Oregon. pp. 216–216.

Montgomery, J., Evans, J.A., Cooper, R.E., 2007. Resolving archaeological populations with Sr-isotope mixing models. Applied Geochemistry. 22, 1502–1514.

Montgomery, J., Evans, J.A., Wildman, G., 2006. 87Sr/86Sr isotope composition of bottled British mineral waters for environmental and forensic purposes. Applied Geochemistry. 21, 1626–1634.

Montuire, S., Desclaux, E., 2008. Palaeoecological analysis of mammalian faunas and environmental evolution in the South of France during the Pleistocene. Boreas. 26, 355–365.

Moore, L.J., Murphy, T.J., Barnes, I.L., Paulsen, P.J., 1982. Absolute isotopic abundance ratios and atomic weight of a reference sample of strontium. Journal of Research of the National Institute of Standards and Technology. 87, 1–8.

Müller, W., Anczkiewicz, R., 2016. Accuracy of laser-ablation (LA)-MC-ICPMS Sr isotope analysis of (bio)apatite – a problem reassessed. Journal of Analytical Atomic Spectrometry. 31, 259–269.

Müller, W., Bondioli, L., Rossi, P.F., Williams, I.S., Anczkiewicz, R., 2013. Spatially-resolved O & Sr isotope ratios by SHRIMP and LA-(MC-)ICPMS – implications for high time resolution profiles in tooth enamel. In: 7th Bone Diagenesis Meeting. Lyon, France.

Nanci, A., 2012. Ten Cate's Oral Histology: Development, Structure, and Function, 8th ed. Elsevier.

Négrel, P., 1999. Geochemical Study of a Granitic Area – The MargerideMountains, France: Chemical Element Behavior and 87Sr/86Sr Constraints. Aquatic Geochemistry. 5, 125–165.

Négrel, P., Casanova, J., Aranyossy, J.F., 2001. Strontium isotope systematics used to decipher the origin of groundwaters sampled from granitoids: The Vienne Case (France). Chemical Geology. 177, 287–308.

Négrel, P., Deschamps, P., 1996. Natural and anthropogenic budgets of a small watershed in the massif central (France): Chemical and strontium isotopic characterization of water and sediments. Aquatic Geochemistry. 2, 1–27.

Négrel, P., Fouillac, C., Brach, M., 1997. A strontium isotopic study of mineral and surface waters from the Cézallier (Massif Central, France): implications for mixing processes in areas of disseminated emergences of mineral waters. Chemical Geology. 135, 89–101.

Négrel, P., Guerrot, C., Millot, R., 2007. Chemical and strontium isotope characterization of rainwater in France: influence of sources and hydrogeochemical implications. Isotopes in environmental and health studies. 43, 179–196.

Négrel, P., Petelet-Giraud, E., 2005. Strontium isotopes as tracers of groundwater-induced floods: The Somme case study (France). Journal of Hydrology. 305, 99–119.

Négrel, P., Petelet-Giraud, E., Widory, D., 2004. Strontium isotope geochemistry of alluvial groundwater: a tracer for groundwater resources characterisation. Hydrology and Earth System Sciences. 8, 959–972.

Négrel, P., Roy, S., 1998. Chemistry of rainwater in the Massif Central (France): A strontium isotope and major element study. Applied Geochemistry. 13, 941–952.

Nelson, B.K., Deniro, M.J., Schoeninger, M.J., De Paolo, D.J., Hare, P.E., 1986. Effects of diagenesis on strontium, carbon, nitrogen and oxygen concentration and isotopic composition of bone. Geochimica et Cosmochimica Acta. 50, 1941–1949.

Niven, L., Steele, T.E., Rendu, W., Mallye, J.B., McPherron, S.P., Soressi, M., Jaubert, J., Hublin, J.J., 2012. Neandertal mobility and large-game hunting: The exploitation of reindeer during the Quina Mousterian at Chez-Pinaud Jonzac (Charente-Maritime, France). Journal of Human Evolution. 63, 624–635.

Nomade, S., Renne, P.R., Vogel, N., Deino, A.L., Sharp, W.D., Becker, T.A., Jaouni, A.R., Mundil, R., 2005. Alder Creek sanidine (ACs-2): A Quaternary 40Ar/39Ar dating standard tied to the Cobb Mountain geomagnetic event. Chemical Geology. 218, 315–338.

Nowell, G.M., Horstwood, M.S.A., 2009. Comments on Richards et al., Journal of Archaeological Science 35, 2008 "Strontium isotope evidence of Neanderthal mobility at the site of Lakonis, Greece using laser-ablation PIMMS." Journal of Archaeological Science. 36, 1334–1341.

O'Connell, T.C., Kneale, C.J., Tasevska, N., Kuhnle, G.G.C., 2012. The diet-body offset in human nitrogen isotopic values: A controlled dietary study. American Journal of Physical Anthropology. 149, 426–434.

Paton, C., Woodhead, J.D., Hergt, J.M., Phillips, D., Shee, S., 2007. Strontium Isotope Analysis of Kimberlitic Groundmass Perovskite via LA-MC-ICP-MS. Geostandards and Geoanalytical Research. 321–330.

Patou-Mathis, M., 2000. Neanderthal subsistence behaviours in Europe. International Journal of Osteoarchaeology. 10, 379–395.

Pestle, W.J., Simonetti, A., Curet, L.A., 2013. 87Sr/86Sr variability in Puerto Rico: Geological complexity and the study of paleomobility. Journal of Archaeological Science. 40, 2561–2569.

Pilz, J., Spöck, G., 2008. Why do we need and how should we implement Bayesian kriging methods. Stochastic Environmental Research and Risk Assessment. 22, 621–632.

Pollard, A.M., 1993. Tales told by dry bones. Chemistry & industry. 359–362.

Pollard, A.M., Pellegrini, M., Lee-Thorp, J.A., 2011. Technical note: some observations on the

conversion of dental enamel δ18O(p) values to δ18O(w) to determine human mobility. American Journal of Physical Anthropology. 145, 499–504.

Porat, N., Zhou, L.P., Chazan, M., Noy, T., Horwitz, L.K., 1999. Dating the Lower Paleolithic Open-Air Site of Holon, Israel by Luminescence and ESR Techniques. Quaternary Research. 51, 328–341.

Poszwa, A., Dambrine, E., Ferry, B., Pollier, B., Loubet, M., 2002. Do deep tree roots provide nutrients to the tropical rainforest? Biogeochemistry. 60, 97–118.

Poszwa, A., Ferry, B., Dambrine, E., Pollier, B., Wickman, T., Loubet, M., Bishop, K., 2004. Variations of bioavailable Sr concentration and 87Sr/ 86Sr ratio in boreal forest ecosystems: Role of biocycling, mineral weathering and depth of root uptake. Biogeochemistry. 67, 1–20.

Poulson, S.R., Kuzminsky, S.C., Scott, G.R., Standen, V.G., Arriaza, B., Muñoz, I., Dorio, L., 2013. Paleodiet in northern Chile through the Holocene: extremely heavy δ15N values in dental calculus suggest a guano-derived signature? Journal of Archaeological Science. 40, 4576–4585.

Prescott, J.R., Hutton, J.T., 1988. Cosmic ray and gamma ray dosimetry for TL and ESR. International Journal of Radiation Applications and Instrumentation. Part D. Nuclear Tracks and Radiation Measurements. 14, 223–227.

Price, T.D., Blitz, J., Burton, J., Ezzo, J.A., 1992. Diagenesis in prehistoric bone: Problems and solutions. Journal of Archaeological Science. 19, 513–529.

Price, T.D., Burton, J.H.H., Bentley, R.A., 2002. The Characterization of Biologically Available Strontium Isotope Ratios for the Study of Prehistoric Migration. Archaeometry. 44, 117–135.

Price, T.D., Grupe, G., Schröter, P., 1998. Migration in the Bell Beaker period of central Europe. Antiquity. 72, 405–411.

Price, T.D., Knipper, C., Grupe, G., Smrcka, V., 2004. Strontium Isotopes and Prehistoric Human Migration: The Bell Beaker Period in Central Europe. European Journal of Archaeology. 7, 9–40.

Prieto Martínez, M.P., Salanova, L., 2009. Coquilles et Campaniforme en Galice et en Bretagne: mécanismes de circulation et stratégies identitaires on JSTOR. Bulletin de la Société préhistorique française. 1, 73–93.

Privat, K.L., O'Connell, T.C., Richards, M.P., 2002. Stable isotope analysis of human and faunal remains from the Anglo-Saxon cemetery at Berinsfield, Oxfordshire : dietary and social implications. Journal of Archaeological Science. 29, 779–790.

Probst, A., El Gh'mari, A., Aubert, D., Fritz, B., McNutt, R., 2000. Strontium as a tracer of weathering processes in a silicate catchment polluted by acid atmospheric inputs, Strengbach, France. Chemical Geology. 170, 203–219.

Prohaska, T., Wenzel, W.W., Stingeder, G., 2005. ICP-MS-based tracing of metal sources and mobility in a soil depth profile via the isotopic variation of Sr and Pb. International Journal of Mass Spectrometry. 242, 243–250.

R Core Team, 2013. R: A language and environment for statistical computing. R Foundation for Statistical Computing,Vienna, Austria. http://www.R-project.org/.

Rao, C.R.M., Sahuquillo, A., Lopez Sanchez, J.F., 2008. A review of the different methods applied in environmental geochemistry for single and sequential extraction of trace elements in soils and related materials, Water, Air, and Soil Pollution.

Reimann, C., Birke, M., Demetriades, A., Filzmoser, P., O'Connor, P., O'Connor, P., 2014. Chemistry of Europe's Agricultural Soils. Part A: Methodology and Interpretation of the GEMAS Data Set.

Reimer, P., 2013. IntCal13 and Marine13 Radiocarbon Age Calibration Curves 0–50,000 Years cal BP. Radiocarbon. 55, 1869–1887.

Reynolds, A.C., Quade, J., Betancourt, J.L., 2012. Strontium isotopes and nutrient sourcing in a semi-arid woodland. Geoderma. 189-190, 574–584.

Richards, M., Grimes, V., Smith, C., Smith, T., Harvati, K., Hublin, J.J., Karkanas, P., Panagopoulou, E., 2009. Response to Nowell and Horstwood (2009). Journal of Archaeological Science. 36,

1657–1658.

Richards, M., Harvati, K., Grimes, V., Smith, C., Smith, T., Hublin, J.J., Karkanas, P., Panagopoulou, E., 2008. Strontium isotope evidence of Neanderthal mobility at the site of Lakonis, Greece using laser-ablation PIMMS. Journal of Archaeological Science. 35, 1251–1256.

Richards, M.P., 2002. A brief review of the archaeological evidence for Palaeolithic and Neolithic subsistence. European Journal of Clinical Nutrition. 56, 1270–1278.

Richards, M.P., Hedges, R.E.M., 1999. Stable isotope evidence for similarities in the types of marine foods used by Late Mesolithic humans at sites along the Atlantic coast of Europe. Journal of Archaeological Science. 26, 717–722.

Richards, M.P., Trinkaus, E., 2009. Isotopic evidence for the diets of European Neanderthals and early modern humans. Proceedings of the National Academy of Sciences. 106, 16034–16039.

Rigo, M., Trotter, J.A., Preto, N., Williams, I.S., 2012. Oxygen isotopic evidence for Late Triassic monsoonal upwelling in the northwestern Tethys. Geology. 40, 515–518.

Rosman, K.J.R., Taylor, P.D.P., 1998. Isotopic compositions of the elements 1997 (Technical Report). Pure and Applied Chemistry. 70, 217–235.

Sambridge, M., Grün, R., Eggins, S., 2012. U-series dating of bone in an open system: The diffusion-adsorption-decay model. Quaternary Geochronology. 9, 42–53.

Sanzelle, S., Pilleyre, T., Montret, M., Faïn, J., Miallier, D., Camus, G., de Goër de Hervé, A., Defleur, A., 2000. Thermoluminescence dating: study of a possible chronological correlation between the maar of La Vestide-du-Pal and a tephra layer from La Baume-Moula-Guercy (Ardèche, France). Comptes Rendus de l'Académie des Sciences - Series IIA - Earth and Planetary Science. 330, 541–546.

Saos, T., 2003. Cadre stratigraphique, paléoclimatique et géochronologie du Languedoc-Roussillon au cours du Pléistocène supérieur d'après l'étude des remplissages de grottes. Université de Perpignan.

Saos, T., Djerrab, A., Defleur, A.R., 2014. Étude stratigraphique, sédimentologique et magnétique des dépôts Pléistocène moyen et supérieur de la Baume Moula-Guercy (Soyons, Ardèche). Quaternaire. 237–251.

Scheib, A.J., Birke, M., Dinelli, E., GEMAS Project Team, 2014. Geochemical evidence of aeolian deposits in European soils. Boreas. 43, 175–192.

Schoeninger, M., DeNiro, M., Tauber, H., 1983. Stable Nitrogen Isotope Ratios of Bone Collagen Reflect Marine and Terrestrial Components of Prehistoric Human Diet. Science. 220, 1381–1383.

Schoeninger, M.J., 1985. Trophic level effects on 15N/14N and 13C/12C ratios in bone collagen and strontium levels in bone mineral. Journal of Human Evolution. 14, 515–525.

Schoeninger, M.J., DeNiro, M.J., 1984. Nitrogen and carbon isotopic composition of bone collagen from marine and terrestrial animals. Geochimica et Cosmochimica Acta. 48, 625–639.

Schoeninger, M.J., Hallin, K., Reeser, H., Valley, J.W., Fournelle, J., 2003. Isotopic alteration of mammalian tooth enamel. International Journal of Osteoarchaeology. 13, 11–19.

Schulting, R.J., Blockley, S.M., Bocherens, H., Drucker, D., Richards, M., 2008. Stable carbon and nitrogen isotope analysis on human remains from the Early Mesolithic site of La Vergne (Charente-Maritime, France). Journal of Archaeological Science. 35, 763–772.

Sealy, J., Armstrong, R., Schrire, C., 1995. Beyond lifetime averages: tracing life histories through isotopic analysis of different calcified tissues from archaeological human skeletons. Antiquity. 69, 290–300.

Sealy, J.C., van der Merwe, N.J., Thorp, J.A.L., Lanham, J.L., 1987. Nitrogen isotopic ecology in southern Africa: Implications for environmental and dietary tracing. Geochimica et Cosmochimica Acta. 51, 2707–2717.

Semhi, K., Clauer, N., Probst, J.L., 2000. Strontium isotope compositions of river waters as records of lithology-dependent mass transfers: the Garonne river and its tributaries (SW France). Chemical

Geology. 168, 173–193.

Shackleton, J., Elderfield, H., 1990. Strontium isotope dating of the source of Neolithic European Spondylus shell artefacts. Antiquity. 64, 312–315.

Shand, P., Darbyshire, D.P.F., Love, A.J., Edmunds, W.M., 2009. Sr isotopes in natural waters: Applications to source characterisation and water-rock interaction in contrasting landscapes. Applied Geochemistry. 24, 574–586.

Sillen, A., 1992. Strontium-calcium ratios (Sr/Ca) of Australopithecus robustus and associated fauna from Swartkrans. Journal of Human Evolution. 23, 495–516.

Sillen, A., Hall, G., Richardson, S., Armstrong, R., 1998. 87Sr/86Sr ratios in modern and fossil food-webs of the Sterkfontein Valley: Implications for early hominid habitat preference. Geochimica et Cosmochimica Acta. 62, 2463–2473.

Simmons, L.M., Montgomery, J., Beaumont, J., Davis, G.R., Al-Jawad, M., 2013. Mapping the spatial and temporal progression of human dental enamel biomineralization using synchrotron X-ray diffraction. Archives of Oral Biology. 58, 1726–1734.

Simonetti, A., Buzon, M.R., Creaser, R.A., 2008. In-situ elemental and Sr isotope investigation of human tooth enamel by Laser Ablation-(MC)-ICP-MS: Successes and pitfalls. Archaeometry. 50, 371–385.

Slovak, N.M., Paytan, A., 2012. Handbook of Environmental Isotope Geochemistry, Handbook of Environmental Isotope Geochemistry. Springer, Berlin, Heidelberg.

Song, B.-Y., Ryu, J.-S., Shin, H.S., Lee, K.-S., 2014. Determination of the Source of Bioavailable Sr Using 87Sr/86Sr Tracers: A Case Study of Hot Pepper and Rice. Journal of agricultural and food chemistry. 62, 9232–9238.

Sponheimer, M., Lee-Thorp, J.A., 1999. Alteration of Enamel Carbonate Environments during Fossilization. Journal of Archaeological Science. 26, 143–150.

Stevens, R.E., Balasse, M., O'Connell, T.C., 2011. Intra-tooth oxygen isotope variation in a known population of red deer: Implications for past climate and seasonality reconstructions. Palaeogeography, Palaeoclimatology, Palaeoecology. 301, 64–74.

Storm, P., Wood, R., Stringer, C., Bartsiokas, A., de Vos, J., Aubert, M., Kinsley, L., Grün, R., 2013. U-series and radiocarbon analyses of human and faunal remains from Wajak, Indonesia. Journal of human evolution. 64, 356–65.

Stosch, H.-G., 2004. Einführung in die Isotopengeochemie, basierend auf Vorlesungen am Mineralogisch- Petrographischen Institut der Universität zu Köln zwischen 1988 und 1994 überarbeitet und ergänzt ab Winter 1999. Institut für Mineralogie und Geochemie Universität Karlsruhe.

Suga, S., 1989. Enamel Hypomineralization Viewed From the Pattern of Progressive Mineralization of Human and Monkey Developing Enamel. Advances in Dental Research. 3, 188–198.

Thirlwall, M.F., 1991. Long-term reproducibility of multicollector Sr and Nd isotope ratio analysis. Chemical Geology: Isotope Geoscience section. 94, 85–104.

Trickett, M.A., Budd, P., Montgomery, J., Evans, J., 2003. An assessment of solubility profiling as a decontamination procedure for the 87Sr/86Sr analysis of archaeological human skeletal tissue. Applied Geochemistry. 18, 653–658.

Trotter, J.A., Williams, I.S., Barnes, C.R., Lécuyer, C., Nicoll, R.S., 2008. Did cooling oceans trigger Ordovician biodiversification? Evidence from conodont thermometry. Science (New York, N.Y.). 321, 550–554.

Trueman, C.N., Kocsis, L., Palmer, M.R., Dewdney, C., 2011. Fractionation of rare earth elements within bone mineral: A natural cation exchange system. Palaeogeography, Palaeoclimatology, Palaeoecology. 310, 124–132.

Trueman, C.N., Palmer, M.R., Field, J., Privat, K., Ludgate, N., Chavagnac, V., Eberth, D.A., Cifelli, R., Rogers, R.R., 2008. Comparing rates of recrystallisation and the potential for preservation of biomolecules from the distribution of trace elements in fossil bones. Comptes Rendus Palevol. 7,

145–158.

Trueman, C.N., Tuross, N., 2002. Trace Elements in Recent and Fossil Bone Apatite. Reviews in Mineralogy and Geochemistry. 48, 489–521.

Valensi, P., Crégut-Bonnoure, E., Defleur, A., 2012. Archaeozoological data from the Mousterian level from Moula-Guercy (Ardèche, France) bearing cannibalised Neanderthal remains. Quaternary International. 252, 48–55.

van Klinken, G.J., 1999. Bone Collagen Quality Indicators for Palaeodietary and Radiocarbon Measurements. Journal of Archaeological Science. 26, 687–695.

Vander Linden, M., 2006. For Whom the Bell Tolls: Social Hierarchy vs Social Integration in the Bell Beaker Culture of Southern France (Third Millennium BC). Cambridge Archaeological Journal. 16, 317.

Vander Linden, M., 2007. What linked the Bell Beakers in third millennium BC Europe ? Antiquity. 81, 343–352.

Vanhaeren, M., D'Errico, F., Billy, I., Grousset, F., 2004. Tracing the source of Upper Palaeolithic shell beads by strontium isotope dating. Journal of Archaeological Science. 31, 1481–1488.

Viner, S., Evans, J.A., Albarella, U., Parker Pearson, M., 2010. Cattle mobility in prehistoric Britain: Strontium isotope analysis of cattle teeth from Durrington Walls (Wiltshire, Britain). Journal of Archaeological Science. 37, 2812–2820.

Vitòria, L., Otero, N., Soler, A., Canals, A., 2004. Fertilizer characterization: isotopic data (N, S, O, C, and Sr). Environmental science & technology. 38, 3254–3262.

Vitousek, P.M., Kennedy, M.J., Derry, L.A., Chadwick, O.A., 1999. Weathering versus atmospheric sources of strontium in ecosystems on young volcanic soils. Oecologia. 121, 255–259.

Voerkelius, S., Lorenz, G.D., Rummel, S., Quétel, C.R., Heiss, G., Baxter, M., Brach-Papa, C., Deters-Itzelsberger, P., Hoelzl, S., Hoogewerff, J., Ponzevera, E., Van Bocxstaele, M., Ueckermann, H., 2010. Strontium isotopic signatures of natural mineral waters, the reference to a simple geological map and its potential for authentication of food. Food Chemistry. 118, 933–940.

Vroon, P.Z., van der Wagt, B., Koornneef, J.M., Davies, G.R., 2008. Problems in obtaining precise and accurate Sr isotope analysis from geological materials using laser ablation MC-ICPMS. Analytical and Bioanalytical Chemistry. 390, 465–476.

West, J.B., Bowen, G.J., Dawson, T.E., Tu, K.P., 2010. Isoscapes: Understanding movement, pattern, and process on earth through isotope mapping. In: West, J.B., Bowen, G.J., Dawson, T.E., Tu, K.P. (Eds.), Isoscapes: Understanding Movement, Pattern, and Process on Earth Through Isotope Mapping. Springer Netherlands, pp. 1–487.

Whipkey, C.E., Capo, R.C., Chadwick, O.A., Stewart, B.W., 2000. The importance of sea spray to the cation budget of a coastal Hawaiian soil: A strontium isotope approach. Chemical Geology. 168, 37–48.

White, C.D., Price, T.D., Longstaffe, F.J., 2007. Residential Histories of the Human Sacrifices At the Moon Pyramid, Teotihuacan . Ancient Mesoamerica. 18, 159.

Willmes, M., McMorrow, L., Kinsley, L., Armstrong, R., Aubert, M., Eggins, S., Falguères, C., Maureille, B., Moffat, I., Grün, R., 2014. The IRHUM (Isotopic Reconstruction of Human Migration) database – bioavailable strontium isotope ratios for geochemical fingerprinting in France. Earth System Science Data. 6, 117–122.

Willmes, M., Moffat, I., Mcmorrow, L., Kinsley, L., Armstrong, R., Eggins, S., Grün, R., n.d. Spatial variability of bioavailable 87Sr/86Sr isotope ratios in France as a framework for archaeological provenance studies. submitted to Applied Geochemistry.

Wood, R.E., Ramsey, C.B., Higham, T.F.G., 2010. Refining Background Corrections for Radiocarbon Dating of Bone Collagen at Orau. Radiocarbon. 52, 600–611.

Woodhead, J., Swearer, S., Hergt, J., Maas, R., 2005. In situ Sr-isotope analysis of carbonates by LA-MC-ICP-MS: interference corrections, high spatial resolution and an example from otolith studies. Journal of Analytical Atomic Spectrometry. 20, 22.

Zazzo, A., Balasse, M., Patterson, W.P., 2005. High-resolution δ13C intratooth profiles in bovine enamel: Implications for mineralization pattern and isotopic attenuation. Geochimica et Cosmochimica Acta. 69, 3631–3642.

8 Appendix

8.1 Laboratory and analytical method details for the IRHUM database

This chapter expands on the quality control section of chapter 2 and includes updates to our standard, blank, and reproducibility measurements. Furthermore, it discusses our data reduction schema for $^{87}Sr/^{86}Sr$ isotope measurements of soil and plant samples on the Neptune MC-ICP-MS at the Research School of Earth Sciences, ANU.

8.1.1 Soil standards

The comparability of our dataset was tested by carrying out a blind test on a grazing soil standard from the GEMAS project (Geochemical Mapping of Agricultural and Grazing Land Soil). Measurements at RSES gave an average value of 0.70634±0.00002 (n=14, 2σ) which is in agreement with the GEMAS value of 0.70638±0.00003 (n=39, 2σ), see Figure 8-1. For future comparability studies we have commenced measuring an in-house soil standard which is available upon request. Measurements between 2011 and 2014 gave an average value of 0.70465±0.00004 (n=22, 2σ), see Figure 8-2.

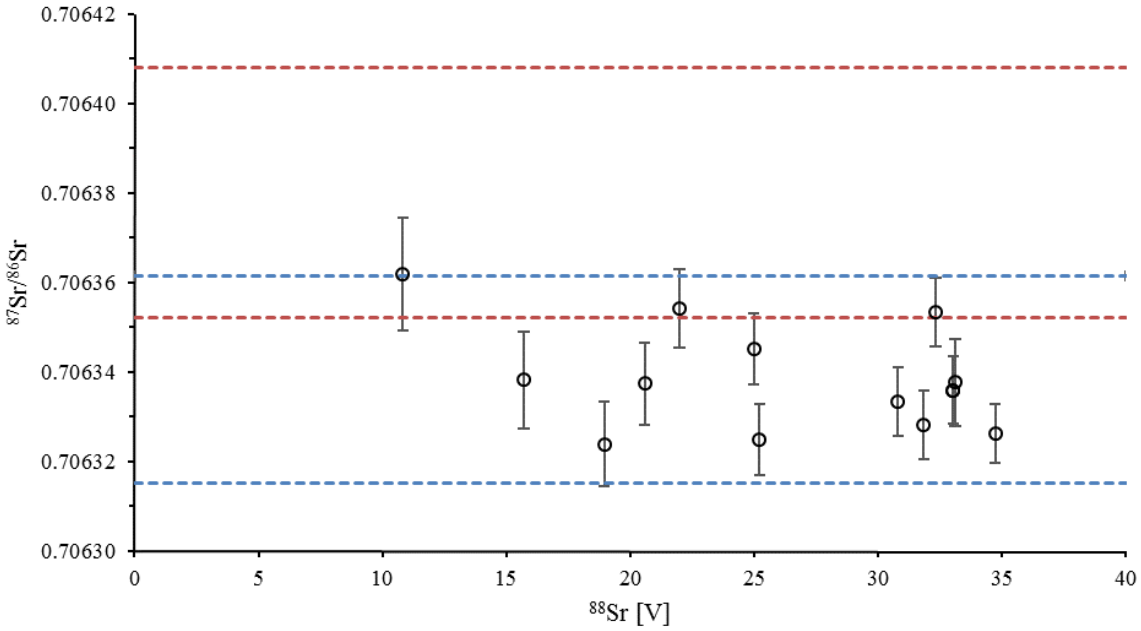

Figure 8-1: Comparison of the grazing soil standard measured at RSES and by the GEMAS project. Error bars are 2σ.

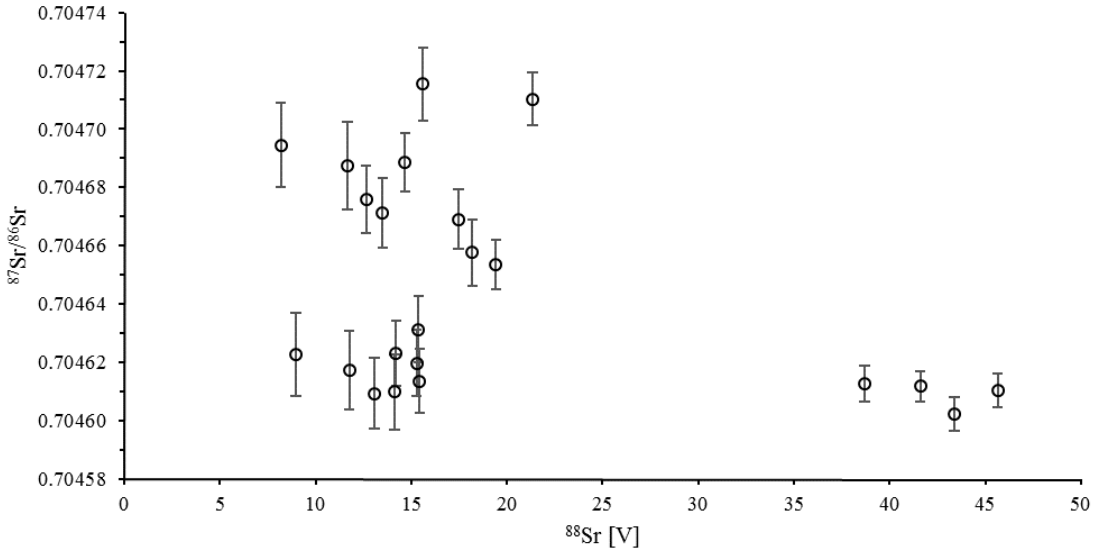

Figure 8-2: Measurements of the RSES soil standard between 2011 and 2014. Error bars are 2σ.

8.1.2 SRM987 standard

The Sr carbonate standard SRM987 (National Institute of Standards and Technology) is commonly used as a standard for $^{87}Sr/^{86}Sr$ isotope studies. It original certified $^{87}Sr/^{86}Sr$ isotope value is 0.71034±0.00026 (Moore et al., 1982). Most studies however quote the accepted $^{87}Sr/^{86}Sr$ value for SRM987 of 0.71025±0.00001 (Thirlwall, 1991; McArthur, 1994; Faure and Mensing, 2005; Hans et al., 2013). Direct measurements of SRM987 on the Neptune MC-ICP-MS at RSES gave an average $^{87}Sr/^{86}Sr$ value of 0.71024±0.00003 (n=256, 2σ). We also measured SRM987 after passing through the ion exchange column chemistry, which gave $^{87}Sr/^{86}Sr$ value of 0.71024±0.00003 (n=35, 2σ) and after our total procedure which gave $^{87}Sr/^{86}Sr$ value of 0.71024±0.00002 (n=26, 2σ). All of these results are in excellent agreement with the literature values and with measurements of the same standard by TIMS at RSES, ANU, which gave an average $^{87}Sr/^{86}Sr$ value of 0.71023±0.00003 (n=99, 2σ).

8.1.3 Blank levels and reproducibility

Blanks (n=278) were monitored during each step of the analytical procedure and representative blanks were measured by isotope dilution with an ^{84}Sr enriched isotope spike using a TRITON Plus Thermal Ionisation Mass Spectrometer (TIMS) at RSES, ANU. Blank levels were found to vary between 50-250 pg Sr, which represents an insignificant contribution to the amount of sample Sr measured (>100 ng). We tested the reproducibility of our analysis by running duplicate and triplicate samples through the entire procedure and found differences between $^{87}Sr/^{86}Sr$ ratios measured for the same sample to be <0.004% (n=42).

8.1.4 Rubidium interference of plant samples

Rubidium can cause an interference on mass 87 and as such influence the final $^{87}Sr/^{86}Sr$ isotope ratio. It can potentially reach the final sample due to problems or errors in the operation of the column chemistry,

especially when the sample started out with high Rb concentrations and low Sr concentrations. A number of plant samples (n=65) from the IRHUM dataset showed high Rb concentrations even after multiple passes through the column chemistry. The level of Rb after column chemistry was found to be independent of the initial Rb level of the sample, the type of plant, or the amount of sample loaded onto the columns. At this stage we suggest that organic compounds from the plants may block columns and leach Rb into the sample aliquot. This requires careful monitoring of the Rb concentration in the samples after column chemistry and potentially to reanalyse samples using stronger acid digestion to remove residual organic compounds.

8.2 Supplementary material: Spatial variability of bioavailable $^{87}Sr/^{86}Sr$ isotope ratios in France as a framework for archaeological provenance studies

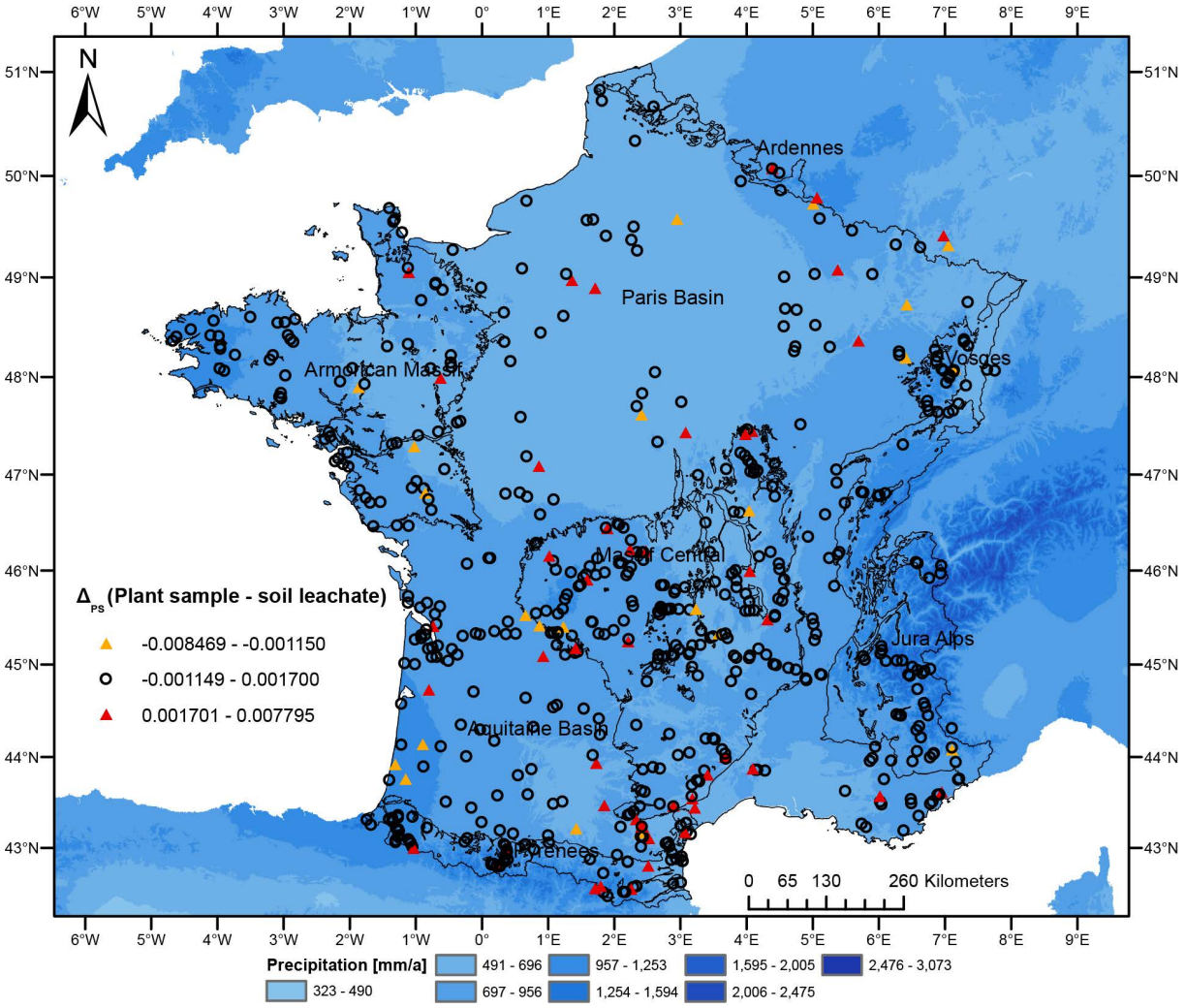

Figure 8-3: Average annual precipitation map of France created from data of worldclim.org (Hijmans et al., 2005). No spatial correlation is observed with the differences in $^{87}Sr/^{86}Sr$ isotope ratios between plant samples and soil leachates.

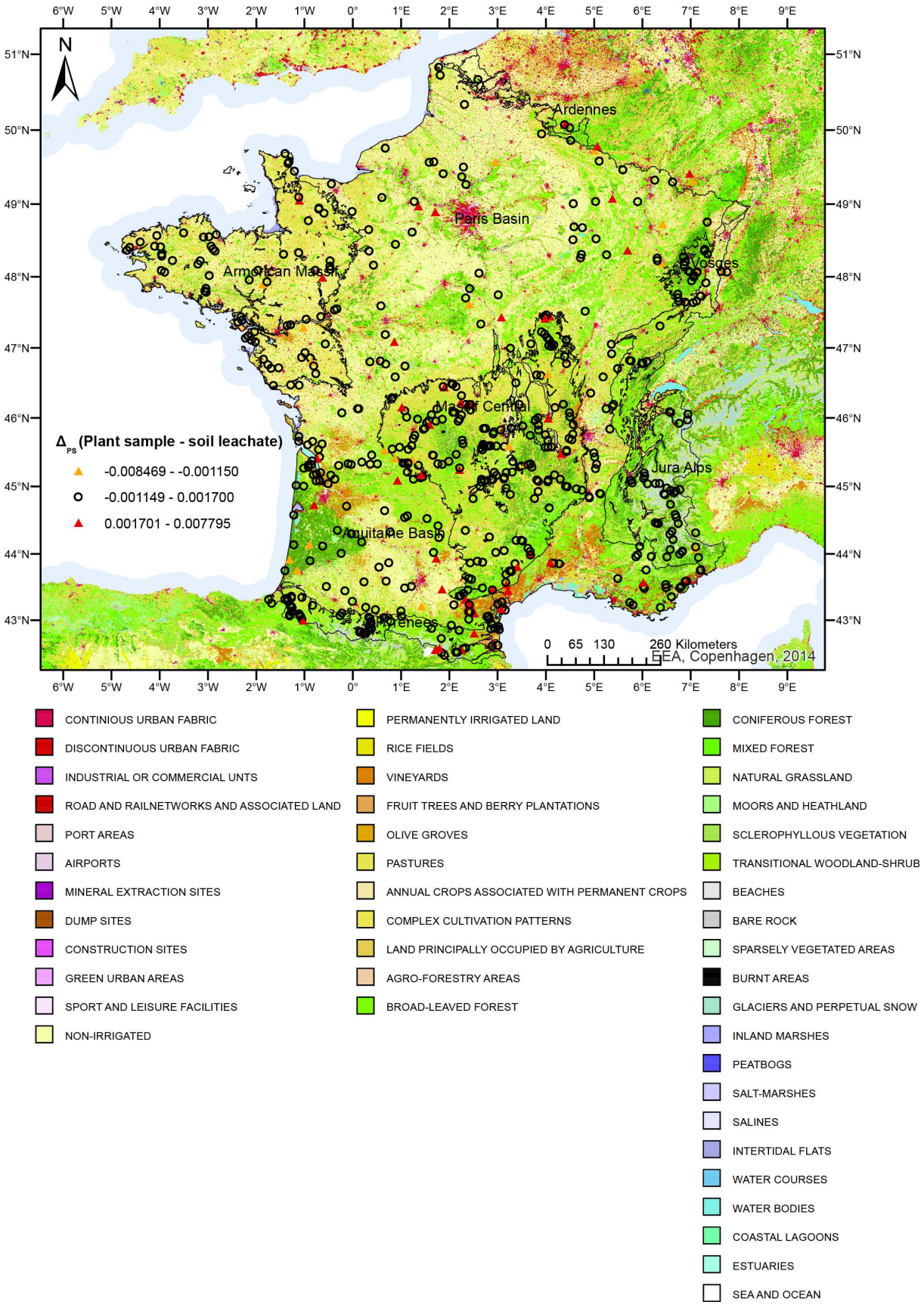

Figure 8-4: CORINE 2006 land cover data (European Environment Agency (EEA), 2009) of France. No spatial correlation is observed with the differences in $^{87}Sr/^{86}Sr$ isotope ratios between plant samples and soil leachates.

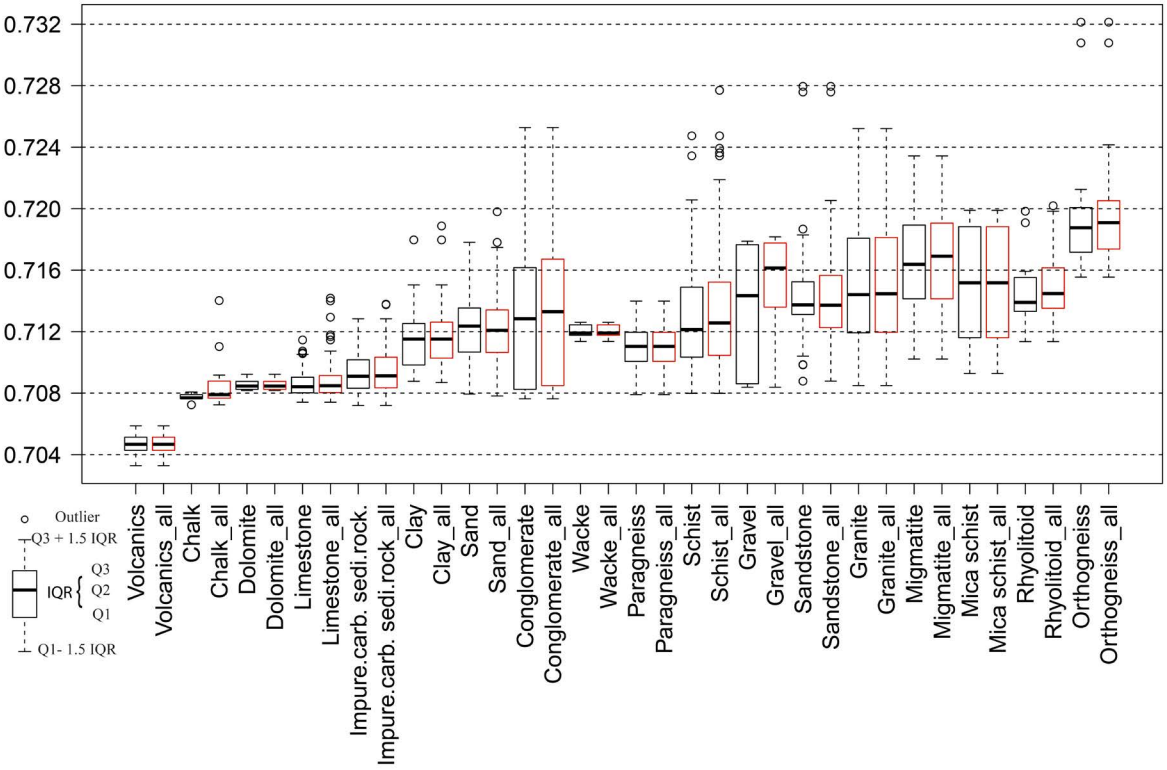

Figure 8-5: Boxplot of the bioavailable $^{87}Sr/^{86}Sr$ isotope range for the different lithological units of France. In red the uncorrected dataset, in black the corrected dataset with sample location with large Δ_{PS} values removed.

Empirical Bayesian Kriging

In order to incorporate the spatial variability within lithological units into the bioavailable $^{87}Sr/^{86}Sr$ isotope map we performed Empirical Bayesian Kriging (EBK) and compared the results to the isotope package approach discussed in chapter 3. EBK generates a smooth continuous surface and does not rely on any external input from the surface geologic map. Empirical Bayesian kriging (EBK) was performed using the geostatistical analyst in ESRI ArcGIS™. Kriging is a complex geostatistical interpolation technique and a detailed evaluation of this method is outside the scope of this chapter, for details see Pilz and Spöck, (2007). In short, EBK automates the building of a valid kriging model through a process of subsetting and simulations and thus reduces the amount of interactive modelling. It also provides more accurate uncertainty estimates by accounting for the error introduced by estimating the underlying semivariogram. We performed an empirical data transformation and used the K-Bessel semivariogram type. Maximum neighbours were set to 30, minimum to 15 and the model was run for 500 simulations. A subset size of 120 with an overlap of 2 was chosen after varying these parameters to create a best visual fit to the empirical semivariances for the complete dataset. To simulate the sharp geologic boundaries, we performed a second EBK analysis where the dataset was split EBK was performed separately for the different geologic regions of France. We used a subset size of 40 for the Armorican Massif, 50 for the Pyrenees, 60 for Massif Central, 40 for the Alps, and 140 for the Aquitaine and Paris Basins, which include the Vosges and Black forest. All of these used an overlap of 2, with 30 maximum and 5 minimum neighbours. The results from the geostatistical layers were exported into raster format, plant data and soil data were merged and averaged, using the raster calculator.

The EBK maps allow us to investigate subtle changes in $^{87}Sr/^{86}Sr$ isotope ratios within lithological units across France (Figure 8-6). However, the EBK method also introduces errors, by creating a smooth continuous change in $^{87}Sr/^{86}Sr$ isotope ratios across otherwise sharp geologic boundaries, and ignoring compositional gaps in $^{87}Sr/^{86}Sr$ isotope ratios. In addition, the fundamental assumption that the sample at a certain location is representative of the surrounding area limits the use of this method using the comparatively small IRHUM dataset compared to the size of France. These limitations of the EBK map can be evaluated by taking the prediction standard error map into account (Figure 8-6C, D). The prediction standard error incorporates two processes. Firstly, it increases in areas of low sample density. Secondly, it increases in areas where the $^{87}Sr/^{86}Sr$ isotope ratio changes rapidly over small spatial scales. The first effect is visible at the northern boundary of the Massif Central. Here high bioavailable $^{87}Sr/^{86}Sr$ isotope ratios occur in the Massif Central and extend far into the Paris Basin. This is caused by the interpolation from the igneous and metamorphic units of the Massif Central into the carbonaceous sediments of the Paris Basin across the geologic boundary. In the IRHUM dataset there are no sample locations in this part of the Paris Basin from the carbonaceous sediments. This is reflected in the high prediction standard errors. Interpolation across geologic boundaries may be reasonable in the direction from mountainous areas into basins, to simulate sediment transport. However, the basins should not have an effect on the mountainous areas at all. This calls for the implementation of boundaries, to restrict the interpolation to within geologic regions. We can simulate this effect by splitting the dataset between

the geologic regions and running EBK separately (Figure 8-6B). Investigating the area north of the Massif Central now shows a much better fit of bioavailable $^{87}Sr/^{86}Sr$ isotope ratios with the surface geology. Prediction standard errors are now also much lower for this area. This shows that the composite EBK is advantageous, since it avoids the large interpolation errors that can occur when crossing sharp geologic boundaries, while maintaining the subtle changes in bioavailable $^{87}Sr/^{86}Sr$ ratios within geologic regions. Large standard prediction error remains in some geologic regions, mainly the Massif Central. This reflects the rapid changes in surface lithology connected to large variability in bioavailable $^{87}Sr/^{86}Sr$ ratios that are poorly constrained using the current sample collection density. While this method certainly shows great promise using the current dataset it is not possible to adequately predict the bioavailable $^{87}Sr/^{86}Sr$ ratio at a specific location within large areas of the Massif Central. The prediction standard errors shown for this map also do not capture the full uncertainties that arise from the underlying assumptions of using this interpolation technique. For now, it is thus best to use the isotope package approach and further test the EBK kriging approach and its associated uncertainties in smaller areas with a well-established $^{87}Sr/^{86}Sr$ isotope baseline.

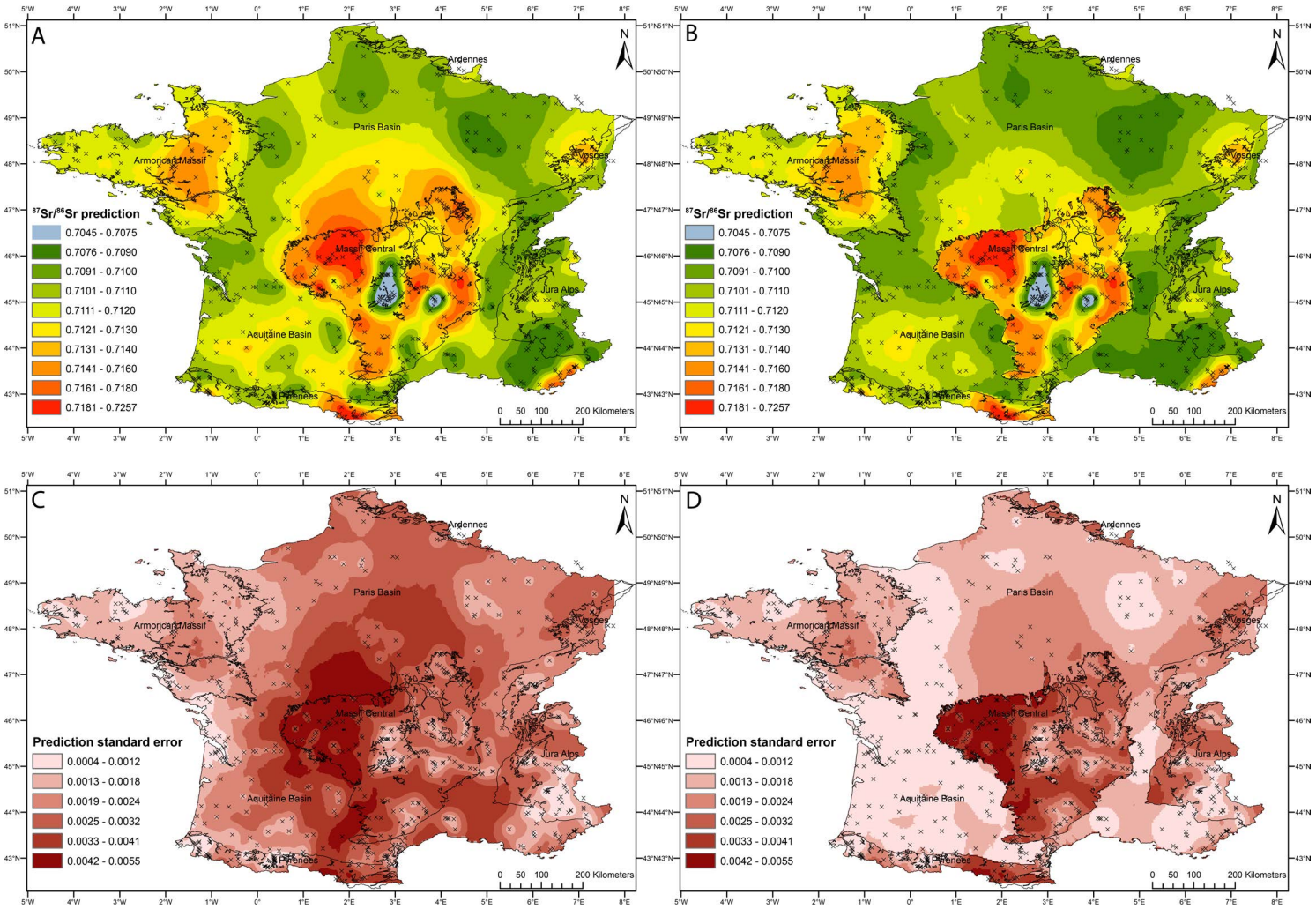

Figure 8-6: A: EBK map created using the complete dataset. B: Composite EBK map created by splitting the dataset and performing EBK separately the different geologic regions. C, D: Prediction standard error maps for the EBK map and composite EBK map, respectively.